THE COMPUTER MODELLING AND EXPERIMENTAL STUDY OF CONFINED JET MIXING WITH APPLICATION TO JET PUMP DESIGN

BY

SEOW NGIE TAY

Thesis submitted for the Degree of
Doctor of Philosophy
of the
Council for National Academic Awards

Department of Mechanical and Production Engineering
Sheffield City Polytechnic

June 1980

COLLABORATING ESTABLISHMENT : GODWIN PUMPS

SOME PARTS EXCLUDED UNDER INSTRUCTION FROM THE UNIVERSITY

CONTENTS

	Page
Acknowledgements	v
Declaration	vi
Summary	vii
Nomenclature	ix
Introduction	1
Chapter 1 Previous Related Studies	7
1.1 Historical Development of the theory of Jet Pumps	7
1.2 Numerical Methods for Predicting Turbulent Flows	10
1.2.1 The Integral Methods	10
1.2.2 The Finite Difference Methods	12
1.3 Previous Experimental Studies	19
1.3.1 Experimental Studies on Confined Jet Mixing	19
1.3.2 Experimental Studies on Jet Pumps and Ejectors	20
1.4 Previous Applications of Laser Doppler Anemometry on Related Flow Measurements	22
Chapter 2 The Mathematical Model	24
2.1 The Equations of Motion for an Incompressible Viscous Fluid	24
2.2 The Need for Turbulence Modelling	25
2.3 The Differential Equations of Conservation Applied to Two-Dimensional Axisymmetrical Flows	27
2.3.1 The Coordinate System	27
2.3.2 The Differential Equations of Conservation	30
2.4 The Choice and Application of Two-Equation k-ε Model	32
2.5 Modification of the Model for 'Near Wall' Flow	36
2.5.1 The 'Law of the Wall'	36
2.5.2 Modifications of k and ε in the 'Near Wall' Region	40
2.6 The Boundary Conditions	42

		Page
Chapter 3	The Numerical Methods	43
	3.1 The Finite Difference Equations	43
	3.1.1 The Staggered Grid and Control Volume	44
	3.1.2 The General Expression of the Finite Difference Equation	46
	3.1.3 The Finite Difference Equation for Pressure Correction	53
	3.2 The Solution of the Finite Difference Equation	56
	3.3 The Overall Procedure of Solution	59
Chapter 4	The Computer Model	62
	4.1 Introduction	62
	4.2 The Basic Structure of the Computer Program	62
	4.3 The Simulation of Various Flow Components	64
	4.3.1 Uniform Mixing Duct	64
	4.3.2 Typical Jet Pump Mixing Tube Including Secondary Inlet Region	67
	4.3.3 Conical Diffuser	72
Chapter 5	Flow Prediction	76
	5.1 Flow in Uniform Diameter Mixing Tube	76
	5.1.1 Introduction	76
	5.1.2 Results and Discussion	78
	5.2 Flow in Typical Mixing Tube Including Secondary Inlet Region	98
	5.2.1 Introduction	98
	5.2.2 Results and Discussion	99
	5.3 Flow in a Conical Diffuser	107
	5.3.1 Introduction	107
	5.3.2 Results and Discussion	110
	5.4 The Prediction of Overall Performance of Typical Jet Pump	114
	5.4.1 Introduction	114
	5.4.2 The Procedure of Calculating the Overall Performance	117
	5.4.3 Results and Discussion	119

		Page
Chapter 6	Experimental Investigation	123
	6.1 Introduction	123
	6.2 The Jet Pump Test Rig	125
	6.2.1 The Flow Circuit	125
	6.2.2 The Components of the Test Pump	128
	6.3 The Laser Doppler Anemometry	136
	6.3.1 The Measurement of Turbulent Flow	136
	6.3.2 The Basic Principles of L.D.A.	137
	6.3.3 The Optical Systems	140
	6.3.4 Methods for Frequency Signal Processing	145
	6.3.5 Signal Quality	148
	6.3.6 Frequency Shift	153
	6.4 The Measurement of Mean and Fluctuating Velocities Using L.D.A.	154
	6.4.1 The Components of the Laser Doppler Anemometer	154
	6.4.2 The Measurement of Three Orthogonal Velocity Components in a Circular Mixing Tube	160
	6.4.3 Experimental Procedure	177
	6.4.4 The Limitation of L.D.A. and Design Criteria of the Optical Components	179
	6.5 Results and Discussion	183
	6.5.1 L.D.A. Experimental Results	183
	6.5.2 Comparison of L.D.A. Measurement with Prediction	194
	6.5.3 Discussion	197
	6.6 Measurement of Static Pressure in Mixing Tube and Diffuser	204
Chapter 7	Application of the Computer Model for Jet Pump Design	209
	7.1 Performance Prediction of Any Proposed Design	209
	7.2 Effect of Geometry on Jet Pump Performance	212
	7.2.1 The Influence of Diameter Ratio	212
	7.2.2 The Influence of Mixing Tube Length	215
	7.2.3 The Influence of Diffuser Included Angle	218
	7.2.4 The Effect of Nozzle Exit to Mixing Throat Spacing	221
	7.3 An Optimizing Procedure for Jet Pump Design	224

		Page
Chapter 8	Conclusions and Suggestions for Future Research	227
8.1	Conclusions	227
8.2	Suggestions for Further Research	230
Appendix A		
A.1	One-Dimensional Theory of Jet Pumps, Gosline and O'Brien(1934)	232
A.2	Momentum Integral Method of P.G.Hill for Axisymmetric Ducted Jets	236
A.3	Derivation of Momentum Equation for a Two-Dimensional Axisymmetric Flow	243
A.4	Derivation of k-Production Terms	247
A.5	Derivation of the General Finite Difference Equation for ϕ	249
A.6	Linearization of Source Terms	255
A.7	Derivation of the Finite Difference Equation for P'	259
A.8	Calculation of Orthogonal Grid in the Secondary Inlet Region of Jet Pump	262
A.9	Inlet Conditions for Turbulent Kinetic Energy k and Length Scale l	267a
Appendix B	Listing of Computer Programs	268
References		306

ACKNOWLEDGEMENTS

I should like to thank my supervisor, Mr. D.R. Croft, for his guidance and generous help throughout the project. I should also like to thank my second supervisor, Dr. M.J. Denman, for many helpful suggestions and comments on the experimental aspect of this project and the presentation of this thesis. My thanks are also due to Dr. P.D. Williams for his advice and encouragement in the early stages of this work.

There are many staff in the Department of Mechanical and Production Engineering and the Department of Computer Services to whom my thanks are also due but I should particularly like to mention Mr. D. Allen and Mr. R. Wilson for their assistance and contribution in the construction of the experimental rig.

I am also in debt to Mr. I. Rothwell of B.I.R.A.L. for the loan of a TSI tracker and several useful discussions.

The work reported in this thesis was carried out during the tenure of a LEA research assistantship provided by the Sheffield City Polytechnic , without such financial support this work would not have been possible.

Finally, I should like to thank my wife for her continuing patience and help in the preparation of this thesis; and to my parents, who, from the other side of the world, consistently give me encouragement and moral support during my pursual of this work.

S. N. TAY

JUNE 1980

DECLARATION

Apart from the references cited, this thesis is the original work of the author.

Some of the computer predicted results have been used in a joint paper 'Numerical Analysis of Jet Pump Flows' published by the author and his supervisors at the First International Conference on Numerical Methods in Laminar and Turbulent flow held at the University College, Swansea on 17th to 21st July 1978.

SUMMARY

As an aid to jet pump design and performance analysis, a theoretical investigation on turbulent confined jet mixing in a non-uniform axisymmetric duct typically used in jet pumps and ejectors has been undertaken. A so-called Prandtl-Kolmogorov two-equation turbulence model, with turbulent kinetic energy k and turbulent energy dissipation rate ε as the two parameters, is incorporated into the time-mean Navier-Stokes equations to form a complete set of partial differential equations which describes the turbulent flow mathematically. The equations are solved numerically via a primitive pressure-velocity finite-difference procedure using a digital computer. The time-mean static pressure, velocities, turbulent kinetic energy and dissipation rate are predicted directly throughout the whole flow field.

To validate the computer model, predicted time-mean static pressure and velocity as well as turbulent shear stress for flow in a uniform bore mixing tube are compared with the published results. The method is then extended to predict flows in conical diffusers and typical jet pumps. The predictions are also compared with the available experimental data.

A laser Doppler anemometer is used to measure the mean and fluctuating velocities of water jet mixing in a uniform perspex mixing tube with a centrally located

nozzle. The measured data which enable turbulent kinetic energy to be evaluated, are compared with the computer predictions to further consolidate the theoretical model.

Finally, the computer model is used to predict the performance of a proposed jet pump and to investigate the influence of various geometrical parameters on jet pump performance. The capability of the computer model as a useful design tool is also demonstrated via an optimization procedure to give the optimum geometry for a given design specification.

NOMENCLATURE

The symbols are explained as they are introduced throughout the thesis. Inevitably, some of the symbols are used to represent more than one quantity. Unless otherwise stated, the symbols will have the following meanings.

Symbol	Meaning
A_P, A_E, A_W, A_N, A_S	Coefficients in the general difference equation
a^u, a^v	Surface areas of control volumes for U and V
a_j, b_j, c_j, d_j	Coefficients of the general algebraic equation for ϕ in tri-diagonal matrix form
C_1, C_2	Constants in the source terms for turbulent energy dissipation ε
C_D	Constant in the source term for turbulent kinetic energy
C_e, C_w, C_n, C_s	Coefficients in the convective terms of the difference equation
C_t	Craya-Curtet Number for confined jet flow
$C\mu$	A constant in the equation for turbulent viscosity
c	Velocity of light
D_e, D_w, D_n, D_s	Coefficients in the diffusive terms of the difference equation
d	Diameter
E	A function of wall roughness in the logarithmic velocity distribution near the wall
F	Force
f	Frequency of light

f_D	Doppler frequency
G	Turbulent energy production term
H	Total head
i	Incident angle of a light beam
k	Turbulent kinetic energy
$\bar{k}$	Unit vector
k_f	Roughness parameter of a wall
l	Length in general or length scale in the turbulence models
l_m	Mixing length in Prandtl's model
M	Flow ratio of a jet pump
$\dot{m}$	Mass flow rate
N	Head ratio of a jet pump
P	Time-mean static pressure
p, p'	Instantaneous and fluctuating static pressures
Q_1, Q_2	Primary and secondary flow rates of a jet pump
R_i, R_o	Radii of curvature of the nozzle wall and inlet duct wall respectively; also refer to inner and outer pipe radii in Chapter 6
Re	Reynolds number
r	Distance of a point from the axis of symmetry; also represents refractive angle in Chapter 6
r_i, r_o	Radii of the central jet and mixing duct for an uniform mixing duct
r_x, r_y	Radii of curvature for x and y surfaces respectively
S_ϕ	Source term in the differental equation for ϕ
S_u^ϕ, S_p^ϕ	Source terms in the difference equation for ϕ

s	Spacing between nozzle exit and mixing tube inlet
t	Time in general; also thickness of a perspex wall in Chapter 6
U,V	Time-mean velocities in the x and y directions
$U_m,\bar{U}$	Area-mean velocity of a duct
u,v	Instantaneous velocities in x and y directions
u',v',w'	Fluctuating velocity components in three orthogonal directions
u_t	Turbulent velocity
$\bar{v}$	Velocity vector
x,y	Streamwise and cross-stream coordinates for a general 2-D orthogonal axisymmetric coordinate system
x_1,x_2	2-D Cartesian coordinates
z	A turbulent quantity, $k^m l^n$ where m,n are constants; also represents the axial direction of cylindrical polar coordinates
β	Angle between the axis of symmetry and direction x
η	Efficiency; also represents refractive index in Chapter 6
θ	Diffuser included angle
λ	Wave length of light
μ, μ_t, μ_{eff}	Laminar, turbulent and effective viscosities of the fluid
ρ	Density
$\sigma_k, \sigma_\varepsilon$	Turbulent Prandtl/Schmidt numbers for k and ε
ε	Turbulent energy dissipation rate
τ	Shear stress
ν	Kinematic viscosity
ϕ	A variable represents U,V,k or ε

κ	von Karman constant in the logarithmic velocity distribution
φ	Beam intersecting angle

Subscripts

0	Mixing tube inlet section
1	Diffuser inlet section
a	Quantity measured in air
c	Centre-line value
d	Diffuser
e	Entrained quantity
i	Refers to inner in general; also refers to incident beam in Chapter 6
in	Inlet condition
j	Primary jet
N,S,E,W	Pertaining to neighbouring nodes which lie respectively north, south, east and west of node P
n	Nozzle exit
n,s,e,w	Pertaining to the four sides of the control volume surrounding node P
o	Outer
P	Pertaining to node P
p	Quantity measured in perspex wall
s	Secondary inlet section; also refers to scattered beam in Chapter 6
t	Mixing tube
w	Quantity measured in water
x	Refers to section at a distance x downstream of mixing tube inlet

INTRODUCTION

Confined jet mixing is a fundamental fluid flow phenomenon of practical engineering importance. It is concerned with the mixing of a high velocity jet with a slow-moving fluid stream in a duct. The design of many devices such as jet pumps and ejectors, gas turbine combustors, gas burners, etc., are all benefited from the understanding of the mechanism of such flow. Despite the wide application of confined jet mixing, the subject received relatively little attention in the past as compared with free jet flow or other boundary layer flows. The present study is mainly aimed at confined jet mixing related to jet pump design and performance analysis.

Jet pumps and ejectors are simple pumping devices directly derived from the principle of confined jet mixing. When a high velocity jet ejects into a mixing chamber, the slow-moving adjacent fluid is dragged along in the jet direction. The mixing between the driving and entrained fluid results in momentum transfer from the high velocity driving jet to the low speed entrained fluid. It is obvious that the increase in velocity in the entrained fluid is achieved at the expense of the energy of the driving jet.

Unlike other pumping devices such as positive displacement, centrifugal or rotary pumps, a jet pump does not require any moving part. Its working principle is based on a purely fluid dynamic phenomenon. No mechanical

energy is being used to increase the energy of the entrained fluid. The advantages of such a primitive device are its simplicity, reliability, absence of moving parts, and cheapness.

Jet pumps are being used in many areas, such as process industries; STOL aircraft augmentation and space-oriented systems; recirculation devices in nuclear reactors; and more common, in deep-well pumping, booster pumping as well as dredging and priming devices. Because of their low cost and easily replaceable nature, jet pumps are especially suitable for pumping hostile fluids such as slurry which might be harmful to other expensive pumps.

A typical jet pump consists essentially of a primary nozzle, a suction chamber, a mixing tube and a diffuser as shown in Fig.0-1. The nozzle and the suction chamber are connected to the driving line and suction line respectively. The two fluids undergo turbulent mixing in a mixing tube and the combined fluids then pass through a diffuser which serves as a pressure head recovery device. The relevant geometries and flow conditions are also indicated in the diagram.

The four fundamental parameters used for jet pump design and performance analysis are usually presented in non-dimensional forms. These are:

(i) the ratio of the entrained flow rate to the primary flow rate, known as the flow ratio M;

$$M = \frac{Q_2}{Q_1}$$

(ii) the ratio of total head gained by the entrained fluid to total head lost by the primary fluid, known as the head ratio N;

$$N = \frac{H_d - H_s}{H_j - H_d}$$

(iii) the area ratio of nozzle to mixing tube, R;

$$R = \left(\frac{d_n}{d_t}\right)^2$$

and (iv) the efficiency η , which is equivalent to the output power divided by the net input power

$$\eta = \frac{Q_2(H_d - H_s)}{Q_1(H_j - H_d)} = MN$$

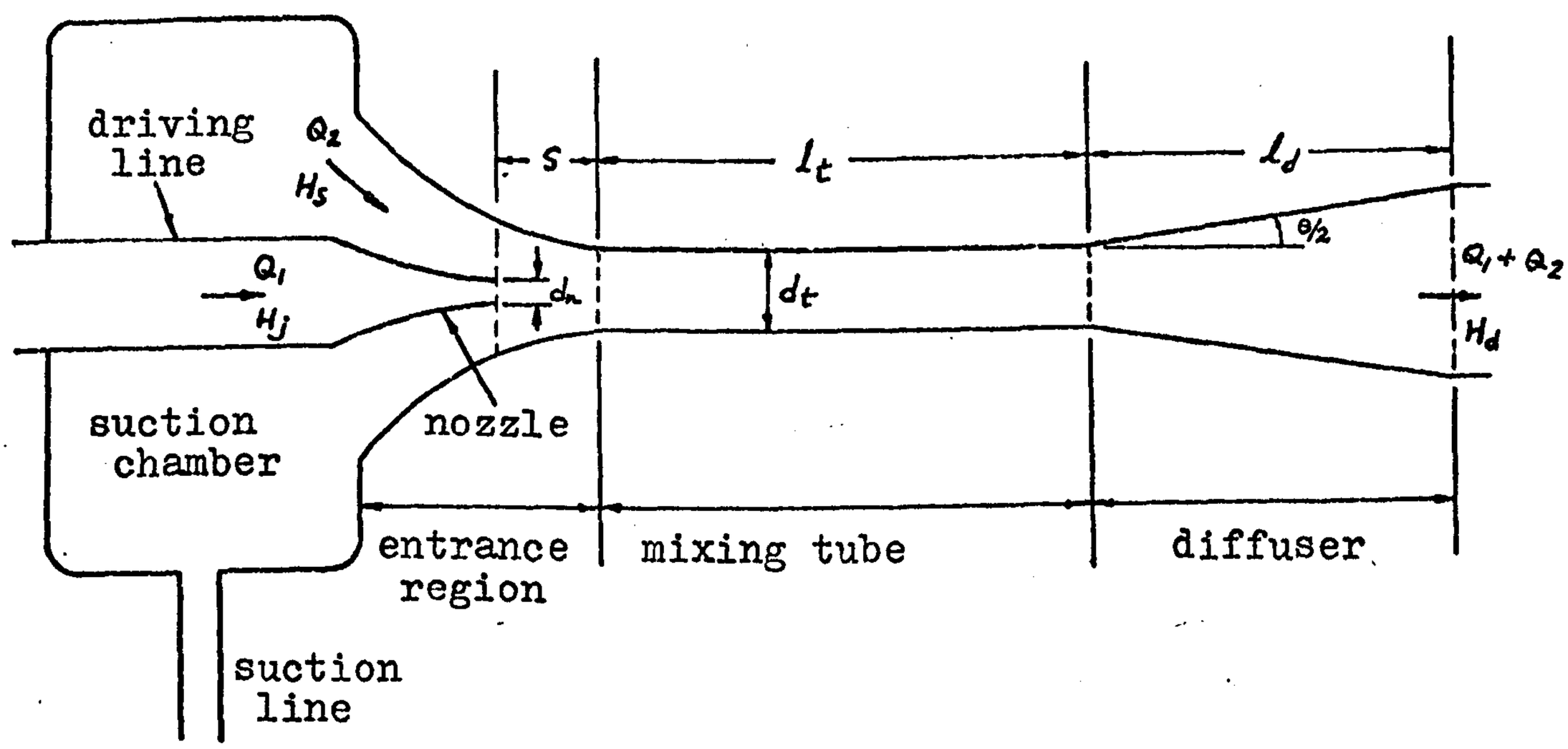

Fig.0-1 Typical Jet Pump Configuration

Other geometrical variables of significant importance on performance and design are mixing tube length l_t, nozzle to mixing tube spacing s and diffuser included

angle θ . Wall profiles of the secondary entrance region may also have some influence over the performance.

Although jet pumps have been the subject of extensive experimental studies, very few investigations have dealt with the basic flow behaviour. The inadequacy of theoretical and experimental studies on confined jet mixing has led to a situation whereby the designs of jet pumps and ejectors in the past have largely relied on empirical data obtained from model pump testing. Performance prediction is unreliable as it varies for each individual design. Owing to the large number of geometrical parameters involved, the previous research has not been able to provide consistent design recommendations. There is also a lack of a satisfactory explaination on the limitation of jet pump performance such as low head rise, low entrainment ratio or low efficiency.

This thesis reports the research work carried out by the author. The thesis can be divided into three parts:

(i) The development of a set of computer models which predict flows in (a) the mixing tube region; (b) the entrance region; and (c) the diffuser region of a typical jet pump device.

(ii) Experimental studies of turbulent confined jet mixing using a laser Doppler anemometer for the measurements of mean and fluctuating velocities.

(iii) The application of the computer prediction technique to the design and performance prediction

of jet pumps.

The present theoretical approach, unlike the previous analytical methods which relied on large amount of empirical input data, is to incorporate the Prandtl-Kolmogorov two equation k- ε turbulence model into the time-mean Navier Stokes equations to form a set of partial differential equations. The equations, which are elliptic in character, are solved numerically by a finite difference procedure using a semi-implicit line by line method together with a tri-diagonal matrix algorithm. The primitive variables, pressure and velocity are solved directly rather than using the vorticity-stream function approach.

The flows in the entrance region, mixing tube and diffuser are solved through using similar but separate computer programs. This enables the use of the most appropriate co-ordinates system for each flow configuration as well as avoids the excessive storage requirement on the computer. The computed time-mean velocity, turbulent shear stress and static pressure distributions in these flow regions are compared with the existing experimental results from various sources.

The laser Doppler anemometry (L.D.A.) technique is employed to measure the time-mean and fluctuating r.m.s. velocities in the mixing tube where turbulent mixing of two co-axial jet streams takes place. The turbulent kinetic energy in the mixing tube is calculated from the three orthogonal r.m.s. velocities. The measured

time-mean velocity and turbulent kinetic energy are then compared with the computer prediction. The accuracy and limitation of using the L.D.A. for the measurement of turbulent water jet mixing are also discussed.

Finally, the computer programs are used to predict pressure and velocity fields for various geometrical combinations, i.e. area ratio, nozzle spacing, mixing tube length and diffuser included angle. The effect of varying any geometrical parameter on jet pump performance is also studied. The final development computer model provides a useful tool for jet pump and ejector design. The designer needs only to specify geometry and required flow ratio in order to obtain information such as pressure rise, thrust augmentation, and efficiency. An optimization procedure is also developed to enable the designer to obtain optimum geometrical combination with best efficiency for a given design requirement.

CHAPTER 1

PREVIOUS RELATED STUDIES

1.1 Historical Development of the Theory of Jet Pumps

The use of water jet pumps has existed for more than a hundred years. The first known application of a water jet pump was made by James Thomson in 1852. Since then, numerous theoretical and experimental studies on jet pump design and performance have been carried out. The theory of pumping through the mixing of two jet streams was first developed by J. M. Rankine (1870) based on the one-dimensional continuity and momentum equations. This concept of analysis is still widely used at the present time, with little or no addition to improve the prediction.

Gosline et al (1934) applied the one-dimensional concept to derive the head ratio and efficiency for water jet pumps with cylindrical mixing chambers. The details of the derivation are described in Appendix A.1. Reasonable prediction of performance was obtained by the authors using the analysis but only by assuming empirical loss coefficients for the driving line, suction line, mixing tube and diffuser. The treatment is a simple method used in general fluid flow analysis which ignores the details of the mechanism by which the two streams mix with one another. No generality can be claimed by such an analysis as its prediction is based on the experimental-determined loss-coefficients on specific jet pumps. However, owing

to its simplicity, the method was employed by many other workers, including Cunningham et al (1954), Mueller (1964), Reddy et al (1968), and Sanger (1968a, 1971) etc. An attempt was made by Mueller to improve the prediction using two frictional loss-coefficients to account for the developing and developed flows in the mixing tube, but the modified version did not improve the prediction (Sanger, 1968a). A method of designing liquid-to-liquid jet pumps using a simple computer program based on the one-dimensional analysis was developed by Sanger (1971).

Cunningham (1975) also derived a modified head ratio expression which took into account the 'jet loss' due to the space between the nozzle and the mixing tube. It was found that the improvement in prediction was only marginal and not applicable to all cases.

Two-dimensional analysis of axisymmetric confined jet mixing using momentum integral methods has been carried out by several researchers. The earlier works of this kind can be found in Curtet (1958), and Dealy (1964). More comprehensive theoretical analysis was done by P. G. Hill (1965, 1967). After assuming a virtual source located at nozzle exit plane, Hill divided the downstream into three distinct flow regions, namely, potential outer flow region, recirculation region and wall-jet interaction region as shown in Fig. 1.1-1. He was able to predict the mean velocity and pressure distributions using empirical data of velocity and turbulent shear stress distribution from a round free jet. However, Hill's method was limited

to confined jet flow with relatively small nozzle diameter as compared with that of mixing tube. The main deficiency was thus its inability to predict the flow behaviour in the potential core region for high nozzle to mixing tube diameter ratios frequently used in jet pumps and ejectors. The analysis is fully described in Appendix A.2.

Fig.1.1-1 Flow Regimes of Hill's (1965) Analysis

The development of momentum integral method was carried a step forward by B. J. Hill (1971, 1973). He extended the analysis to include the potential core region and used empirical data directly derived from jet pump measurement. The major shortcoming of the integral method is the necessity to use a large amount of empirical input data. The accuracy of analysis thus depends on the range of geometrical and flow conditions under which the empirical data was evaluated.

More recent theoretical development of jet pump and confined jet mixing is focused on solving turbulent trans-

port equations using finite difference procedures. Hedges et al (1972, 1974) devised a finite difference model based on the conservation equations and Prandtl's mixing length hypothesis to predict the mean velocity and pressure distributions. Pope (1972) also used the Patankar-Spalding finite difference procedure (1967) incorporating a mixing-length hypothesis to solve for the mean flow behaviour. However, no prediction of turbulent shear stress or other turbulent quantity is reported. It is clear that in order to study the turbulent nature of confined jet mixing and to predict jet pump flow more reliably, a more advanced turbulence model must be employed.

1.2 Numerical Methods for Predicting Turbulent Flows

In the past twenty years, following the development and application of high speed digital computers, tremendous amount of research works have been devoted to the field of numerical methods for predicting turbulent flows. To summarized the various methods being used and published, it would require a relatively long chapter. However, despite the great variety of methods, it is possible to divide them, according to the computational procedures involved, into two main categories, i.e.,(i)integral methods, and (ii) finite-difference methods.

1.2.1 The Integral Methods

The integral methods require empirical data obtained

from experimental measurements, such as the shape of the velocity profile, the shear stress distribution and skin friction coefficient for the solid wall, to incorporate into the integral equations of conservation. The resulting set of ordinary differential equations are then solved by some appropriate numerical integration procedures such as Runge-Kutta method. The applications of these methods to predict turbulent boundary layer flows were reported by Truckenbrodt (1952), Head (1960), Escudier and Spalding (1965) and Escudier and Nicoll (1966). Curtet (1958), Mikhail (1960), Dealy (1964), Hill (1965), Exley and Brighton (1971) and Hill (1973) have applied the integral methods to predict confined jet flows. The detail description of Hill's (1965) approach which is a typical integral method is included in Appendix A.2.

The widespread use of integral methods lies on the fact that much less computer time is required as compared with the finite difference methods. However, the integral methods are lacking in generality and large amount of empirical information is required. In order to predict different flow regions, various empirical forms for velocity profile and shear stress distribution to suit various flow components are therefore needed as input data to obtain reasonable result. In view of these deficiencies, the search for more general methods to predict turbulent flows through solving the governing partial differential equations numerically was the main concern in this field for the past two decades.

1.2.2 The Finite Difference Methods

The solving of partial differential equations of mass, momentums and other variables for turbulent flows could only be achieved if the flow could be treated as obeying the Newton's viscosity law with an appropriate effective viscosity. Such concept of "turbulent" or "eddy" viscosity was first introduced by Boussinesq in 1877. He proposed that the effective turbulent shear stress τ_t could be replaced by the product of the time-mean velocity gradient and the turbulent viscosity μ_t

$$\tau_t = \mu_t \frac{\partial U}{\partial y} \qquad (1.2\text{-}1)$$

where U is the time-mean velocity and y is the cross-stream distance.

The introduction of the turbulent viscosity concept does not solve the problem completely but at least provides a basis for turbulence modelling. The main task left behind is to express the turbulent viscosity in terms of quantities which can be determined, either by solving some algebraic equations or partial differential equations.

Prandtl's mixing length hypothesis Based on the analogy to the kinetic theory of gases, i.e., the viscosity is proportional to the product of the density, the r.m.s. velocity of the molecules and the mean free path, Prandtl (1925) proposed that the turbulent viscosity might be determined by the local product of the density

the turbulent velocity u_t and a length l_m called mixing length,

$$\mu_t = \rho l_m u_t \tag{1.2-2}$$

He then further proposed that the turbulent velocity was equal to the mixing length l_m times the longitudinal time-mean velocity gradient,

$$u_t = l_m \left|\frac{\partial U}{\partial y}\right| \tag{1.2-3}$$

Thus, the complete mixing-length hypothesis will have the following mathematical relationship

$$\mu_t = \rho l_m^2 \left|\frac{\partial U}{\partial y}\right| \tag{1.2-4}$$

Prandtl went on to suggest that l_m was proportional to the distance from the nearest wall. In the case of free turbulent flows, Prandtl made an assumption that l_m was proportional to the width of the turbulent mixing zone and thus only dependent upon the distance along the main flow direction but not the lateral direction.

Prandtl's mixing length hypothesis was incorporated into the partial differential equations of conservation for boundary layer flows and solved numerically by Patankar and Spalding (1967). The predictions of time-mean velocity distribution in free jets and in

turbulent flow on flat-plate were found to agree reasonably well with measurements. The method was also extended to predict the temperature, mass concentration in boundary layer flows by the same authors. Application of the method to predict mean flow behaviour of jet pump was reported by Pope (1972).

The main shortcomings of the mixing length hypothesis are (1) turbulent viscosity is zero at those location where $\frac{\partial U}{\partial y} = 0$ whereas experiments have shown otherwise; (2) no account is taken of the processes of convection and diffusion of turbulence in which the local turbulent velocity is affected by the neighbouring fluids.

<u>One-equation models of turbulence</u> The shortcomings of the mixing length hypothesis was overcome by the proposals of Prandtl (1945) and Kolmogorov (1942) who independently suggested that the turbulent viscosity was proportional to the square root of the turbulent kinetic energy k as

$$\mu_t = \rho k^{\frac{1}{2}} l \qquad (1.2\text{-}5)$$

where $k = \frac{1}{2}(\overline{u'^2} + \overline{v'^2} + \overline{w'^2})$

u', v' and w' are the three orthogonal r.m.s. velocities, l is a length scale and k is to be determined from a transport equation. Prandtl and Kolmogorov derived the k-transport equation separately from the Navier-Stokes equations. The final approximated form of the k-equation can then be solved simultaneously with the momentum and continuity equations. The model was used by Runchal(1969)

to predict the turbulent flow in a sudden enlarged pipe and by Wolfshtein (1968) in predicting the impinge jet flow. Pun and Spalding (1967) also succeeded in applying the similar model to predict turbulent confined jet mixing in cylindrical combustion chamber.

Instead of using the concept of turbulent viscosity, Bradshaw et al (1967) assumed that the turbulent shear stress is proportional to a variable called turbulent energy k',

$$\tau_t = C\rho k'$$

where C is a constant. They derived a transport equation for k' which was then solved together with other conservation equations. Satisfactory predictions were obtained for a number of external wall boundary layer flows. Nee and Kovasznay (1969) also proposed that the kinematic turbulent viscosity should be determined directly by a transport equation. All the above methods are always referred to as one-equation models of turbulence. The major shortcoming of these models is that the length scale l which always appeared in the transport equation is needed to be prescribed algebraically. A precise prescription of l is, however, rarely possible except for boundary-layer flows.

<u>Two-equation models of turbulence</u> The deficiency of the one-equation models has led to the search for more competent models to be able to predict turbulent flows without prescribing the length scale algebraically. Such

models require that another variable related to the length scale should be determined by an additional transport equation and can thus be referred to as two-equation models. Perhaps Komogorov (1942) was the first person to propose the idea of two-equation model. In 1942, he suggested that the turbulent viscosity could be determined by the turbulent kinetic energy k and the characteristic frequency of energy-containing motions f so that

$$\mu_t = \rho \frac{k}{f} \tag{1.2-6}$$

Both k and f should be determined from separate differential transport equations. Comparing equation (1.2-6) with equation (1.2-5), it can easily be seen that Komogorov actually chose $k^{\frac{1}{2}}/l$ as his second dependent variable. From then onwards, many authors have proposed various two-equation models using different dependent variables, among them are Rotta(1951) and Spalding (1967) who used k and l; Harlow and Nakayama (1968) who used k and $k^{3/2}/l$ Rotta (1971), Ng and Spalding (1972) who used k and kl and Spalding (1969) who used k and k/l^2. It is apparent that the difference among various two-equation models is the choice of the second dependent variable to determine the length scale. If the second variable is designated by $z = k^m l^n$ with m and n being constants, a summary of various two-equation model can be listed in Table 1.2-1.

All the two-equation models provide facility for both variables k and l to appear in the Prandtl-Kolmogorov formula for μ_t and they are both determined by solving the appropriate transport equations.

The successful applications of two-equation models, especially the k-ε model, for predicting turbulent flows, both boundary layer type and recirculating type, were reported by many authors. The decay of a plane jet in a moving stream was predicted by Launder et al (1972) and the agreement with experimental data was found to be much better as compared with predictions using mixing-length and one-equation models. Other boundary layer flows predictions include the turbulent pipe flows obtained by Jones and Launder (1973) and wall-jet flow

predicted by Sharma (1972). In recirculating flows, prediction of film cooling was obtained by Matthews and Whitelaw (1971), cylindrical furnace flow was predicted by Elghobashi and Pun (1974) and forced cavity flow was reported by Nielson (1973).

Multi-equation models of turbulence Other turbulence models being proposed include the three-equation model of Hanjalic (1970) who used k, ε and $\overline{u'v'}$ as dependent variables and the five-equation model of Daly and Harlow (1970) in which the normal turbulent stresses $\overline{u'^2}$, $\overline{v'^2}$ and $\overline{w'^2}$ together with $\overline{u'v'}$ and ε are determined by five differential transport equations. However, few successful prediction based on the multi-equation models has been reported. This suggests that a model of such complexity is not yet well established for general application.

The solution procedures employed Almost all the early solution procedures for calculating turbulent flows using finite-difference method were based on the computer code developed by Patankar and Spalding (1967) and Gosman et al (1969). The former solved parabolic equations in boundary layer flows and the later solved elliptic equations in recirculating flows. Both procedures employed the stream function-vorticity approach which solved the stream-function and vorticity together with the turbulent parameters and then transformed back to time-mean velocities and pressure. New solution procedures which solved the primitive variables,velocities and pressure,were developed by Patankar and Spalding (1972) and Caretto et al (1972).

They were widely tested in many flow predictions as reported by Gosman and Pun (1974) and Pun and Spalding (1976).

1.3 Previous Experimental Studies

1.3.1 Experimental Studies on Confined Jet Mixing

The early experimental studies of confined jet mixing were mainly concerned with mean flow behaviour. The centre-line velocity, the static pressure and the velocity profiles were the main interests to many researchers. Measurements of centre-line velocity decay and velocity profiles across various sections in uniform duct were first obtained by Forstall and Shapiro (1950). Static pressure along the duct wall and velocity profiles were measured by Helmbold et al (1954) who used both uniform and non-uniform mixing ducts. Other similar measurements of mean flow behaviour include those made by Mikhail (1960), Becker, Hottel and Williams (1962), Dealy (1964), etc., all using Pitot static tube for their velocity measurements.

Turbulent fluctuating velocities in both longitudinal and radial direction of a confined jet flow were first measured by Curtet and Ricou (1964) using a constant-temperature hot-wire anemometer. The most complete measurement of confined jet mixing to date was probably done by Razinsky and Brighton (1971) who measured the centre-line velocity, the wall static pressure, the velocity profiles, the longitudinal r.m.s. velocity as

well as the Reynolds stress. The mean velocity was measured by a Pitot static tube and the turbulent quantities were measured by a constant-temperature hot-wire anemometer. All these works have contributed a great deal to the understanding of the mixing behaviour in ducts.

1.3.2 Experimental Studies on Jet Pumps and Ejectors

Large amounts of literature on experimental studies of jet pumps and ejectors have been accumulated in the past fifty years. Most of the literature is summarised in a BHRA Review compiled by Bonnington and King (1972). The earlier works on jet pumps are mainly concerned with performance tests and pressure rise measurement along the duct wall. Typical works of such are those of Gosline et al (1934), Keenan et al (1942), Folsom (1948) and Kastner et al (1950).

Many experimental investigations have also been devoted to various geometrical effects on jet pump performance. Gosline et al (1934), Vogel (1956), Mueller (1964) and Hansen et al (1965) carried out experimental tests and recommended a mixing tube length ranging from 3.5 to 8.0 diameters for optimum performance. As for the effect of nozzle to mixing tube spacing, Schulz (1952) established that the optimum spacing lie between 1 and 2 nozzle diameters whereas Hansen et al (1965) recommended a value between 0.8 and 1.4. Schulz (1958) and Mueller (1964) also discovered that a better performance was obtained by

having the secondary flow inlet in the shape of a rounded bell mouth. The diffuser angle is another geometrical variable which many workers have made considerable experimental studies in order to give a recommendation to achieve a good performance. Mueller (1964) recommended a 5° diffuser included angle for best efficiency whereas an 8° included angle was proposed by Vogel (1956). It is clear that although many efforts have been devoted to the investigation of geometrical effects on jet pump performance, no consistent recommendation of optimum geometrical configuration has been made. The facts that a large number of geometrical variables are involved and their interrelated effects on the flow behaviour in mixing tube and diffuser make it extremely difficult to generalize the problem.

Experimental studies of several low-area-ratio water jet pumps were carried out by Sanger (1968a, 1968b, 1970). Static pressure and efficiency were obtained for two area ratios of 0.066 and 0.197. The mixing tube lengths used were 7.25 and 5.66 diameters whereas nozzle spacing ranging from 0 to 2.9 tube diameters. It was observed that the efficiency for the shorter mixing tube pump was about 2% higher for both area ratios which suggested that for these area ratios, mixing tube length between 5 and 6 diameters was sufficient for optimum mixing. However, it was concluded by the author that because of the interdependence among the various geometrical parameters, no optimum geometries can be established for all jet pumps.

Other experimental studies on jet pumps are concerned with applications of jet pump devices under various operating conditions, cavitation studies and using jet pumps to pump a dissimilar fluid.

1.4 Previous Applications of Laser Doppler Anemometry on Related Flow Measurements

The first successful application of laser Doppler anemometry to the measurement of fluid velocity can be attributed to Yeh and Cummins (1964). In their pioneering work, they measured the velocity in a fully developed laminar pipe flow of water. The technique was later applied to turbulent water flows by others including Goldstein and Hagen (1967), Welch and Tomme (1967), etc. The measurement of turbulent air flow was carried out by Lewis, Foreman, Watson and Thornton (1968) and Haffaker, Fuller and Lawrence (1969). The technique has been used, for example, by Durst and Whitelaw (1971) to measure the mean and fluctuating velocities of an axisymmetric air jet; by Melling and Whitelaw (1973) to measure the three orthogonal components of mean and r.m.s. fluctuating velocities of a rectangular water channel flow. Measurements of turbulent shear stresses in pipe flow using two trackers and a correlator were obtained by Bourke et al (1971) and Morton and Clark (1971).

More recently, laser Doppler anemometry has been applied to measure some highly turbulent flows using frequency shifting techniques. Durst, Wigley and Zaire

(1974) carried out measurement of mean and fluctuating velocities downstream of a square flow obstacle with turbulent intensity up to 50%. Baker (1974) reported the measurement of three orthogonal r.m.s. velocities in the fully developed region of a turbulent jet. The mean and fluctuating velocities downstream of an annular jet with substantial recirculation were measured by Durao and Whitelaw (1974). It is obvious that the laser Doppler anemometry, although a rather new technique, will emerge as a very powerful tool in the future fluid flow measurements.

CHAPTER 2

THE MATHEMATICAL MODEL

In this chapter, the partial differential equations governing the basic laws of conservation of mass and momentum for a incompressible viscous fluid are first described. The equations, when apply to a turbulent flow, require the additional terms to account for the fluctuating components of the variables. A two-equation k-ε turbulence model which provides informations for the extra terms is incorporated into the time-mean differential equations to form a complete mathematical model for the two-dimensional axisymmetric turbulent flows. Appropriate boundary conditions which simulate the practical jet pump situation in order to obtain realistic prediction are discussed.

2.1 The Equations of Motion for an Incompressible Viscous Fluid

The derivation of the equations of motion based on the basic laws of conservation are readily available in many standard text books on fluid mechanics such as Schlichting (1960) and Hinze (1975). The equations, according to Hinze (1975), when expressed in a tensor notation using Cartesian coordinates takes the following forms:

Continuity:

$$\frac{\partial \rho}{\partial t} + \frac{\partial}{\partial x_j} \rho u_j = 0 \qquad (2.1\text{-}1)$$

$$j = 1, 2, 3$$

Momentum equation in x_i-direction:

$$\rho \frac{Du_i}{Dt} = \frac{\partial}{\partial x_j} \sigma_{ji} + F_i \qquad (2.1\text{-}2)$$
$$j = 1, 2, 3$$

where σ_{ji} is the stress in the x_i-direction operates in a plane which is perpendicular to the direction x_j. F_i is an external force per unit volume acting on the fluid in x_i-direction.

For an incompressible fluid,

$$\frac{\partial}{\partial x_j}\sigma_{ji} = -\frac{\partial p}{\partial x_i} + \frac{\partial}{\partial x_j}\left[\mu\left(\frac{\partial u_i}{\partial x_j} + \frac{\partial u_j}{\partial x_i}\right)\right]$$

equation (2.1-2) can be written as

$$\rho \frac{Du_i}{Dt} = -\frac{\partial p}{\partial x_i} + \frac{\partial}{\partial x_j}\left[\mu\left(\frac{\partial u_i}{\partial x_j} + \frac{\partial u_j}{\partial x_i}\right)\right] + F_i \qquad (2.1\text{-}3)$$
$$j = 1, 2, 3$$

where p is the static pressure and μ is the dynamic viscosity of the fluid. Equations (2.1-1) and (2.1-3) are usually referred to as the Navier-Stokes equations which form the basis of the whole theory of viscous fluid mechanics.

2.2 The Need for Turbulence Modelling

The equations of motion described in section 2.1 are generally applicable to laminar flows but not turbulent flows. In brief, a turbulent flow is defined as an irregular fluid motion in which the various quantities show a random variation with time and space coordinates. Turbulent flows can occur when fluids flow through

conduits (turbulent pipe flow), pass over solid bodies (wake), or when neighbouring stream of the fluids with different velocities pass over one another (jet mixing). At present, one is unable to obtain solution for the time-dependent turbulent flow field using existing computers. Fortunately, it is possible to describe turbulent flow with distinct average values of various quantities such as velocity, pressure and temperature, etc. If a turbulent flow field is quasi-steady, averaging with respect to time can be used. But for a homogeneous turbulent flow field, averaging with respect to space is preferred. In most of the engineering problems, time-averaged values are more useful for engineers and designers.

The instantaneous values of velocity and pressure can be written as

$$u_i = U_i + u_i' \qquad (2.2\text{-}1)$$

and

$$p = P + p' \qquad (2.2\text{-}2)$$

where U_i and P are the time-mean values and u_i', p' are the fluctuating values.

The equations of motion for the average values in turbulent flow were first derived by Osborne Reynolds. He substituted the instantaneous values of u_i and p into the equation (2.1-3) to give the following form.

$$\rho \frac{DU_i}{Dt} = -\frac{\partial P}{\partial x_i} + \frac{\partial}{\partial x_j}\left[\mu\left(\frac{\partial U_i}{\partial x_j} + \frac{\partial U_j}{\partial x_i}\right) - \rho\overline{u_i' u_j'}\right] + F_i \qquad (2.2\text{-}3)$$

$$j = 1, 2, 3$$

Compare this equation with the original momentum equation (2.1-3), it can be seen that the extra-terms $-\rho\overline{u_i'u_j'}$ are required to add to the viscous stresses in order that the instantaneous variables can be substituted by their time-mean values. Because Reynolds was the first person to derive the equation for turbulent flow in this form, the turbulent terms $-\rho\overline{u_i'u_j'}$ are often called Reynolds stresses.

To solve equation (2.2-3), the terms $-\rho\overline{u_i'u_j'}$ must be known. Since there is no direct way of knowing the magnitude of these terms, a mathematical model to relate effect with known quantities is therefore required. Thus, a model of turbulence, in the words of Launder and Spalding (1972) will 'propose a set of equations which, when solved with the mean-flow equations, allows calculation of the relevant correlations and so simulates the behaviour of real fluid in important respects'.

2.3 The Differential Equations of Conservation Applied to Two-Dimensional Axisymmetrical Flows

2.3.1 The Coordinate System

Before making any attempt to express any equation for a particular flow configuration, an appropriate coordinates system must be chosen. In this thesis, owing to the fact that fluid flows take place at various flow components, the most general two-dimensional orthogonal axisymmetrical

coordinate system is used. Fig. 2.3-1 illustrates such a coordinate system in which the coordinates x and y characterise the members of two orthogonal families of surfaces of revolution. r_x and r_y are the radii of curvature for x and y surfaces intercepting at point P and r is the distance from P to the axis of symmetry.

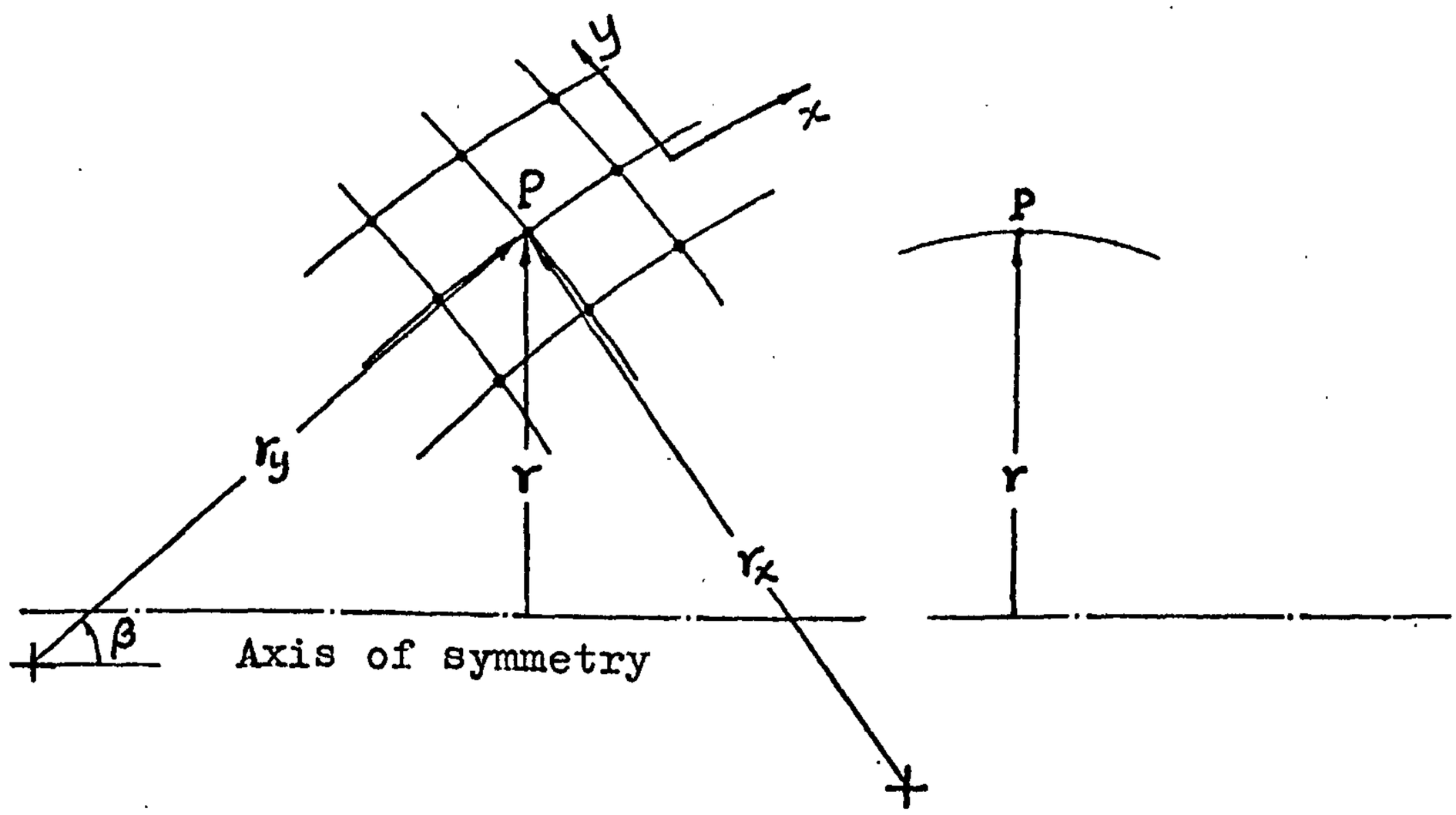

Fig.2.3-1 The Orthogonal Axisymmetric Coordinate System.

The merit of using such a general arbitrary orthogonal coordinate system is that the coordinates can be so chosen that all the flow boundaries are parallel to the grid surfaces. In the present investigation, a typical jet pump flow field consists of (i) an annular entrance region,(ii) a cylindrical mixing tube and (iii) a diffuser. By using the coordinate system outlined above, a grid pattern can be devised to accommodate all the three

flow regions as shown in Fig.2.3-2.

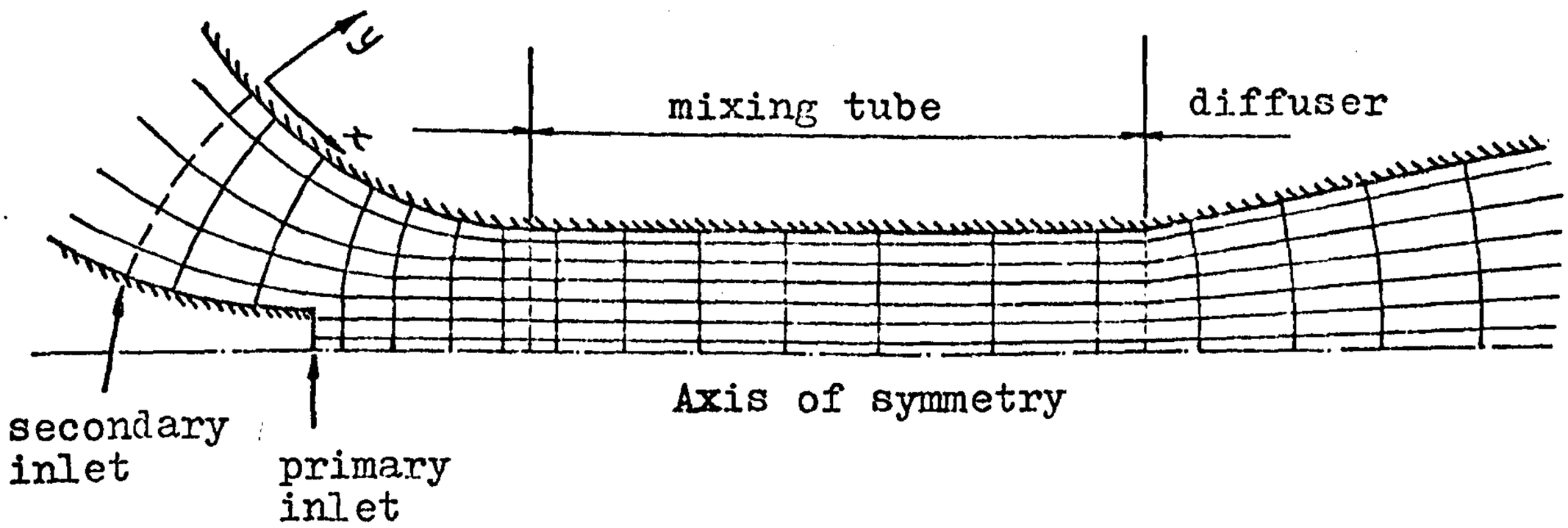

Fig.2.3-2 The coordinate system applied to jet pump configuration

In general, r_x, r_y and r are function of x and y. In the uniform mixing tube region,

$$r_x = \infty$$
$$r_y = \infty \qquad (2.3\text{-}1)$$
$$r = y$$

In the diffuser region,

$$r_x = \infty$$
$$r_y = x + x_o \qquad (2.3\text{-}2)$$
$$r = (x + x_o)\sin\beta$$

where x_o and β are given in Figure 2.3-3 and their values depend on the diffuser included angle and the inlet diameter.

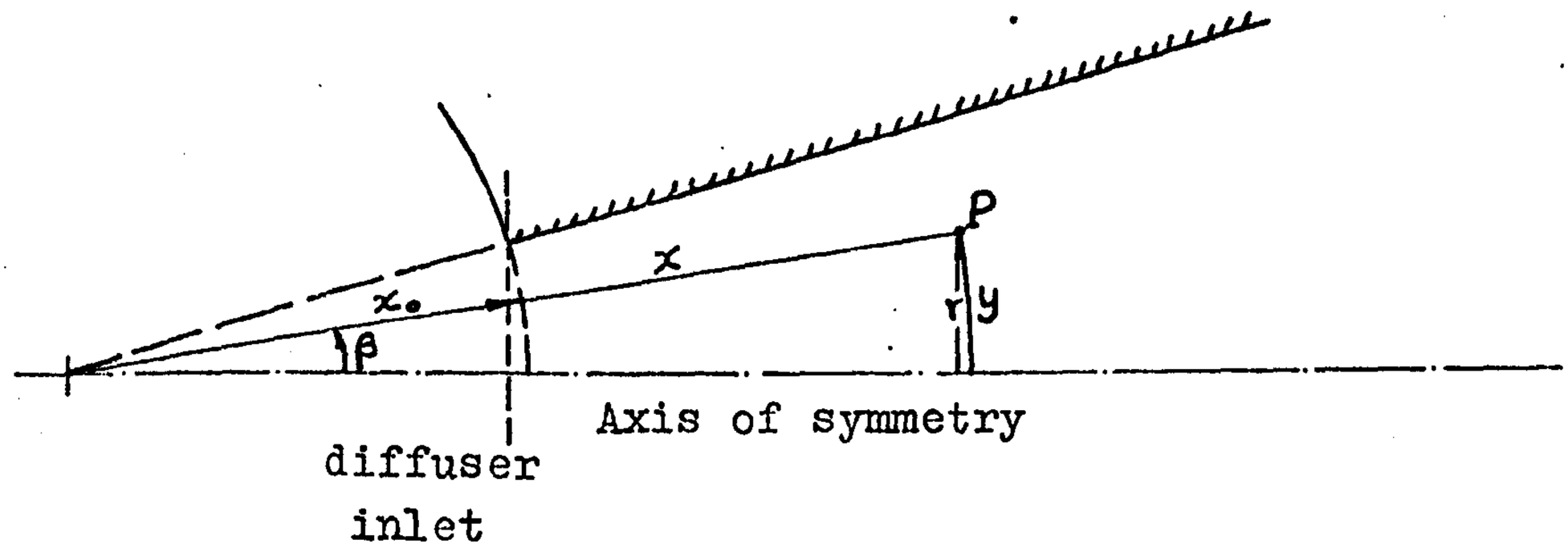

Fig.2.3-3 Diffuser geometry

In the annular entrance region, explicit expressions for r_x, r_y and r are much more cumbersome. However, all the variables x, y, r_x, r_y and r can conveniently be calculated in terms of Cartesian coordinates. Details of the calculation will be illustrated in section 4.3.2.

2.3.2 The Differential Equations of Conservation

The equations for conservation of mass and momentum, when expressed in the general orthogonal x, y coordinate system described above for a steady flow, will take the following forms.

The continuity equation,

$$\frac{\partial}{\partial x}(\rho r U) + \frac{\partial}{\partial y}(\rho r V) = 0 \qquad (2.3\text{-}3)$$

The momentum equation in x-direction,

$$\frac{1}{r}\left[\frac{\partial}{\partial x}(\rho U r U) + \frac{\partial}{\partial y}(\rho V r U) - \frac{\partial}{\partial x}\left(r\mu_{eff}\frac{\partial U}{\partial x}\right) - \frac{\partial}{\partial y}\left(r\mu_{eff}\frac{\partial U}{\partial y}\right)\right]$$
$$= -\frac{\partial P}{\partial x} + S^u$$

where

$$S^u = \frac{1}{r}\left[\frac{\partial}{\partial x}(r\mu_{eff}\frac{\partial U}{\partial x}) + \frac{\partial}{\partial y}(r\mu_{eff}\frac{\partial V}{\partial x})\right] + \frac{\rho V^2}{r_y} - \frac{2\mu_{eff}(U\sin\beta + V\cos\beta)}{r^2}\sin\beta \qquad (2.3\text{-}4)$$

The momentum equation in y-direction,

$$\frac{1}{r}\left[\frac{\partial}{\partial x}(\rho UrV) + \frac{\partial}{\partial y}(\rho VrV) - \frac{\partial}{\partial x}(r\mu_{eff}\frac{\partial V}{\partial x}) - \frac{\partial}{\partial y}(r\mu_{eff}\frac{\partial V}{\partial y})\right] = -\frac{\partial P}{\partial y} + S^v$$

$$S^v = \frac{1}{r}\left[\frac{\partial}{\partial x}(r\,\mu_{eff}\frac{\partial U}{\partial y}) + \frac{\partial}{\partial y}(r\mu_{eff}\frac{\partial V}{\partial y})\right] + \frac{\rho U^2}{r_x} - \frac{2\mu_{eff}(U\sin\beta + V\cos\beta)}{r^2}\cos\beta \qquad (2.3\text{-}5)$$

where U, V, P are time-mean velocities and static pressure. The full derivation of the momentum equations is given in Appendix A.3.

The momentum equations are obtained by assuming that the fluid is treated as obeying Newton's viscosity law. For a turbulent flow, μ_{eff} accounts for both viscous stress and Reynolds stress. By comparing equation (2.3-4) with equation (2.2-3), one can write

$$\mu_{eff}(\frac{\partial U_i}{\partial x_j} + \frac{\partial U_j}{\partial x_i}) = \mu(\frac{\partial U_i}{\partial x_j} + \frac{\partial U_j}{\partial x_i}) - \rho\overline{u_i'u_j'} \qquad (2.3\text{-}6)$$

An appropriate model of turbulence is thus required to relate the turbulent stresses $-\rho\overline{u_i'u_j'}$ to some known quantities throughout the flow field.

2.4 The Choice and Application of Two-Equation k-ε Model

It was first proposed by Boussinesq in 1877 that the turbulent shear stress could be replaced by the product of the time-mean velocity gradient and the turbulent viscosity μ_t, i.e.,

$$-\rho\overline{u_i'u_j'} = \mu_t\left(\frac{\partial U_i}{\partial x_j} + \frac{\partial U_j}{\partial x_i}\right) \tag{2.4-1}$$

Substituting Equation (2.4-1) into (2.3-6), one gets

$$\mu_{eff} = \mu + \mu_t \tag{2.4-2}$$

Thus, the effective viscosity in a turbulent flow is equal to the sum of the molecular viscosity and the turbulent viscosity. Unlike the molecular viscosity which is the real property of the fluid, the turbulent viscosity can become effective only when there is flow and its value varies from point to point in the flow depending upon the turbulent structure at that particular location.

Many turbulence models have been proposed to relate μ_t to some quantities which can be determined. The outline of various models and their merits and shortcomings have been described in section 1.2.2. In the present studies of confined jet mixing and jet pump flows, owing to the interaction between the mixing shear region and the wall shear region, the length scale profile is unable to be prescribed throughout the flow field. The mixing length and one-equation models will not be able to predict these

flows satisfactorily. However, in view of the fact that the multi-equation models are far less established and more computing time is required, the choice of a two-equation model is a compromise of accuracy and economics unless a more complicated multi-equations model is proved to be necessary.

The Prandtl-Komogorov two-equation model states that the turbulent viscosity μ_t can be written as

$$\mu_t = C_\mu \rho k^{\frac{1}{2}} l \qquad (2.4\text{-}3)$$

where $k = \frac{1}{2}(\overline{u'^2} + \overline{v'^2} + \overline{w'^2})$, l is the length scale and C_μ is a constant. k and l are to be determined by their transport equations. However, it turns out that the length scale itself is not the most appropriate dependent variable. Various workers have selected different combinations of m and n of a quantity $k^m l^n$ as their second dependent variable instead of using l itself. (See Table 1.2-1). A quantity, called turbulence energy dissipation rate ε, first proposed by Harlow and Nakayama (1968) and subsequently favoured by many other workers is chosen as the second dependent variables in the present work where

$$\varepsilon = \frac{k^{3/2}}{l} \qquad (2.4\text{-}4)$$

The reasons for this choice are : (i) it is relatively easy to derive the exact equation for ε ; (ii) ε appears

directly as an unknown in the transport equation for k; (iii) the effective turbulent Prandtl Number σ_ε appeared in the ε-equation as a constant irrespective of the distance from the wall whereas for other combinations, such as kl and k/l^2, this is not so, as proved by Launder and Spalding (1973).

Furthermore, the k-ε model are well established and has been incorporated into standard computer code by Gosman and Pun (1974) for solving turbulent recirculating flows. The model was widely tested and enjoyed satisfactory predictions for a wide range of flows. Examples of such applications of k-ε model can be found in the works of Hanjalic (1970), Elghoboshi and Pun (1974), Matthews and Whitelaw (1971) and Nielson (1973).

The k- and ε- equations, when using a general orthogonal axisymmetric coordinate system described in section 2.3.1, may be expressed in the following form at high Reynolds numbers.

k-equation:

$$\frac{1}{r}\left[\frac{\partial}{\partial x}(\rho U r k) + \frac{\partial}{\partial y}(\rho V r k) - \frac{\partial}{\partial x}\left(\frac{r\mu_{eff}}{\sigma_k}\frac{\partial k}{\partial x}\right) - \frac{\partial}{\partial y}\left(\frac{r\mu_{eff}}{\sigma_k}\frac{\partial k}{\partial y}\right)\right]$$

$$= G - C_D \rho \varepsilon \qquad (2.4\text{-}5)$$

ε-equation:

$$\frac{1}{r}\left[\frac{\partial}{\partial x}(\rho U r \varepsilon) + \frac{\partial}{\partial y}(\rho V r \varepsilon) - \frac{\partial}{\partial x}\left(\frac{r\mu_{eff}}{\sigma_\varepsilon}\frac{\partial \varepsilon}{\partial x}\right) - \frac{\partial}{\partial y}\left(\frac{r\mu_{eff}}{\sigma_\varepsilon}\frac{\partial \varepsilon}{\partial y}\right)\right]$$

$$= C_1 \varepsilon G/k - C_2 \rho \varepsilon^2/k \qquad (2.4\text{-}6)$$

where
$$G = \mu_t \left\{ 2 \left[\left(\frac{\partial U}{\partial x}\right)^2 + \left(\frac{\partial V}{\partial y}\right)^2 + \frac{V}{r_x}\left(\frac{\partial U}{\partial x}\right) + \frac{U}{r_y}\left(\frac{\partial V}{\partial y}\right) \right] + \left(\frac{\partial U}{\partial y} + \frac{\partial V}{\partial x}\right)^2 \right\} \qquad (2.4\text{-}7)$$

These equations are modified from the cylindrical polar forms used by Gosman and Pun (1974). They differ in the expression of the turbulent energy production term G. The derivation of G, equation (2.4-7) is given in Appendix A.4.

By combining equations (2.4-3) and (2.4-4), μ_t is related to k and ε as

$$\mu_t = C_\mu \rho k^2/\varepsilon \qquad (2.4\text{-}8)$$

It is now possible to obtain the five unknown variables, namely, U, V, P, k, ε by solving five simultaneous equations (2.3-3), (2.3-4), (2.3-5), (2.4-5) and (2.4-6) with the help of the auxilliary equations (2.4-2) and (2.4-8).

The values of the constants C_μ, C_D, C_1, C_2, σ_k and σ_ε must be prescribed to complete the specification of the model. At high Reynolds, these constants are given the values listed in Table 2.4-1 as recommended by Launder and Spalding (1973) and Gosman and Pun (1974). This set of values has been widely used in various flow problems and is generally accepted for flows of plane jets, mixing layers and the plane and axisymmetric wall flows.

C_μ	C_D	C_1	C_2	σ_k	σ_ε
0.09	1.00	1.44	1.92	1.00	1.21

Table 2.4-1 The values of the constants used in the k-ε model

In the present study of jet pump flows, these values are chosen for the whole flow field without any modification.

2.5 Modification of the Model for 'Near Wall' Flow

The model described in section 2.3 and 2.4 is only valid for fully turbulent flow. When close to a solid wall, there are regions where viscous effect are significant compared with turbulent effect. In these regions, some modifications on the transport equations are therefore necessary.

2.5.1 The 'Law of the Wall'

In the vicinity of a solid wall, the flow is determined by (i) wall shear stress, and (ii) roughness. The mean velocity component U in this region, according to the classical theory of turbulent boundary layer along a flat plate (Hinze, 1975), is a function of (i) wall shear stress τ_w; (ii) roughness parameter k_f; (iii) normal distance from the wall y and (iv) kinematic viscosity ν .

i.e.

$$U = f\left(\sqrt{\frac{\tau_w}{\rho}}\ ,\ k_f\ ,\ \nu\ ,\ y\right) \qquad (2.5\text{-}1)$$

where $\sqrt{\frac{\tau_w}{\rho}}$ has the dimension of velocity and is usually referred to as wall-friction velocity or wall shear stress velocity U*, i.e.,

$$\sqrt{\frac{\tau_w}{\rho}} = U^* \tag{2.5-2}$$

From the dimensional analysis,

$$\frac{U}{U^*} = f\left(\frac{U^* y}{\nu}, \frac{U^* k_f}{\nu}\right) \tag{2.5-3}$$

For a smooth wall where $k_f = 0$

$$\frac{U}{U^*} = f\left(\frac{U^* y}{\nu}\right) \tag{2.5-4}$$

In the viscous sublayer,

$$\mu \frac{\partial U}{\partial y} = \tau_w$$

and

$$U = \frac{\tau_w}{\mu} y$$

From equation (2.5-2), it follows that

$$\frac{U}{U^*} = \frac{U^* y}{\nu} \tag{2.5-5}$$

If it is assumed that, for the wall region, the shear stress remain constant and equal to the wall shear stress, the following relationship can be written for the turbulent part of the wall region,

$$\mu_t \frac{\partial U}{\partial y} = \tau_w \tag{2.5-6}$$

In the neighbourhood of the wall, it may be assumed that turbulent viscosity is proportional to the distance from the wall. From dimensional analysis,

$$\mu_t = \kappa \rho U^* y \tag{2.5-7}$$

where κ is a dimensionless constant called von Kàrmàn constant and having a numerical value of 0.4187. Substituting equation (2.5-7) to equation (2.5-6) gives

$$\kappa U^* y \frac{\partial U}{\partial y} = U^{*2}$$

Using the dimensionless expression $U^+ = \frac{U}{U^*}$ and $y^+ = \frac{U^* y}{\nu}$, one gets

$$\kappa y^+ \frac{\partial U^+}{\partial y^+} = 1 \tag{2.5-8}$$

The solution obtained by integration is

$$U^+ = \frac{1}{\kappa} \ln y^+ + \text{const.} \tag{2.5-9}$$

For a rough wall with roughness parameter k_f, a similar solution can be obtained

$$U^+ = \frac{1}{\kappa} \ln \frac{y^+}{k_f} + \text{const.} \tag{2.5-10}$$

Equation (2.5-9) and (2.5-10) can be combined into a general form

$$U^+ = \frac{1}{\kappa} \ln E y^+ \tag{2.5-11}$$

where E is a function of the wall roughness. According to Launder and Spalding (1973), E approximately equal to 9.0 for a smooth wall.

Equation (2.5-11) is the well-known expression of the logarithmic 'law of the wall' applied to the turbulent part of the wall region and only determined by the wall roughness and the distance from the wall. Even in the outer region of the boundary layer, the logarithmic velocity distribution only deviates slightly from the actual experimental results. Thus, from a practical engineering viewpoint, the logarithmic velocity distribution can provide acceptable mean-velocity profile for turbulent flows in a pipe or boundary layer.

In the near-wall region where generation and dissipation of energy are in balance, it can be shown that

$$\frac{\tau_w}{\rho} = (C_\mu C_D)^{\frac{1}{2}} k \qquad (2.5\text{-}12)$$

Combining equations (2.5-12) and(2.5-11) gives

$$\frac{U}{\left(\frac{\tau_w}{\rho}\right)} (C_\mu C_D)^{\frac{1}{4}} k^{\frac{1}{2}} = \frac{1}{\kappa} \ln E y^+ \qquad (2.5\text{-}13)$$

where

$$y^+ = \frac{\rho (C_\mu C_D)^{\frac{1}{4}} k^{\frac{1}{2}}}{\mu} y$$

This is the final expression where the turbulent wall shear stress can be evaluated from the values of k, y and U adjacent to the wall. If the value of y^+ is less than

11.63, the laminar shear stress expression is used

$$\tau_w = \mu \frac{U}{y} \qquad (2.5\text{-}14)$$

The wall shear stress is then incorporated into the source term S^u of the U-momentum equation (2.3-4) for flow next to the duct wall.

2.5.2 Modification of k and ε in the 'Near Wall' Region

In the near wall region the shear stress components can no longer be calculated from the fully developed turbulent flow. Thus the turbulent energy production term G appeared in k- and ε- equations has to be modified. Using the original G term from Appendix A.4,

$$G = \tau_{ij} \frac{\partial U_i}{\partial x_j} \qquad (2.5\text{-}15)$$

The normal stress components τ_{xx} and τ_{yy} remain unchanged ,

$$\tau_{xx} = 2\mu_t \left(\frac{\partial U}{\partial x} + \frac{V}{r_x}\right) \qquad (2.5\text{-}16)$$

$$\tau_{yy} = 2\mu_t \left(\frac{\partial V}{\partial y} + \frac{U}{r_y}\right) \qquad (2.5\text{-}17)$$

The shear stress components τ_{yx} and τ_{xy} should be calculated from equation (2.5-13) or (2.5-14). The modified G near the wall then takes the following form:

$$G = 2\mu_t\left[\left(\frac{\partial U}{\partial x}\right)^2 + \left(\frac{\partial V}{\partial y}\right)^2 + \frac{V}{r_x}\left(\frac{\partial U}{\partial x}\right) + \frac{U}{r_y}\left(\frac{\partial V}{\partial y}\right)\right]$$
$$+ \tau_w\left(\frac{\partial U}{\partial y} + \frac{\partial V}{\partial x}\right) \qquad (2.5\text{-}18)$$

To determine the near wall value of ε , equation (2.5-7) is substituted into equation (2.4-8),

$$\varepsilon = \frac{C_\mu k^2}{\kappa U^* y}$$

From equation (2.5-12)

$$U^* = \sqrt{\frac{\tau_w}{\rho}} = (C_\mu C_D)^{\frac{1}{4}}\, k^{\frac{1}{2}} ,$$

the near-wall ε - value can now be expressed as follows :

$$\varepsilon = \frac{(C_\mu C_D)^{\frac{3}{4}}\, k^{3/2}}{C_D \kappa y} \qquad (2.5\text{-}19)$$

It should be noted that equation (2.5-19) does not give the value of ε at the wall but the value of ε at the point P next to the wall as shown in Fig.2.5-1.

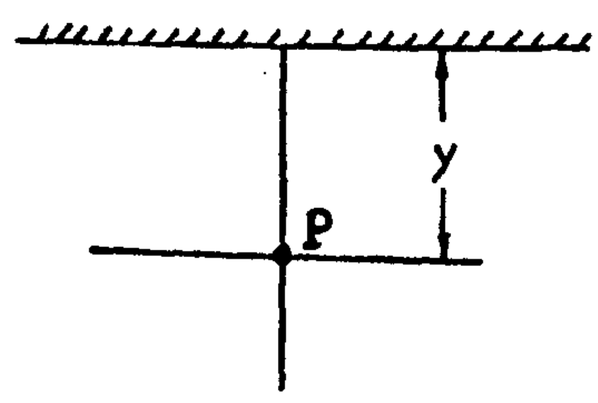

Fig.2.5-1 The 'near wall' node

2.6 The Boundary Conditions

There are basically four different types of boundary conditions needed to be specified so as to complete the flow description. They are: (1) the wall boundary, (2) the axis of symmetry, (3) the inlet flow condition, and (4) the outlet flow condition.

At a solid wall, both velocities along the wall U and normal to the wall V are set to zero for no-slip and non-permeable conditions. The shear stress at the wall is calculated from equation (2.5-13) or (2.5-14) so that it can be included in the source term S^u for those grid nodes adjacent to the wall.

For k and ε , the near-wall values are calculated with a modified G-terms and the modified ε values, i.e., equations (2.5-18) and (2.5-19) respectively.

On the axis of symmetry, radial velocity V is zero and the gradients $\frac{\partial U}{\partial y}$, $\frac{\partial k}{\partial y}$ and $\frac{\partial \varepsilon}{\partial y}$ are all zero too.

Appropriate profiles for U, V, k and ε are necessary to specify in the inlet section. The outlet U-velocity is specified by considering the overall mass conservation, V can be set to zero and k and ε are assumed to be fully developed. The assumption for outlet flow specification is acceptable when the outlet section is fixed beyond the region of interest.

CHAPTER 3

THE NUMERICAL METHODS

3.1 The Finite Difference Equations

The steady two-dimensional axisymmetrical turbulent flow without swirl which occurs in jet pumps can be described by the five partial differential equations given in Chapter 2. It is possible to solve these equations by some appropriate finite-difference techniques. There are basically two distinct methods of solution. In the first method, the continuity and the momentum equations are transformed into two partial differential equations of stream function ψ and vorticity ω to eliminate the pressure. Together with k and ε , the four partial differential equations are solved numerically throughout the flow field first and the pressure field is then deduced separately. The second method is based on a novel procedure known as SIMPLE (Semi-Implicit Method for Pressure Linked Equations) developed by Patankar and Spalding (1972), Caretto et al (1972), etc., which solve for the primitive variables U, V and P together with k and ε .

The advantage of the velocity-pressure approach over the stream function-vorticity approach is that flows with pressure-dependent density can be handled which provides wider scope of applications to compressible flows. In an attempt to compare the two procedures, Ha Minh et al (1978) applied both methods to predict flow in a sudden

enlarged pipe and observed that the velocity-pressure approach gave better predictions of pressure and turbulent properties (k and $\overline{u'v'}$) as compared with measuring data. It is the velocity-pressure approach which is being employed in the present work and is to be discussed in the following sections.

3.1.1 The Staggered Grid and Control Volume

Before deriving the finite difference equations from the governing partial differential equations , a gird arrangement and the control volumes for the variables have to be specified. Fig.3.1-1 illustrates part of the grid arrangement for a general 2-D orthogonal coordinate system. The intersections of the solid lines

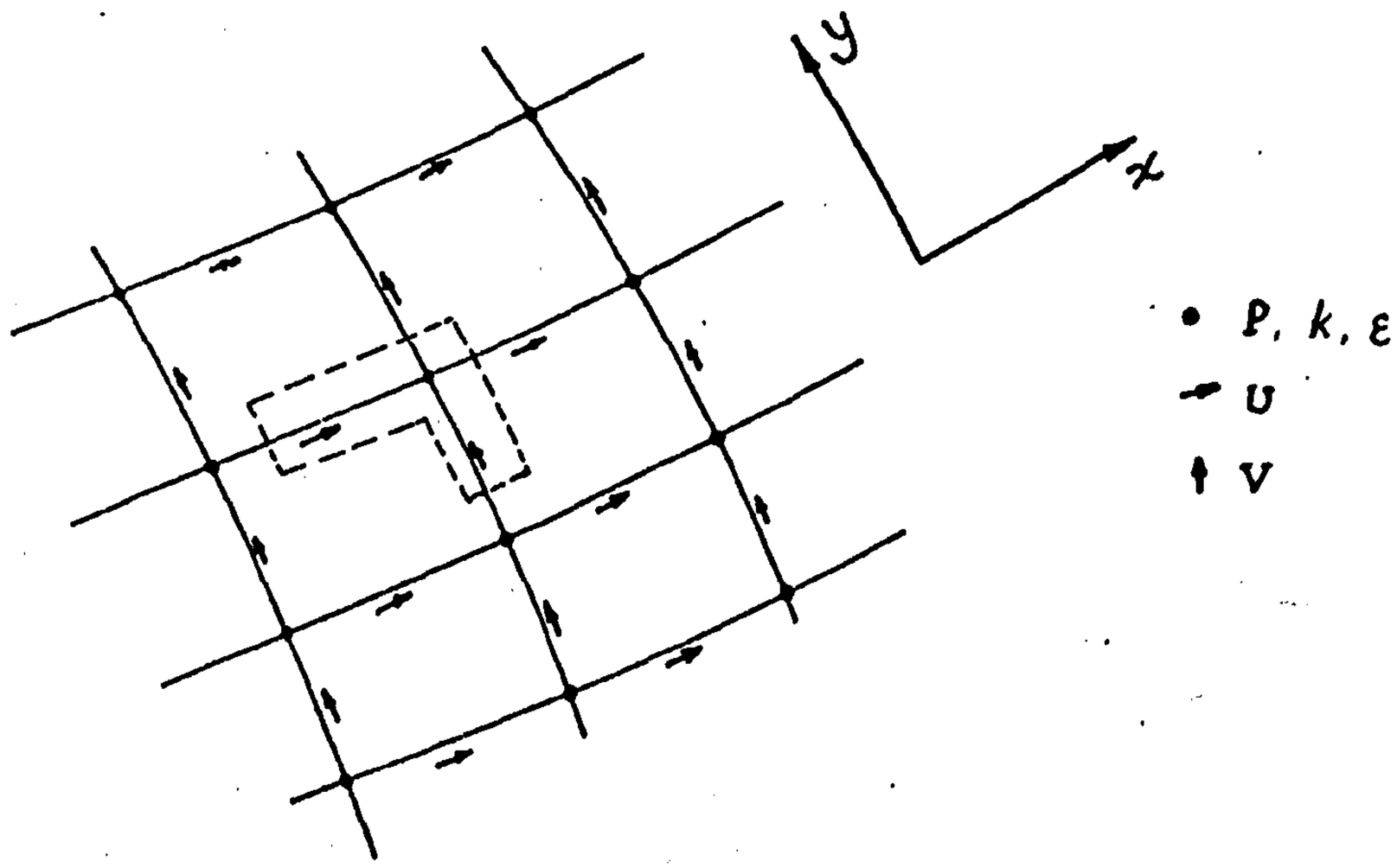

Fig.3.1-1 A typical grid arrangement

mark the grid nodes where all the scalar variables (i.e., p, k, ε) are calculated and stored. The U and V velocity

components are computed and stored at the midway between a node and its upstream neighbour as shown by the arrows → and ↑ respectively. The control volume boundaries are placed midway between the locations where the values of the variable are stored. Thus, for any point P, there are three different control volumes as shown in Fig.3.1-2. Such a grid arrangement is often referred to as staggered grid.

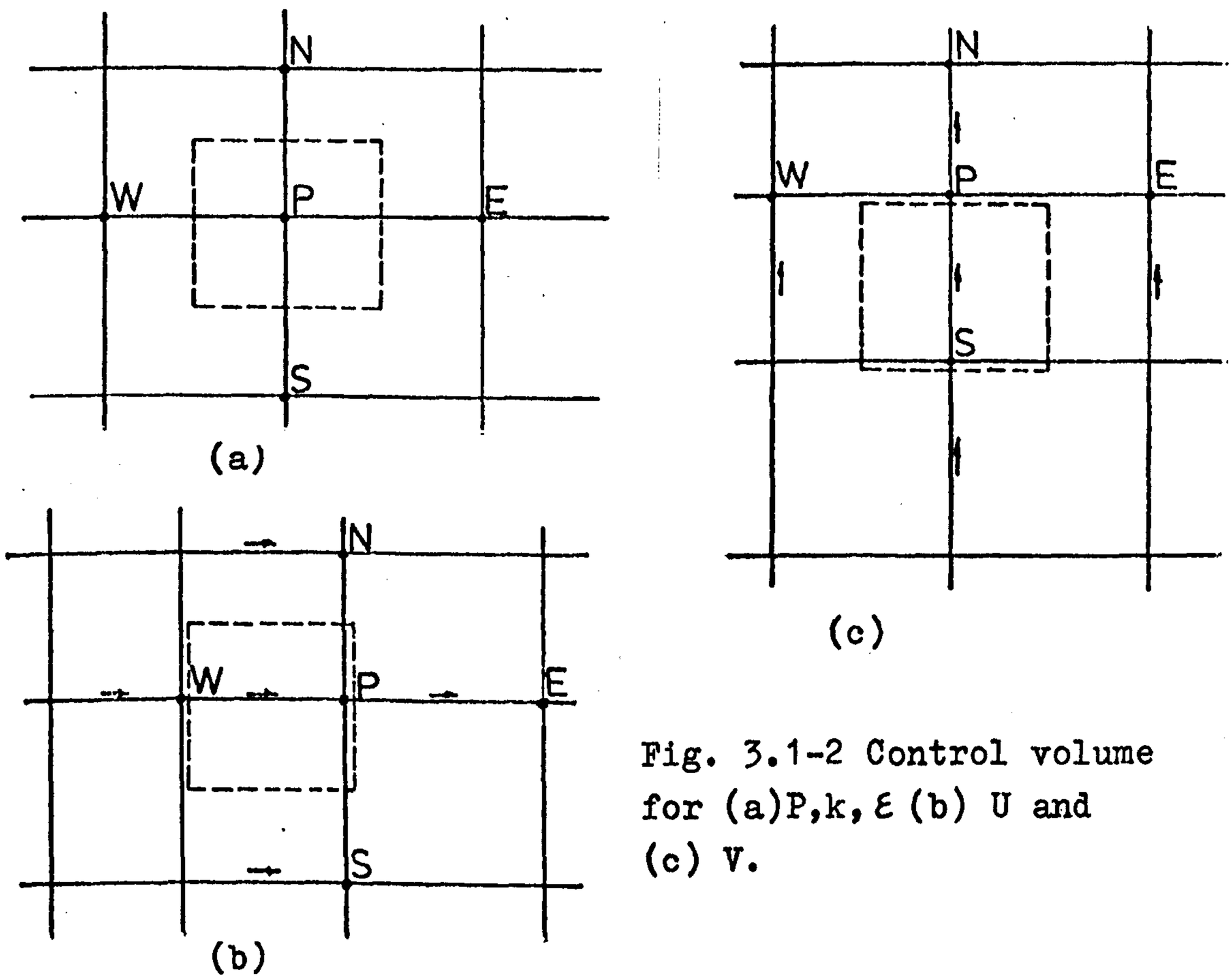

Fig. 3.1-2 Control volume for (a)P,k,ε (b) U and (c) V.

The advantages of the staggered grid are: (i) From a computational viewpoint, since the U and V velocities are placed between the pressures which featured in the momentum balance, the pressure gradients can be evaluated

directly without interpolation; (ii) based on the same argument, these velocities lie on the boundaries of the control volumes of P, ε and k and can therefore be used directly for the calculation of convective fluxes across these boundaries; (iii) the flow boundaries which are located midway between the grid lines can easily be simulated by specifying the U and V values.

3.1.2 The General Expression of the Finite Difference Equation

The partial differential equations for U, V, k and ε are in fact similar and can be expressed in a general form for a 2-D orthogonal axisymmetrical coordinates described in Chapter 2, i.e.,

$$\frac{1}{r}\left[\frac{\partial}{\partial x}(\rho U r\phi) + \frac{\partial}{\partial y}(\rho V r\phi) - \frac{\partial}{\partial x}\left(\frac{r\mu_{eff}}{\sigma_\phi}\frac{\partial\phi}{\partial x}\right) - \frac{\partial}{\partial y}\left(\frac{r\mu_{eff}}{\sigma_\phi}\frac{\partial\phi}{\partial y}\right)\right] = S_\phi \qquad (3.1\text{-}1)$$

where ϕ is a dependent variable stands for U, V, k or ε. σ_ϕ and S_ϕ have the values given in Table 3.1-1.

ϕ	σ_ϕ	S_ϕ
U	1	$-\frac{\partial P}{\partial x} + S^u$
V	1	$-\frac{\partial P}{\partial y} + S^v$
k	σ_k	$G - C_D\rho\varepsilon$
ε	σ_ε	$(C_1\varepsilon G - C_2\rho\varepsilon^2)/k$

Table 3.1-1 Values of σ_ϕ and S_ϕ for U, V, k and ε

A finite difference equation for ϕ can then be derived by integrating equation (3.1-1) over a control volume enclosing a point P in the flow field. Fig. 3.1-3 shows a curvilinear orthogonal grid around P of which the double

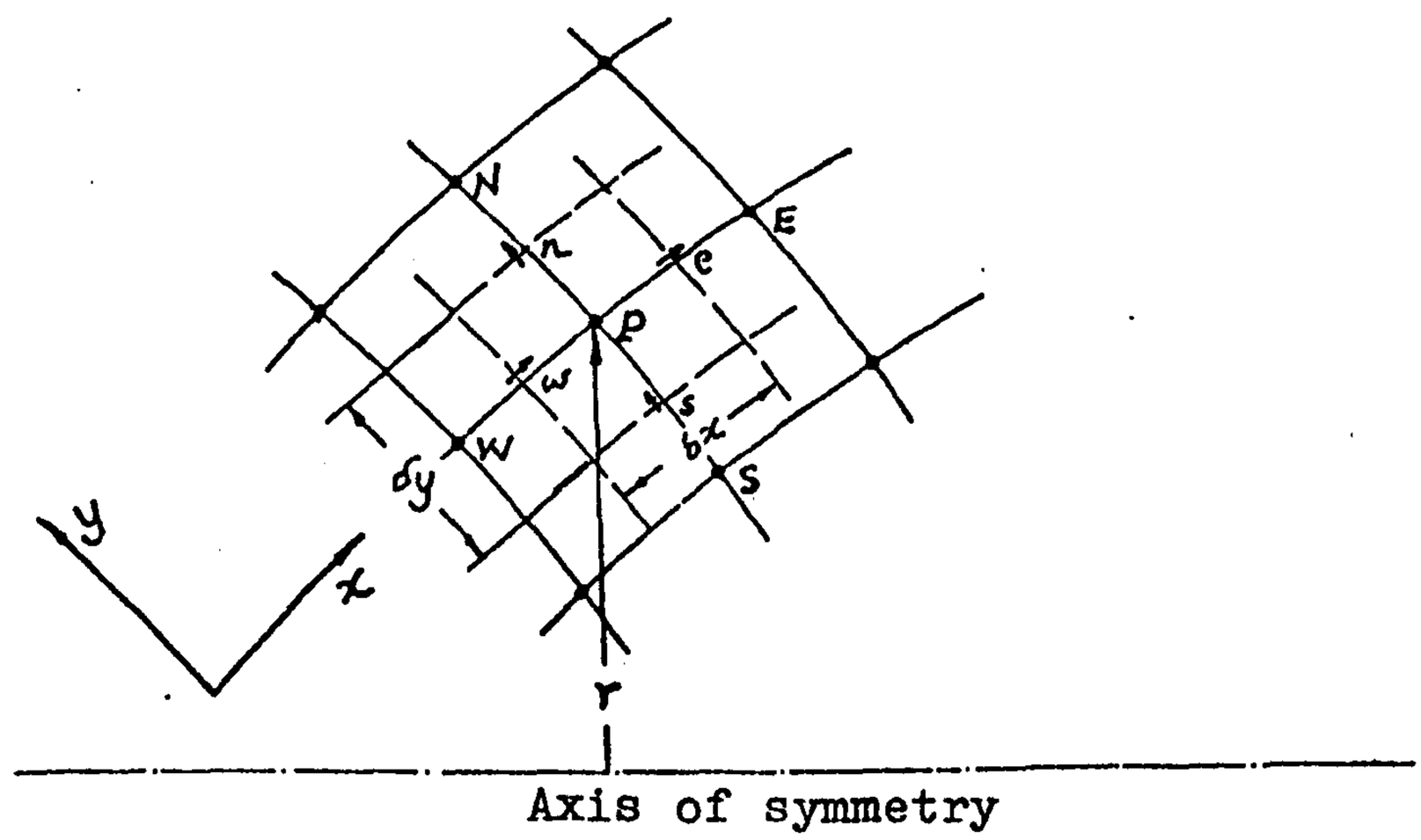

Fig. 3.1-3 Control volume around point P.

integration will take place. N, S, E, W represent the four neighbouring points around P. The control volume boundaries in x and y directions are placed at midway of the main grid lines. Integrating equation (3.1-1) with respect to x and y over the control volume boundaries surrounding P and rearranging gives (detailed integrations are given in Appendix A.5),

$$\left[(A_E + A_W + A_N + A_S) + (C_e - C_w + C_n - C_s) - S_P^{\phi}\right] \phi_P$$

$$= A_E \phi_E + A_W \phi_W + A_N \phi_N + A_S \phi_S + S_u^{\phi} \qquad (3.1\text{-}2)$$

where the A's are the coefficients expressing the combined effects of convection and diffusion and the C's are the convective coefficients account for the mass flow rate across the surfaces of the control volume surrounding P, i.e.,

$$C_e = (\rho U r \delta y)_e$$

$$C_w = (\rho U r \delta y)_w$$

$$C_n = (\rho V r \delta x)_n \qquad (3.1\text{-}3)$$

$$C_s = (\rho V r \delta x)_s$$

The subscripts e, w, n, s denote the four surfaces of the control volume as shown in Fig.3.1-3. The values of A's depend on the difference scheme. If the central difference scheme is employed to evaluate the convective terms,

$$A_E = D_e - 0.5\ C_e$$

$$A_W = D_w + 0.5\ C_w \qquad (3.1\text{-}4)$$

$$A_N = D_n - 0.5\ C_n$$

$$A_S = D_s + 0.5\ C_s$$

where the D's are the diffusive coefficients given as follows

$$D_e = \left(\frac{r\mu_{eff}\delta y}{\sigma_\phi \delta x}\right)_e$$

$$D_w = \left(\frac{r\mu_{eff}\delta y}{\sigma_\phi \delta x}\right)_w \qquad (3.1\text{-}5)$$

$$D_n = \left(\frac{r\mu_{eff}\delta x}{\sigma_\phi \delta y}\right)_n$$

$$D_s = \left(\frac{r\mu_{eff}\delta x}{\sigma_\phi \delta y}\right)_s$$

If, instead, a upwind difference scheme is used to evaluate the convective terms, the A's will take the following values:

$$A_E = D_e + 0.5(|C_e| - C_e)$$

$$A_W = D_w + 0.5(|C_w| + C_w) \qquad (3.1\text{-}6)$$

$$A_N = D_n + 0.5(|C_n| - C_n)$$

$$A_S = D_s + 0.5(|C_s| + C_s)$$

S_p^ϕ and S_u^ϕ are obtained from linearizing the source term S_ϕ listed in Table 3.1-1 such that

$$\int_{y_s}^{y_n}\int_{x_w}^{x_e} rS_\phi \, dxdy = S_p^\phi \phi + S_u^\phi \qquad (3.1\text{-}7)$$

The complete derivation of equation (3.1-2) as well as all the coefficients above are given in detail in

Appendix A.5.

The choice of central or upwind difference scheme depends on the contribution from the convective term. If the contribution from the convective term is greater than that of the diffusive term, upwind difference is used. Otherwise, central difference should be employed. Such choice is based on the fact that as the convective contribution is greater than the diffusive contribution, the directional effect is important. The upwind difference scheme which stresses more on the influence of the upstream conditions is thus preferred. The combined effect can be expressed in the following mathematical relationships

$$A_E = \begin{cases} D_e - 0.5C_e & \text{if } |0.5C_e| \leqslant D_e \\ D_e - 0.5C_e + 0.5|C_e| & \text{if } |0.5C_e| > D_e \end{cases}$$

$$A_W = \begin{cases} D_w + 0.5C_w & \text{if } |0.5C_w| \leqslant D_e \\ D_w + 0.5C_w + 0.5|C_w| & \text{if } |0.5C_w| > D_e \end{cases} \qquad (3.1\text{-}8)$$

$$A_N = \begin{cases} D_n - 0.5C_n & \text{if } |0.5C_n| \leqslant D_n \\ D_n - 0.5C_n + 0.5|C_n| & \text{if } |0.5C_n| < D_n \end{cases}$$

$$A_S = \begin{cases} D_s + 0.5C_s & \text{if } |0.5C_s| \leqslant D_s \\ D_s + 0.5C_s + 0.5|C_s| & \text{if } |0.5C_s| > D_s \end{cases}$$

The term $C_e - C_w + C_n - C_s$ appearing in the left-hand-side of equation (3.1-2) is the net mass flow rate out from the control volume. If the continuity equation is satisfied, i.e., when the final solution is reached, this should be zero. But in the intermediate iteration, the net mass flow rate may not be zero and a false source can be calculated from the previous value of ϕ_P, if

$$\dot{m}_P = C_e - C_w + C_n - C_s \qquad (3.1\text{-}9)$$

then the false source = $\dot{m}_P \phi_P^{old}$, where ϕ_P^{old} is the value of ϕ at P evaluated from the last iteration. The finite difference equation (3.1-2) becomes

$$\left(\sum_{j=E,W,N,S} A_j + \dot{m}_P - S_P^{\phi}\right)\phi_P = \sum_{j=E,W,N,S} A_j\phi_j + \dot{m}_P \phi_P^{old} + S_u^{\phi} \qquad (3.1\text{-}10)$$

The inclusion of $\dot{m}_P\phi_P$ and $\dot{m}_P\phi_P^{old}$ into the finite difference equation will not affect the final solution as when the solution is approached, both $\dot{m}_P$ and $(\phi_P - \phi_P^{old})$ are small. It will only be necessary to include these terms if they can help to stabilize the iteration process. Since the convergence criteria for the above equation is

$$\left(\sum_{j=E,W,N,S} A_j + \dot{m}_P - S_P^{\phi}\right) \geqslant \sum_{j=E,W,N,S} A_j$$

it is clear that only when $\dot{m}_P$ is positive will the terms $\dot{m}_P\phi_P$ and $m_P\phi_P^{old}$ be included in the equation. Thus, the complete finite difference equation for ϕ can be written as

$$A_P\phi_P = \Sigma A_j\phi_j + S_u^{\phi}$$
$$j = N, S, E, W$$

where (3.1-11A)

$$A_P = \Sigma A_j - S_P^{\phi}$$
$$j = N, S, E, W$$

$$\text{for } \dot{m}_P \leqslant 0$$

and

$$A_P\phi_P = \Sigma A_j\phi_j + \dot{m}_P\phi_P^{old} + S_u^{\phi}$$
$$j = N, W, E, W$$

where (3.1-11B)

$$A_P = \Sigma A_j + \dot{m}_P - S_P^{\phi}$$
$$j = N, S, E, W$$

$$\text{for } \dot{m}_P > 0$$

Equations (3.1-11) are the general forms of all the finite difference equations for U, V, k and ε. The equations differ in the source term expressions S_P^{ϕ} and S_u^{ϕ} which can be obtained by integrating S_{ϕ} listed in Table 3.1-1 via equation (3.1-7). If ϕ is a velocity component, S_u^{ϕ} has two distinct parts, a pressure-gradient term and an additional term due to radius of curvature.

The pressure is a unique variable in this solution procedure as it is not governed by a transport equation but enters through the momentum source term. The values of $S_u\phi$ and $S_p\phi$ appropriate for the present flow situation are tabulated in Table 3.1-2. The integration and approximation are given in Appendix A.6.

Variable ϕ	$S_p\phi$	$S_u\phi$
U	0	$0.5(a_e^u+a_w^u)(P_w-P_P)+(\frac{\rho V^2}{r_y})_P v_P$
V	$-(\frac{\mu_{eff}}{r^2})_P v_P$	$0.5(a_n^v+a_s^v)(P_s-P_P)+(\frac{\rho U^2}{r_x})_P v_P$
k	$-(\frac{C_D C_\mu \rho^2 k}{\mu_{eff}})_P v_P$	$G_P v_P$
ε	$-(\frac{C_2 \rho \varepsilon}{k})_P v_P$	$(\frac{C_1 C_\mu \rho k G}{\mu_{eff}})_P v_P$

Table 3.1-2 Values of $S_p\phi$ and $S_u\phi$. a_e^u, a_w^u, a_n^v and a_s^v are surface areas of the appropriate control volumes for U and V. v_P is the control volume for the variable concerned.

3.1.3 The Finite Difference Equation for Pressure Correction

To solve the finite difference equations for U and V, it is necessary to have the values of pressures. However, these values are not known in advance. The normal practice

is to initially guess the best estimated pressure (denoted by P*) so that the velocity field U* and V* can be obtained. The U* and V* velocity field will not in general satisfy the continuity equation. The pressure corrections are made such that the velocity field is brought into conformity with the continuity equation. The true pressure P is thus given by

$$P = P^* + P' \qquad (3.1\text{-}12)$$

where P' is the pressure correction. By applying the general finite difference equation for ϕ to U*, V* and U, V respectively and subtracting the guessed momentum equation from the corresponding momentum equation with appropriate approximation, one gets

$$U_P = U_P^* + D_w^u(P_W' - P_P') \qquad (3.1\text{-}13)$$

$$V_P = V_P^* + D_s^v(P_S' - P_P') \qquad (3.1\text{-}14)$$

where $D_w^u = \dfrac{0.5(a_e^u + a_w^u)}{A_P^u}$ and $D_s^v = \dfrac{0.5(a_n^v + a_s^v)}{A_P^v}$. A_P^u and A_P^v are the coefficient A_P for U and V respectively.

The substitution of equations (3.1-13) and (3.1-14) into the finite difference form of the continuity equation gives

$$A_P^P \, P_P' = \sum A_j^P \, P_j' + S_u^P \qquad (3.1\text{-}15)$$

$$j = N, S, E, W$$

where

$$A_P^P = \sum A_j^P$$

$$j = N, S, E, W$$

and

$$S_u^P = -\dot{m}_P$$

The coefficient are given by

$$A_W = D_w^u \, (\rho r \delta y)_w$$

$$A_E = D_e^u \, (\rho r \delta y)_e$$

$$(3.1\text{-}16)$$

$$A_N = D_n^v (\rho r \, \delta x)_n$$

$$A_S = D_s^v (\rho r \, \delta x)_s$$

The full derivation of equations (3.1-13), (3.1-14) and (3.1-15) are given in Appendix A.7.

By solving P' throughout the flow field, a better estimated pressure field can be obtained by adding P' to the existing pressure field after each iteration; i.e.,

$$P^{n+1} = P^n + P'$$

where P^n is the pressure used for n^{th} iteration, P' is the solution obtained from the nth iteration and P^{n+1} is

the updated pressure to be used for $n+1^{th}$ iteration.

3.2 The Solution of the Finite Difference Equations

The finite difference equation for ϕ at a point P(I,J) can be written as

$$A_P\phi_{i,j} = A_E\phi_{i+1,j} + A_W\phi_{i-1,j} + A_N\phi_{i,j+1} + A_S\phi_{i,j-1} + S_u\phi \tag{3.2-1}$$

In such a typical equation , there are five variables in existence. If, however, the values of $\phi_{i+1,j}$ and $\phi_{i-1,j}$ are taken from the previous iteration or in the case of the first iteration given by some initial values, equation (3.2-1) can then be reduced to three unknown variables, i.e.,

$$-b_j\phi_{i,j-1} + d_j\phi_{i,j} - a_j\phi_{i,j+1} = c_j \tag{3.2-2}$$

where

$$b_j = A_S$$

$$d_j = A_P$$

$$a_j = A_N$$

and

$$c_j = A_E\phi_{i+1,j} + A_W\phi_{i-1,j} + S_u\phi$$

Equation (3.2-2) is an algebraic equation relating the value of ϕ at P and its two neighbouring points N and S. Fig. 3.2-1 illustrates a typical grid line arrange-

ment where the axis of symmetry is placed between j=1 and j=2 and the wall boundary is placed midway of j=NJ-1 and j=NJ. In the case where the node is next to the axis of symmetry, i.e., j=2, the usual link between $\phi_{i,2}$ and its southern neighbour $\phi_{i,1}$ no longer in existence and A_S is set to zero. Similarly, when the node is next to a solid wall, no linkage between $\phi_{i,NJ-1}$ and $\phi_{i,NJ}$, and $A_N=0$. A set of such equations for all the nodes along the ith grid line can then be assembled in a tri-diagonal matrix form.

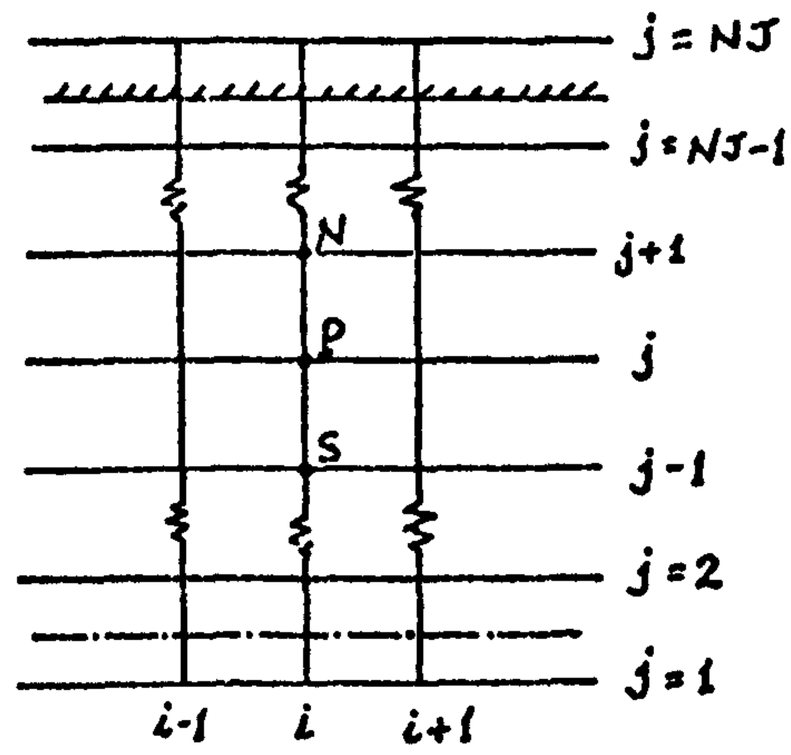

Fig3.2-1 The ith grid line

$$\begin{bmatrix} d_2 & -a_2 & & & & & \\ -b_3 & d_3 & -a_3 & & & & \\ & & \text{------} & & & & \\ & & -b_j & d_j & -a_j & & \\ & & & & \text{---------} & & \\ & & & & -b_{NJ-2} & d_{NJ-2} & -a_{NJ-2} \\ & & & & & -b_{NJ-1} & d_{NJ-1} \end{bmatrix} \begin{bmatrix} \phi_{i,2} \\ \phi_{i,3} \\ \vdots \\ \phi_{i,j} \\ \vdots \\ \phi_{i,NJ-2} \\ \phi_{i,NJ-1} \end{bmatrix} = \begin{bmatrix} c_2 \\ c_3 \\ \vdots \\ c_j \\ \vdots \\ c_{NJ-2} \\ c_{NJ-1} \end{bmatrix} \tag{3.2-3}$$

The above set of equations, with a maximum of 3 unknowns per equation, can be solved by Gaussian elimination using a recurrence formula

$$\phi_{i,j} = \alpha_j + \beta_j \phi_{i,j+1} \qquad (3.2\text{-}4)$$

$$\alpha_j = \frac{c_j + b_j \alpha_{j-1}}{-b_j \beta_{j-1} + d_j} \qquad (3.2\text{-}5)$$

and

$$\beta_j = \frac{a_j}{-b_j \beta_{j-1} + d_j} \qquad (3.2\text{-}6)$$

The solution is obtained by back substitution solving for $\phi_{i,NJ-1}$, $\phi_{i,NJ-2}$, ... till $\phi_{i,2}$.

The overall procedure is in such a manner that solution start from i=2, obtaining all the ϕ's values at i=2 then proceed to i=3,4,.... etc., so that all the ϕ's of the whole flow field are obtained. This is called the Tri-Diagonal Matrix Algorithm (TDMA) of the line by line procedure.

It has been found that some degree of under-relaxation is necessary in order to achieve stability during the iteration. By using an under-relaxation factor f, A_P and S_u^{ϕ} in equation (3.2-1) will be modified to A_P' and $S_u^{\phi}{}'$ as follows:

$$A_P' = \frac{A_P}{f} \qquad (3.2\text{-}7)$$

$$S_u^{\phi}{}' = S_u^{\phi} + (1-f)\frac{A_P}{f}\phi_P \qquad (3.2\text{-}8)$$

where ϕ_P is the existing ϕ value at P. From experience by trial and error, the values of f are set to 0.5 for U and V, 0.7 for k and ε and 1 for P'.

3.3 The Overall Procedure of Solution

Before proceeding to the solution of the finite difference equation (F.D.E.) for various variables, initial values for all the variables throughout the flow field are specified. The solution procedure is the cyclic repetition of the following steps:

(i) The effective viscosity is calculated by equations (2.4-2) and (2.4-8) using the existing stored values of k and ε .

(ii) The F.D.E. of U and V are solved by TDMA using the existing pressure field P* to calculate the source terms. The resulting values of U* and V* are usually not satisfied with the local continuity equation and an 'error' mass source $\dot{m}$ for each cell can be calculated.

(iii) The F.D.E. for pressure correction (3.1-15) is solved by TDMA using the 'error' source $-\dot{m}_P$ as S_u^P . The new pressure field is obtained by adding P' to P*, i.e., P = P* + P'. The U and V velocities are also corrected using equations (3.1-13) and (3.1-14).

(iv) The F.D.E. for k and ε are solved by TDMA.

(v) The updated values of the variables are used to compute the coefficients and source terms of the

F.D.E.'s for the next iteration. The above procedure (i) to (iv) are repeated until the pressure correction P' is small enough throughout the flow field. This ensures that both momentum and continuity equations are satisfied simultaneously.

To improve the rate of convergence of the procedure, certain variable can be solved more than once before proceeding to solve the next variable. This idea is called the number of sweep in solving a specific variable. It is found that in solving P', the increase of the number of sweep to 2 in the case of jet mixing problem and to 5 in the case of diffuser problem will improve the rate of convergence.

The termination of the iteration procedure is based on the 'error' mass source term $\dot{m}$. The procedure is deemed to have converged when the sum of the absolute 'error' mass source throughout the flow field is small compared with the inlet mass flow rate $\dot{m}_{in}$, i.e.,

$$\frac{\sum\left|C_e - C_w + C_n - C_s\right|}{\dot{m}_{in}} \leq \delta \qquad (3.3\text{-}1)$$

where δ is a small positive value depending on the requirement of accuracy. In most cases, $\delta = 10^{-4}$ will give a fairly good accuracy for the solution. Besides depending upon the δ which determines the number of iteration, the accuracy also depends on the number of gridlines specified in the flow field. More grid lines will require more

computer time. The choices of the number of grid lines and the value of δ apparently depend on the compromise between the accuracy and economy.

CHAPTER 4

THE COMPUTER MODEL

4.1 Introduction

The set of partial differential equations discussed in Chapter 2 and the numerical method described in Chapter 3 were embodied into a basic computer program called TEACH (teaching elliptic axisymmetric characteristic heuristically) by Gosman and Pun (1974). The original program can only handle cylindrical pipe flows. The present computer models for predicting the flows in various components of a typical jet pump are devised based on the basic TEACH program. In order to predict the upstream entrance region and the downstream diffuser region, the models must be able to accommodate the general two-dimensional orthogonal axisymmetric coordinates described in Chapter 2. The present Chapter describes only briefly the basic structure of the computer program as more details are available in the report written by Gosman and Pun (1974). However, detailed description of modelling the various flow components are included.

4.2 The Basic Structure of the Computer Program

The computer program in the present work is written in Fortran IV. It consists of a main program and ten subroutines. The flow chart of the program is shown in Fig. 4.2-1. The geometry specification, grid calculation and

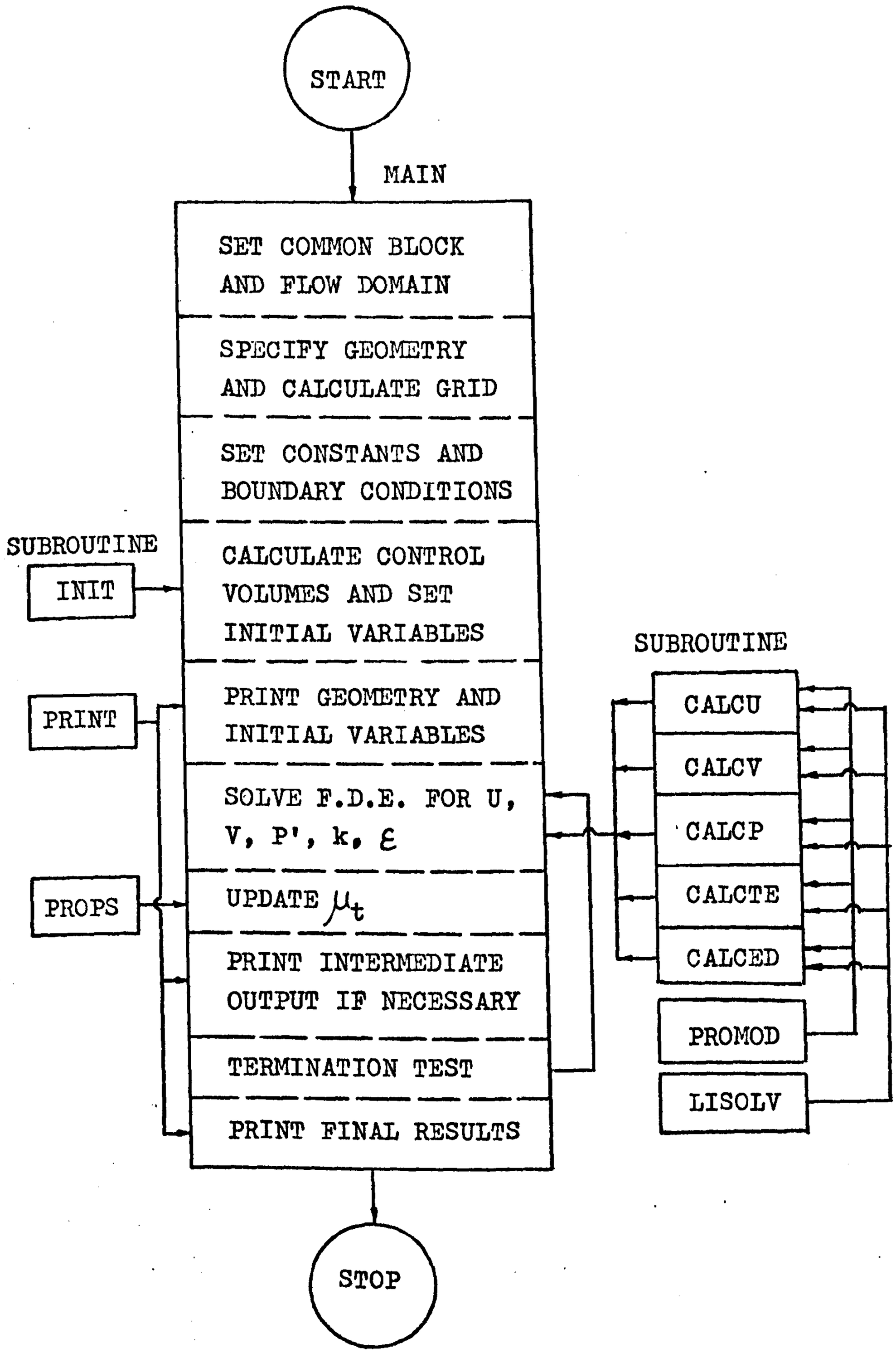

Fig. 4.2-1 Flow chart of the computer program

simulation of boundary conditions are done at the beginning of the main program. The duties of the subroutines are briefly described in the main program block. The solving of finite difference equation for each variable is carried out in the individual subroutine, i.e., CALCU for solving U, CALCP for solving P', etc. The 'near-wall' modification for all the variable is done in the subroutine PROMOD and the line by line procedure of solving simultaneous algebraic equations using the TDMA technique is performed in the subroutine LISOLV. The updating of viscosity after each iteration is carried out in the subroutine PROPS. The solving of finite difference equations is repeated until the termination test as described in Chapter 3 is fulfiled and final results are printed. A complete listing of the computer program for calculating typical jet pump mixing tube including secondary inlet region is given in Appendix B.1.

It should be noted that except for the subroutine INIT, other subroutines are applicable to various flow configurations subject to minor changes in evaluating the source terms of the finite difference equations. Programs for various flows differ in the main program and the subroutine INIT where the setting up of the geometry, grid, boundary conditions and control volumes must be able to simulate a particular flow accurately.

4.3 The Simulation of Various Flow Components

4.3.1 Uniform Mixing Duct

A uniform mixing duct consists of a round nozzle

located at the centre of the inlet section of a uniform diameter mixing duct is shown in Fig.4.3-1. A high velocity jet meets the secondary fluid at the inlet section. Both the primary and the secondary velocities can be taken as uniform across the inlet section as indicated by U_i and U_o respectively. The radius of the central jet is r_i and the inner radius of the mixing duct is r_o .

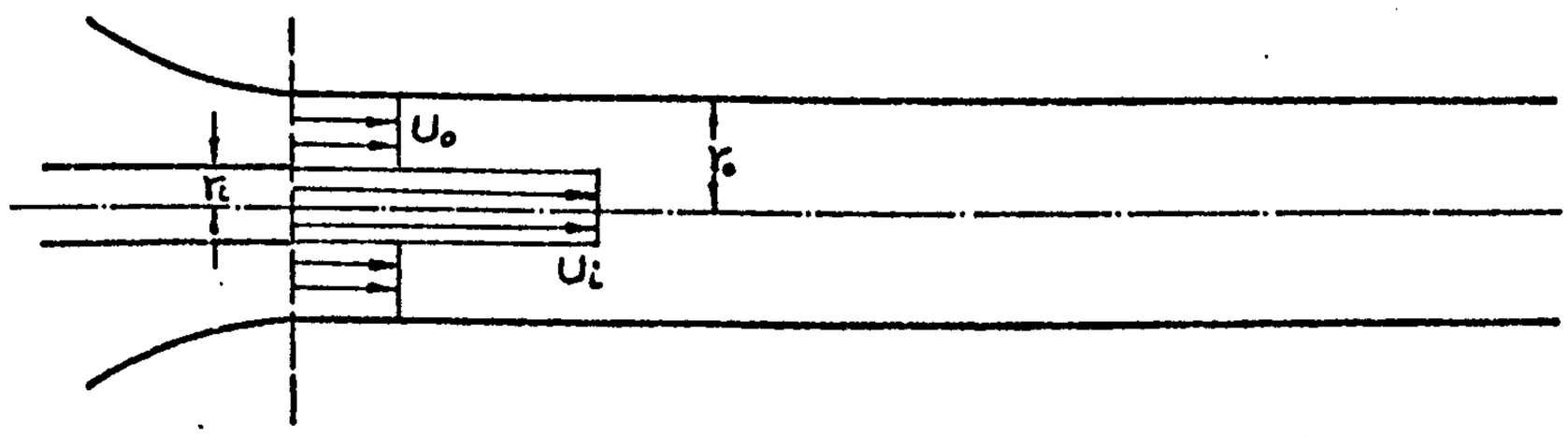

Fig. 4.3-1 Uniform mixing duct

The general 2-D orthogonal axisymmetric coordinate described in Chapter 2 when applied to such a uniform mixing duct, is reduced to a cylindrical polar coordinates with x and y as coordinates in the axial and radial directions respectively, i.e., x = z and y = r. The grid for such a coordinate system is shown in Fig.4.3-2. The grid lines are specified throughout the flow domain which is bounded by the axis of symmetry and the duct wall from the inlet to the exit. NI radial grid lines and NJ axial grid lines are used. Uniform grid spacings are used in the radial direction whereas a geometrical expansion of grid spacing is used in the axial direction so that the up-stream region where the mixing is more vigorous will have a finer grid. The radial grid spacing in the central

jet region is DY1 and that in the outer region is DY2 as shown in Fig.4.3-2.

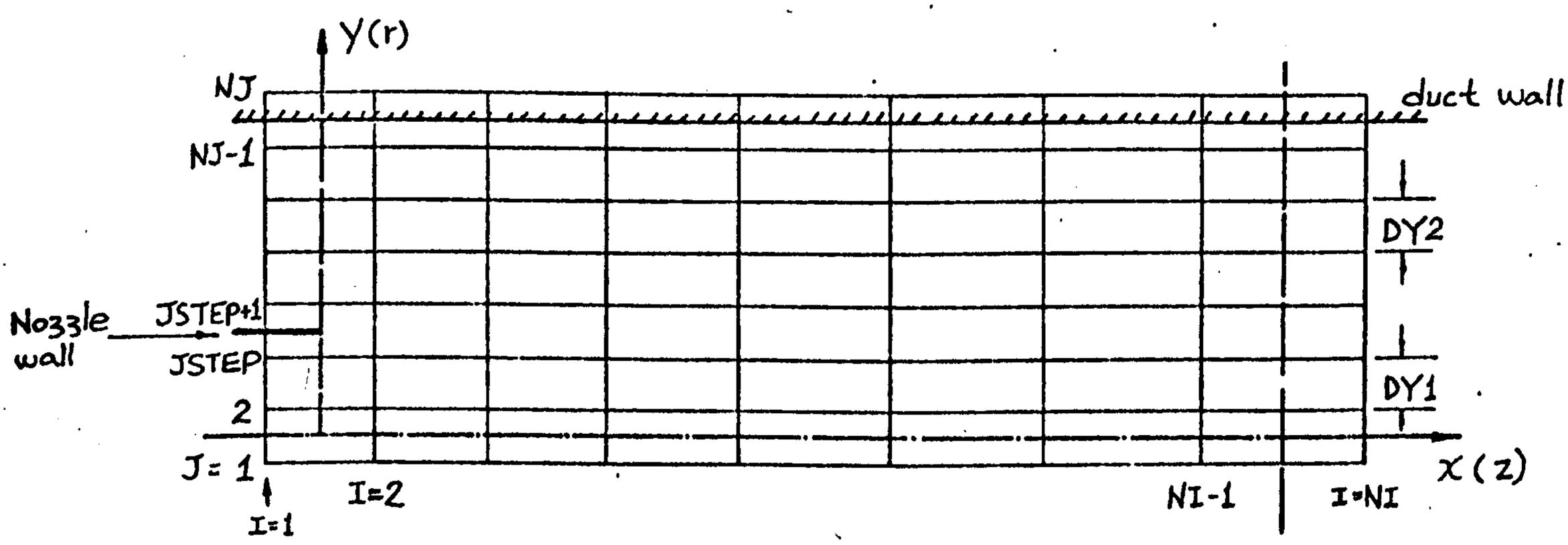

Fig. 4.3-2 The grid and boundary for uniform mixing duct

The flow boundaries are specified according to Table 4.3-1.

Flow Boundary	Grid Location
Axis of symmetry	Midway of J = 1 and J = 2
Duct wall	Midway of J = NJ-1 and NJ
Initial jet boundary	Between J=JSTEP and J=JSTEP+1
Inlet section	Midway of I=1 and I=2
Outlet section	Midway of I=NI-1 and NI

Table 4.3-1 Flow boundary specification for uniform mixing duct

Thus, the radial grid spacings are given by

$$DY1 = \frac{r_i}{JSTEP - 1} \qquad (4.3\text{-}1)$$

and $$DY2 = \frac{r_o - r_i}{NJ - JSTEP - 1} \qquad (4.3\text{-}2)$$

The listing of the main program and subroutine INIT is given in Appendix B.2.

4.3.2 Typical Jet Pump Mixing Tube Including Secondary Inlet Region

A typical jet pump mixing tube including secondary inlet region is shown in Fig.4.3-3. The configuration of the inlet region is governed by (1) the profile of the secondary inlet duct leading to the constant diameter mixing tube, (2) the profile of the external surface of the nozzle, and (3) the distance between the nozzle exit and the mixing tube inlet.

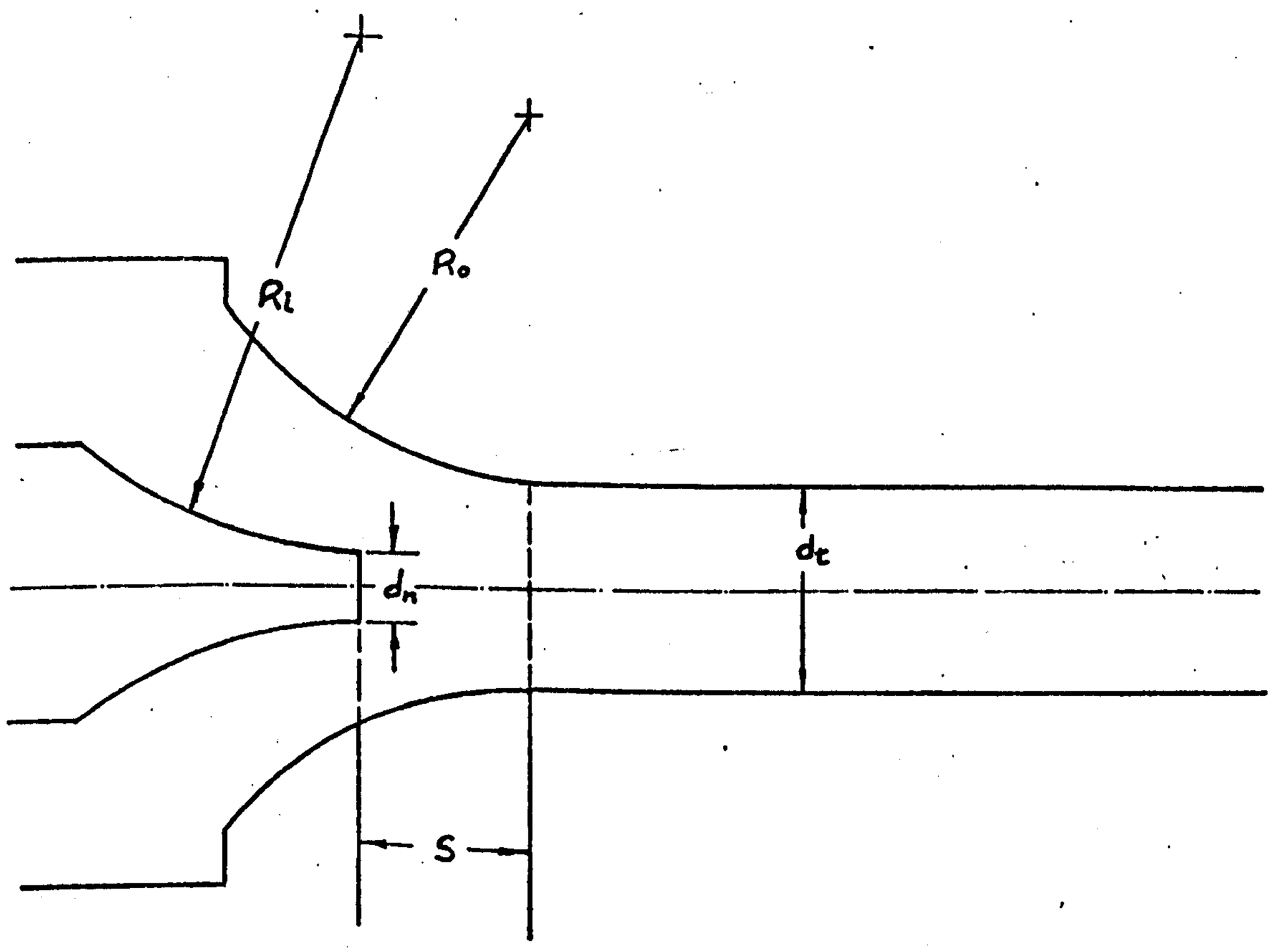

Fig. 4.3-3 Typical jet pump mixing tube including inlet region

The profiles of both the nozzle and the secondary inlet duct are described by circular arcs with radii R_i and R_o respectively. The annular passage formed by these profiles will provide a continuous convergence of flow area which ascertains flow with less loss. Although other inlet profiles are possible, it is shown by Mueller (1964) and Fasol et al (1958) that circular arc profiles give better performance. The distance from the nozzle exit to the mixing tube inlet is s and the diameters of mixing tube and nozzle exit are d_t and d_n respectively. By varying these five geometrical variables, a wide range of entry configuration can be obtained and investigated using a common computer program.

A general 2-D orthogonal curvillinear coordinate system is devised to specify grid positions in the flow field. Coordinate x is in the streamwise direction where the grid lines are drawn so as to lay between boundary wall and the axis of symmetry. The grid lines for coordinate y are orthogonal to the x grid lines everywhere. The complete secondary inlet grid together with part of the mixing tube grid is shown in Fig.4.3-4. The positions of the grid nodes in the annular region are calculated in terms of a Cartesian coordinates x_1 and x_2 as shown in Fig. 4.3-5. The inlet duct wall can be described by an equation of circle in x_1 - x_2 coordinates with centre at (0,0). Similarly, the nozzle wall can be represented by another equation of circle with centre at (-s, b) where s is the nozzle spacing, i.e.,

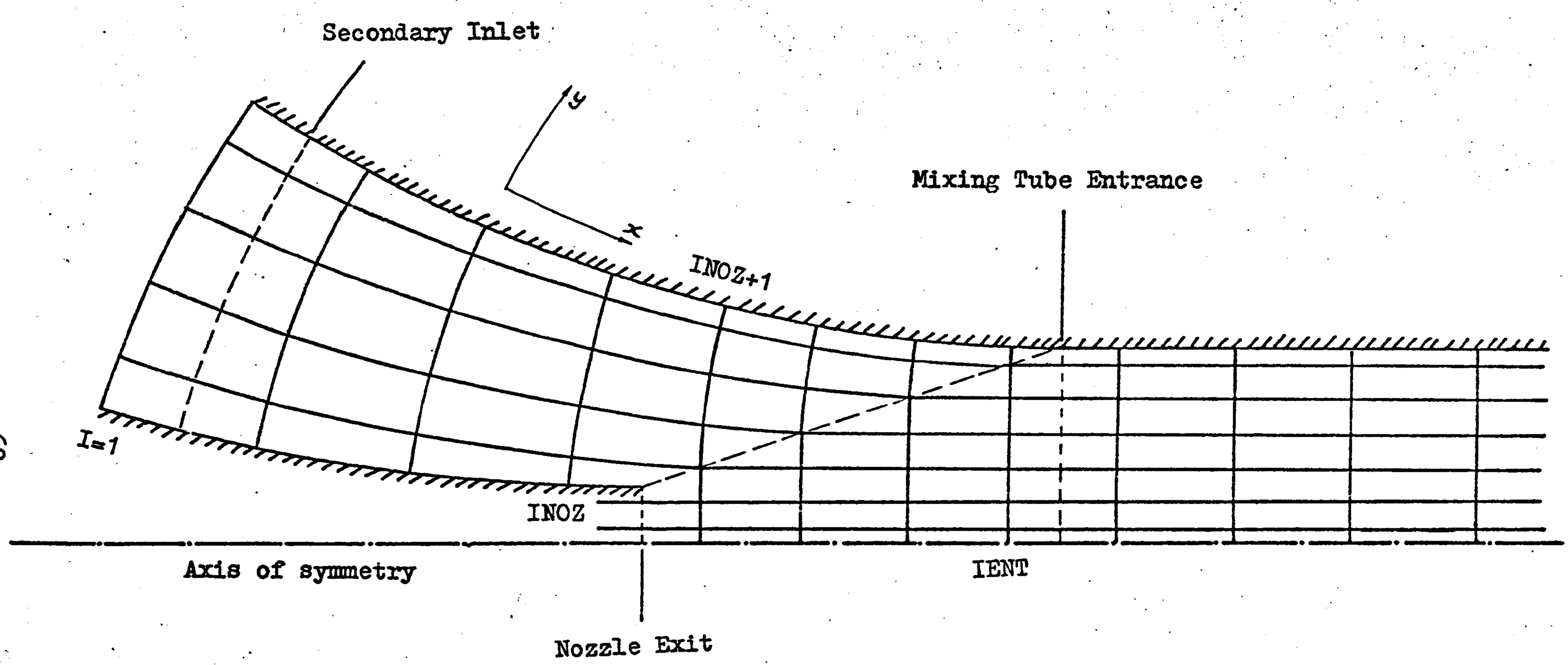

Fig. 4.3-4 Grid for the Secondary Inlet Region

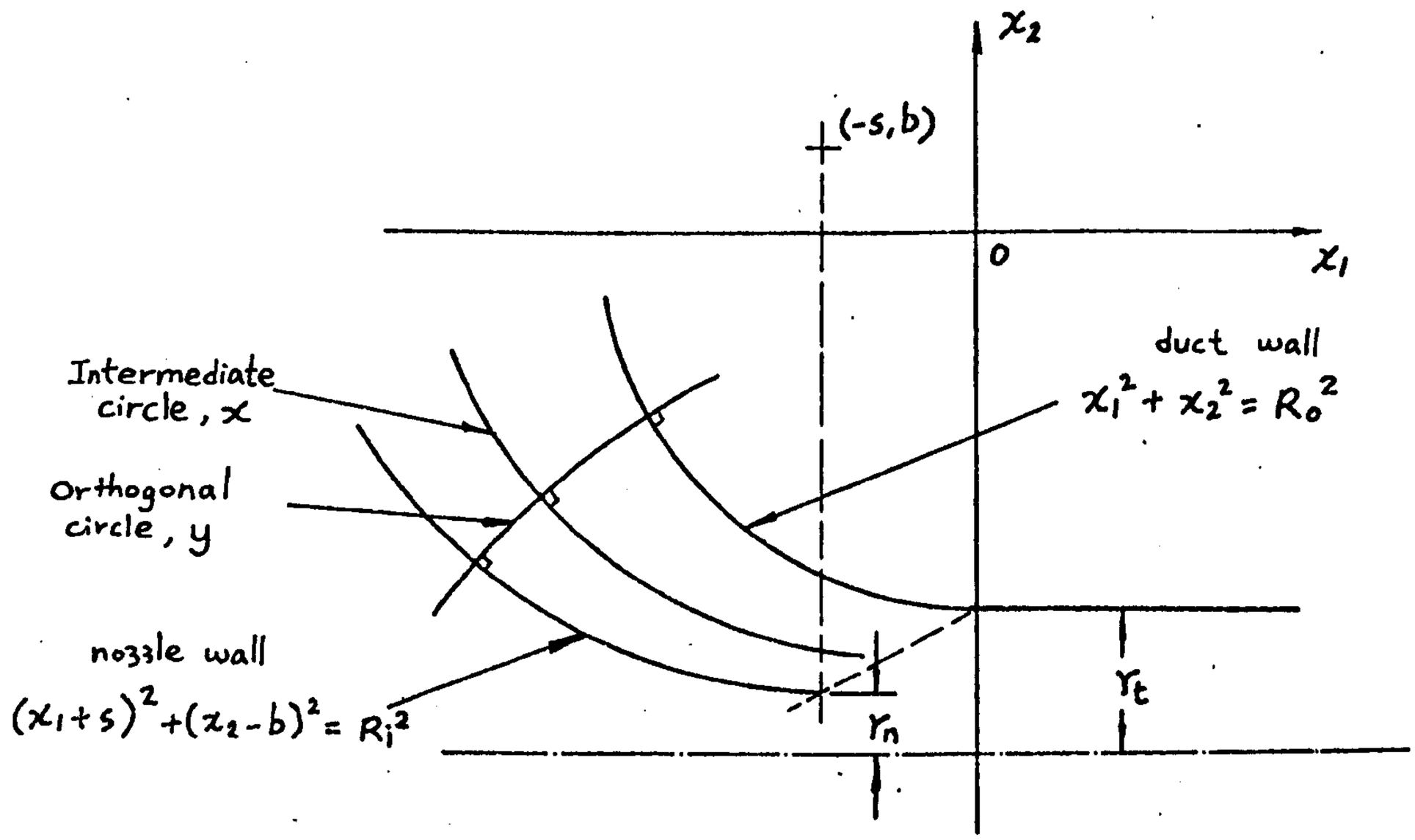

Fig.4.3-5 Calculation of grid nodes

For duct wall,

$$x_1^2 + x_2^2 = R_o^2 \qquad (4.3\text{-}3)$$

For nozzle wall,

$$(x_1 + s)^2 + (x_2 - b)^2 = R_i^2 \qquad (4.3\text{-}4)$$

where $\qquad b = R_i + r_n - R_o - r_t$

From any point at the nozzle wall, it is possible to determine the centre and radius of a orthogonal circle which forms a y grid line. A series of intermediate circles which lie between nozzle and duct walls and cut orthogo-

nally with the orthogonal circle can be devised to form the x grid lines. The intersections of the orthogonal and intermediate circles are thus the grid nodes in the inlet region. The detailed calculation of the positions of these grid nodes are given in Appendix A.8.

The treatments of the duct wall, the axis of symmetry and the outlet section are similar to those used for uniform diameter mixing tube described in section 4.3.1. Other boundaries as shown in Fig.4.3.4 are specified according to Table 4.3-2.

Flow Boundary	Grid Location
Primary Inlet (Nozzle exit)	Between I=INOZ and I=INOZ+1
Secondary Inlet	Midway of I=1 and I=2
Mixing Tube Entrance	Between I=IENT and I=IENT+1
Nozzle Wall	Between J=JNOZ and JNOZ+1

Table 4.3-2 Flow boundary specification for typical jet pump mixing tube

The selection of INOZ depends on the length of the annular flow region. The value of IENT can be calculated from

$$IENT = INOZ + NJ - (JNOZ + 1) \qquad (4.3\text{-}5)$$

The whole flow domain is thus completely specified

by two inlet sections, the nozzle wall, the duct wall, the axis of symmetry and the outlet section. Uniform primary jet velocity and secondary annular velocity are specified at the two inlet sections according to the primary and secondary flow rates of the jet pump under investigation. In order to calculate the secondary inlet velocity, the annular flow area at the secondary inlet section is calculated by a separate short program AREA listed in Appendix B.4. Other boundary conditions are specified according to section 2.6. The listing of the complete computer program for calculating flow in jet pump mixing duct is given in Appendix B.1.

4.3.3 Conical Diffuser

Fig. 4.3-6 shows the geometry of a typical conical diffuser with inlet diameter d_1 , included angle θ and axial length l_d .

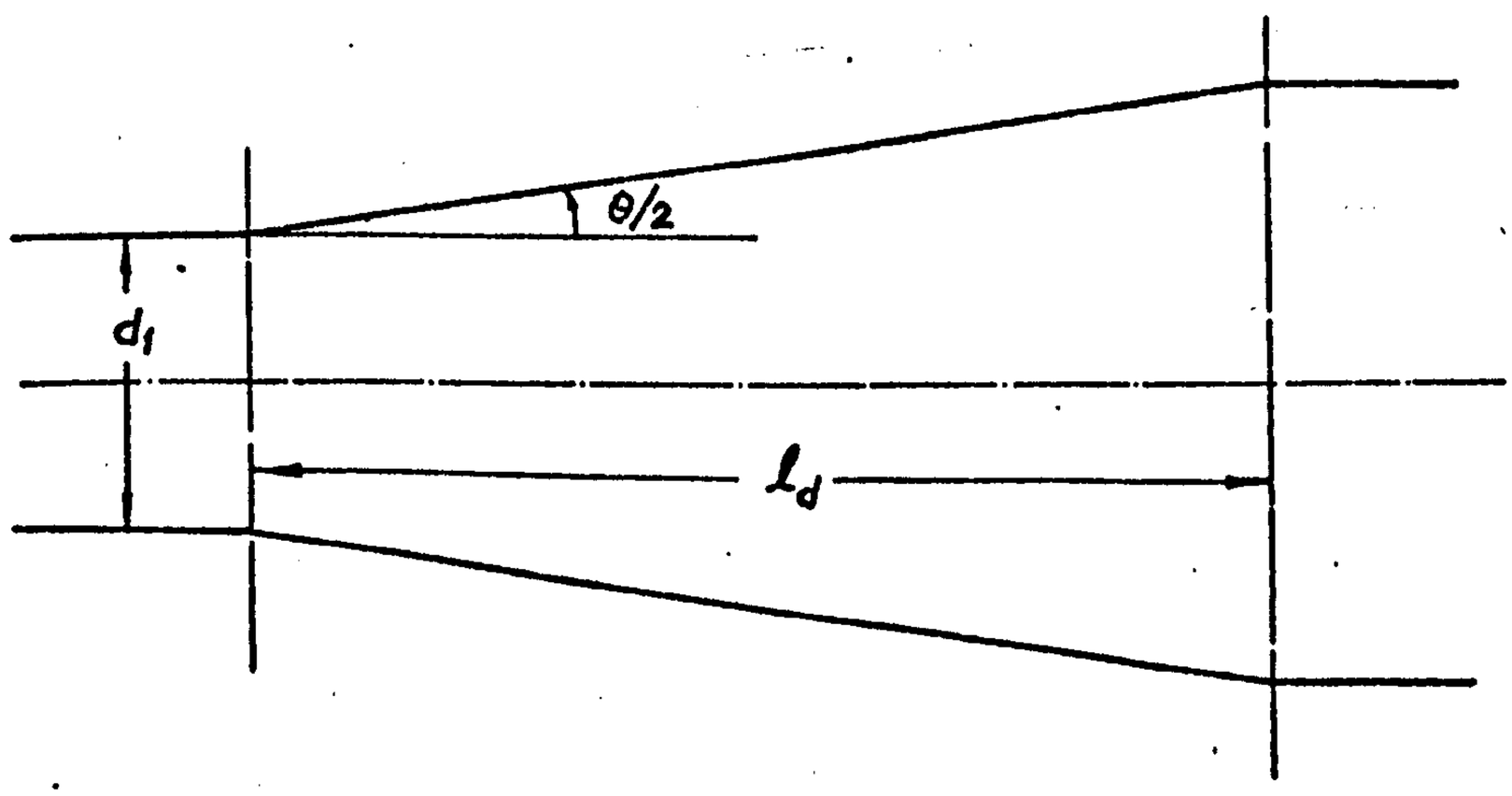

Fig. 4.3-6 Geometry of a typical conical diffuser

The geometry of a diffuser is completely described by these three variables. If the diffuser wall is extrapolated to meet the axis of symmetry at a point O as shown in Fig. 4.3-7.

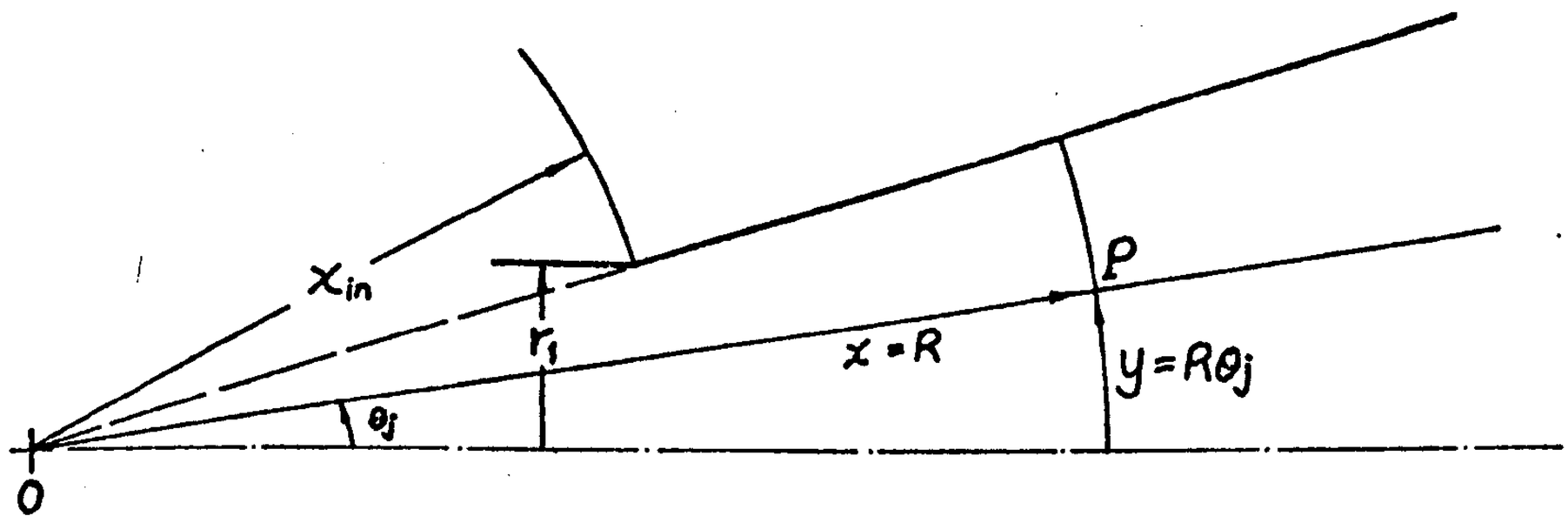

Fig. 4.3-7 Coordinate system for conical diffuser

The position at any point P in the flow field is determined by distance OP or R and the angle between OP and the axis of symmetry θ_j. The general 2-D orthogonal coordinates x and y as described in Chapter 2 can then be expressed in terms of R and θ_j, i.e.,

$$x = R \tag{4.3-6}$$

$$y = R\theta_j \tag{4.3-7}$$

A complete grid of the diffuser flow region using a 8 x 8 grid is shown in Fig. 4.3-8.

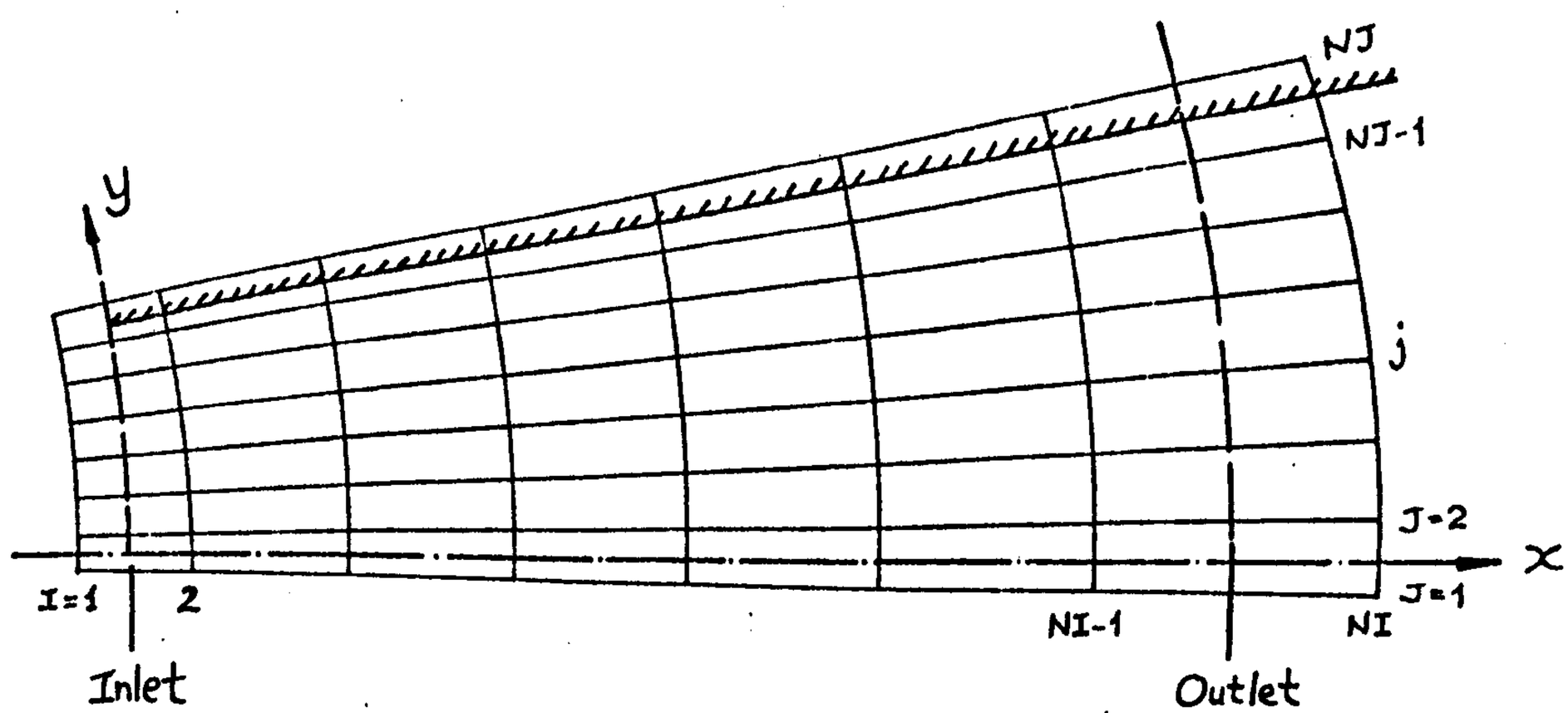

Fig. 4.3-8 The grid of a conical diffuser

The angle θ_j at every node on the jth grid line can be calculated from NJ, j, and θ as follows:-

$$\theta_j = \frac{j - 1.5}{NJ - 2}\left(\frac{\theta}{2}\right) \qquad (4.3\text{-}8)$$

The value of x at the inlet section x_{in} is obtained from d_1 and θ , i.e.,

$$x_{in} = \frac{\frac{d_1}{2}}{\sin\frac{\theta}{2}} \qquad (4.3\text{-}9)$$

The specification of flow boundaries is similar to the mixing duct problem. However, it is necessary to specify the U-velocity at outlet section from the overall mass flow conservation considering the increase in flow area. The procedures are as follows:

(i) Evaluate the mass flow rate at I=NI-1, $\dot{m}_{NI-1}$

(ii) Calculate the velocity correction U_{cor} from $\dot{m}_{NI-1}$

and the inlet mass flow rate $\dot{m}_{in}$.

$$U_{cor} = \frac{\dot{m}_{in} - \dot{m}_{NI-1}}{A_{NI-1}\rho} \qquad (4.3\text{-}10)$$

where A_{NI-1} is the flow area corresponding to $I = NI - 1$.

(iii) Add U_{cor} to every U-velocity at $I = NI - 1$ and calculate U at $I = NI$ using the continuity relationship.

$$U(NI,J) = \left[U(NI-1,\ J) + U_{cor}\right] \left(\frac{A_{NI-1}}{A_{NI}}\right) \qquad (4.3\text{-}11)$$

Other boundary conditions are specified according to section 2.6. A listing of the main program and subroutine INIT for solving the diffuser flow is given in Appendix B.3.

CHAPTER 5

FLOW PREDICTION

It is now possible to apply the computer models described in Chapter 4 for flow predictions. In order to validate the theoretical approach described in this thesis, the computer programs are first employed individually to predict flows in (i) uniform mixing duct, (ii) typical jet pump mixing tube with secondary inlet region and (iii) conical diffuser. The predicted results are compared with the published experimental data. The computer models are then used subsequently to simulate the flow in a typical jet pump system which consists of a entrance region, a mixing tube and a conical diffuser. Predictions of the pressure rise and the overall performance parameters are then obtained and compared with the available experimental data.

5.1 Flow in Uniform Diameter Mixing Tube

5.1.1 Introduction

A typical uniform mixing tube with a round nozzle located at the centre of the inlet section as shown in Fig.4.3-1 is the simplest design of a jet pump. Experimental studies of jet mixing in such a uniform duct were carried out by many workers. Among them, Helmbold et al (1954) carried out the measurements of the axial static pressure and the radial total pressure profiles at various

stations downstream of the nozzle. Razinsky and Brighton (1971) measured the mean and fluctuating velocities, static pressures as well as the turbulent shear stress throughout the whole flow field. Sanger (1968a, 1968b) carried out comprehensive tests of several jet pumps, all having uniform mixing ducts followed by conical diffusers.

Theoretical analyses of confined jet flows were carried out by Curtet (1958), Dealy(1964), Hill (1964), Exley and Brighton (1971) and Hill (1973). Baker, Hottel and Williams (1962) derived a non-dimensional parameter called Craya-Curtet Number C_t , based on the ratio of kinematic-mean and dynamic-mean inlet velocities, to determine the character of the flow in the mixing duct. In a mixing duct of constant diameter, as shown in Fig. 4.3-1, C_t can be expressed in terms of the radius ratio and the initial velocity ratio.

$$C_t = \frac{U_c}{\left[(U_i^2 - U_o^2)(\frac{r_i}{r_o})^2 + \frac{1}{2}(U_o^2 - U_c^2)\right]^{\frac{1}{2}}} \qquad (5.1\text{-}1)$$

where

$$U_c = (U_i - U_o)(\frac{r_i}{r_o})^2 + U_i$$

Hill (1964) proposed that the flow behaviour of confined jet mixing was a function of a non-dimensional parameter $\frac{m}{(M\rho)^{\frac{1}{2}}}$ which when applied to a constant diameter mixing tube gave the following value,

$$\frac{m}{(M\rho)^{\frac{1}{2}}} = \frac{\lambda_o + (r_i/r_o)^2}{\left[\lambda_o^2 + 2(1 + 2\lambda_o)(r_i/r_o)^2\right]^{\frac{1}{2}}} \qquad (5.1\text{-}2)$$

where $\lambda_o = \dfrac{U_o}{U_i - U_o}$

It is apparent that both parameters are solely determined by the area ratio and the initial velocity ratio. The character of jet mixing in a uniform duct is thus determined by the radius ratio and the initial velocity ratio of the primary jet to the secondary flow.

5.1.2 Results and Discussion

The computer model described in section 4.3.1 has been used to predict the flows of the air jet mixing in two uniform ducts measured by Razinsky and Brighton (1971) as well as the water jet mixing tested by Sanger (1968a). The geometries of the ducts and the inlet flow conditions are listed in Table 5.1-1. All the results for comparison

were obtained from an IBM 370/158 computer using a 14 x 14 grid. However, the effect of the number of grid lines being employed on the predicted result was studied and discussed

<u>The mean axial velocity prediction</u> The axial velocity profiles at various stations downstream of the nozzle exit are of significant importance in the studies of confined jet mixing. They indicate the degree of mixing between the two streams as well as the degree of entrainment. Fig. 5.1-1 presents the predicted velocity profiles, non-dimensionalized by the area-mean velocity U_m , as compared with the four combinations of inlet velocity ratio and radius ratio reported by Razinsky and Brighton (1971) [see Table 5.1-1]. Fig.5.1-2 shows the comparison of predicted and measured centre-line velocity decays. The agreement between the prediction and the measurement is fairly good despite the fact that no detailed information regarding the inlet turbulent kinetic energy and energy dissipation rate was reported. The inlet k-profile was calculated from the r.m.s. velocity $\sqrt{\overline{u'^2}}$ by assuming isotropic turbulence in both primary and secondary flows, i.e.

$$k_{in} = \frac{3}{2}\,\overline{u'^2_{in}} \qquad (5.1\text{-}3)$$

The inlet ε profile was calculated via

$$\varepsilon_{in} = \frac{k_{in}^{3/2}}{l_{in}} \qquad (5.1\text{-}4)$$

Fig.5.1-1(a)
Comparison of predicted velocity variation in mixing duct with experimental data from Razinsky and Brighton, $\frac{U_i}{U_o} = 3$, $\frac{r_i}{r_o} = \frac{1}{3}$.

Fig. 5.1-1(b)

Comparison of predicted velocity variation in mixing duct with experimental data from Razinsky and Brighton, $\frac{U_i}{U_o} = 10$, $\frac{r_i}{r_o} = \frac{1}{3}$.

Fig. 5.1-1(c)

Comparison of predicted velocity variation in mixing duct with experimental data from Razinsky and Brignton, $\frac{U_i}{U_o} = 3$, $\frac{r_i}{r_o} = \frac{1}{6}$.

Fig. 5.1-1(d)

Comparison of predicted velocity variation in mixing duct with experimental data from Razinsky and Brighton, $\frac{U_i}{U_o} = 10$, $\frac{r_i}{r_o} = \frac{1}{6}$.

Fig. 5.1-2(a)

Comparison of predicted centre-line velocity decay in mixing duct with experimental data from Razinsky and Brighton, $\frac{r_i}{r_o} = \frac{1}{3}$.

Fig. 5.1-2(b)

Comparison of predicted centre-line velocity decay in mixing duct with experimental data from Razinsky and Brighton, $\frac{r_i}{r_o} = \frac{1}{6}$.

where l_{in} is the length scale at the inlet section. Without better information, l_{in} may be taken as constant across the inlet section. In the prediction of Razinsky and Brighton's work, the following assumption was made in order to give a good agreement between prediction and measurement.

$$l_{in} = 0.005r_o{}^{*} \qquad (5.1\text{-}5)$$

The influence of the inlet length scale on the axial mean velocity field has been investigated by running the computer program with varying l_{in} while keeping other flow conditions unchanged. The results obtained from a radius ratio of 0.25 and inlet velocity ratio of 6.0 are shown in Fig.5.1-3 which compares the centre-line velocity decays. It is apparent that a larger inlet length scale causes the velocity on the axis to decay at a faster rate, i.e. larger eddy size can lead to better mixing. However, the effect is relatively small over a large range of l_{in}.

<u>Pressure prediction</u> The static pressure rise in the mixing tube is of vital important in jet pump performance. The capability of the computer model to predict accurately the static pressure variation along a uniform mixing tube is an essential indicator to determine the success of the model for this particular application. The predicted pressure variations along the duct wall of a uniform mixing tube with various radius ratios are compared in Fig. 5.1-4 with the experimental data from Razinsky and

* See Appendix A.9

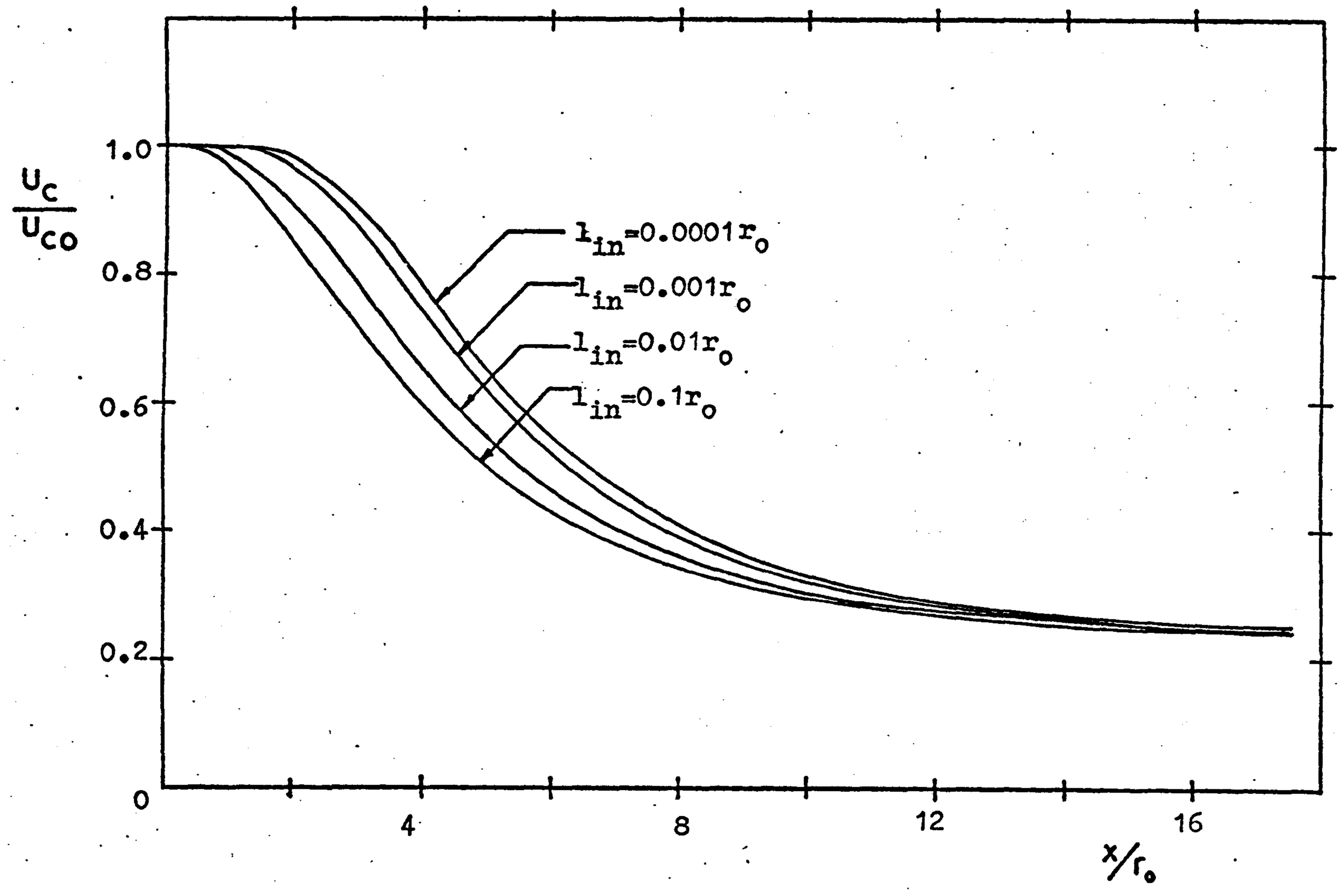

Fig. 5.1-3 The influence of inlet length scale on the predicted centre-line velocity variation, $\frac{r_i}{r_o}=0.25$, $\frac{U_i}{U_o}=6.0$.

Fig.5.1-4 Comparison of predicted pressure rise with data from Razinsky and Brighton, $U_i/U_o=10$.

Brighton (1971) for incompressible air flow. In the case of water jet mixing, predicted pressures are compared with the data from Sanger (1968a) as shown in Fig. 5.1-5. All the pressures were taken with reference to the inlet section and non-dimensionalized using the area-mean or the nozzle exit velocity. In general, the agreement between the predicted and measured distributions are acceptable. The influence of the inlet length scale on the static pressure distribution was studied by the computer program. The results are presented in Fig. 5.1-6. It appears that a larger inlet length scale will lead to an earlier recovery of pressure which is resulted from a better mixing due to larger eddy size at inlet. However, the effect on pressure variation over a wide range of inlet length scale is also relatively small.

<u>Turbulent energy and shear stress predictions</u> One major advantage of the computer model is its capability of predicting the turbulent behaviour throughout the whole flow field. Since the turbulent kinetic energy k and energy dissipation ε are the two dependent variables used in the transport equations, k and ε are calculated directly via the numerical procedure. The predicted k-distribution for the case of $\frac{U_i}{U_o} = 3$ and $\frac{r_i}{r_o} = \frac{1}{3}$ is presented in Fig.5.1-7. The profiles of k/U_m^2 at various stations downstream reveal that there is a very thin but high turbulent energy zone between the primary and secondary streams at the beginning of the duct. This can be explained as the result of vigo-

Fig.5.1-5(a) Comparison of predicted pressure rise with data from Sanger, $r_i/r_o=0.257$.

Fig.5.1-5(b) Comparison of predicted pressure rise with data from Sanger, $r_i/r_o=0.444$.

Fig. 5.1-6 The influence of inlet length scale on predicted pressure rise in mixing tube, $r_i/r_o=0.257$, data from Sanger.

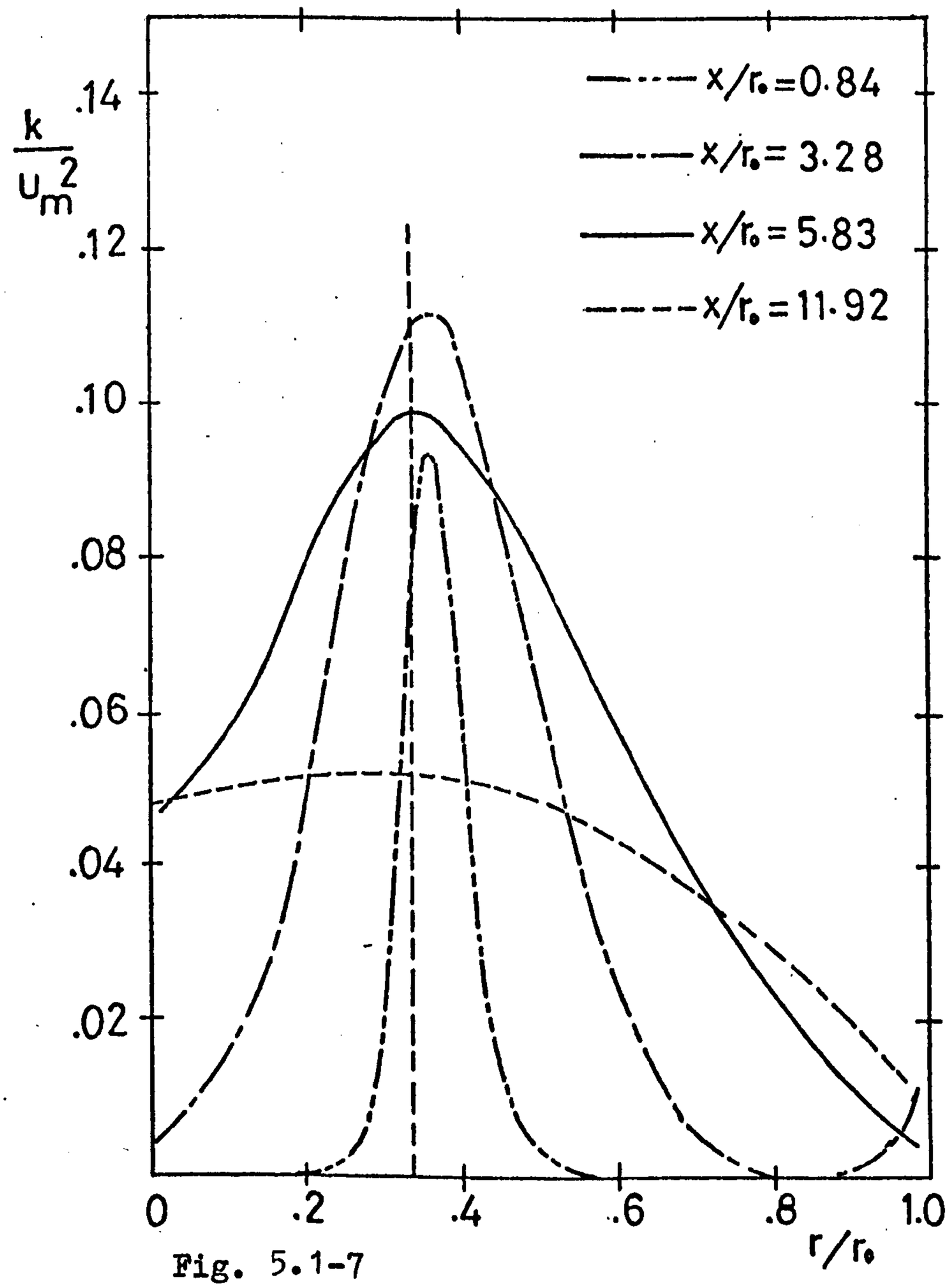

Fig. 5.1-7

Predicted radial distributions of turbulent kinetic energy in mixing duct, $\frac{U_i}{U_o} = 3$, $\frac{r_i}{r_o} = \frac{1}{3}$.

rous mixing between the two streams. The jet growth further down-stream is made clear by the spread of the high turbulent energy zone. The peak of the k-profile is increased at first and then decreases. This shows that the degree of mixing is intensified at first and then diminished gradually. The profile at about 12 radius downstream suggests that the mixing is almost completed there as no obvious peak is observed. Since there is no existing experimental data of k for comparison, experimental studies using a laser Doppler anemometer to measure the mean and the three orthogonal fluctuating velocities were carried out in a uniform mixing duct. The results are reported in Chapter 6 and compared with the predicted values.

The turbulent shear stresses which arise from the cross-correlation of fluctuating velocities as given by equation (2.4-1) can be re-written for cylindrical polar coordinates as

$$-\rho\overline{u'v'} = \mu_t \left(\frac{\partial U}{\partial r} + \frac{\partial V}{\partial z}\right) \qquad (5.1\text{-}5)$$

In the mixing duct case,

$$\frac{\partial U}{\partial r} \gg \frac{\partial V}{\partial z}$$

Thus

$$-\rho\overline{u'v'} = \mu_t \frac{\partial U}{\partial r} \qquad (5.1\text{-}6)$$

From equation (2.4-8),

$$\mu_t = C_\mu \rho k^2/\varepsilon \ ,$$

the Reynolds shear stress term can then be expressed as

$$\overline{u'v'} = - C_\mu \frac{k^2}{\varepsilon} \frac{\partial U}{\partial r} \qquad (5.1\text{-}7)$$

As U, k and ε are predicted throughout the whole flow field, $\overline{u'v'}$ can be evaluated everywhere. The predicted $\overline{u'v'}$ profiles across various stations of a uniform mixing duct are non-dimensionalized by U_m^2 and the results are compared with Razinsky and Brighton's (1971) data as shown in Fig. 5.1-8. The agreement appears to be satisfactory.

<u>The influence of grid spacing</u> To investigate the influence of the grid spacing on the predicted results, three different grids were used to predict the same flow situation with radius ratio of $\frac{1}{3}$ and velocity ratio of 10. The comparison of centre-line velocity decay and static pressure rise are shown in Fig. 5.1-9. It can be observed that by increasing the grid from 11 x 11 to 18 x 18, the results do not show drastic change, especially when the flow is far enough downstream. However, the computer time required for 18 x 18 grid is almost three times that of 11 x 11. It is thus necessary to choose an appropriate grid size based on the compromise of economy and accuracy.

Fig. 5.1-8(a) Comparison of Predicted Shear Stress with data from Razinsky and Brighton, $\frac{r_o}{r_i} = 3$, $\frac{U_o}{U_i} = \frac{1}{3}$

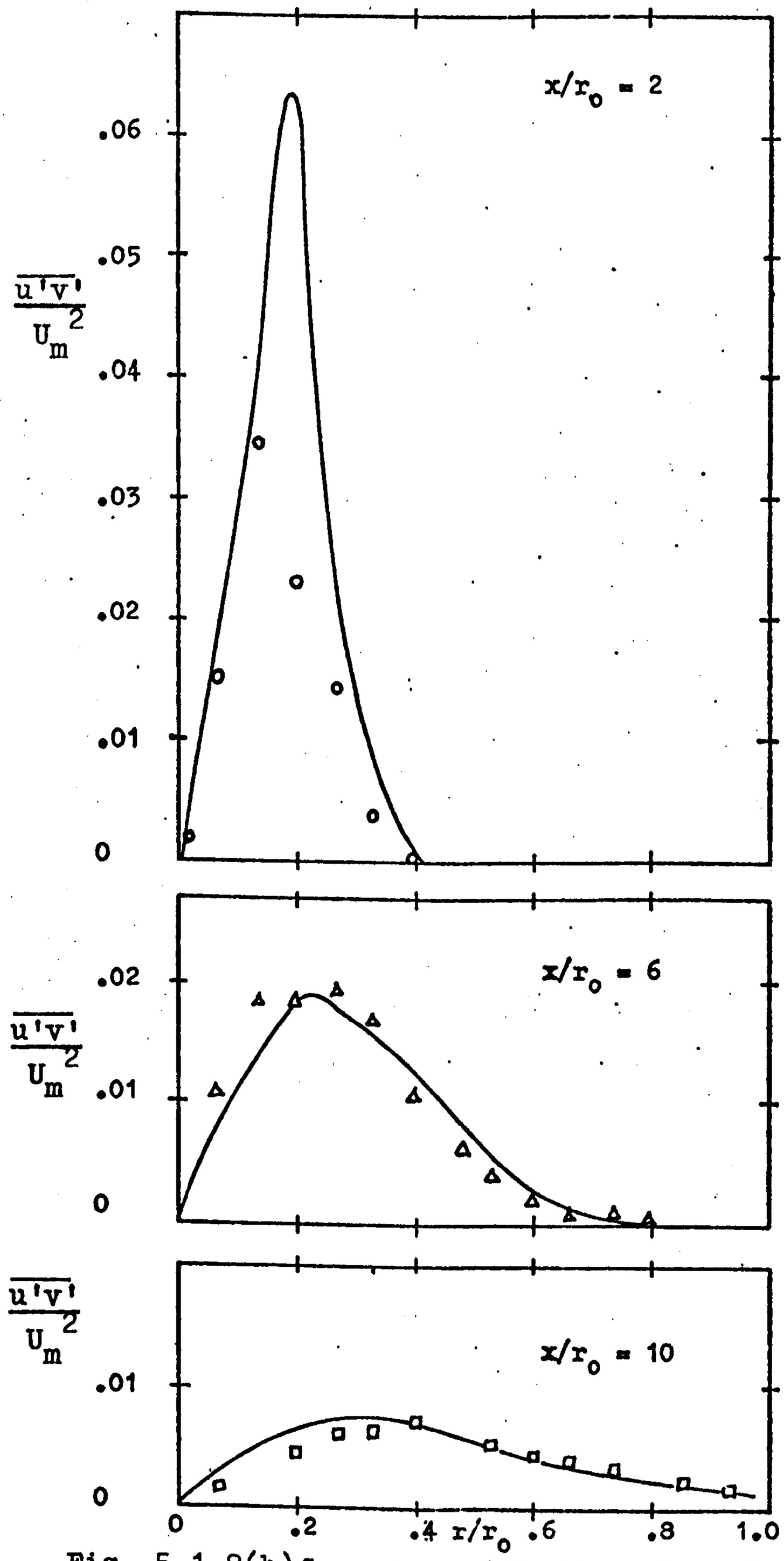

Fig. 5.1-8(b) Comparison of Predicted Shear Stress with data from Razinsky and Brighton, $\frac{r_o}{r_i} = 6$, $\frac{U_o}{U_i} = \frac{1}{3}$.

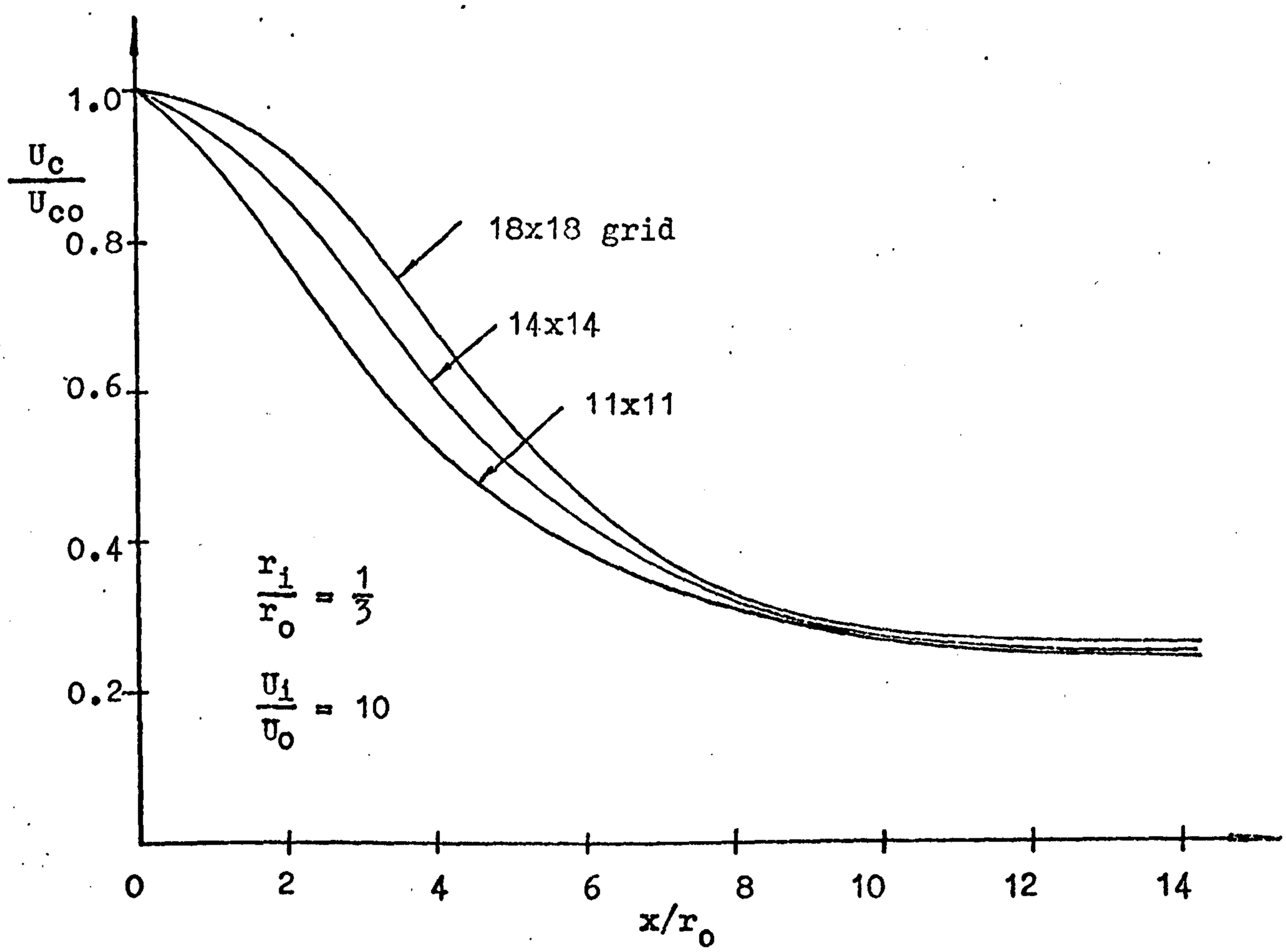

Fig.5.1-9 (a) The influence of grid on centre-line velocity.

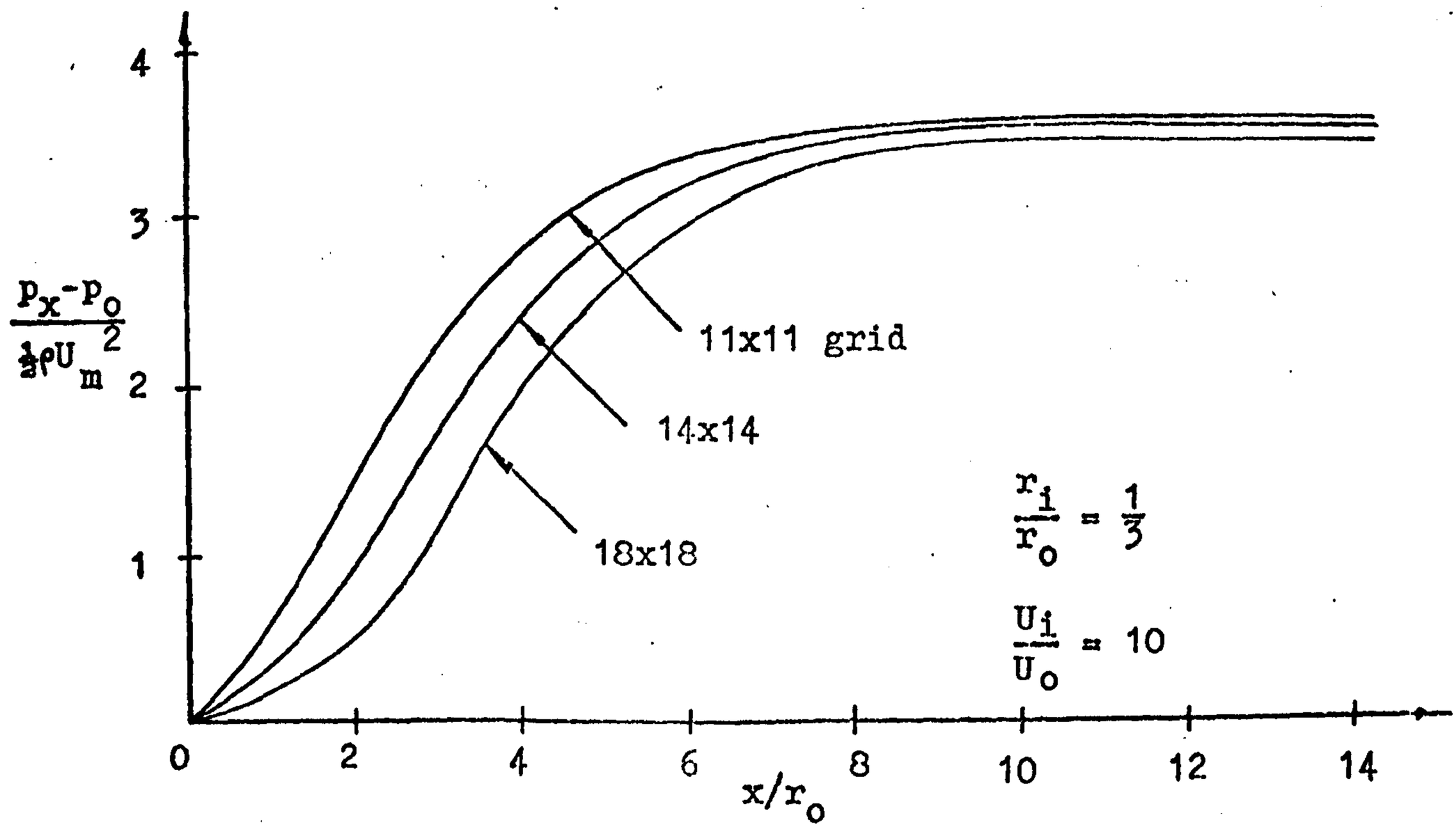

Fig.5.1-9 (b) The influence of grid on static pressure.

Some comments on the accuracy and possible improvements

In general, the agreement between prediction and measurement is acceptable for axial velocity, static pressure and turbulent shear stress. The accuracy might be improved, especially in the case of high velocity ratio and small radius ratio, by specifying a finer radial grid spacing in the mixing region where velocity gradient is high. To some extent, the empirical constants listed in Table 2.4-1 may have some effect on the accuracy of the prediction. By improving these constants, a better result can be expected. However, it is anticipated that large amount of measurements are necessary before a better set of constants can be established.

The results obtained so far reveal that the two-equation turbulence model is capable of predicting, with acceptable accuracy, the time-mean velocity and static pressure as well as the turbulent behaviour of the flow in an uniform mixing duct. The next task is to apply the model to predict the flow in a typical jet pump mixing tube with a secondary inlet region where flow area is reducing and the nozzle is placed at some distance upstream of the inlet section of the mixing duct.

5.2 Flow in Typical Mixing Tube Including Secondary Inlet Region

5.2.1 Introduction

The geometrical configuration of a typical jet pump mixing tube with nozzle exit placed in the varying-area

inlet region is shown in Fig. 4.3-3. A computer model which simulates the mixing tube together with such a secondary inlet region is developed and described in section 4.3.2. The model was used to predict the flows in the domain and compared with the experimental data from Sanger (1968a). Flow conditions were varied so that their effects on the performance were discussed. All the predictions were obtained using a 26 x 12 grid.

5.2.2 Results and Discussion

The computer model was used to predict two mixing tube tested by Sanger (1968a). The geometries of the two mixing tube A and B are listed in Table 5.2-1.

Mixing Tube	d_t(m)	d_n/d_t	s/d_t	R_o(m)	R_i(m)
A	0.0342	0.257	1.05	0.127	0.165
B	0.0342	0.444	0.96	0.127	0.1903

Table 5.2-1 Geometries of mixing tubes used for prediction

The predicted pressures along the duct wall were plotted and compared with the measured values obtained by Sanger as shown in Fig. 5.2-1. It is clearly demonstrated that the correlation between the predicted and the measured values is fairly good. The predicted pressure profiles for various flow ratios in mixing tube A are also presented in Fig. 5.2-2. The results shows that the locations of minimum and maximum pressure points are closer to the nozzle exit at lower flow ratio. As the flow ratio increases, these locations move further downstream from

Fig.5.2-1(a) Comparison of predicted static pressure rise with data from Sanger, $\frac{d_n}{d_t} = 0.257$, $\frac{s}{d_t} = 1.05$, M=3.5.

Fig. 5.2-1(b) Comparison of predicted static pressure rise with data from Sanger, $\frac{d_n}{d_t} = 0.444$, $\frac{s}{d_t} = 0.96$, $M=1.4$.

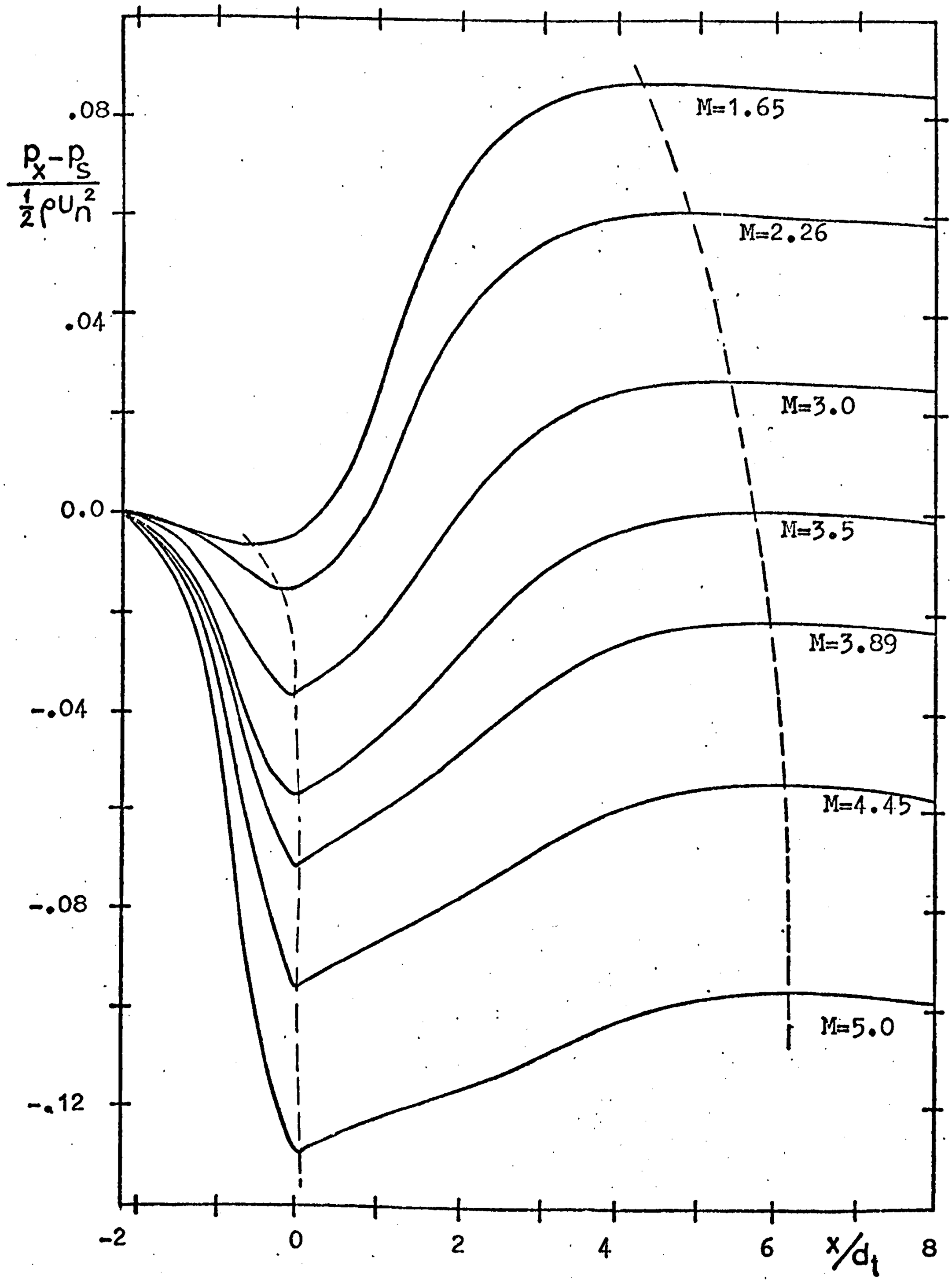

Fig.5.2-2 Predicted pressure profiles in mixing tube for various flow ratios, $\frac{d_n}{d_t} = 0.257$, $\frac{s}{d_t} = 1.05$.

the nozzle exit. This tendency is more obvious for the maximum pressure point. It is also observed that the pressure in the mixing tube increases more abruptly in the case of smaller flow ratio possibly due to larger initial velocity ratio between the primary and the secondary flows which leads to a more vigorous mixing.

It may be concluded that for the same nozzle to mixing tube area ratio, a higher flow ratio will require a longer mixing tube to achieve the maximum possible pressure rise. This discovery explains the inconsistency of the optimum mixing tube lengths recommended by various authors as the flow conditions under investigations differ widely.

To ensure that the prediction is acceptable for a wide range of flow ratios, the pressure rise in the constant diameter mixing tube is non-dimensionalized by $\frac{1}{2}\rho U_n^2$ and plotted against the flow ratio so as to compare with Sanger's data. Fig. 5.2-3 shows a satisfactory comparison between the prediction and the measurement.

The predicted streamwise velocity profiles across various flow sections throughout the whole flow field are shown in Fig. 5.2-4. Comparison for two different flow ratios is also shown. The centre-line velocity decays are shown in Fig. 5.2-5. The results show that the centre-line velocity decays faster as flow ratio reduces. If the centre-line velocity decay is taken as a measure of the degree of mixing, then it can be concluded that mixing is completed earlier in the case of a

Fig.5.2-3 Comparison of predicted and measured pressure rise in mixing tube, $\frac{d_n}{d_t}=0.257$, $\frac{s}{d_t}=1.05$.

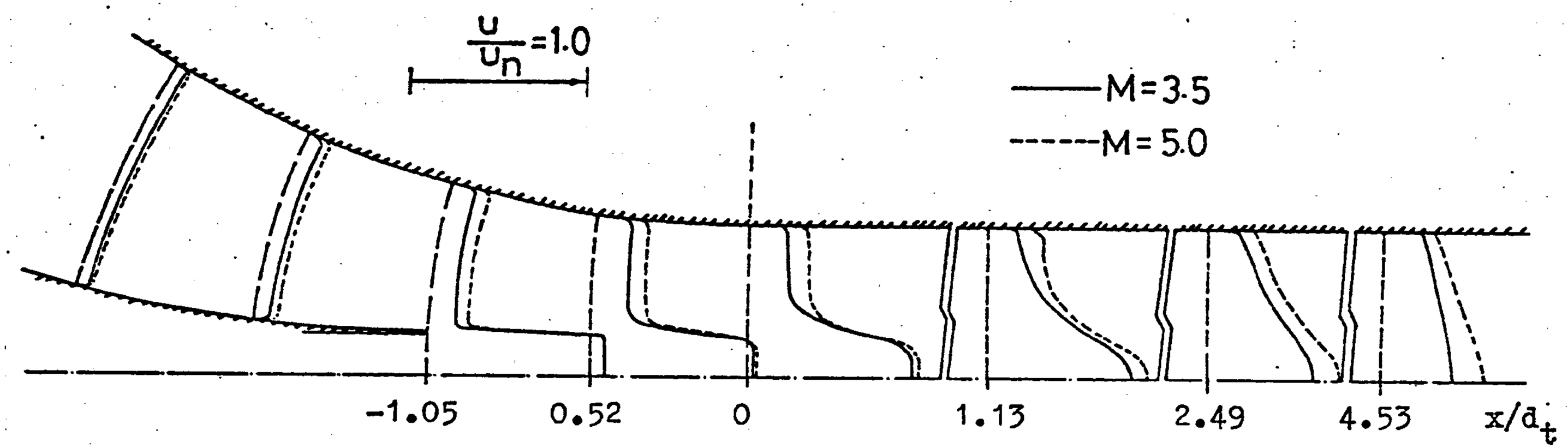

Fig. 5.2-4 Predicted streamwise velocity profiles in mixing tube, $\frac{d_n}{d_t}=0.257$, $\frac{s}{d_t}=1.05$.

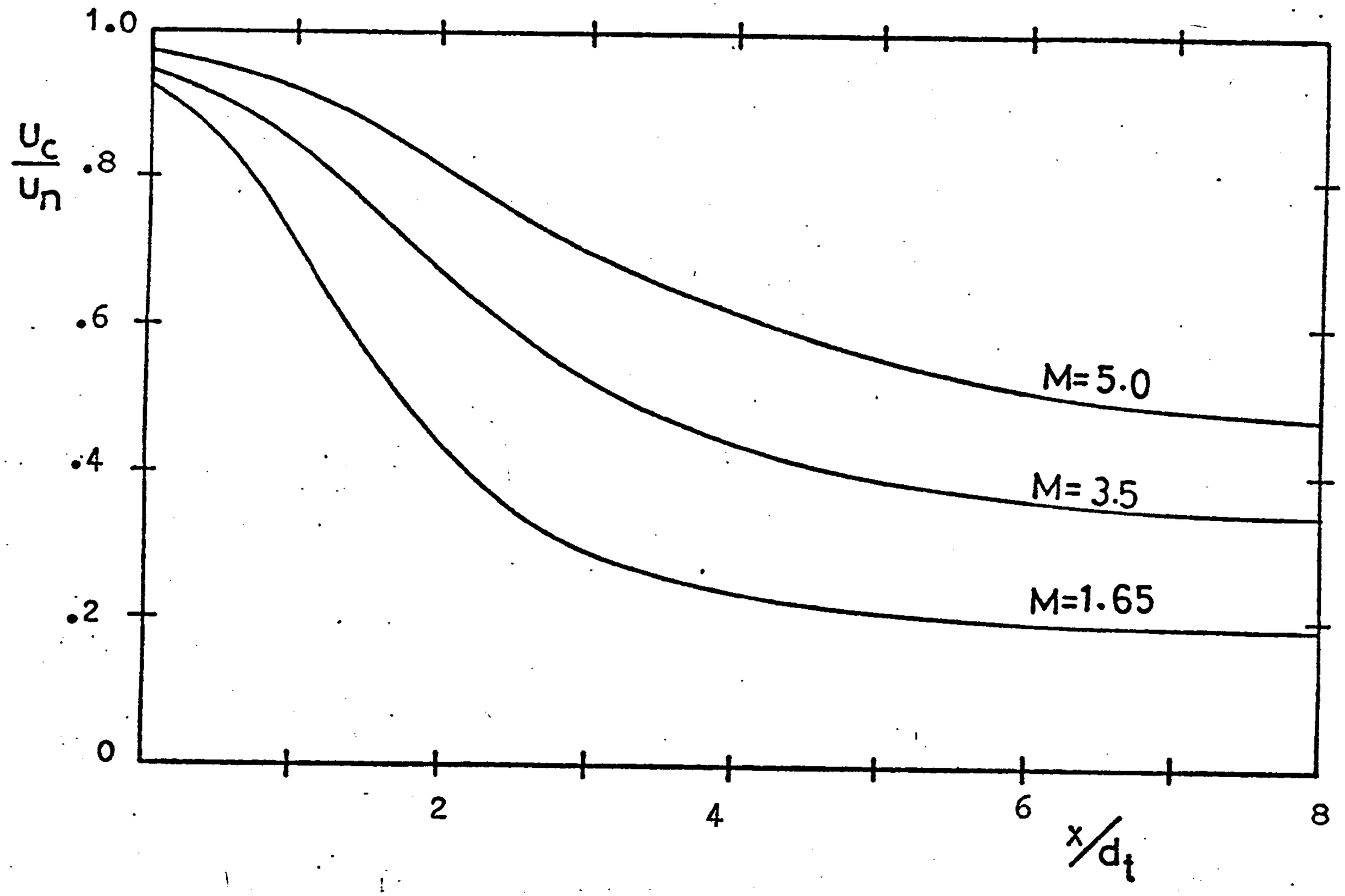

Fig. 5.2-5 Predicted centre-line velocity decay in mixing tube, $\frac{d_n}{d_t}=0.257$, $\frac{s}{d_t}=1.05$.

lower flow ratio. A longer mixing tube is thus required for a higher flow ratio. This has coincided well with the conclusion drawn from the pressure prediction.

Although no detailed information is given for the turbulent intensity or turbulent kinetic energy distribution at the inlet in Sanger's work, uniform k-profile were assumed for nozzle exit and secondary inlet region as follows.

$$k_n = 0.001U_n^2 \ * \qquad (5.2\text{-}1)$$

$$k_s = 0.003U_s^2 \ * \qquad (5.2\text{-}2)$$

where U_n and U_s are the mean velocities at nozzle exit and secondary inlet respectively. The choice was based on an estimation that the local turbulent intensities at the nozzle exit and the secondary inlet were around 3% and 4.5% respectively, and the flow was assumed to be isotropic turbulence. The inlet ε-profile was specified according to equation (5.1-4) with $l_{in} = 0.0025 d_t$.*

A typical k-distribution profile is presented in Fig. 5.2-6. It is clear that the results reflect reasonably well the turbulent behaviour of the confined jet mixing with the mixing zone having a higher turbulent kinetic energy.

5.3 Flow in A Conical Diffuser

5.3.1 Introduction

A conical diffuser is often used as the pressure head

* See Appendix A.9

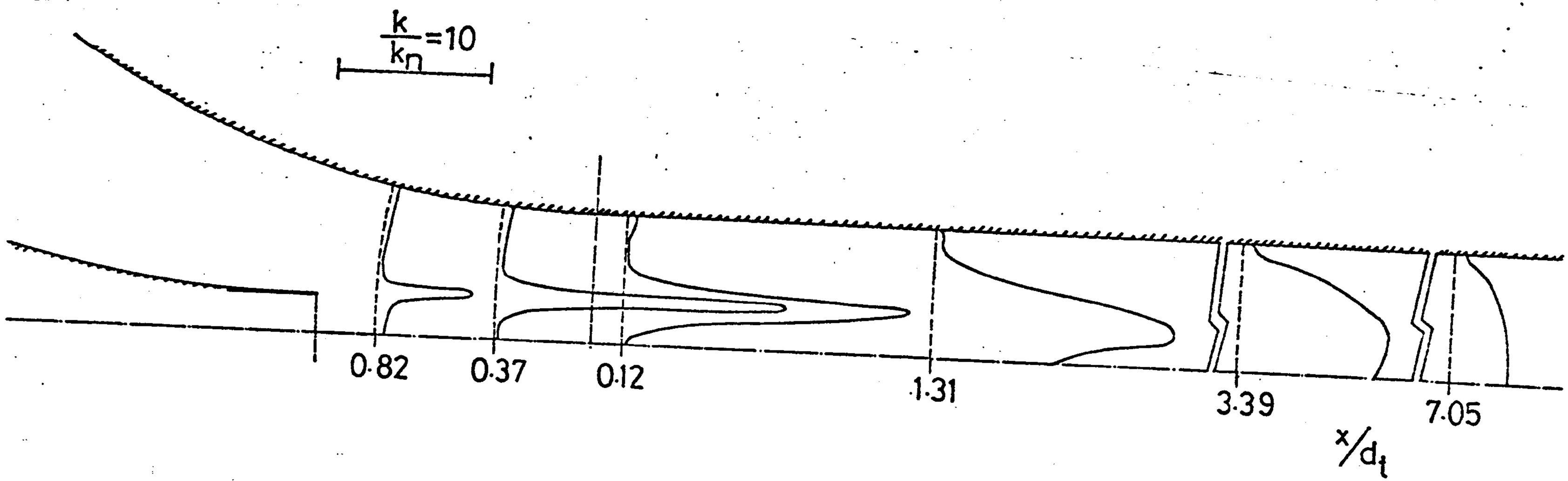

Fig. 5.2-6 Predicted turbulent intensity profiles in mixing tube, $\frac{d_n}{d_t}=0.257$, $\frac{s}{d_t}=1.05$, M=3.5.

recovery device in jet pump systems. McDonald et al (1966) tested various conical diffusers of different included angles and length to investigate their performances. Mueller (1964) studied a series of diffusers in jet pumps having included angles ranging from 3.5^{o} to 10.7^{o}. He concluded that for optimum jet pump performance with best efficiency, the diffuser with larger included angles must be used in conjunction with a longer mixing tube in order to prevent separation in the diffuser. The results of Mueller also reveal that the best efficiency occurs at a combination of 5° diffuser included angle with a mixing tube length of 6.5 diameters. By testing two sets of jet pumps, Sanger (1968a, 1968b) showed that a combination of a 6° diffuser included angle with a mixing tube length of 5.66 diameters gives a better performance than a 8.1^{o} diffuser combined with a mixing tube of 7.25 diameters long. It is apparent that the diffuser performance depends upon the inlet velocity profile which itself depends on a number of factors in the jet pump system, i.e., mixing tube length, nozzle spacing, area ratio and flow ratio.

Besides being used in a jet pump device, the conical diffuser is also widely used in many other fluid flow systems. A reliable prediction of diffuser flow behaviour and performance is certainly required.

The present study is to use the computer model described in section 4.3.3 to predict the flows in conical diffusers. The inlet velocity profile which is dictated by the upstream geometries and flow conditions is specified as the inlet boundary condition.

5.3.2 Results and Discussion

The computer programme for calculating the flow in conical diffuser has been run for two diffusers with included angles of 4° and 8° and inlet Reynolds Number of 1.25×10^5 so as to predict the experimental performance obtained by McDonald et al (1966). The two included angles are chosen based on the fact that most diffusers used in jet pumps are within the range of 3.5^o to 8°. As no information on turbulent intensity at the inlet was reported by the authors, the following inlet k-values and length scale were used as they produced good predicted results compared with the experimental data.

$$k_1 = 0.001U_1^2 \quad *$$

$$l_1 = 0.05r_1 \quad *$$

where 1 denotes the diffuser inlet section.

The results are presented in Fig. 5.3-1 where the predicted and the experimental pressures are compared. The prediction in the region up to 10 radius of the diffuser inlet section are in excellent agreement with the measurement. Further downstream, the prediction is slightly higher than the measurement in both cases.

To study the flow behaviour in the diffuser, mean velocity profiles at various sections were also plotted. Fig. 5.3-2 presents the mean velocity development of the 8° included angles diffuser with uniform inlet velocity.

* See Appendix A.9

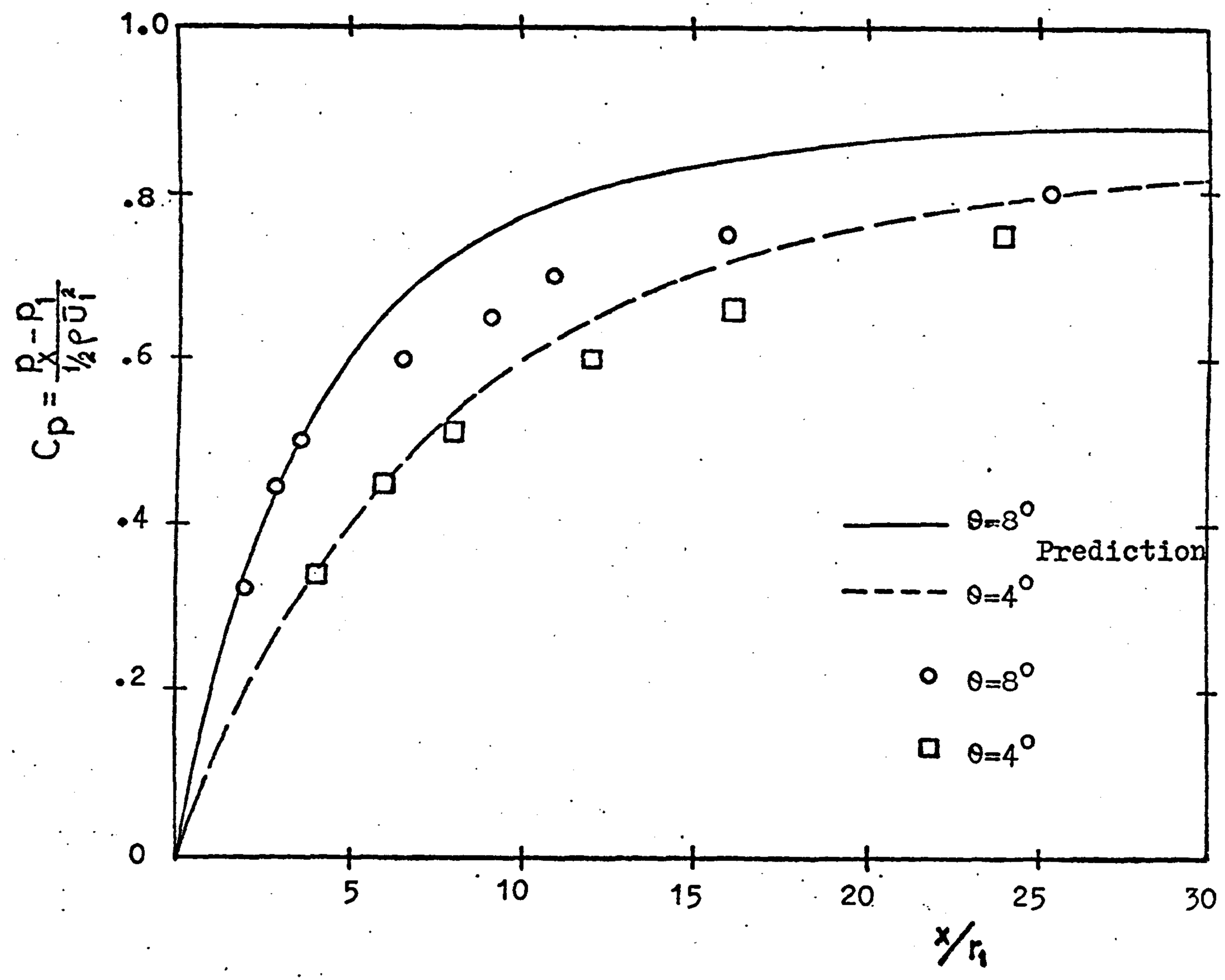

Fig. 5.3-1 Comparison of predicted pressure recovery in conical diffuser with Mcdonald's data, $Re_1=1.25\times10^5$.

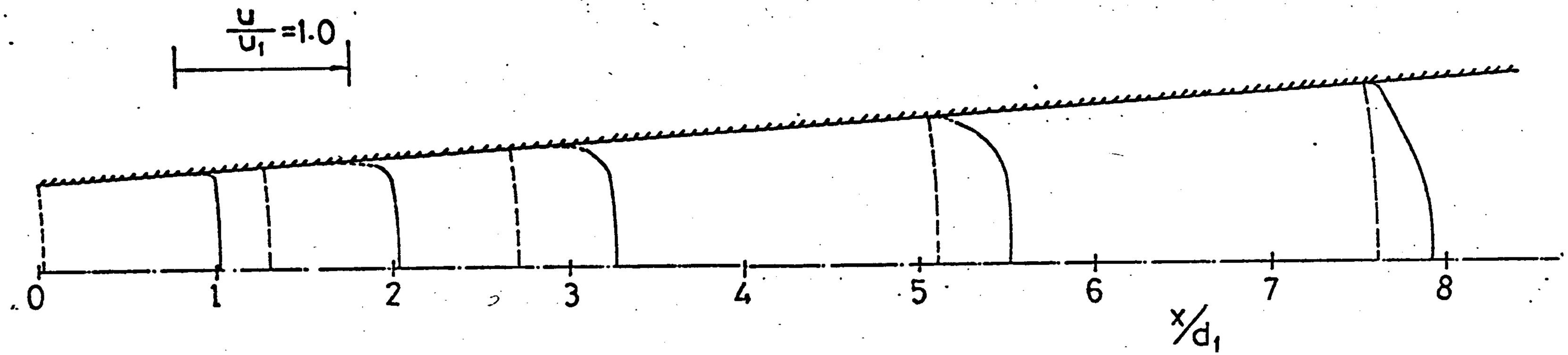

Fig. 5.3-2 Predicted mean velocity profiles in diffuser, $\theta=8^{\circ}$.

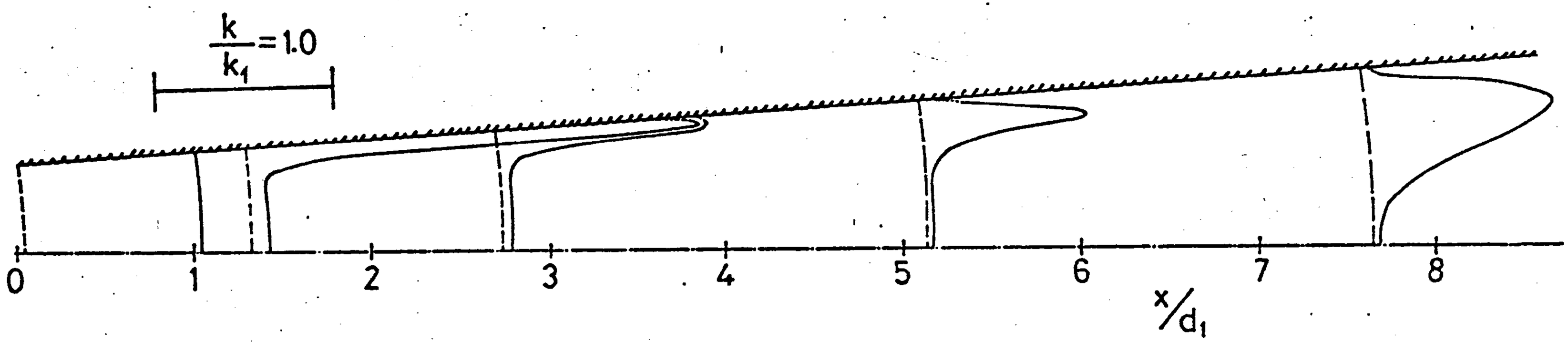

Fig. 5.3-3 Predicted turbulent kinetic energy in diffuser, $\theta=8^{\circ}$.

The results clearly demonstrate the development of the turbulent boundary layer in diffuser flow. Fig. 5.3-3 presents the non-dimensional turbulent kinetic energy profiles with an assumed uniform k-profile prescribed at the inlet. Once again, the turbulent boundary layer development is clearly shown. At the initial region of the diffuser, there is a very thin but high turbulent energy zone close to the diffuser wall. Further downstream, owing to the growth of turbulent boundary layer, the high turbulent energy zone increases its thickness with a reduction in its magnitude. The peak of the k-profile also moves further away from the wall as the flow developed downstream.

Diffuser flow in conjunction with a mixing tube as used in typical jet pumps were also studied. The jet mixing computer programme was run using various area ratios and flow ratios. The predicted velocity profiles at the end of the mixing tube were then used as inlet velocity profiles for the diffuser programme. Predictions were obtained for two jet pump configurations tested by Sanger (1968a). The detailed geometries are tabulated in Table 5.3-1.

Area Ratio	d_n/d_t	l_t/d_t	θ	s/d_t
0.066	0.257	7.25	8.1^o	0
0.197	0.444	5.66	6°	0

Table 5.3-1 Geometries of two jet pump diffusers used for prediction

Fig. 5.3-4 and 5.3-5 present the predicted static pressure along the wall for various flow ratios. Both cases show good correlation between predicted and measured values. All the diffuser predictions were obtained using a 14 x 12 grid.

The results so far reveal that the k- ε turbulence model is capable of predicting satisfactory results in conical diffusers not only by itself but also in conjunction with a mixing tube. They are expecially encouraging in view of the fact that both mean flow behaviour as well as turbulent structure are obtainable at the same time. Since the mean velocity and k-profiles at the inlet are prescribed as inlet boundary conditions, the programme can readily be used to investigate many other flow problems where the diffuser is one of the flow components.

5.4 The Prediction of Overall Performance of Typical Jet Pump

5.4.1 Introduction

The successful predictions of the flows in jet pump components using the computer models described in Chapter 4 have led to a conclusion that it is possible to predict the overall performance, i.e., pressure rise, efficiency, etc., in a typical jet pump system. Once the flow ratio of a jet pump is specified, the head ratio will be the only parameter to determine the efficiency of the pump. The prediction of the static pressure throughout the whole flow field will enable the head ratio and thus

Fig.5.3-4 Comparison of predicted axial static pressure rise with experimental data from Sanger, $\frac{d_n}{d_t}=0.257$, $\frac{l_t}{d_t}=7.25$, $\theta=8.1^\circ$

Fig.5.3-5 Comparison of predicted axial static pressure rise with experimental data from Sanger, $M=1.4$, $\frac{d_n}{d_t}=0.444$, $\theta=6°$, $\frac{l_t}{d_t}=5.66$.

the efficiency of the pump to be evaluated. Although it is theoretically possible to simulate the entire flow domain of a jet pump using a single computer program, this will require excessive storage space unless the job was run on a very large computer. As an alternative, the mixing tube program and the diffuser program were run successively to obtain a complete prediction.

5.4.2 The Procedure of Calculating the Overall Performance

The total head at any station x of a horizontal jet pump is given by

$$H_x = P_x + \tfrac{1}{2}\rho \bar{U}_x^{\,2} \qquad (5.4\text{-}1)$$

where P_x and $\bar{U}_x$ are the static pressure and the area-mean velocity at station x. Since the area-mean velocity at any station can readily be deduced from the continuity equation, the total head will solely depend on the static pressure at that station. The correct prediction of the static pressure along a jet pump is thus of vital importance to its design and performance analysis.

The present prediction procedure can be summarised as follows:

(i) Specify the geometry of a jet pump together with the primary and secondary inlet flow rates for the jet mixing program; run the program to obtain pressure and velocity fields

(ii) The velocity profile at the end section of the mixing tube is used as inlet velocity profile

for the diffuser program; the program is run to obtain the static pressure rise in diffuser

(iii) The static pressure from the secondary inlet to the exit of the diffuser is then plotted and the overall static pressure rise evaluated

(iv) The total head gained by the entrained fluid is obtained from static pressure rise and the increase in dynamic head, i.e.,

$$H_d - H_s = P_d - P_s + \tfrac{1}{2}\rho\overline{U}_d^{\,2} - \tfrac{1}{2}\rho\overline{U}_s^{\,2} \qquad (5.4\text{-}2)$$

(v) The total head lost by primary fluid can be calculated similarly

$$H_j - H_d = P_j - P_d + \tfrac{1}{2}\rho(\overline{U}_j^{\,2} - \overline{U}_d^{\,2}) \qquad (5.4\text{-}3)$$

However, the position of station j which is upstream of the primary nozzle is fixed arbitrary. From station j to the nozzle exit plane n, only frictional losses occur. The loss from j to n is relatively small compared with other losses and can often be ignored if the distance between j and n is small. The total head lost by the primary fluid can then be written as

$$\begin{aligned} H_j - H_d &= H_n - H_d \\ &= P_n - P_d + \tfrac{1}{2}\rho\overline{U}_n^{\,2} - \tfrac{1}{2}\rho\overline{U}_d^{\,2} \qquad (5.4\text{-}4) \end{aligned}$$

(vi) The head ratio N and the efficiency η can be calculated as follows:

$$N = \frac{H_d - H_s}{H_j - H_d} \qquad (5.4\text{-}5)$$

$$\eta = \frac{Q_2(H_d - H_s)}{Q_1(H_j - H_d)} \quad . \qquad (5.4\text{-}6)$$

5.4.3 Results and Discussion

Fig. 5.4-1 presents the predicted static pressure rise along the wall of a jet pump used by Sanger (1968a). The agreement between prediction and measurement is fairly good. The satisfactory prediction of the static pressure along the entire jet pump wall enable the head ratio and the efficiency to be calculated. Fig. 5.4-2 presents the predicted performance curves, plotted with head ratio and efficiency against the flow ratio, for a specific geometrical combination used by Sanger (1968a). Quantitatively, both the predicted head ratio and efficiency are slightly higher than the measurements obtained by Sanger. However, bearing in mind that minimum amount of empirical coefficients are used to evaluate these performances, the achievement is considered satisfactory. The prediction clearly shows the maximum efficiency point which agrees very closely with the measured value. With these achievement, the model may safely be used to predict the performance for any proposed geometry. Studies of new design proposals no longer have to rely on prototype testings or analyses based on empirical

Distance from secondary inlet,

Fig. 5.4-1 Comparison of predicted static pressure with Sanger's data, $\frac{d_n}{d_t}=0.257$, $\frac{s}{d_t}=1.05$, $M=3.5$, $\theta=8.1°$.

Fig.5.4-2 Comparison of predicted performance curves with Sanger's data, $\frac{d_n}{d_t}=0.257$, $\frac{s}{d_t}=1.05$, $\frac{l_t}{d_t}=7.25$, $\theta=8.1^{\circ}$.

coefficients obtained from other pumps. The computer model can, not only be used to investigate the influence of individual geometrical parameter on performance, but also be used to optimize the design. The application of the model for these purposes will be discussed in Chapter 7.

CHAPTER 6

EXPERIMENTAL INVESTIGATION

6.1 Introduction

Although jet pumps have been the subject of extensive experimental studies, comparatively little work has been devoted to detailed studies of the flow field behaviour occuring in various flow regions. Many experimental investigations were mainly concerned with performance testing, pressure distribution along the duct walls, measurement of losses in individual components, cavitation studies and operation of jet pumps under various conditions. As a result, design of jet pumps in the past has largely relied upon the empirical coefficients evaluated from other tests rather than based on the flow structure of a proposed pump. Although a typical jet pump consists of a primary nozzle, a mixing tube and a diffuser, it is the mixing tube where mixing between the two streams takes place and thus results in the pumping effect. A thorough study of the flow behaviour in a mixing tube is essential for the better understanding of the mixing process. The detailed measurements of mean and fluctuating velocity components in a mixing tube also provide a basis for validating any flow prediction and theoretical analyses.

Helmbold et al (1954) conducted experimental measurements of mean velocity profiles in both constant and variable area mixing tubes using a Pitot static tube. Curtet and Ricou (1964), in an attempt to study self-preservation

tendency in an axisymmetric ducted air jet, carried out measurements of mean velocity as well as axial and radial components of fluctuating velocity in a constant mixing duct using a hot wire anemometer. The most thorough measurement of confined jet mixing was probably done by Razinsky (1969). The measurements were conducted with two different radius ratios and each with two velocity ratios. The mean velocity was obtained using a Pitot static tube. Longitudinal velocity fluctuation and Reynolds stress were measured using a constant-temperature hot wire anemometer. However, no measurements of fluctuating velocity in the radial and tangential directions were reported.

The lack of experimental data in confined jet mixing is reflected in the incomplete measurement of fluctuating velocity components. A severe lack of information in the tangential fluctuating velocity prevents the thorough understanding of the turbulent structure in confined jet mixing. Moreover, owing to the difficulty in obtaining measurement in water jet mixing, almost all the existing data on confined jet mixing were obtained from air jets.

The present experimental investigation is to use a relatively new technique, laser Doppler anemometry (LDA), to measure the mean and fluctuating velocities in a constant diameter mixing tube with water as the working fluid. The LDA technique allows the measurements of axial mean and fluctuating velocities to be taken simultaneously. Through various suitable arrangements of the optical system, all

the three orthogonal fluctuating velocities are obtained using one laser Doppler anemometer system. The main aim of the present experimental program is to calculate the turbulent kinetic energy k from the data of the three fluctuating velocity components so as to compare it with the predicted k obtained from the two-equation k- ε model. Other important aspects include the studies of improving laser Doppler signals, criteria for selecting optical components, effects of frequency shifting and the limitation of LDA in this particular application.

6.2 The Jet Pump Test Rig

6.2.1 The Flow Circuit

A schematic diagram of the flow circuit is shown in Fig. 6.2-1. Water from a 60 x 90 x 60 cm storing tank was pumped by a 7.5 kW centrifugal pump to a 25mm primary pipe line. After passing through a control gauge valve V1 and a 10-μm filter (ALBANY series 770), the water could be made to flow solely through the primary pipe line, and ejecting through the nozzle by closing the valve V2 connecting the primary and secondary pipe lines. The high velocity jet from the primary nozzle was able to entrain a secondary flow through turbulent mixing in the mixing tube with valve V3 opened. When it reached a steady state, the primary and secondary flows Q_1 and Q_2 remained unchanged. This operation allowed the flow circuit to run as an ordinary jet pump for pressure testing. However, the flow circuit was also operated in such a way

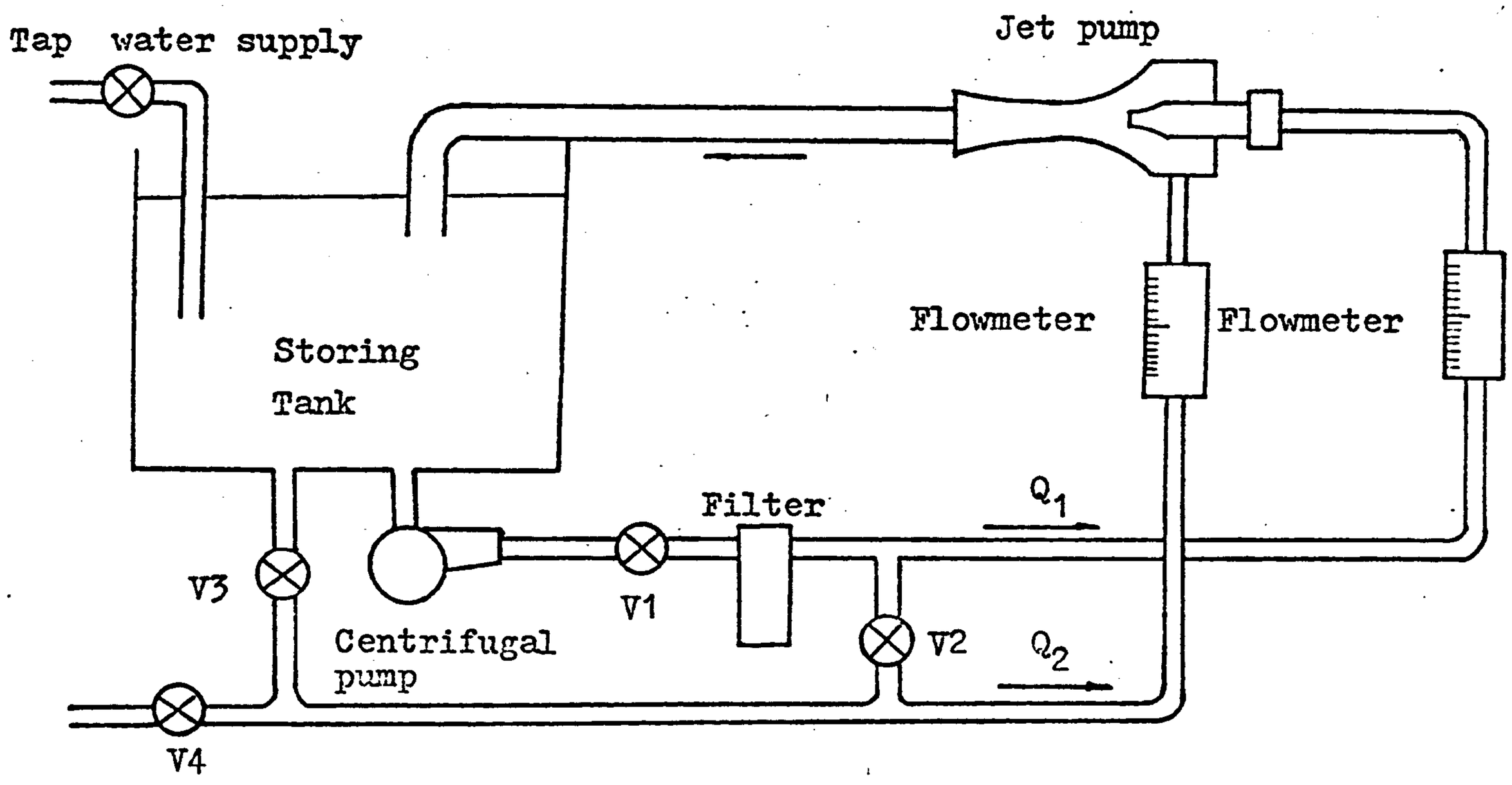

Fig.6.2-1 The experimental flow circuit.

that valve V2 was opened and valve V3 was closed so that the filtered water was diverted to both primary and secondary pipe lines. The two flows Q_1 and Q_2 after passing through two flowmeters, were led to mix in the mixing tube. On leaving the mixing tube, the combined fluids then flowed back to the storing tank via a 38.1mm discharge pipe line. Such operation ensured that both the primary and secondary flows entering the jet pump were being filtered by the 10μm filter. The filtering is crucial for the measurements of mean and fluctuating velocities using a laser Doppler anemometer as particles of diameter larger than 10μm will seriously affect the performance of the signal processor. By careful control of valves V1 and V2, an appropriate velocity ratio at the inlet of the mixing tube was achieved. This was important in view of the fact that the laser Doppler anemometer was unable to cope with very high velocity gradients. If the flow circuit is to be operated as a normal jet pump, the inlet velocity ratio will be well beyond 20 which is far too high for the L.D.A.

A thermometer was inserted into the water in the storage tank to check the temperature of the water. When the temperature of the water was higher than the atmospheric temperature by 5°C, the water was drained away by opening valve V4 and refilled with fresh tap water. The frequent change of water also ensured that the smaller iron oxide particles generated from the cast iron pump would not be accumulated to a high particle concentration affecting the normal performance of the anemometer.

A photograph of the basic jet pump test rig is shown in Plate 6.2-1.

6.2.2 The Components of the Test Pump

The test pump consists of the following components: (i) a primary nozzle, (ii) a suction chamber, (iii) a mixing tube entrance disc, and (iv) a test section. These four components are easily changeable so that the effect of dimensional alteration can be quickly and cheaply achieved. The complete jet pump is shown in Fig. 6.2-2.

Two nozzles of 6.5mm and 12.7mm exit diameter were machined from aluminium. The dimensions of the two nozzles are given in Fig. 6.2-3. The nozzle to be used for the jet pump experiment was screwed into the end of a piston tube which connected with the primary pipe. The piston tube was locked into an adjusting screw tube with external screw threads. The adjusting screw tube screwed into a sleeve which was fastened to the cylinder of the piston tube. A cylindrical suction chamber with an internal diameter of 100mm and length 90mm was then joined to the cylinder. A 25mm copper pipe was connected to the bottom of the suction chamber. To reduce the weight of the jet pump, all the parts mentioned above were made from aluminium. By turning the adjusting screw tube, it was possible to move the piston tube in or out of the cylinder so that the position of the nozzle in the suction chamber could be varied. Two sets of mixing tube entrance discs and mixing tube test sections were produced from clear perspex glass. The mixing tube test section was screwed into the entrance disc which fastened to the suction chamber. The dimensions

Plate 6.2-1 The jet pump rig

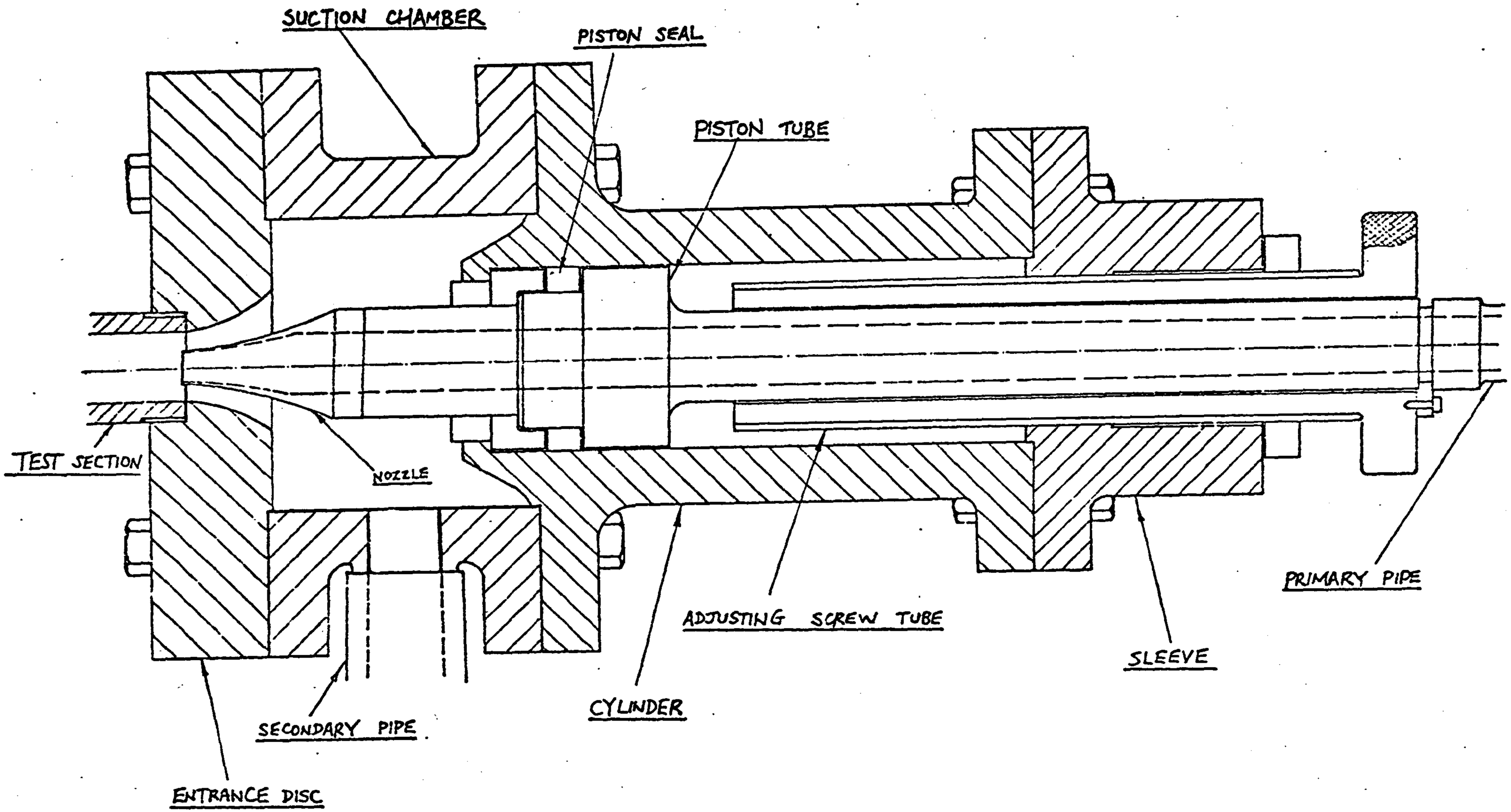

Fig.6.2-2 The suction chamber and nozzle adjusting mechanism.

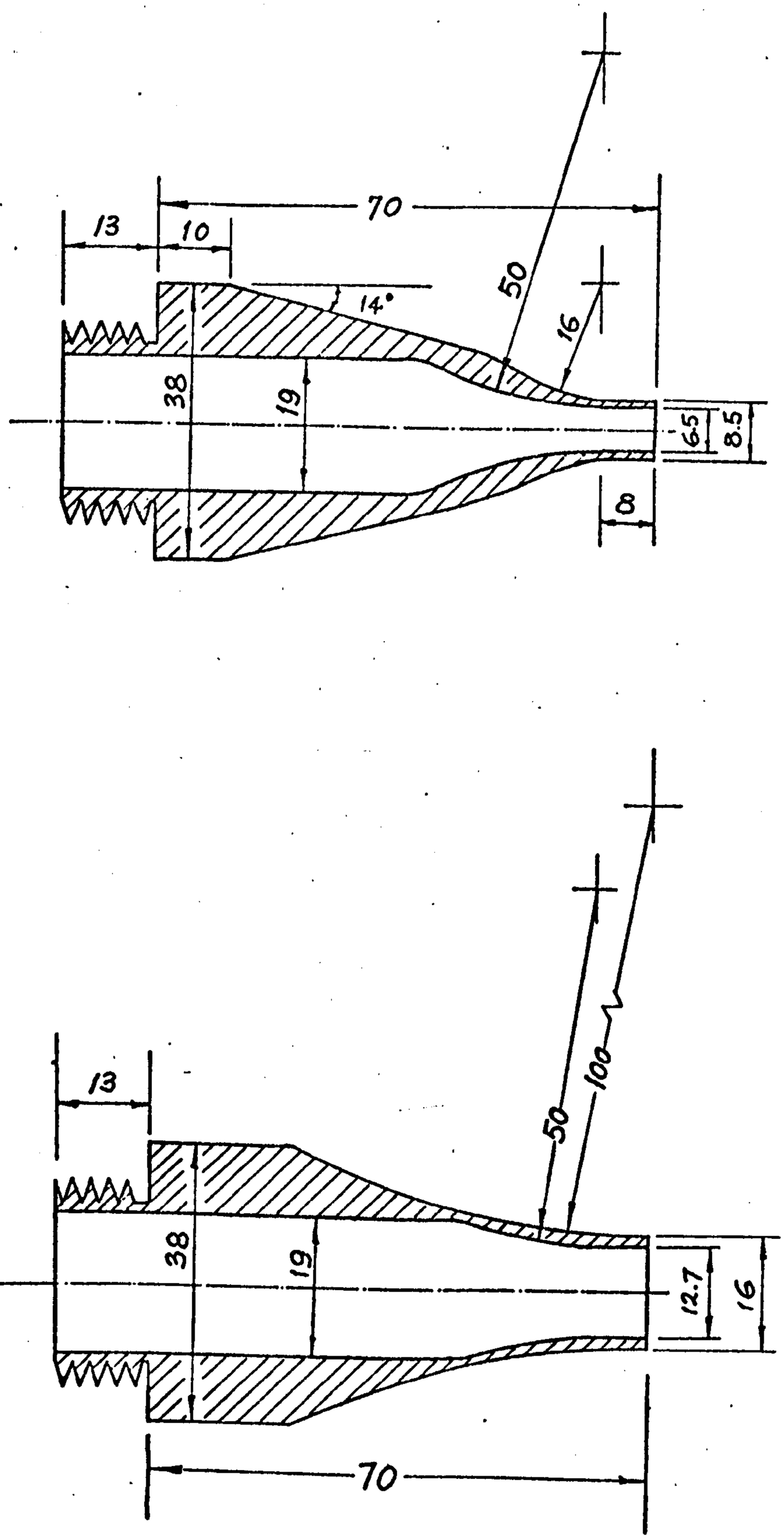

Fig.6.2-3 The nozzles (All dimensions are in mm.)

of these two mixing tubes and entrance discs are shown in Fig. 6.2-4 (a) and (b). The entrance disc provides a bell-mouth secondary inlet contour to the mixing tube.

The mixing tube with an internal diameter of 38mm was used for mean and fluctuating velocity measurements. By using the two nozzles described above, radius ratios of 0.334 and 0.171 were achieved. On the top surface along the length of this mixing tube, a perspex block for holding the probe was fixed. Threaded holes for the probe holder were drilled on this probe holding block at various stations with spacing indicated in Fig. 6.2-4 (a). The details of the probe and its holder are also shown in Fig. 6.2-4 (a). A photograph of the test section is shown in Plate 6.2-2. The probe was mainly used for locating the centre of the mixing tube cross-section so that the two laser beams would be adjusted to cross at the centre. The measuring position at any distance away from the centre was calculated by the movement of the optical unit which is discussed in section 6.4-2. In order to measure the axial velocity near to the nozzle exit, two slots were cut on the outer surface of the entrance disc to enable the laser beams to pass through without any blockage (see Plate 6.2-2).

The mixing tube with an internal diameter of 25mm was used for static pressure measurement. Static pressure taps of 2.0mm diameter were installed along the test section with spacings shown in Fig. 6.2-4 (b). The end of the mixing tube was joined to a short diffuser of 7° inclu-

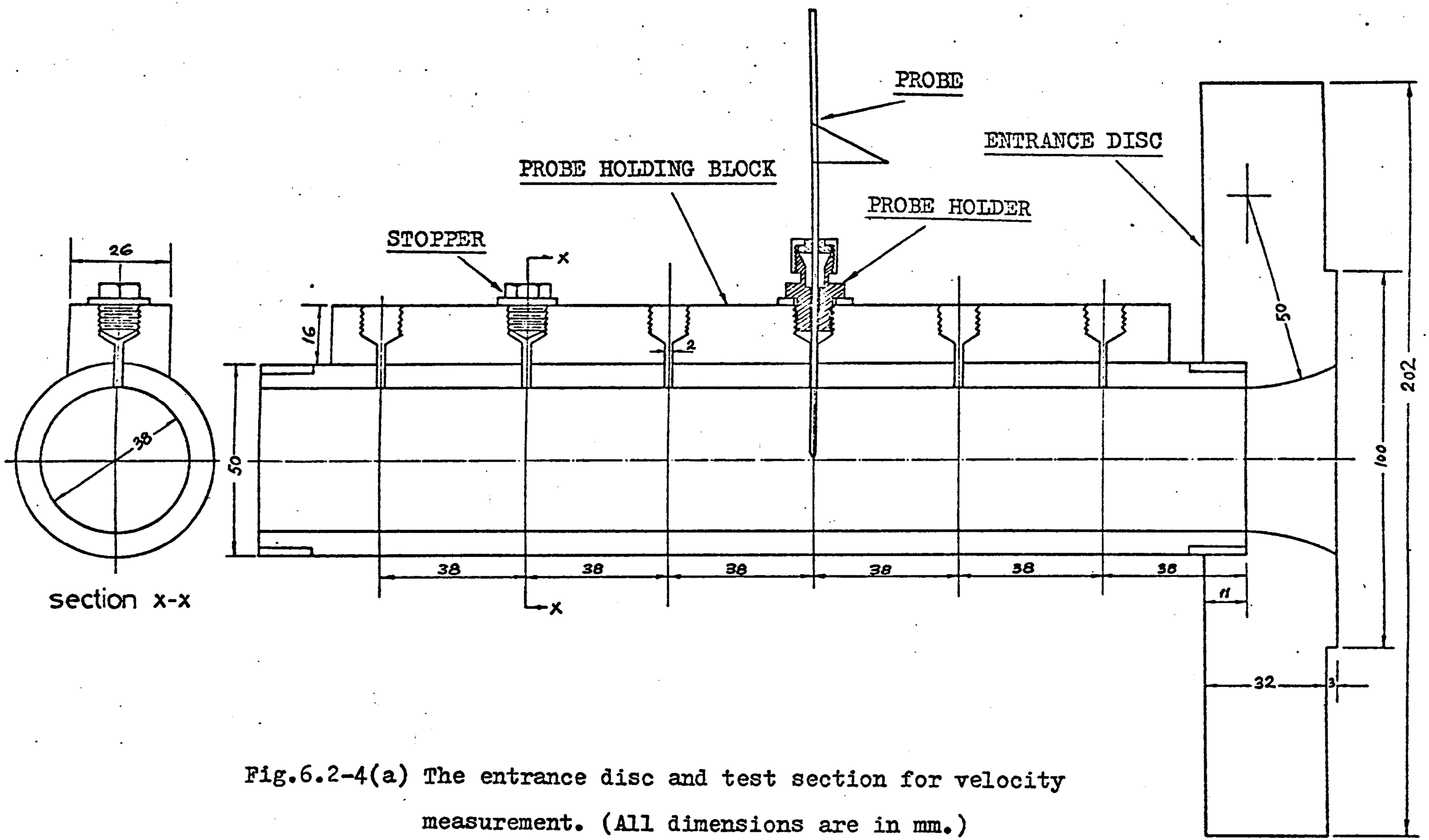

Fig.6.2-4(a) The entrance disc and test section for velocity measurement. (All dimensions are in mm.)

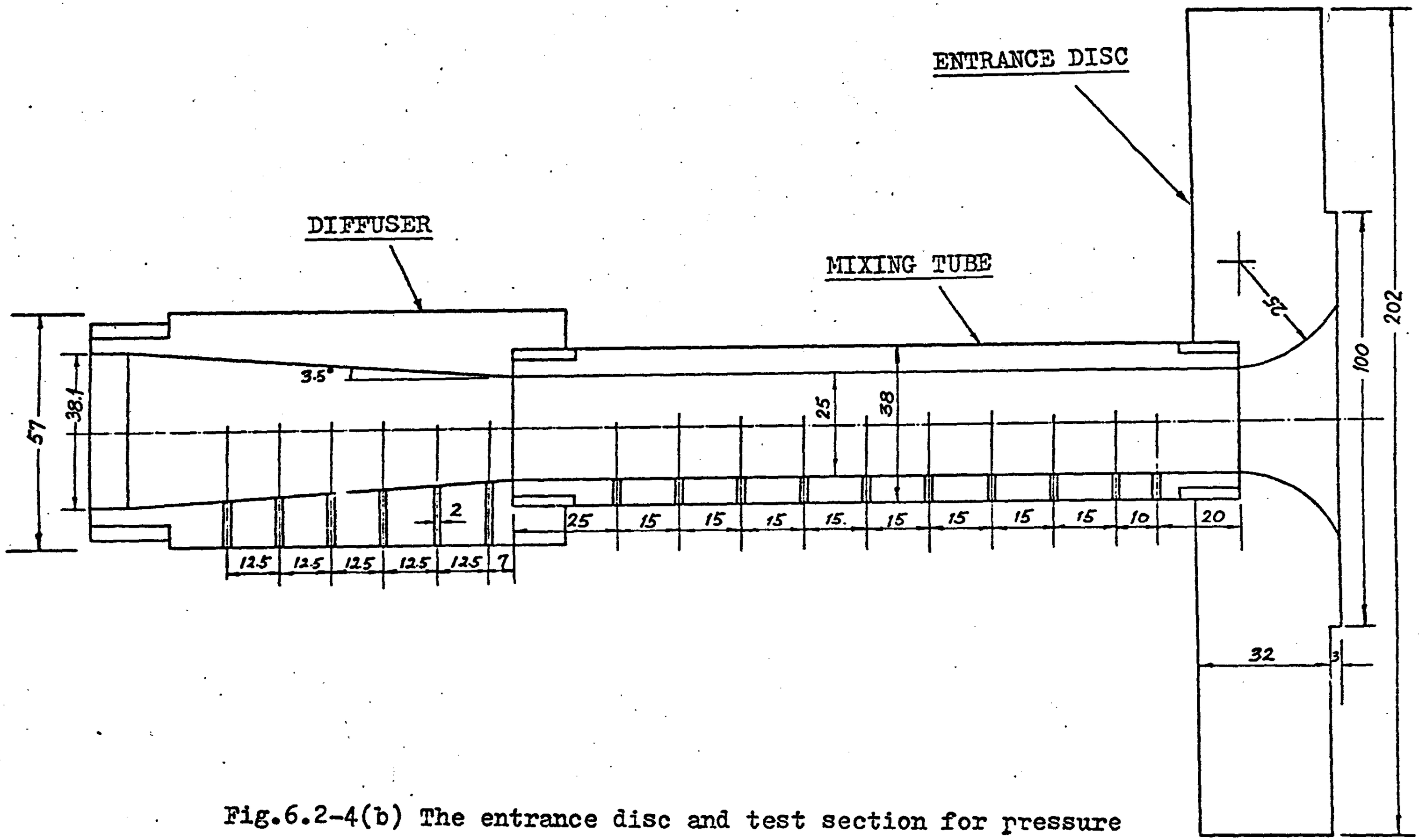

Fig.6.2-4(b) The entrance disc and test section for pressure measurement.(All dimensions are in mm.)

Plate 6.2-2 The test section for velocity measurement

Plate 6.2-3 The test section for pressure measurement

ded angle and an exit diameter of 38.1mm. A photograph of the test section is shown in Plate 6.2-3.

Both test sections were joined to a 38.1mm diameter copper pipe leading to the storage tank.

6.3 The Laser Doppler Anemometry

6.3.1 The Measurement of Turbulent Flows

The measurement of instantaneous velocity provides the necessary information for understanding the structure of turbulent flows. For many years, hot wire or hot-film anemometers have been used as the principal tools for obtaining turbulent flow informations such as r.m.s. velocity and velocity correlations. Although this technique has provided ample quantitative informations, it is limited to flows of low temperature, low speed and low turbulent intensity without recirculation. The development of laser Doppler anemometry represents a significant break-through in fluid flow measurement. The main advantage of such an optical measuring system is the non-contact probing which does not disturb the flow under investigation. Thus, laser Doppler anemometer is particularly favourable for measuring recirculating flows, flows in ducts of small dimension, where the hot wire or hot film is extremely difficult to set up and for hostile environments such as flames. However, laser Doppler anemometers require the wall of the test section to be transparent so that light beams can pass through.

In the present work, the laser Doppler anemometer was

chosen rather than the hot film anemometer for the measurement of mean and fluctuating velocities because

(i) laser beam passes through the flow without using any probe which will disturb the flow,

(ii) the relatively small mixing tube creates great difficulty in setting up a hot film probe in the flow,

(iii) the use of water as working fluid solves the seeding problem,

(iv) the Doppler frequency is directly proportional to the velocity enabling greater accuracy of measurement.

6.3.2 The Basic Principles of Laser Doppler Anemometry

The laser Doppler anemometry is based on the Doppler shift of the light frequency scattered by particles suspended in the fluid. The scattered light contains information about the velocity of the suspended particles which can be interpreted by photoelectronic means. The Doppler effect, which is named after Christian Doppler who discovered the frequency change of a moving source towards a stationary observer, forms the basic concept for the development of the laser Doppler anemometers.

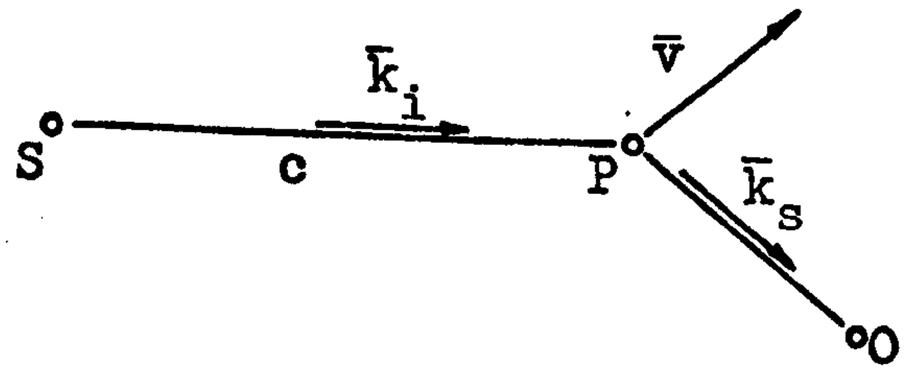

Fig. 6.3-1 Light scattered by a moving particle.

Fig. 6.3-1 shows light which is propagated from a fixed source S in the direction $\bar{k}_i$ and scattered by a particle at point P moving with velocity $\bar{v}$, the scattered light is detected by an observer O where $\bar{k}_s$ is the unit vector from P to O. The relative velocity of the light with respect to the moving particle P, c', will be

$$c' = c - \bar{v}\cdot\bar{k}_i \qquad (6.3\text{-}1)$$

where c is the velocity of light to a stationary observer. Thus, the light will arrive to the moving particle at a frequency,

$$f' = \frac{c'}{\lambda} = \frac{1}{\lambda}(c - \bar{v}\cdot\bar{k}_i) = f(1 - \frac{1}{c}\,\bar{v}\cdot\bar{k}_i) \qquad (6.3\text{-}2)$$

Now, the particle can be considered as a moving source emitting a light of frequency f'. The stationary observer at O will observe the light from a moving source with a wave length

$$\lambda'' = \frac{c - \bar{v}\cdot\bar{k}_s}{f'} \qquad (6.3\text{-}3)$$

The corresponding frequency is then

$$f'' = \frac{f'}{1 - \frac{1}{c}\,\bar{v}\cdot\bar{k}_s} \qquad (6.3\text{-}4)$$

Substituting equation (6.3-2) into equation (6.3-4) yields

the expression of the final frequency detected by the stationary observer at O,

$$f'' = \frac{f(1 - \frac{1}{c}\,\bar{v}\cdot\bar{k}_i)}{1 - \frac{1}{c}\,\bar{v}\cdot\bar{k}_s} \qquad (6.3\text{-}5)$$

The overall frequency shift is then given by

$$\Delta f = f'' - f$$

$$= \frac{\bar{v}\cdot(\bar{k}_s - \bar{k}_i)}{\lambda(1 - \frac{1}{c}\,\bar{v}\cdot\bar{k}_s)} \qquad (6.3\text{-}6)$$

Since the velocity of the moving particle $\bar{v}$ is negligible compared with c,

i.e.,

$$\frac{|\bar{v}|}{c} \doteqdot 0$$

thus,

$$\Delta f = \frac{1}{\lambda}\,\bar{v}\cdot(\bar{k}_s - \bar{k}_i) \qquad (6.3\text{-}7)$$

The frequency shift, Δf, which is also referred to as the Doppler frequency, f_D , is directly proportional to the particle velocity $\bar{v}$.

The laser, which emits highly coherent monochromatic light waves is the most suitable light source for the measurement of particle velocity utilising the above

principle.

6.3.3 The Optical Systems

In practice, it is more convenient to employ two incident light beams which cross at the measuring point in the flow. Appropriate optical components such as beam splitters, lens and filter may be arranged in different modes of operation. The most commonly used optical arrangements are "reference-beam" mode and "dual beam" mode.

The "Reference-Beam" Mode In the reference-beam mode, the laser beam is split into two beams and directed towards the measuring point by an optical unit which consists of a beam splitter and a convergent lens as shown in Fig. 6.3-2.

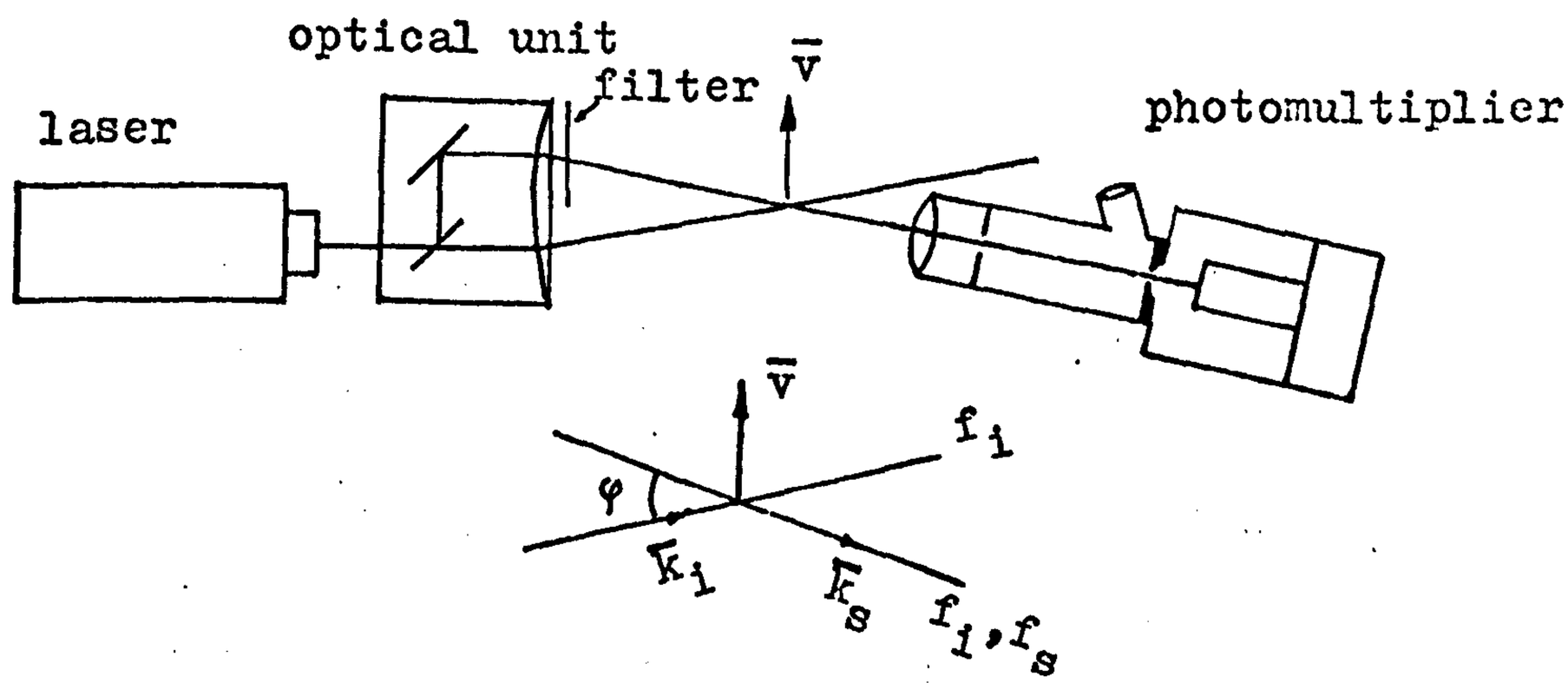

Fig. 6.3-2 Reference-beam mode

The intensity of the reference beam is reduced by a filter so as to optimize the quality of the Doppler signal. A photomultiplier is placed to face the reference beam so that the frequency difference between the reference

beam and the scattered beam can be detected. The frequency difference, according to equation (6.3-7), is

$$f_D = f_s - f_i = \frac{1}{\lambda}\,\bar{v}\cdot(\bar{k}_s - \bar{k}_i)$$

The photomultiplier then emits modulated current with a frequency equal to f_D. The velocity component measured by the above arrangement is parallel to $\bar{k}_s - \bar{k}_i$, or normal to the bisector of the beam intersecting angle φ. Its value can be calculated in terms of f_D , λ , and φ as follow

$$v = \frac{f_D \lambda}{2 \sin\frac{\varphi}{2}} \qquad (6.3\text{-}8)$$

<u>The "Dual Beam" or Fringe Mode</u> In this arrangement, the laser beam is split up into two incident beams of equal intensity and is brought to intersect at the place of measurement so that a measuring volume is formed. The scattered light signals of the incident beams are picked up from the same direction by a photomultiplier (see Fig. 6.3-3).

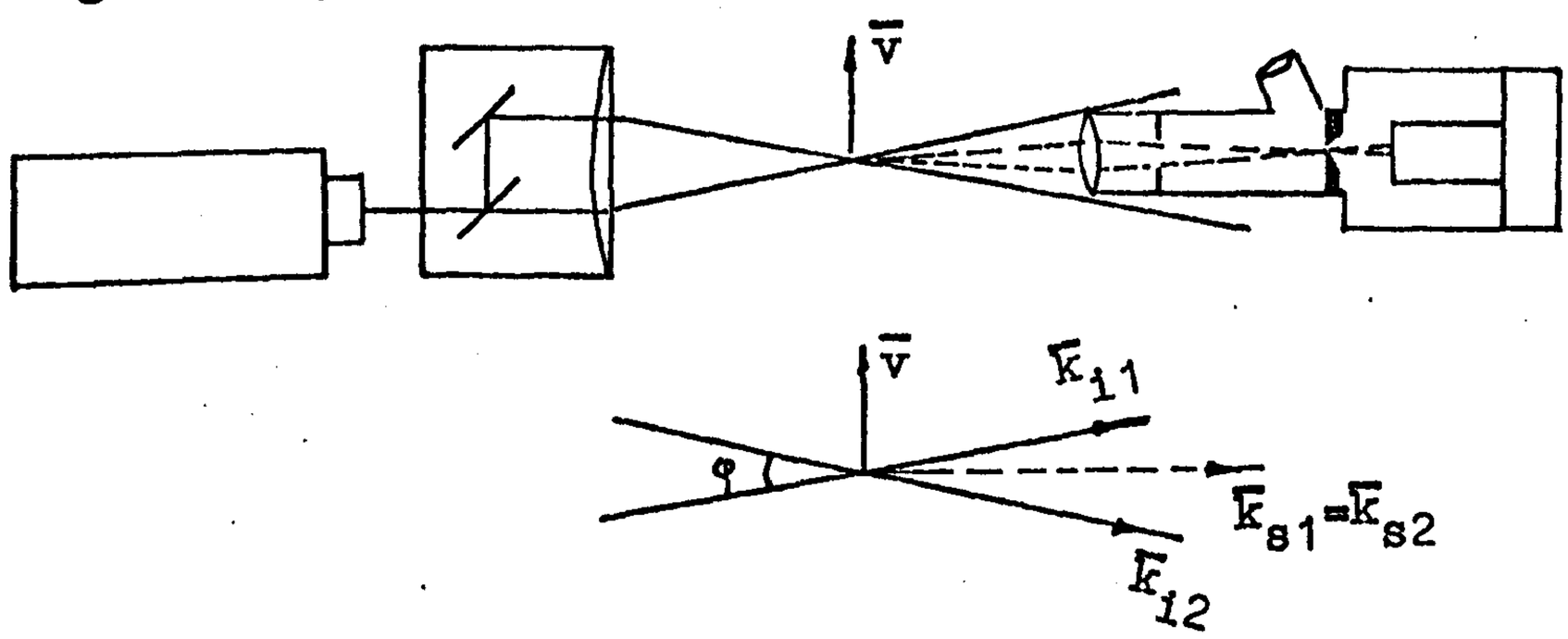

Fig.6.3-3 'Dual beam' or fringe mode.

In this case, each scattered beam has a frequency shift relative to the incident beam that it originates from, i.e.,

$$f_{s1} = f_{i1} + \frac{1}{\lambda}\bar{v}\cdot(\bar{k}_s - \bar{k}_{i1})$$

$$f_{s2} = f_{i2} + \frac{1}{\lambda}\bar{v}\cdot(\bar{k}_s - \bar{k}_{i2})$$

The beat frequency detected by the photomultiplier $f_D = f_{s1} - f_{s2}$ can be deduced to

$$f_D = f_{i1} - f_{i2} + \frac{1}{\lambda}\bar{v}\cdot(\bar{k}_{i2} - \bar{k}_{i1}) \qquad (6.3\text{-}9)$$

If the incident beams arrived at the measuring point without any frequency pre-shift, $f_{i1} = f_{i2}$, and f_D becomes

$$f_D = \frac{1}{\lambda}\bar{v}\cdot(\bar{k}_{i2} - \bar{k}_{i1}) \qquad (6.3\text{-}10)$$

It is obvious that the beat frequency f_D is independent of the direction of detection and the velocity component measured is parallel to $\bar{k}_{i1} - \bar{k}_{i2}$, i.e., normal to the bisector of the beam intersecting angle φ. The velocity can be calculated in terms of f_D , λ and φ according to equation (6.3-8).

<u>The Effect of Refractive Index</u> When a beam of light passes obliquely from one medium to another of different refractive index, its direction is altered and its velocity

and wavelength also changed. The various properties in air and in a fluid of refractive index η is given in Table 6.3-1.

Property	Air	In the Fluid
Intersecting Angle	φ	φ'
Velocity of light	c	c/η
Frequency of light	f	f
Wavelength of light	$\lambda = \frac{c}{f}$	$\lambda' = \frac{\lambda}{\eta}$

Table 6.3-1 Various properties in air and in a fluid of refractive index η

Thus, if the beams are intersected in a fluid of refractive index η and the angle between the beams φ' is measured in the fluid, the velocity, according to equation (6.3-8) will be

$$v = \frac{f_D \lambda'}{2\sin\frac{\varphi'}{2}} = \frac{f_D \lambda}{2\eta\sin\frac{\varphi'}{2}} \qquad (6.3\text{-}11)$$

The "Interference Fringe" Model of the Dual Beam Mode

The dual beam mode is also termed as "fringe" mode because the interference of the two light beams forms a fringe pattern at the intersection volume. This model for analysing laser Doppler signals was first proposed by Rudd (1969). Fig. 6.3-4 shows two coherent light beams having plane wave fronts intersecting at an angle φ. Where the path lengths travelled by the two beams are equal, or

differ by a whole number of wavelengths, the intensities of the beams will add constructively to give a bright fringe. While a difference of path length by ½ of a

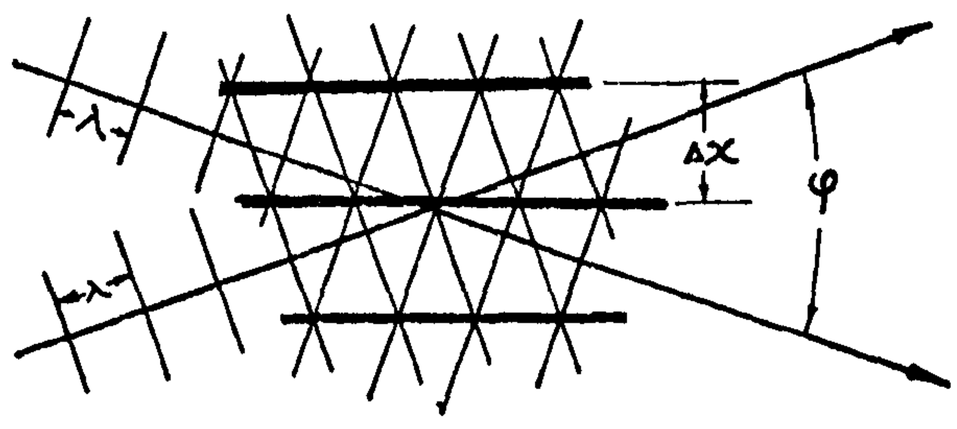

Fig. 6.3-4 Fringe pattern of beam intersection

wavelength will add destructively to give a dark fringe. An interference fringe pattern which consists of a series of bright and dark fringes is formed in the intersection region. From the above diagram, it is obvious that the following relationship between fringe spacing Δx and wavelength of the light λ can be obtained.

$$\Delta x \sin\frac{\varphi}{2} = \frac{\lambda}{2} \qquad (6.3\text{-}12)$$

A particle which moves across the fringe pattern with a velocity v will scatter light whose intensity will vary at a frequency

$$f_D = \frac{v}{\Delta x} = \frac{2v\sin\frac{\varphi}{2}}{\lambda} \qquad (6.3\text{-}13)$$

The relationship between the signal frequency and the particle velocity obtained is exactly identical to that obtained by a Doppler consideration.

In this experimental work, the dual beam mode of optical arrangement was chosen based on the following reasons:-

(1) It is relatively easier to set up the optical system as the laser, the optical unit and the photomultiplier are mounted on the same optical axis; the changes required in measuring different directions involves only minimal re-arrangement of the components.

(2) Since the beat frequency is independent of the direction of detection, the position of the photomultiplier does not require to be precise; good signals can be obtained over a relatively wide angle of detection.

6.3.4 Methods for Frequency Signal Processing

A typical signal from the photomultiplier consists of a low frequency signal which corresponds to the passage of particles across the beams (pedestal), a high frequency signal related to the velocity of individual particles passing through the beam intersection region, and a wide band of noise. A signal processing device is therefore required to extract the velocity-related high frequency signal, measure its mean value and obtain the information about fluctuation, i.e., r.m.s. value.

There are three basic types of signal processing

technique:- frequency spectrum analysis, counting and frequency tracking.

Frequency spectrum analysis is the simplest approach to Doppler signal processing. It was used for most of the early work on L.D.A. For most analysers, a spectrum of probability density function of Doppler frequency can be plotted against the frequency. In such a distribution, the most probable frequency corresponds approximately to the mean value of Doppler frequency and therefore, to the mean velocity; the width of the spectrum is related to the turbulent intensity. The major shortcomings of frequency analysis are (i) instantaneous velocity and energy spectrum cannot be obtained; (ii) processing the signal is time consuming and often lacking in precision.

A counter measures the time taken for a particle to cross a pre-determined numbers of fringes. The velocity can then be calculated from the numbers of fringes, fringe spacing and the time taken. The counting technique cannot measure the oscillations and energy spectra readily. However, counting procedures are not greatly influenced by changes in particle concentration and work well with high dropout values caused by a highly discontinuous signal.

Frequency tracking devices 'lock on' to the Doppler signal from the photomultiplier and yield an analogue output voltage proportional to the instantaneous fluid velocity. The block diagram of a typical frequency tracker is shown in Fig. 6.3-5. The incoming Doppler signal, at a frequency which varies with time, is mixed

with a output signal from a voltage controlled oscillator (V.C.O.). The output signal at a difference frequency is narrow-band filtered by an intermediate filter (I.F.) to remove as much noise as possible. The signal from the I.F. filter is then passed through a limiter which converts the signal to a square wave form and then fed into a frequency discriminator. This provides a d.c. output proportional to the I.F. frequency deviation from a fixed centre value f_o . After suitable smoothing, with a time constant T_o , and d.c. amplification, the resulting error voltage v is fed back to the control input of the V.C.O. The result of the feedback is that, provided a suitable value of loop gain is chosen, the oscillator frequency tracks that of the Doppler signal, maintaining a nearly constant difference equal to f_o . Thus the voltage v provides an electrical analogue of 'instantaneous' Doppler frequency which is in turn proportional to the flow velocity.

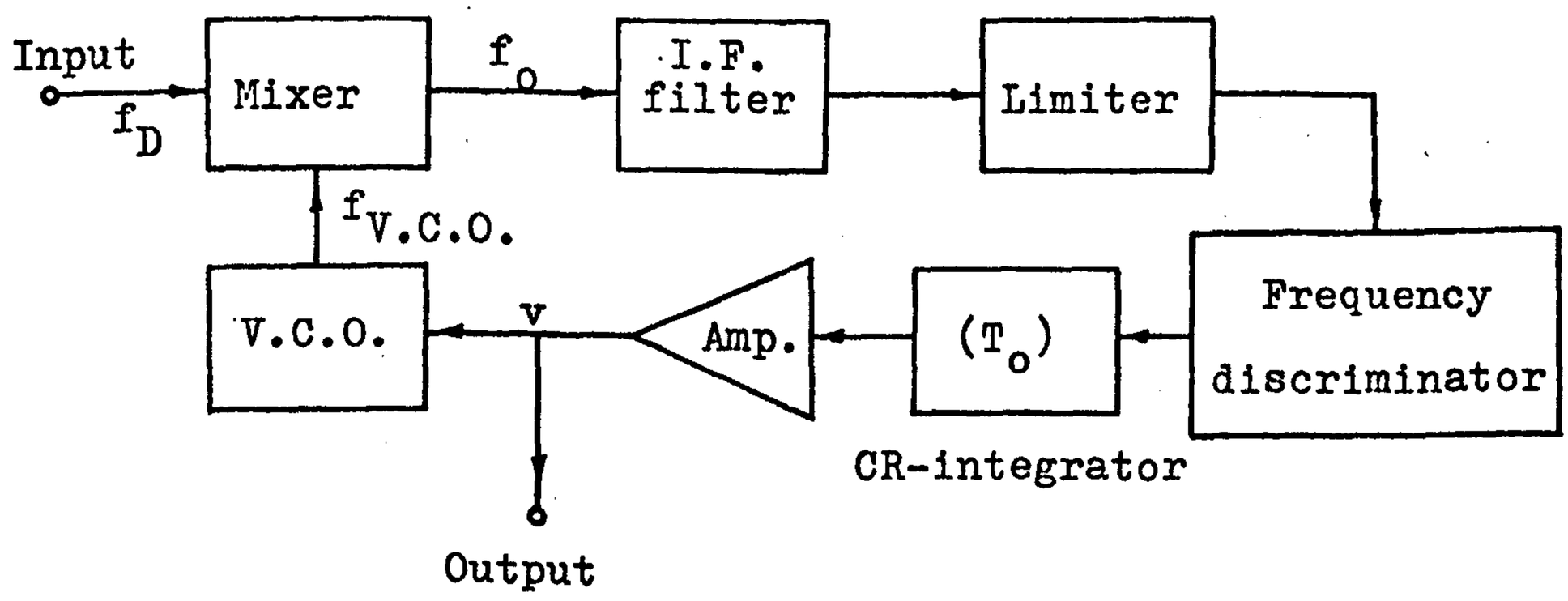

Fig. 6.3-5 Block diagram of frequency tracker

The distinct advantage of frequency trackers over other signal processing devices is that the mean and r.m.s. quantities can be read out directly on the appropriate meters. Frequency trackers are particularly suitable for application with flows where high particle concentration is present. In this experimental study of confined water jet mixing, the high particle concentration in unseeded tap water enables the use of a frequency tracker which is cheaper than a counter.

6.3.5 Signal Quality

As the measurement of fluid velocity in a flow depends on the scattered light signal received by the photomultiplier, a good signal is thus essential for accurate velocity measurement. Since the scattered light signal is produced by the scattering particles suspended in the flow, the qualities of scattering particles, such as particle size, particle concentration will certainly influence the signal quality and thus determine the accuracy of the velocity being measured.

The Doppler signal will also contain a certain amount of noise, partly from the optical system and partly from the electronics. By careful design of the electronics and optical system, the noise level can be reduced but cannot be eliminated totally. A quantity called signal-to-noise ratio is used to define the relative strength of the Doppler signal to the noise signal. Three factors which affect the signal quality are considered.

The Particle Size All measurements of fluid velocity by

laser Doppler anemometry are attempted by measuring the velocity of the particles suspended in the flow. Consequently, the ability of the particles to follow the flow is of great importance. Durst, Melling and Whitelaw (1976) studied the criteria of particle size capable of following turbulent flows. They suggested that for water flows, particles of diameter between 5μm to 16μm will be able to respond to a turbulent frequencies of 1 kHz to 10 kHz; for air flows, particles of diameter near 1μm are required to give the same turbulent response. This variation is due to the difference in viscosities of air and water as well as the particle to fluid density ratio.

Besides considering the ability to follow the flow, to obtain an optimum signal, appropriate matching of particle size with fringe spacing is desirable. An ideal Doppler signal (Fig. 6.3-6(a)) produced by a particle whose diameter is of the order of half the fringe spacing $\frac{1}{2}\Delta x$, contains a low frequency 'envelope' or 'pedestal' related to the Gaussian distribution of the light beam, plus a high frequency fringe crossing signal which contains information on the particle velocity. The signal has a depth of modulation equal to the amplitude of the pedestal.

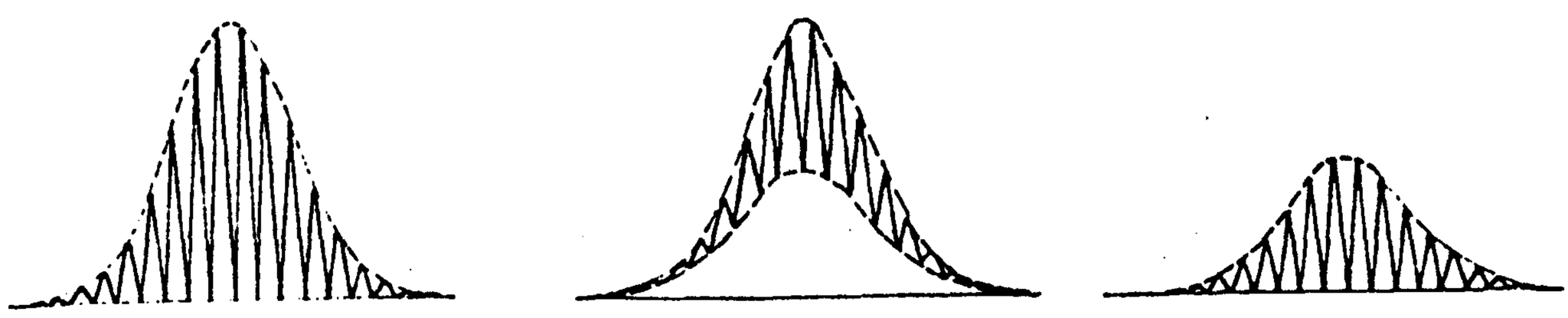

(a) (b) (c)

Fig. 6.3-6 Signals from various particle-sizes

However, for a particle of diameter greater than $\frac{1}{2}\Delta x$, the total light scattered will be greater but the depth of modulation of the signal as it passes through the fringes will be less as shown in Fig. 6.3-6(b). If the particle diameter is less than $\frac{1}{2}\Delta x$, the total light scattered will be reduced, causing a reduction in the total signal level (Fig. 6.3-6(c)). The result of variation in particle size, which is bound to exist, will be a variation in the amplitude of the Doppler signal. It is obvious that if the majority of the particles in the fluid have diameters in the order of half fringe spacing, then better Doppler signal will be obtained.

According to the interference fringe model, the fringe spacing Δx given by equation (6.3-12) can be re-written as

$$\Delta x = \frac{\lambda}{2\sin\frac{\varphi}{2}} \qquad \text{in air,}$$

$$\Delta x = \frac{\lambda}{2\eta\sin\frac{\varphi'}{2}} \qquad \text{in a liquid with refractive index } \eta \text{ and } \varphi' \text{ measured in the liquid.}$$

Thus, the appropriate particle size for a specific fluid should be matched with its refractive index η and the beam intersection angle φ' in order to give an optimal signal.

<u>Particle Concentration</u> An ideal situation for laser Doppler anemometry would be one in which there are sufficient particles in the flow so that at any time there is one particle in the measuring volume. Fig. 6.3-7(a) shows such an ideal

signal. If there are two particles in the control volume, the two particles will interfere constructively if the particles are in phase. The resulting signal will have a larger amplitude due to the extra light scattered as shown in Fig. 6.3-7(b). If the particles are 180° out of phase, destructive interference will occur and there will be no signal modulation since light will be continuously scattered (Fig.6.3-7(c)). In the case of a natural system, random particle separations will yield a signal as shown in Fig.6.3-7(d). The modulation depth is likely to be reduced at large particle concentration.

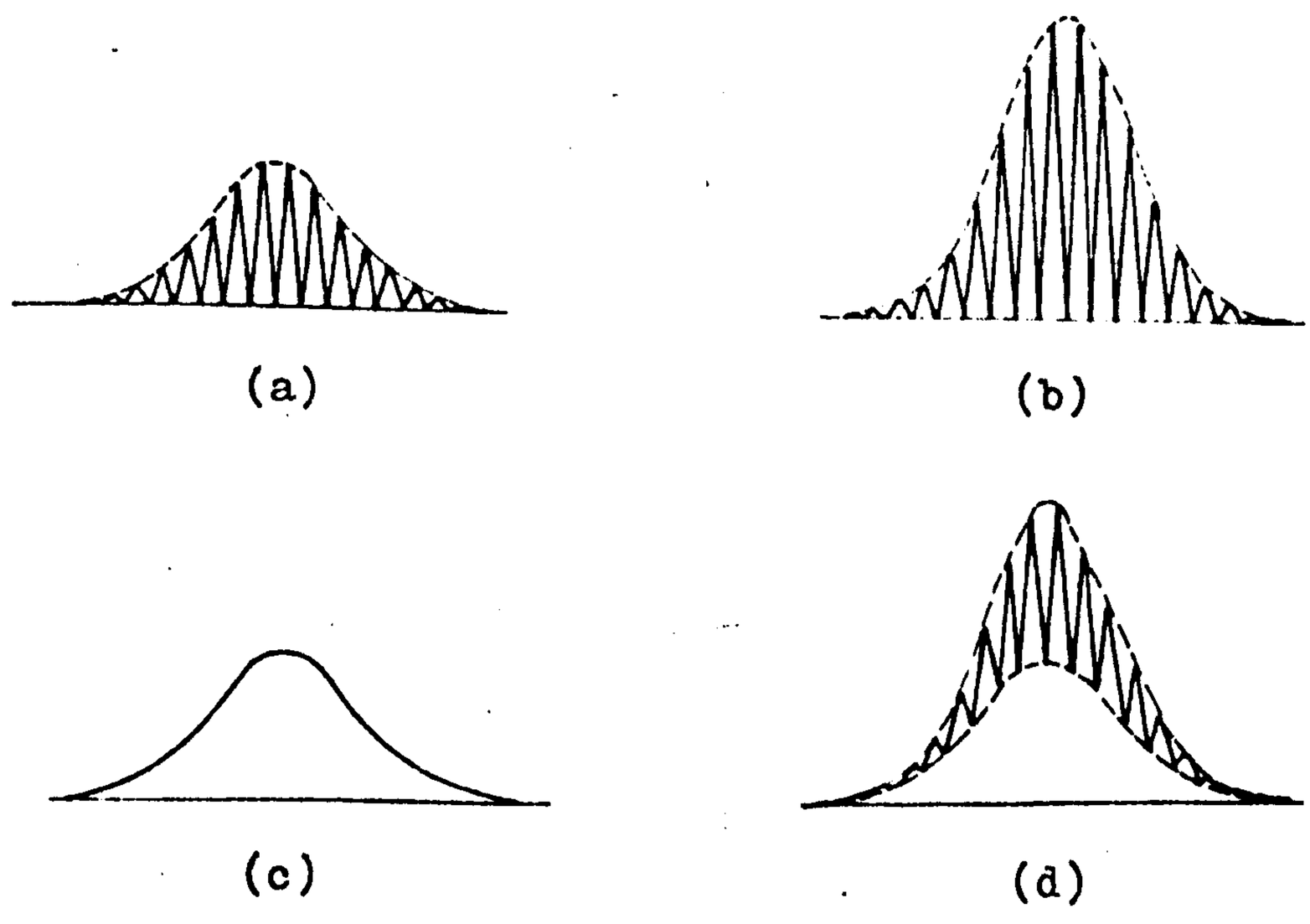

Fig. 6.3-7 Signals from various particle concentration

Durst, Melling and Whitelaw (1976) pointed out that smaller, weak scatterers may be present at a rather high concentration without causing serious defect, except that an excessive concentration give a high d.c. signal compo-

nent; but the concentration of larger particles should be kept to a minimum even if they do not contribute strong Doppler signals. Wang and Snyder (1974) also discovered that the signal-to-noise ratio from the anemometer will deteriorate at high particle concentration. When the Doppler signal is processed by a frequency tracker, the lowest limit of particle concentration will be the one sufficient to maintain at least one particle in the scattering volume for most of the time. According to Durst, Melling and Whitelaw (1976), the maximum concentration at which a fringe mode optical system would be employed is about 100 particles simultaneously present in the scattering region.

Light-collecting System It has been shown by Durst, Melling and Whitelaw (1976) that, for a dual beam anemometer, the signal quality will improve if the light intensities of the two beams are matched. Durst (1972) showed that if the photon shot noise is the predominant noise contribution, the signal-to-noise ratio decreases with increasing angle between the beams as well as with increasing angle of detection. A theoretical analysis by Durst, Melling and Whitelaw (1976) predicted that an increase in detection aperture of the photomultiplier increases the signal strength but not necessary the signal-to-noise ratio. All these results reveal that the light-collecting system represents an important part of laser Doppler anemometer and should be designed carefully in order to achieve the optimal results of signal strength and signal-

to-noise ratio.

6.3.6 Frequency Shift

In the case of measuring highly turbulent flows or the r.m.s. velocity with negligible mean velocity, a large fluctuation of Doppler frequency prevents the use of the frequency tracker as the processing technique. This is because most frequency tracker can only follow frequency fluctuation up to ±70% of the mean frequency. However, such difficulty can be overcome by using two beams of different wavelength to intersect at the flow rather than two beams of the same wavelength. The effect would be to produce a fringe pattern moving across the measuring volume instead of a stationary fringe pattern created by two light beams of same wavelength. Now, a particle with zero mean velocity in the measuring volume with a moving fringe pattern would be equivalent to a moving particle in the measuring volume with a stationary fringe pattern. The Doppler frequency produced by a stationary particle and a moving fringe will depend on the different frequency between the two beams. If, however, a moving particle is present in a moving fringe pattern, the Doppler frequency will increase if the particle and the fringe pattern are moving in the opposite directions. Thus, it is obvious that by creating a fringe pattern moving in the opposite direction of the particle movement, the mean Doppler frequency will increase and hence force the fluctuating frequency to fall within the working range of the frequency

tracker. The Doppler frequency with two incident beams of unequal frequencies f_{i1} and f_{i2} is given by equation (6.3-9) and reproduced as follow:

$$f_D = f_{i1} - f_{i2} + \frac{1}{\lambda}\bar{v}\cdot(\bar{k}_{i2} - \bar{k}_{i1}) \quad ,$$

$f_{i1} - f_{i2} = f_s$ is called the frequency shift.

To include a frequency shift in an optical system, two Bragg cells are installed in the optical unit, so that each beam passes through one cell. The Bragg cells are driven by a driver which has several frequency settings. At each of the shift setting, f_s , the frequency of one beam is increased by $\frac{1}{2}f_s$ and that of the other beam is reduced by $\frac{1}{2}f_s$. The frequency difference of the beams after passing through the Bragg cells is equal to the frequency shift setting f_s . The choice of f_s is dependent upon the turbulent intensity as well as the original mean frequency.

6.4 The Measurement of Mean and Fluctuating Velocities Using L.D.A.

6.4.1 The Components of the Laser Doppler Anemometer

The laser Doppler anemometer used in the present investigation consists of the following components:-

(i) A 10mW, He-Ne laser model Hughes 3225H-PCS with power unit model 3599H-K;

(ii) An integrated optical unit, Type DISA 55L01;

(iii) A flow direction adapter with driver, Type DISA 55L02;

(iv) A photomultiplier Type DISA 55L10;

(v) Frequency tracking signal processing electronics Type DISA55L.

The arrangement of the optical components together with the mixing tube test section is shown diagrammatically in Fig. 6.4-1.

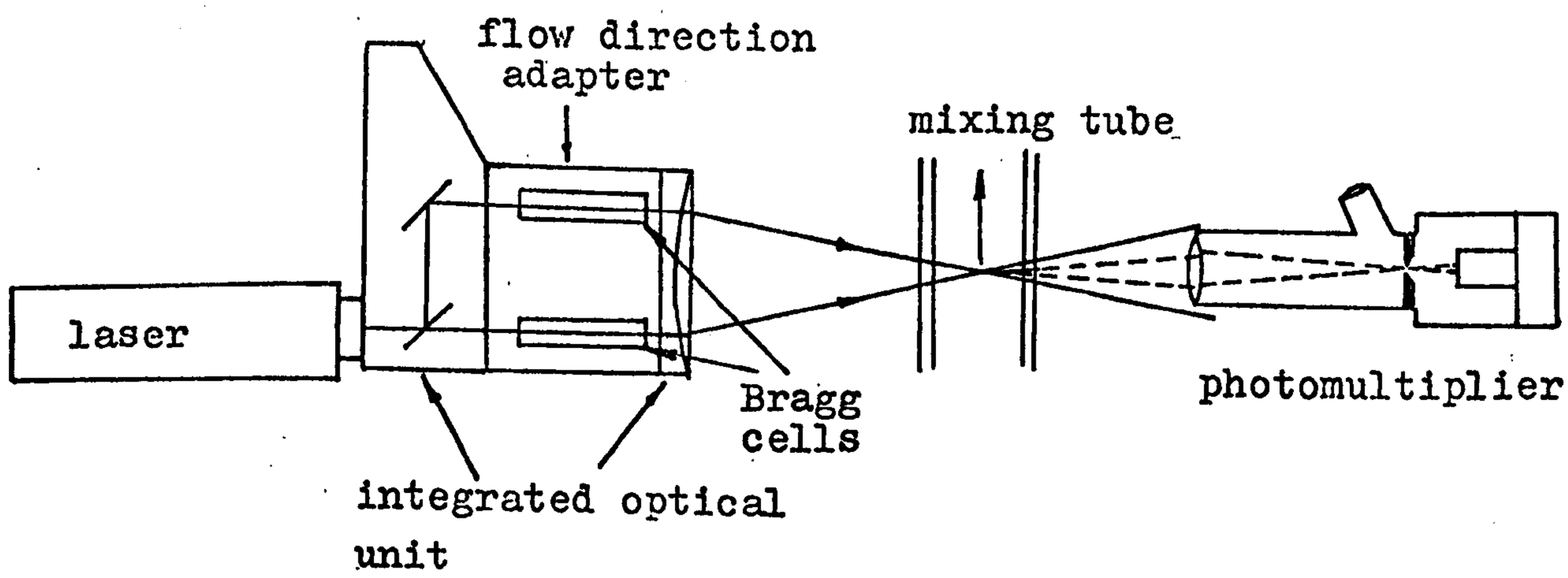

Fig.6.4-1 Optical arrangement of L.D.A.

The laser was directly mounted onto the optical unit so that any rotation of the optical unit for measuring different velocity components does not require re-alignment of the laser. The flow direction adapter which consists of two Bragg cells and a frequency driver, was incorporated into the optical unit so as to facilitate the measurement of highly turbulent mixing region as well as the radial

and tangential r.m.s. velocities where the mean velocity is negligible. The two laser beams were brought to cross at the measuring point in the mixing tube by the convergent lens of the optical unit. The photomultiplier was placed on the same optical bench at the other side of the mixing tube using the dual beam or 'fringe' mode of arrangement.

To ensure that the two laser beams can be brought to cross at any point in the mixing tube, appropriate adjusting mechanisms are required. The integrated optical unit and the photomultiplier were mounted on an optical bench via two adjustable riders. The riders have fine adjusting screws to move the optical unit and the photomultiplier in the vertical and longitudinal directions of the mixing tube. The entire optical bench was supported by two supporting mechanisms fixed on the frame of the rig. Each one of these mechanisms comprised an inverted 'V' base laid parallel to the longitudinal axis of the mixing tube. Along its apex a rack was cut so as to accommodate the pinion of a cross slide mounted on top of the base (see Fig. 6.4-2). By turning the pinion head, the cross-slide can be moved along the base in the longitudinal direction of the mixing tube. Fixed on top of the cross-slide is a thick plate with two 'V' groove cut into it running at right angles to the direction of travel of the cross-slide. A second slide (lateral slide) which held the optical bench was mounted onto this grooved plate. Fine adjustment of this lateral slide was made using threaded link between the slide and a tapped block fixed

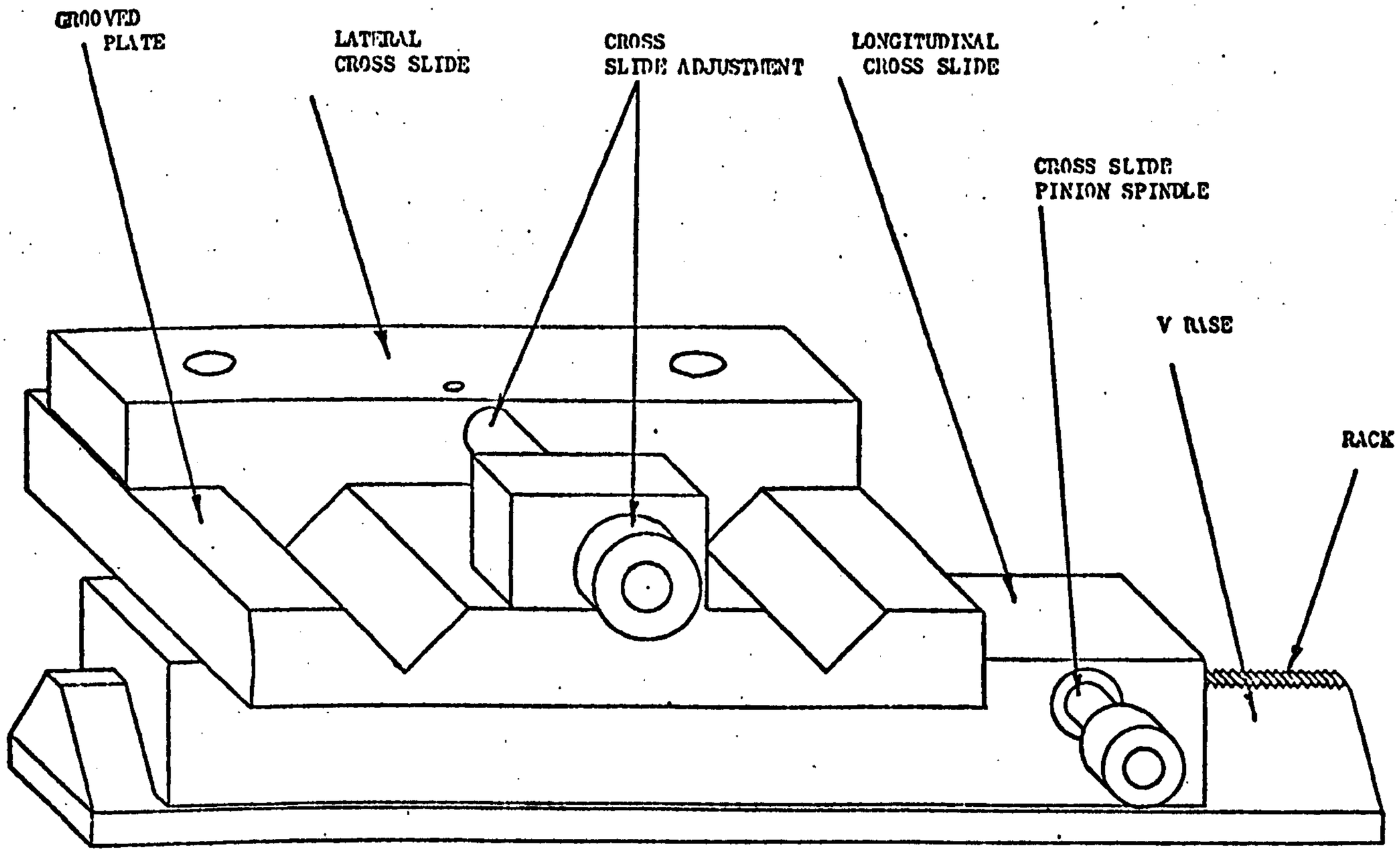

Fig.6.4-2 The adjusting mechanism for optical bench.

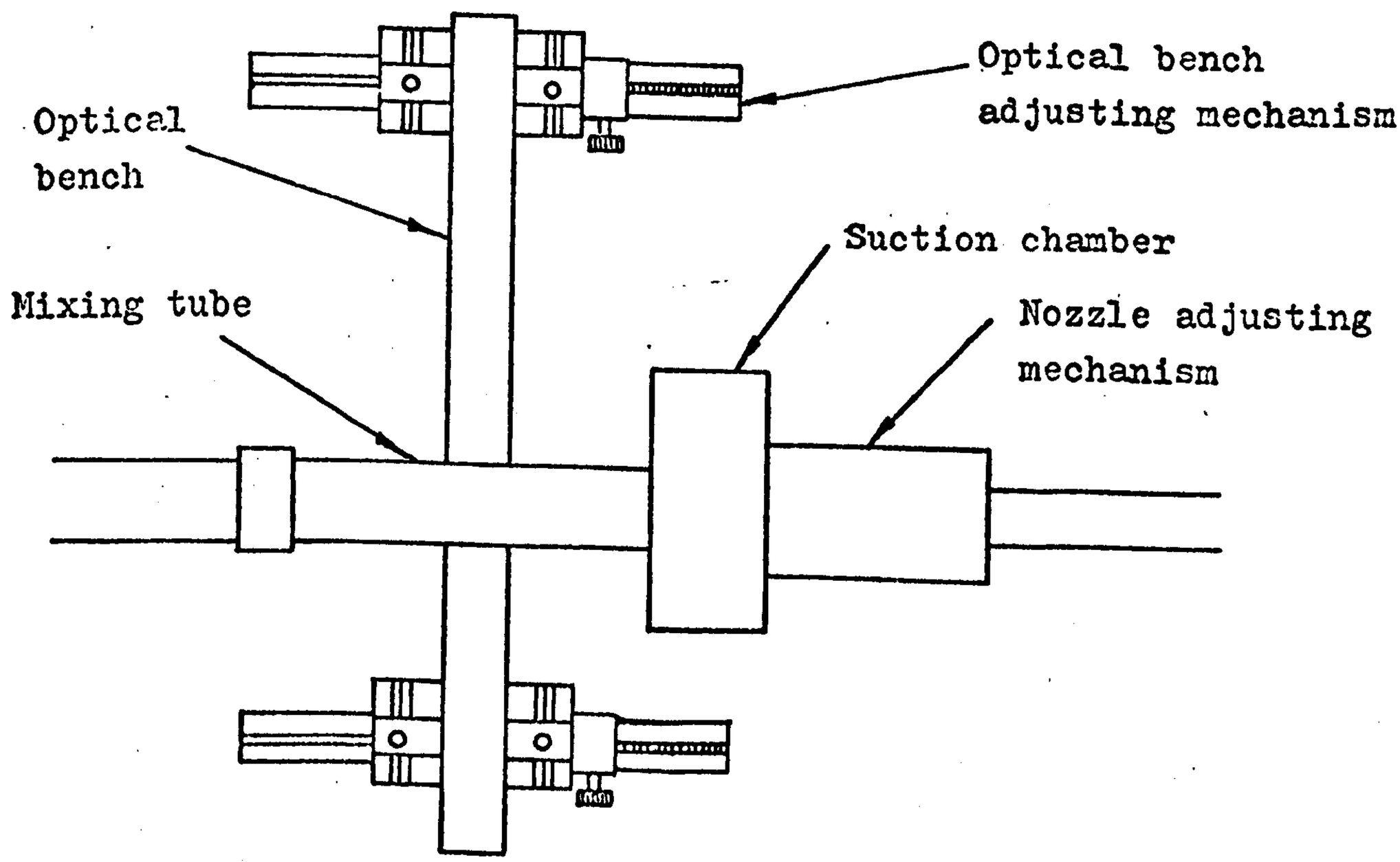

Fig. 6.4-3 Plan view of mixing tube and optical bench.

to the 'V' grooved plate. The mechanism thus provides facilities for the whole optical bench to be moved along the mixing tube axis by rotating the pinion head of the longitudinal cross-slide and across mixing tube by adjusting the lateral slide. The overall plan view of the adjustment mechanism, optical bench and the mixing tube is shown in Fig. 6.4-3.

The block diagram of the frequency tracking signal processing electronics used in this experiment is shown in Fig. 6.4-4. The equipment is a standard package developed by DISA ELEKTRONIK. The high voltage supply unit provides a continuously adjustable D.C. voltage to the photomultiplier. The photomultiplier received a Doppler shifted light signal scattered by particles from the measuring volume. The light signal has a sinusoidal intensity variation with time. It has been shown by the "interference fringe" model proposed by Rudd (1969) that the frequency of this intensity variation is equal to the Doppler frequency of the scattered light (section 6.3-3). The duty of the photomultiplier is to transform the light signal into an electrical signal without changing its frequency. The signal from the photomultiplier goes first to a preamplifier where the signal level is raised to a level which can be accepted by the tracker. The preamplifier also contains the high pass and low pass filters to remove the low frequency pedestal and high frequency noise from the Doppler signal. The signal is then fed to the frequency tracker which produces an

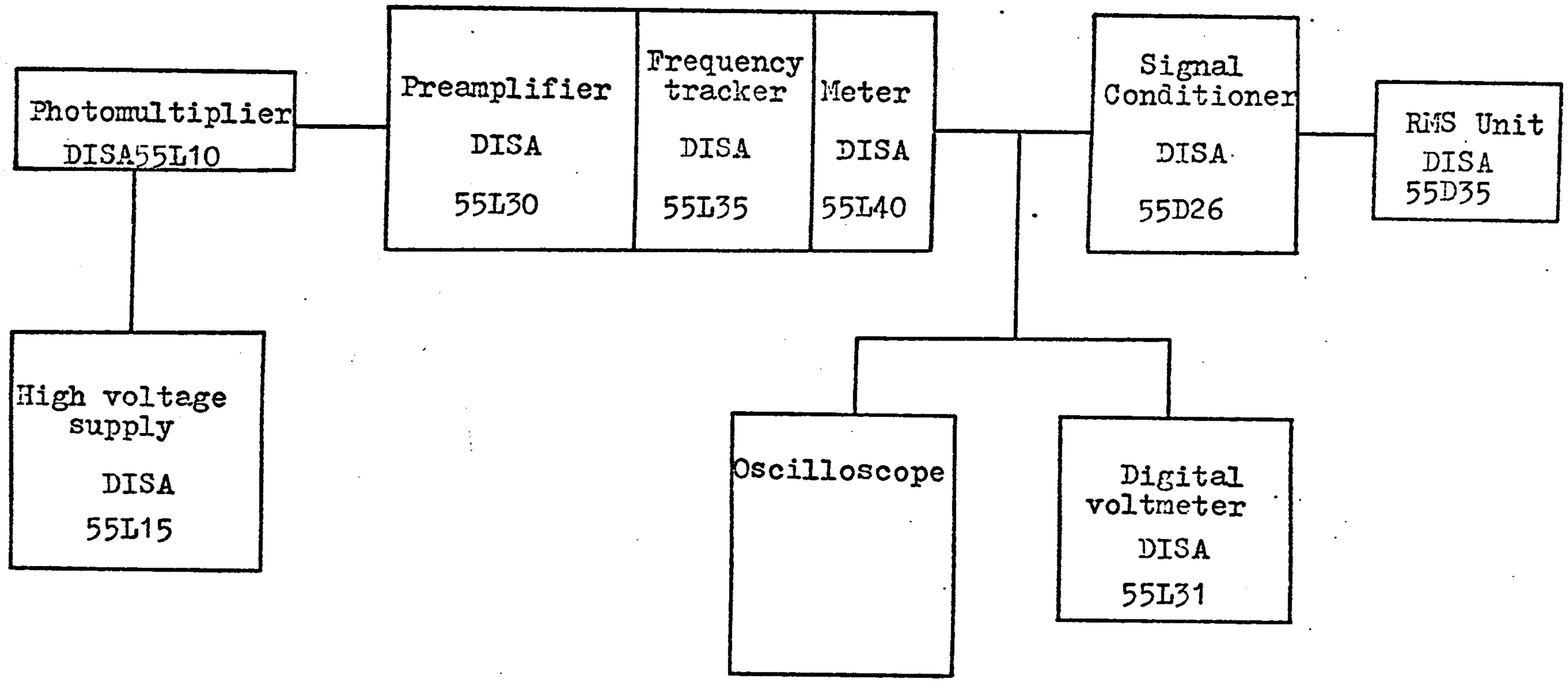

Fig.6.4-4 The frequency tracking signal processing electronics.

analogue voltage directly proportional to the instantaneous Doppler frequency and hence of flow velocity. In order to provide statistical information on the mean and fluctuating velocities the output voltage from the tracker is fed to a digital voltmeter for determining the mean velocity and to a r.m.s. voltmeter via a signal conditioner for determining the r.m.s. velocity.

A photograph of the laser anemometer mounted on the jet pump test rig is shown in Plate 6.4-1 and the signal processing electronics is shown in Plate 6.4-2.

6.4.2 The Measurement of Three Orthogonal Velocity Components in a Circular Mixing Tube

The three orthogonal components of velocity in a circular mixing tube to be measured are shown in Fig. 6.4-5.

The following paragraphs are concerned with details of the geometrical set-up of the laser optics and the necessary calculation procedures for evaluating the mean and r.m.s. velocities in the three orthogonal directions.

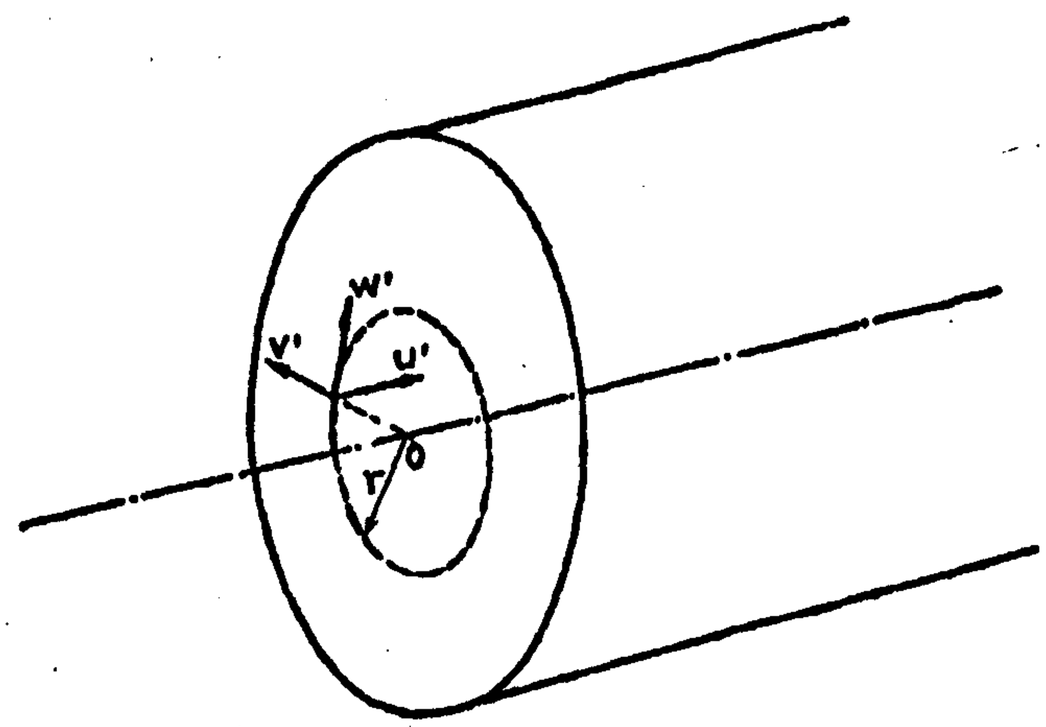

Fig. 6.4-5 The three orthogonal fluctuating velocities

Plate 6.4-1 The laser Doppler anemometer mounted on the rig

Plate 6.4-2 The signal processing electronics

The measurement of mean and fluctuating r.m.s. velocities in the axial (longitudinal) direction The flow in the mixing tube is assumed to be axi -symmetrical. The axial component of velocity was measured in a horizontal plane which cut through the axis of the mixing tube. Two horizontal laser beams from the optical unit were brought to meet at any point on the plane so that the bisector of the beam intersecting angle is perpendicular to the axis of the mixing tube (see Fig. 6.4-6). To ensure that the measurement was taken at the correct plane, a probe was inserted from the top of the mixing tube to locate the centre of the mixing tube. When the two laser beams crossed exactly at the probe tip, the probe was removed and the flow was left undisturbed when actual measurements were taken. By moving the whole optical bench horizontally at right angles to the mixing tube axis, the measuring point was then moved away from the centre such that measurement at various locations of that particular measuring section could thus be achieved.

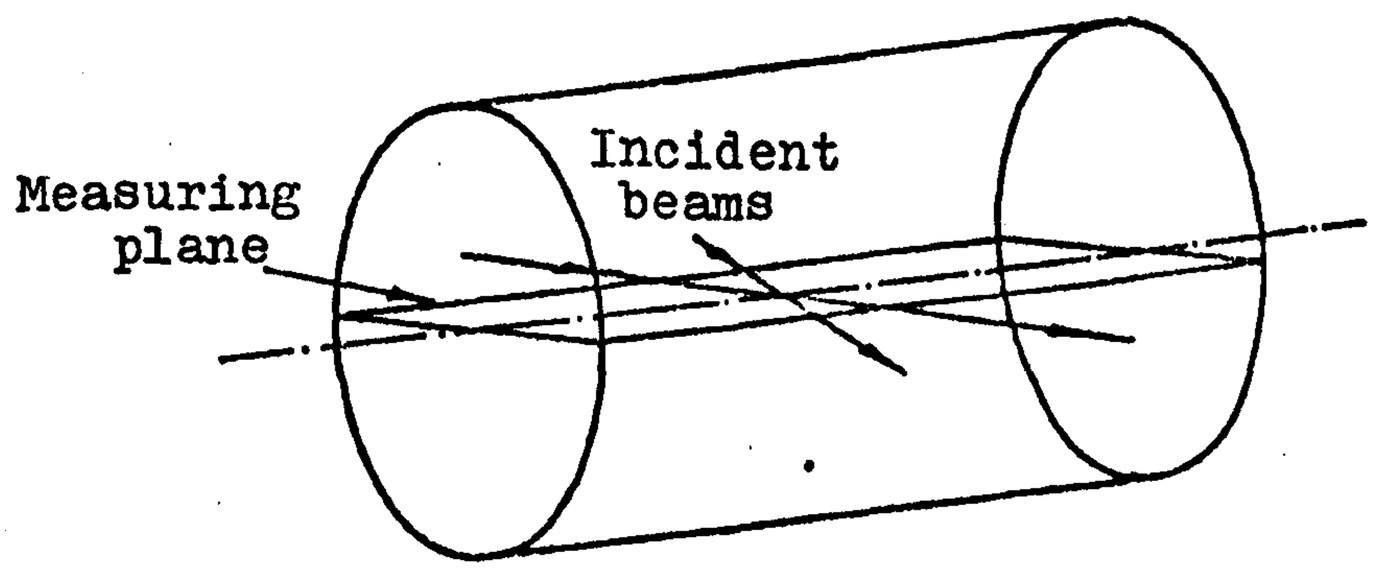

Fig. 6.4-6 Measuring plane for U-velocity

Owing to the refractive effect, the distance travelled by the optical unit is not equal to the distance travelled by the measuring point. A relationship between these two movements is thus needed to be established. Fig. 6.4-7 illustrates the beam intersection for measuring the axial velocity.

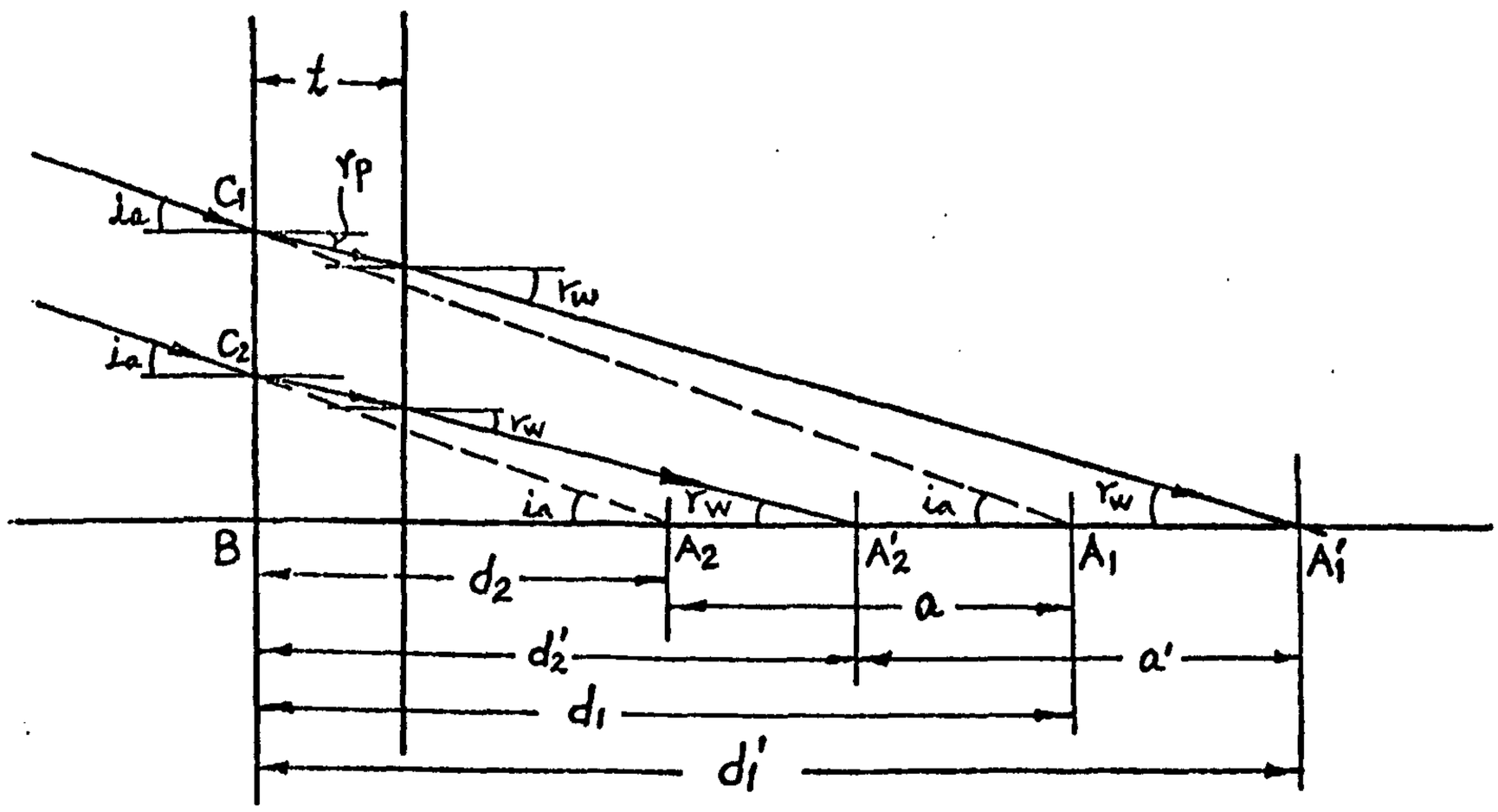

Fig. 6.4-7 Beam intersection for axial velocity measurement

An incident beam, which hits the outer wall surface at C_1, if passes through the wall into the water without any refraction, will meet a symmetrical beam (not shown) at A_1 having a distance d_1 from the outer wall surface. However, due to the refractions in the perspex wall and water, the beams actually intersect at point A_1', with a distance d_1' from the outer wall surface. If i_a is the incident angle in air, r_p is the refractive angle in perspex and r_w is the refractive angle in water, then

$$BC_1 = d_1 \tan i_a$$

$$= t \tan r_p + (d_1' - t)\tan r_w \qquad (6.4\text{-}1)$$

where B is a point on the outer surface of the wall such that $A_1'A_1B$ is a straight line perpendicular to the wall surface, and t is the thickness of the wall.

Similarly, if the optical unit is moved away from the mixing tube by a distance a, the unrefracted beams will meet at A_2 having a distance d_2 and the actual refracted beams will meet A_2' having a distance d_2', then,

$$d_2 \tan i_a = t \tan r_p + (d_2' - t)\tan r_w \qquad (6.4\text{-}2)$$

Subtracting equation (6.4-2) from equation (6.4-1),

$$(d_1 - d_2)\tan i_a = (d_1' - d_2')\tan r_w \qquad (6.4\text{-}3)$$

Since $d_1 - d_2$ is equal to the distance travelled by the optical unit, a, and $d_1' - d_2'$ is the distance travelled by the intersecting point, a', equation (6.4-3) can be written as

$$a' = a \frac{\tan i_a}{\tan r_w} \qquad (6.4\text{-}4)$$

In most measurements, i_a is relatively small and depends on the focal length of the lens used in the optical unit. For a 300mm focal length and 50mm beam seperа-

tion,

$$\tan i_a = \frac{25}{300}$$

i.e.,

$$i_a = 4.764^{\circ}$$

When i_a and r_w are small, $\tan i_a \simeq \sin i_a$ and $\tan r_w \simeq \sin r_w$, equation (6.4-4) can be approximated to

$$a' \simeq a \frac{\sin i_a}{\sin r_w} \simeq a \eta_w \qquad (6.4\text{-}5)$$

where η_w is the refractive index of the water

This relationship allows the relative position of the measuring point to be calculated from the movement of the optical unit and the refractive index of water.

The mean and r.m.s. velocities can then be calculated by the following equations.

$$U = \frac{f\lambda}{2\eta_w \sin r_w} = \frac{f\lambda}{2 \sin i_a} \qquad (6.4\text{-}6)$$

$$\sqrt{\overline{u'^2}} = \frac{f_{r.m.s.}\lambda}{2 \sin i_a} \qquad (6.4\text{-}7)$$

Where $f_{r.m.s.}$ refers to the fluctuation about the mean frequency.

<u>The measurement of r.m.s. fluctuating velocity in the tangential direction</u> To measure the tangential r.m.s. fluctuating velocity, the optical unit must rotate 90° from the position used for axial velocity measurement. The two laser beams which emerge from the optical unit are now in a vertical plane at right angles to the axis

of the mixing tube (Fig. 6.4-8). The optical unit is adjusted vertically such that the beams intersect on the horizontal diameter. By moving the optical bench along its own axis, measurement can be made at any point on the diameter. However, the distance travelled by the optical unit is obviously different from that travelled by the measuring point due to the refractions in perspex and water.

Fig. 6.4-9 shows the beam intersection for such measurement. The two laser beams, when brought to cross at the centre of the measuring section, pass straight through the perspex wall and into the water without any change of direction as the beams are perpendicular to the interface of the two media. However, when the optical unit is moved away from the mixing tube by a distance a, the beams will not enter the perspex wall at right angles. Refractions then take places in the perspex wall as well as in the water. The beams now intersect in the water at P' instead of P where the beams pass straight through without any change of direction. OP represents the distance travelled by the optical unit and OP' represents the distance travelled by the measuring point. From triangle APO,

$$\frac{OP}{\sin i_a} = \frac{AO}{\sin(180^\circ - \alpha)} = \frac{AO}{\sin\alpha}$$

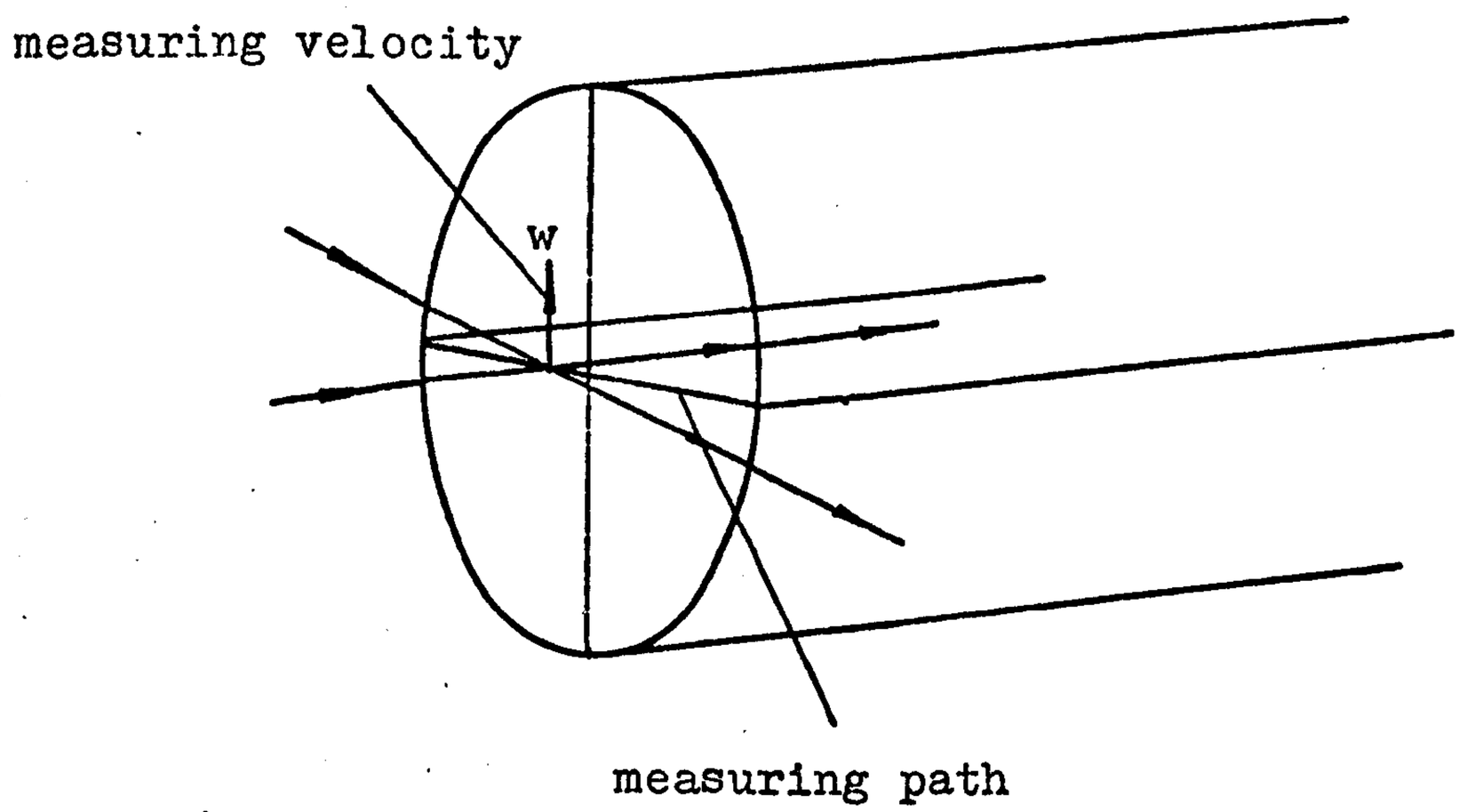

Fig.6.4-8 Measuring path for tangential component.

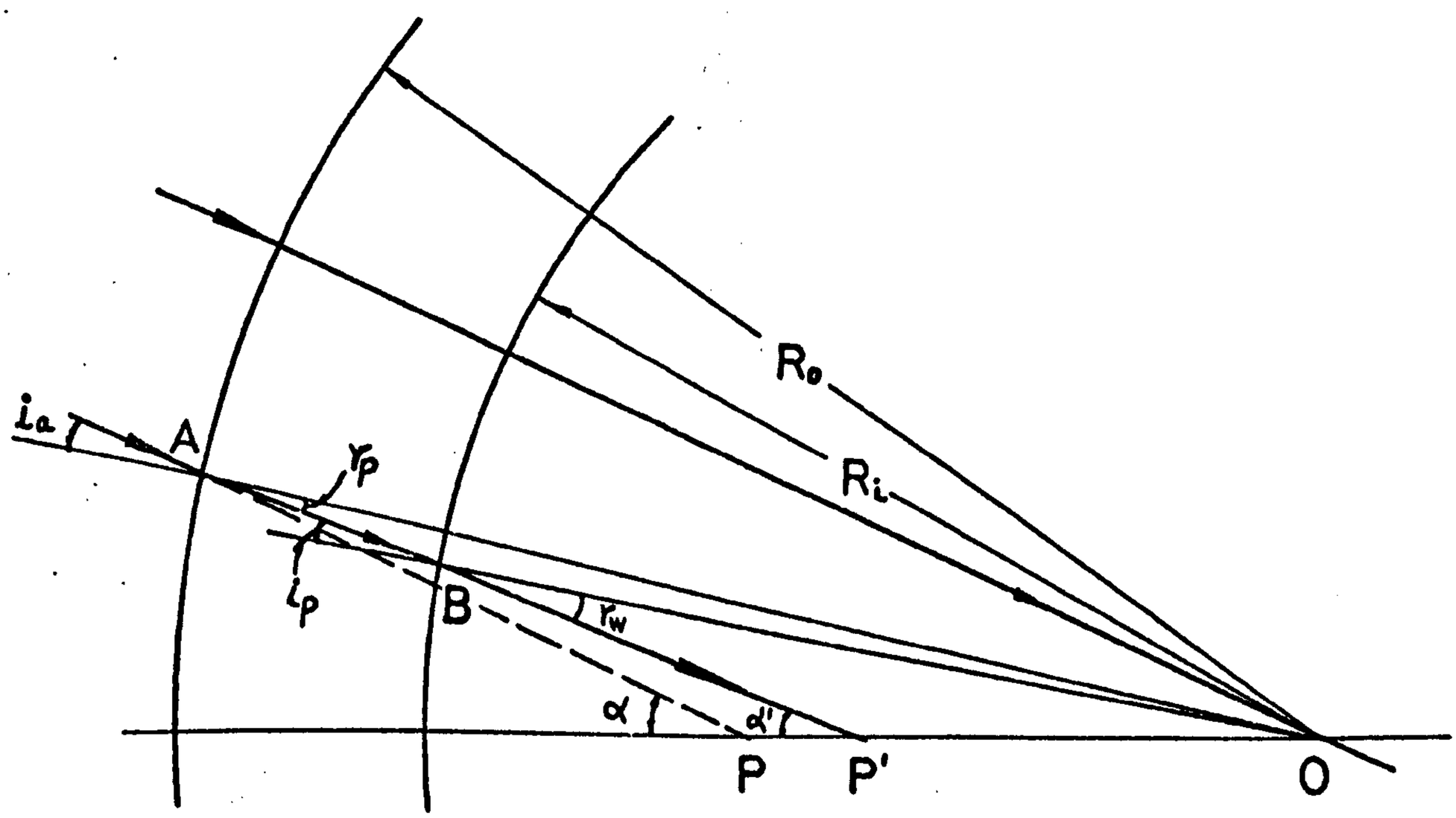

Fig.6.4-9 Beam intersection for tangential velocity measurement.

With $AO=R_o$ and $OP=a$,

$$\frac{a}{\sin i_a} = \frac{R_o}{\sin\alpha}$$

and $$i_a = \sin^{-1}\left(\frac{a \sin\alpha}{R_o}\right) \qquad (6.4\text{-}8)$$

where α is the half angle of the beam intersection in air which depends on the beam separation S_b and focal length f_L of the lens used in the optical unit, i.e.,

$$\alpha = \tan^{-1}\left(\frac{0.5S_b}{f_L}\right)$$

Considering the refraction at outer surface of the wall,

$$\frac{\sin i_a}{\sin r_p} = \eta_p$$

From equation (6.4-8),

$$r_p = \sin^{-1}\left(\frac{a \sin\alpha}{\eta_p R_o}\right) \qquad (6.4\text{-}9)$$

From triangle ABO,

$$\frac{R_i}{\sin r_p} = \frac{R_o}{\sin i_p}$$

and $$i_p = \sin^{-1}\left(\frac{a \sin\alpha}{\eta_p R_i}\right) \qquad (6.4\text{-}10)$$

Considering the refraction at the inner surface of the wall,

$$\frac{\sin i_p}{\sin r_w} = \frac{\eta_w}{\eta_p}$$

$$r_w = \sin^{-1}\left(\frac{a \sin\alpha}{\eta_w R_i}\right) \qquad (6.4\text{-}11)$$

From triangles APO, ABO, and BP'O

$$\measuredangle AOP = \alpha - i_a$$

$$\measuredangle AOB = i_p - r_p$$

and $$\alpha' = r_w + \measuredangle BOP',$$

since $$\measuredangle BOP' = \measuredangle AOP - \measuredangle AOB$$

$$\alpha' = r_w + (\alpha - i_a) - (i_p - r_p) \qquad (6.4\text{-}12)$$

Again, from triangle BP'O,

$$\frac{a'}{\sin r_w} = \frac{R_i}{\sin(180^\circ - \alpha')} = \frac{R_i}{\sin\alpha'}$$

$$a' = \frac{R_i \sin r_w}{\sin\alpha'} \qquad (6.4\text{-}13)$$

The above equations (6.4-8) to (6.4-13) allow the distance travelled by the measuring point a' to be calculated from the optical movement a, the outer and inner radii of the

mixing tube R_o and R_i, half angle of beam intersection α and the refractive indices for perspex and water η_p and η_w.

The r.m.s. fluctuating velocity $\sqrt{\overline{w'^2}}$ can then be calculated from

$$\sqrt{\overline{w'^2}} = \frac{f_{r.m.s.}\lambda}{2\eta_w \sin\alpha'} \qquad (6.4\text{-}14)$$

A short computer program has been written to calculate the value of a', α' and $\lambda/(2\eta_w \sin\alpha')$. The results of the various quantities are tabulated in Table 6.4-1 and the listing of the program is given in Appendix B.5.

a (mm.)	a'(mm.)	α'(rad.)	$\eta_w \sin\alpha'$	$\frac{\lambda}{2\eta_w \sin\alpha'}$(m.)
1.000	0.753	0.082	0.109	0.330E-05
2.000	1.530	0.082	0.109	0.322E-05
3.000	2.316	0.081	0.103	0.324E-05
4.000	3.116	0.080	0.107	0.327E-05
5.000	3.930	0.080	0.106	0.322E-05
6.000	4.759	0.079	0.105	0.302E-05
7.000	5.604	0.078	0.104	0.305E-05
8.000	6.464	0.077	0.103	0.308E-05
9.000	7.341	0.077	0.102	0.311E-05
10.000	8.234	0.076	0.101	0.314E-05
11.000	9.144	0.075	0.100	0.317E-05
12.000	10.072	0.074	0.099	0.320E-05
13.000	11.019	0.074	0.098	0.323E-05
14.000	11.984	0.073	0.097	0.326E-05
15.000	12.968	0.072	0.096	0.329E-05
16.000	13.973	0.072	0.095	0.333E-05
17.000	14.998	0.071	0.094	0.336E-05
18.000	16.044	0.070	0.093	0.340E-05
19.000	17.112	0.069	0.092	0.343E-05
20.000	18.203	0.069	0.091	0.347E-05

Table 6.4-1 <u>The various quantities for calculating the tangential velocity component.</u>

The measurement of r.m.s. fluctuating velocity in the radial direction It is relatively difficult to make measurement in the radial direction of a circular pipe. Fig. 6.4-10 illustrates that in order to measure the radial velocity, the two beam must cross in such a way that the bisector of the beam intersecting angle is perpendicular to the radial direction. To fulfill this requirement, the optical axis has to be inclined at an angle to the horizontal axis. This poses an extremely difficult problem to the alignment of the laser and optical unit. To overcome such difficulty, two perspex blocks with cylindrical inner surfaces identical to the mixing tube wall and flat square outer surfaces were constructed and locked on top of the mixing tube. A cross section with a circular inner surface but square external surfaces was thus formed. The blocks were locked onto the mixing tube by two screws and a joining plate tightened at the bottom surfaces as shwon in Fig. 6.4-11.

To measure the raidal r.m.s. velocity, the optical unit is arranged in a similar way to that for measuring the tangential value. The two laser beams emitted from the optical unit are in the vertical plane perpendicular to the axis of the mixing tube. The two beams are symmetrically inclined to a horizontal axis. When the two beams are brought to cross at the centre of the measuring section, refraction takes place at the outer surface of the perspex cross section but not at the inner surface as they pass

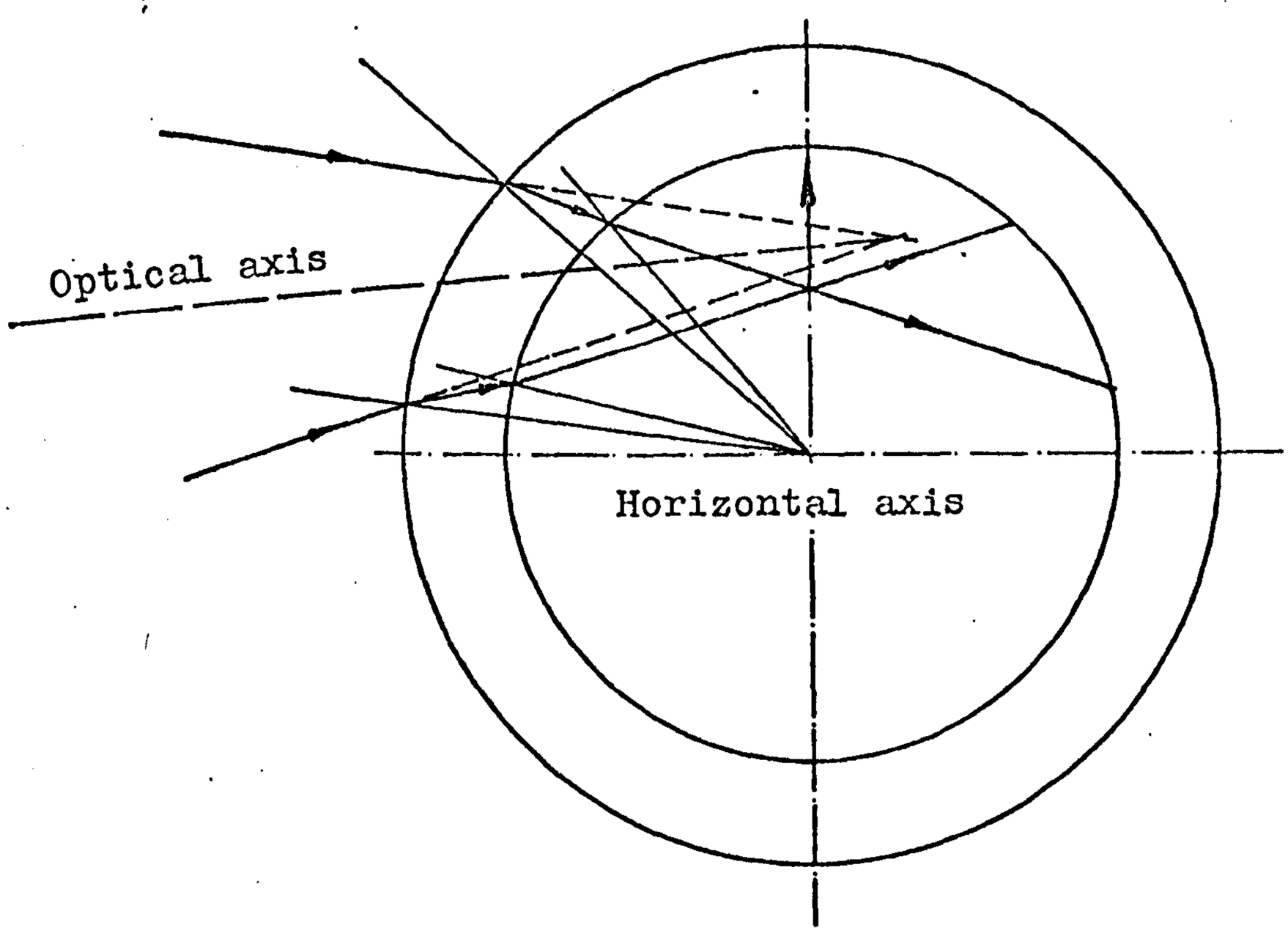

Fig.6.4-10

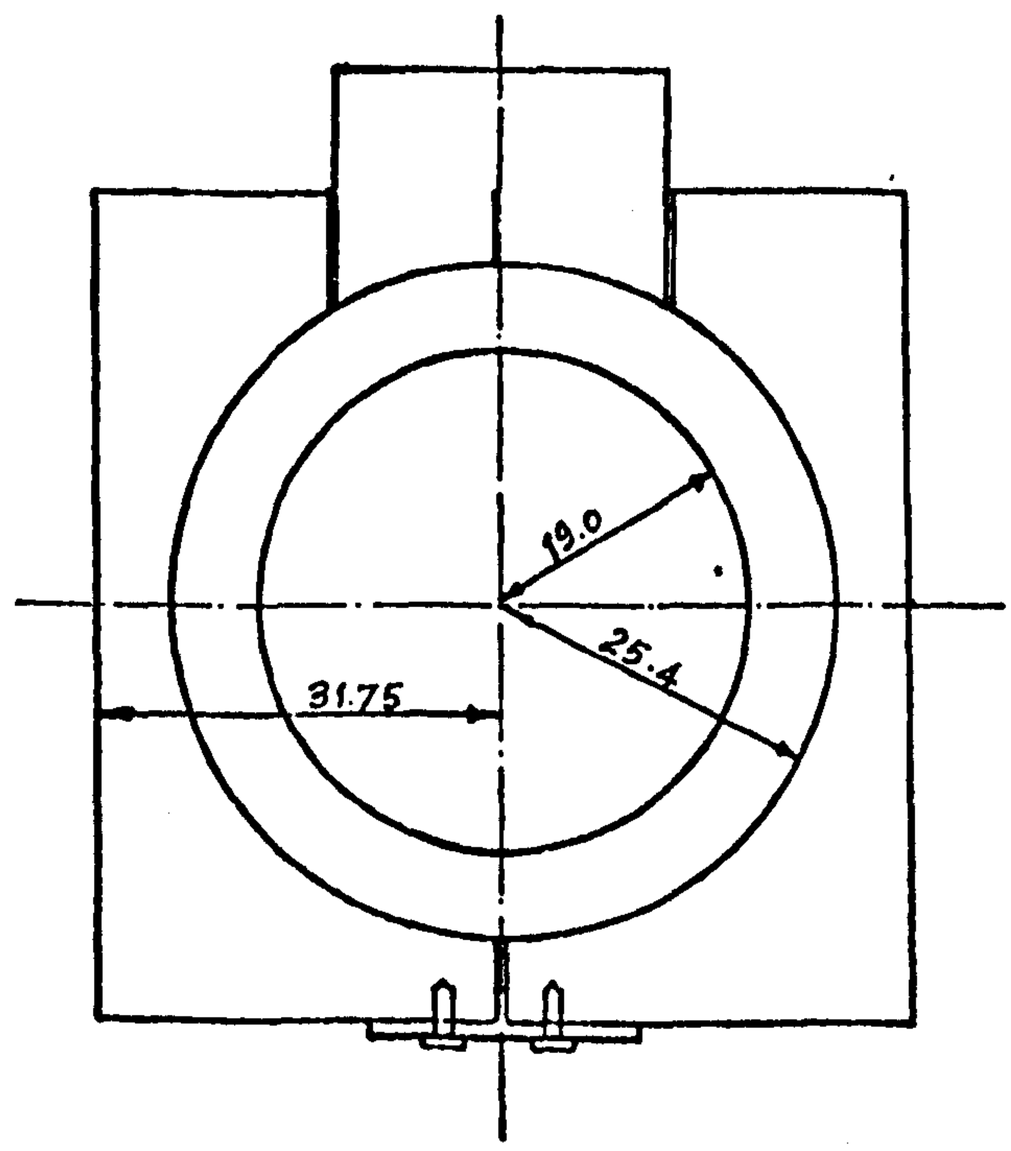

Fig.6.4-11 Cross-section for radial velocity measurement.

perpendicular through it. (see Fig. 6.4-12(a)). The incident angle from the air to the perspex i_a is equal to the half angle of the beam intersection in air, i.e.,

$$i_a = \alpha = \tan^{-1}\left(\frac{0.5S_b}{f_L}\right) \qquad (6.4\text{-}15)$$

The refractive angle in the perspex r_p can be obtained by

$$r_p = \sin^{-1}\left(\frac{\sin i_a}{\eta_p}\right) \qquad (6.4\text{-}16)$$

The distance from the incident point to the symmetrical axis, s, can be calculated from a, the distance from the incident face to the centre of the mixing tube, and r_p, the refractive angle in the perspex,

$$s = a \tan r_p \qquad (6.4\text{-}17)$$

If the centre of the cross-section is considered as the origin of x - y coordinates, the inner surface of the mixing tube can then be described by an equation

$$x^2 + y^2 = R_i^{\,2} \qquad (6.4\text{-}18)$$

where R_i is the internal radius of the mixing tube.

By moving the optical unit vertically upwards a distance h, the beams will meet the incident face of the cross-section at A (-a, h + s) and B (-a, h - s) (see Fig. 6.4-12(b)). After travelling in the perspex along AC and

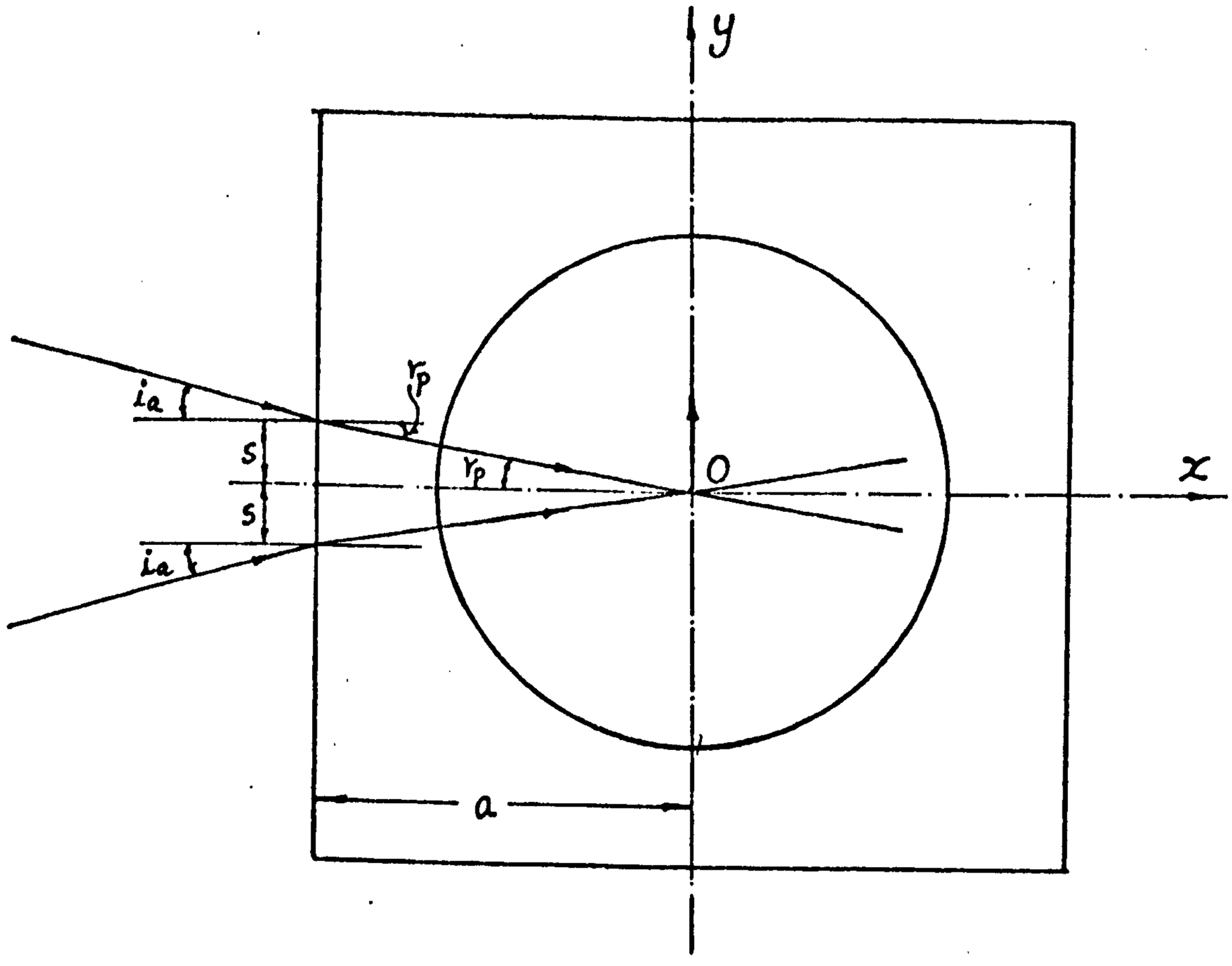

Fig.6.4-12(a)

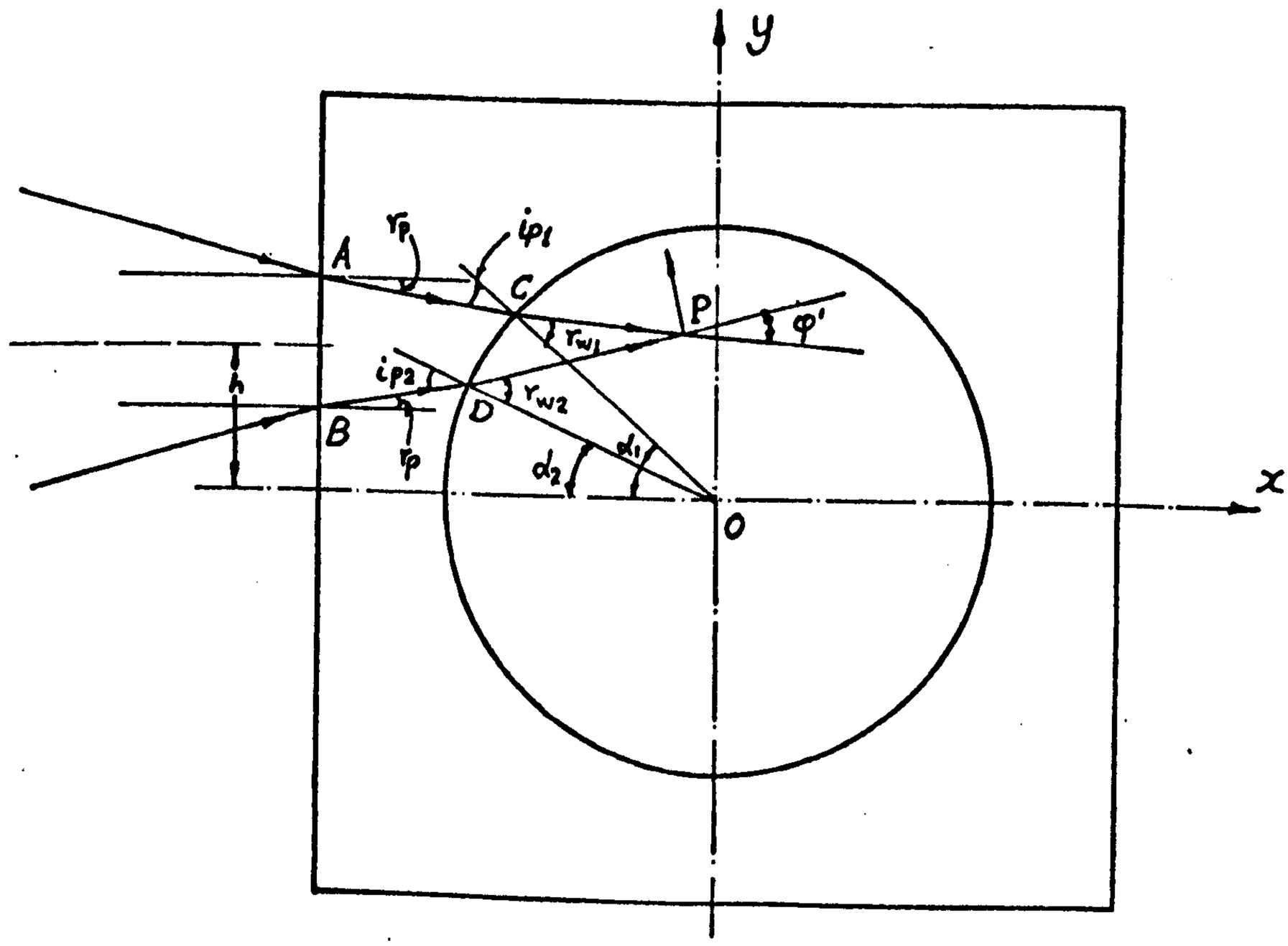

Fig.6.4-12(b) Beam intersection for radial velocity measurement.

BD, the two beams cross in the water at P. Equations of the straight lines AC and BD are given by:

$$\text{AC:} \quad y - h - s = -\tan r_p(x + a) \qquad (6.4\text{-}19)$$

$$\text{BD:} \quad y - h + s = \tan r_p(x + a) \qquad (6.4\text{-}20)$$

To obtain the coordinates of C and D, equations (6.4-19) and (6.4-20) are solved with equation (6.4-18) respectively. Assuming that the coordinates of C and D are (x_C, y_C) and (x_D, y_D), the inclined angles of OC and OD with the horizontal radius, α_1 and α_2 can then be obtained by

$$\alpha_1 = \tan^{-1}\left(\frac{y_C}{-x_C}\right)$$

$$\alpha_2 = \tan^{-1}\left(\frac{y_D}{-x_D}\right)$$

The incident angles at C and D are then given by i_{p1} and i_{p2} as follows:-

$$i_{p1} = \alpha_1 - r_p$$

$$i_{p2} = \alpha_2 + r_p$$

The refractive angles at C and D, i.e., r_{w1} and r_{w2} are related to their respective incident angles and the refractive indices of perspex and water

$$r_{w1} = \sin^{-1}(\frac{\eta_p}{\eta_w}\sin i_{p1}) = \sin^{-1}(\frac{\eta_p}{\eta_w}\sin(\alpha_1 - r_p))$$

$$r_{w2} = \sin^{-1}(\frac{\eta_p}{\eta_w}\sin(\alpha_2 + r_p))$$

The slopes of CP and DP, m_1 and m_2, are then given as follows

$$m_1 = -\tan(\alpha_1 - r_{w1})$$

$$m_2 = \tan(r_{w2} - \alpha_2)$$

The equations of CP and DP can then be written as

$$\text{CP:} \quad y - y_C = -\tan(\alpha_1 - r_{w1})(x - x_C) \qquad (6.4\text{-}21)$$

$$\text{DP:} \quad y - y_D = \tan(r_{w2} - \alpha_2)(x - x_D) \qquad (6.4\text{-}22)$$

The coordinates of $P(x_P, y_P)$ can then be obtained by solving equations (6.4-21) and (6.4-22), i.e.,

$$x_P = \frac{y_C - y_D + x_D\tan(r_{w2} - \alpha_2) + x_C\tan(\alpha_1 - r_{w1})}{\tan(r_{w2} - \alpha_2) + \tan(\alpha_1 - r_{w2})}$$

$$y_P = y_C - \tan(\alpha_1 - r_{w1})(x_P - x_C) \qquad (6.4\text{-}23A)$$

The distance OP can then be calculated from x_P and y_P by

$$OP = \sqrt{x_P^2 + y_P^2} \qquad (6.4\text{-}23B)$$

The angle of beams intersection φ' can be calculated from m_1 and m_2 as follow

$$\varphi' = \measuredangle CPD = \tan^{-1}\left(\frac{m_2 - m_1}{1 + m_1 m_2}\right) \qquad (6.4\text{-}24)$$

A computer program was written to calculate the distance OP and the beam intersecting angle φ' at various values of h. It has also been proved that OP and the bisector of CP and DP are perpendicular to each other as the product of their slopes is equal to -1 at various values of h. Thus, by raising or lowering the optical unit vertically from its central position, the effect of measuring the radial component can be achieved. The position of the measuring point can be calculated from equation (6.4-23). The r.m.s. fluctuating velocity $\sqrt{\overline{v'^2}}$ is given by

$$\sqrt{\overline{v'^2}} = \frac{f_{r.m.s.}\,\lambda}{2\eta_w \sin\frac{\varphi'}{2}} \qquad (6.4\text{-}25)$$

The results of various quantities are tabulated in Table 6.4-2 and the listing of the computer program is given in Appendix B.6.

6.4.3 Experimental Procedure

The step by step procedure of setting up the DISA 55L laser Doppler anemometer is given in detail in the DISA manual. The setting and tunning of the DISA 55L30 signal processor should follow the manufacturer's operation

h(mm.)	OP (mm.)	φ'(rad)	$\eta_w \sin\frac{\varphi'}{2}$	s_1 Slope of bisector of φ'	s_2 Slope of OP	$s_1 x s_2$	$\frac{\lambda}{2\eta_w \sin\frac{\varphi'}{2}}$(m.)
0.500	0.560	0.112	0.074	0.003	-313.753	-0.996	0.427E-05
1.000	1.120	0.112	0.074	0.006	-153.015	-0.995	0.427E-05
1.500	1.630	0.112	0.074	0.009	-105.313	-1.000	0.427E-05
2.000	2.241	0.112	0.074	0.013	-73.775	-0.999	0.427E-05
2.500	2.301	0.112	0.074	0.016	-62.343	-1.000	0.427E-05
3.000	3.361	0.112	0.074	0.019	-52.122	-1.000	0.427E-05
3.500	3.921	0.112	0.074	0.022	-44.439	-1.000	0.427E-05
4.000	4.431	0.112	0.074	0.026	-33.646	-1.000	0.427E-05
4.500	5.041	0.112	0.074	0.029	-34.115	-1.000	0.427E-05
5.000	5.601	0.112	0.074	0.033	-30.460	-1.000	0.427E-05
5.500	6.162	0.112	0.074	0.036	-27.442	-1.000	0.427E-05
6.000	6.722	0.112	0.074	0.040	-24.907	-1.000	0.427E-05
6.500	7.232	0.112	0.074	0.044	-22.735	-1.000	0.427E-05
7.000	7.342	0.112	0.074	0.043	-20.354	-1.000	0.427E-05
7.500	8.402	0.112	0.074	0.052	-19.202	-1.000	0.427E-05
8.000	8.962	0.112	0.074	0.056	-17.736	-1.000	0.427E-05
8.500	9.523	0.112	0.074	0.061	-16.421	-1.000	0.427E-05
9.000	10.033	0.112	0.074	0.066	-15.234	-1.000	0.427E-05
9.500	10.643	0.112	0.074	0.071	-14.150	-1.000	0.427E-05
10.000	11.203	0.112	0.074	0.076	-13.154	-1.000	0.427E-05
10.500	11.763	0.112	0.074	0.082	-12.232	-1.000	0.427E-05
11.000	12.323	0.112	0.074	0.088	-11.372	-1.000	0.427E-05
11.500	12.333	0.112	0.074	0.095	-10.565	-1.000	0.427E-05
12.000	13.444	0.112	0.074	0.102	-9.802	-1.000	0.427E-05
12.500	14.004	0.112	0.074	0.110	-9.074	-1.000	0.427E-05
13.000	14.564	0.112	0.074	0.119	-8.376	-1.000	0.427E-05
13.500	15.124	0.112	0.074	0.130	-7.700	-1.000	0.427E-05

Table 6.4-2 <u>The various quantities for calculating radial velocity component.</u>

manual. During the measurment, an oscilloscope was used to monitor the Doppler signal so that the frequency could be estimated. The frequency range on the tracker was then set to include the Doppler frequency in the recommended region of the frequency meter.

6.4.4 The Limitation of L.D.A. and Design Criteria of the Optical Components

The inlet velocity ratios of the primary jet to the secondary entrained flow used for the present study are 3.72 and 4.67 (see Table 6.5-1). Higher inlet velocity ratios were attempted but the tracker failed to lock to the signal, presumably owing to the following reasons: (i) high turbulent intensity, and (ii) high velocity gradient. However, the use of frequency shift technique improved the tracker's performance for high turbulent intensity but failed to solve the problem of high velocity gradient. It is thus believed that the high velocity gradient which resulted from the high inlet velocity ratio, plays an important part in preventing the tracker to function normally. The limitation of measuring high velocity gradient flow is due to the finite size of the measuring volume. A typical measuring volume formed by two intersecting beams is of ellipsoid shape as shown in Fig. 6.4-13. The particles traversing across the measuring volume have a range of mean velocities. This will result in different Doppler frequency shifts in the light emitted from different parts of the measuring volume.

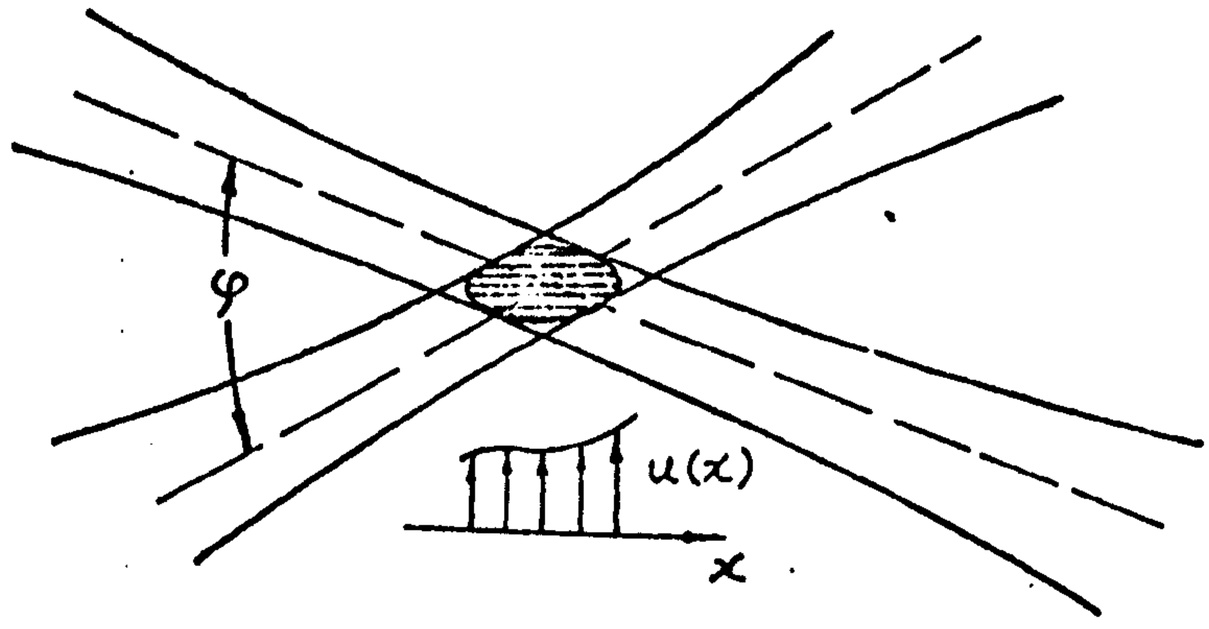

Fig.6.4-13 Typical measuring volume.

Such limitation can be improved, theoretically, by (i) arranging the optical system with a shorter dimension of the measuring volume along the direction of the velocity gradient; or (ii) reducing the size of the measuring volume. Method (i) cannot be achieved in a pipe flow owing to the refraction at the pipe surface. Method (ii) can be accomplished by using lens of shorter focal length in the optical unit. However, a shorter focal length will produce a bigger beam intersecting angle, and subsequently reduce the signal strength and the signal-to-noise ratio as pointed out by Durst, Melling and Whitelaw (1976). The increase of beam intersecting angle also limits the maximal velocity which can be measured by the tracker as most trackers can work up to a specific maximum frequency. By examining the equation relating the velocity and Doppler frequency,

$$U = \frac{f_D \lambda}{2\eta \sin\frac{\varphi'}{2}}$$

f_D is limited to a maximum value which can be handled by

the tracker. The bigger the angle φ', the smaller will be the U which can be measured. Such a situation is even worse in the case of measuring high turbulent flow where the frequency shift technique is necessary. In this case, the maximum velocity can be measured is given by

$$U = \frac{(f_D - f_s)\lambda}{2\eta \sin\frac{\varphi'}{2}}$$

which is less than the case without frequency shift f_s.

The focal length of the optical unit also determines the fringe spacing. According to equation (6.3-12), the fringe spacing Δx is related to λ, η and φ' as follow:

$$\Delta x = \frac{\lambda}{2\eta \sin\frac{\varphi'}{2}}$$

Since λ and η are constants, Δx is inversely proportional to the beam intersecting angle φ'. A shorter focal length will produce a bigger φ' and thus create a fringe pattern of smaller fringe spacing. It has been pointed out in section 6.3.5 that in order to give an optimum signal, the majority of the particles should have diameters in the order of half fringe spacing. A reduction in focal length will require smaller suspended particles. It can thus be concluded that the choice of the focal length is determined by the maximum velocity to be measured and the capability to control the suspended particle size.

In the present measurement, a lens of 300mm focal length was used in the optical unit. With a highest

frequency limit of 15MHz provided by the DISA 55L35 tracker, the maximum velocity range without using frequency shift was 57.15 m/s. This velocity range would be considerably reduced by the use of frequency shift technique. Different fringe patterns were produced for measuring different components in the mixing tube. The fringe spacing was 3.8μm for the axial velocity measurement; 4.27μm for the radial direction measurement and was varied from 2.86μm to 3.48μm for the tangential direction measurement. To ensure that the particles size matched with the fringe spacing, a 10μm filter was installed to filter the larger particles and the signal was found to improve significantly.

The criteria of selecting the light collecting optics, i.e., the close-up lens in front of the photomultiplier objective, depends on the pin-hole size and the focal length of the optical unit's lens. When a laser beam of wavelength λ is focused by a lens of focal length f_L the focused beam D_1 is given by

$$D_1 = \frac{4\lambda f_L}{\pi D_o} \qquad (6.4\text{-}26)$$

where D_o is the diameter of the unfocused beam which contains 86.5% of the emitted light.

It is normally arranged in such a way that the diameter of the measuring control volume observed by the photomultiplier is equal to D_1. By using a fixed pinhole of diameter D_p, and a fixed distance from the collecting lens to the pinhole d_p. The following relationship can

be obtained.

$$\frac{D_p}{D_1} = \frac{d_p - f_c}{f_c} \qquad (6.4\text{-}27)$$

where f_c is the focal length of the collecting lens. Substituting equation (6.4-26) into equation (6.4-27)

$$\frac{d_p}{f_c} = 1 + \frac{\pi D_o D_p}{4\lambda f_L} \qquad (6.4\text{-}28)$$

Thus, the focal length of the collecting lens f_c should be matched with the focal length of the lens used in the optical unit f_L accordingly in order that an appropriate measuring volume is observed. Such matching is essential for ensuring the outer region of the fringe pattern with poor signal quality does not contribute to the measurements.

6.5 Results and Discussion

6.5.1 LDA Experimental Results

The measurements of mean and fluctuating velocities were made in the uniform mixing tube described in section 6.2.2. The geometries and flow conditions are given in Table 6.5-1. All measurements were made using the DISA 55L signal processor described in section 6.4.1. In the case of measuring centre-line axial mean and fluctuating velocities for radius ratio of 0.334, a TSI tracker model 1090 was also used to obtain results for comparison with

those obtained from the DISA tracker. Frequency shifting was employed in most cases except for the potential core region near to the jet exit where turbulent intensity was low.

r_n/r_t	U_n/U_e	d_t(mm)	d_n(mm)	U_n(m/s)	U_e(m/s)
0.334	3.72	38	12.7	3.05	0.82
0.171	4.67	38	6.5	5.72	1.22

where e refers to the entrained value at inlet

Table 6.5-1 Geometrical and flow conditions of measurements

Fig. 6.5-1 and 6.5-2 show the mean and r.m.s velocities along the axis of the mixing tube for radius ratio of 0.334 and velocity ratio of 3.72. The results have been non-dimensionalized by nozzle exit velocity and are plotted against the distance from the nozzle exit. The axial mean and fluctuating velocities obtained from both trackers agree closely with one another.

Fig. 6.5-3 and 6.5-4 show the measured axial mean and fluctuating velocities along the axis of mixing tube for radius ratio 0.171 and inlet velocity ratio 4.67. The above figures reveal that the centre-line velocity begins to decay at a distance of around 4 nozzle diameters downstream of the nozzle exit plane. Both the longitudinal and lateral r.m.s. velocities along the centre-line increase rapidly to a maximum at around 10 nozzle diameters and then decrease gradually. Although the values of

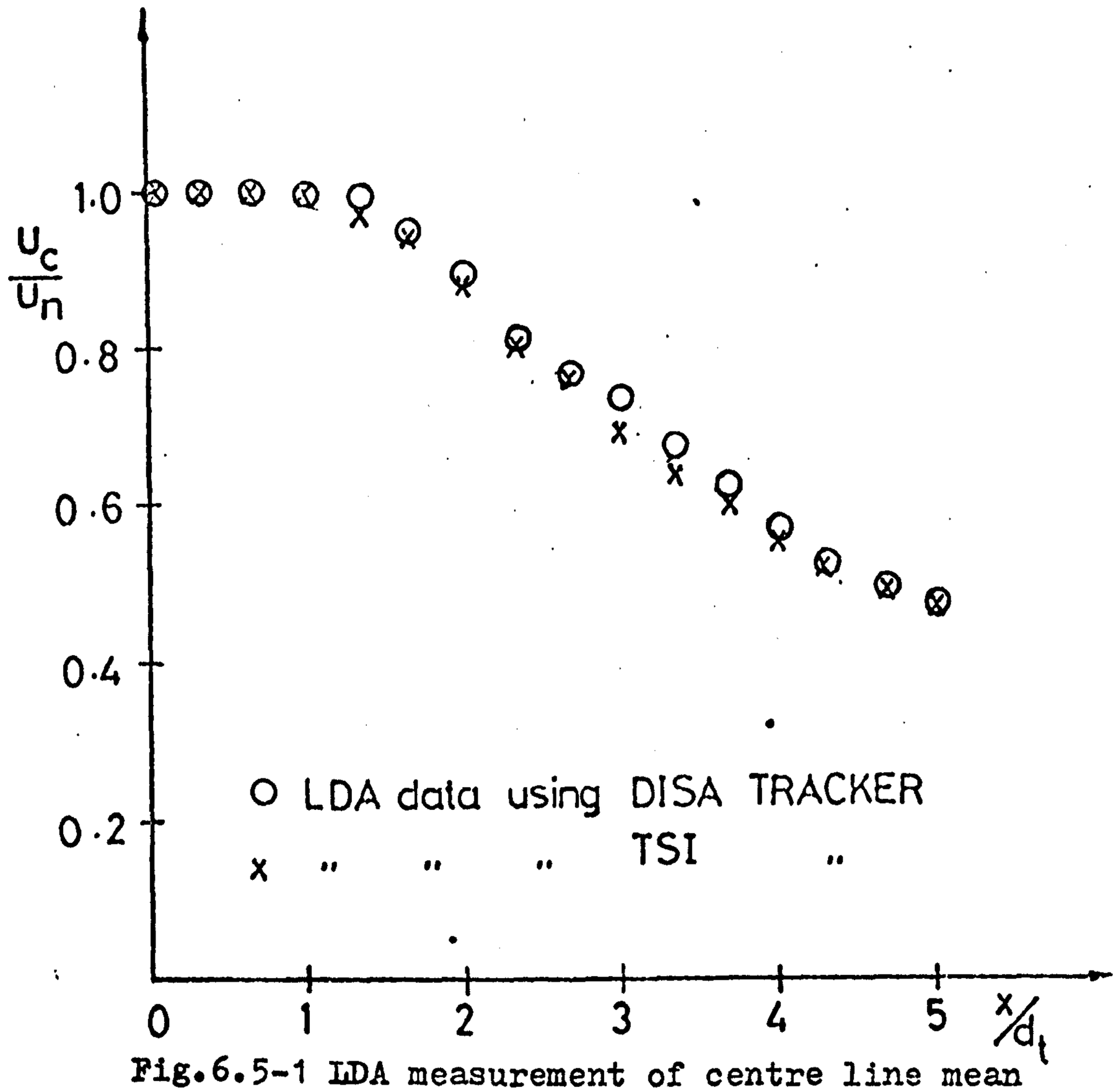

Fig.6.5-1 LDA measurement of centre line mean velocity, r_n/r_t=0.334, U_n/U_e=3.72

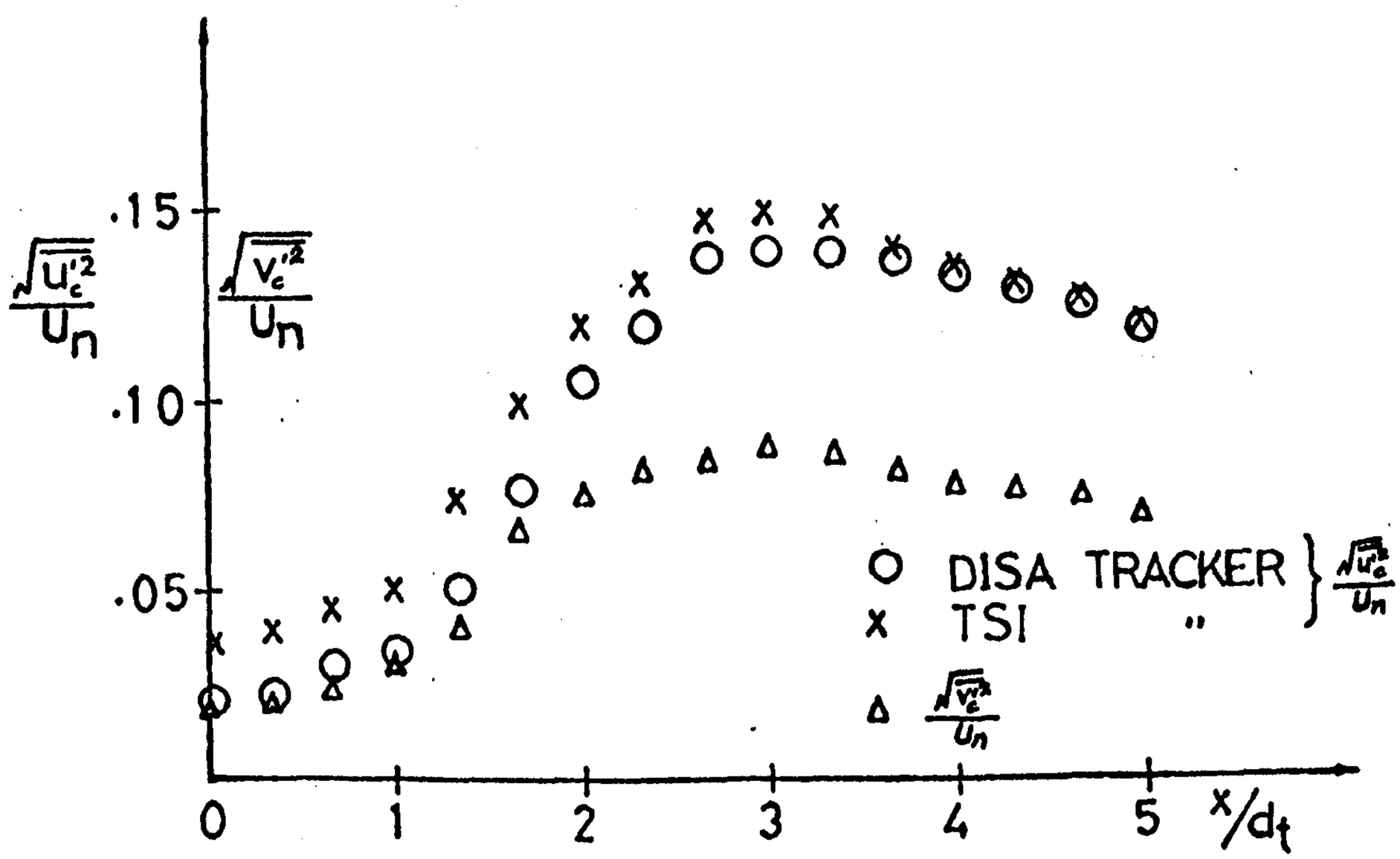

Fig.6.5-2 LDA measurement of centre line r.m.s. velocity, r_n/r_t=0.334, U_n/U_e=3.72.

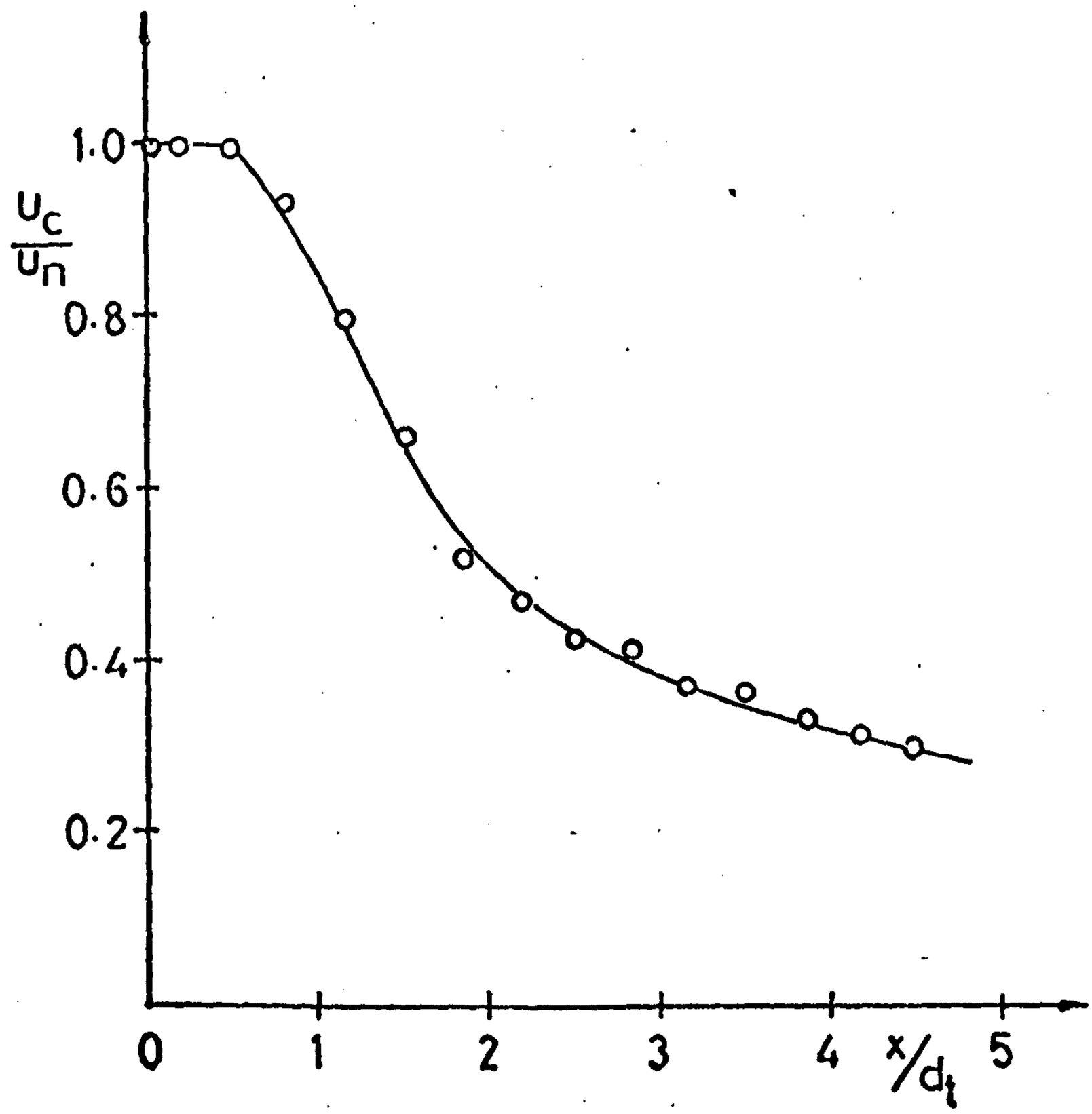

Fig. 6.5-3 Measured centre line mean velocity, r_n/r_t=0.171, U_n/U_e=4.67.

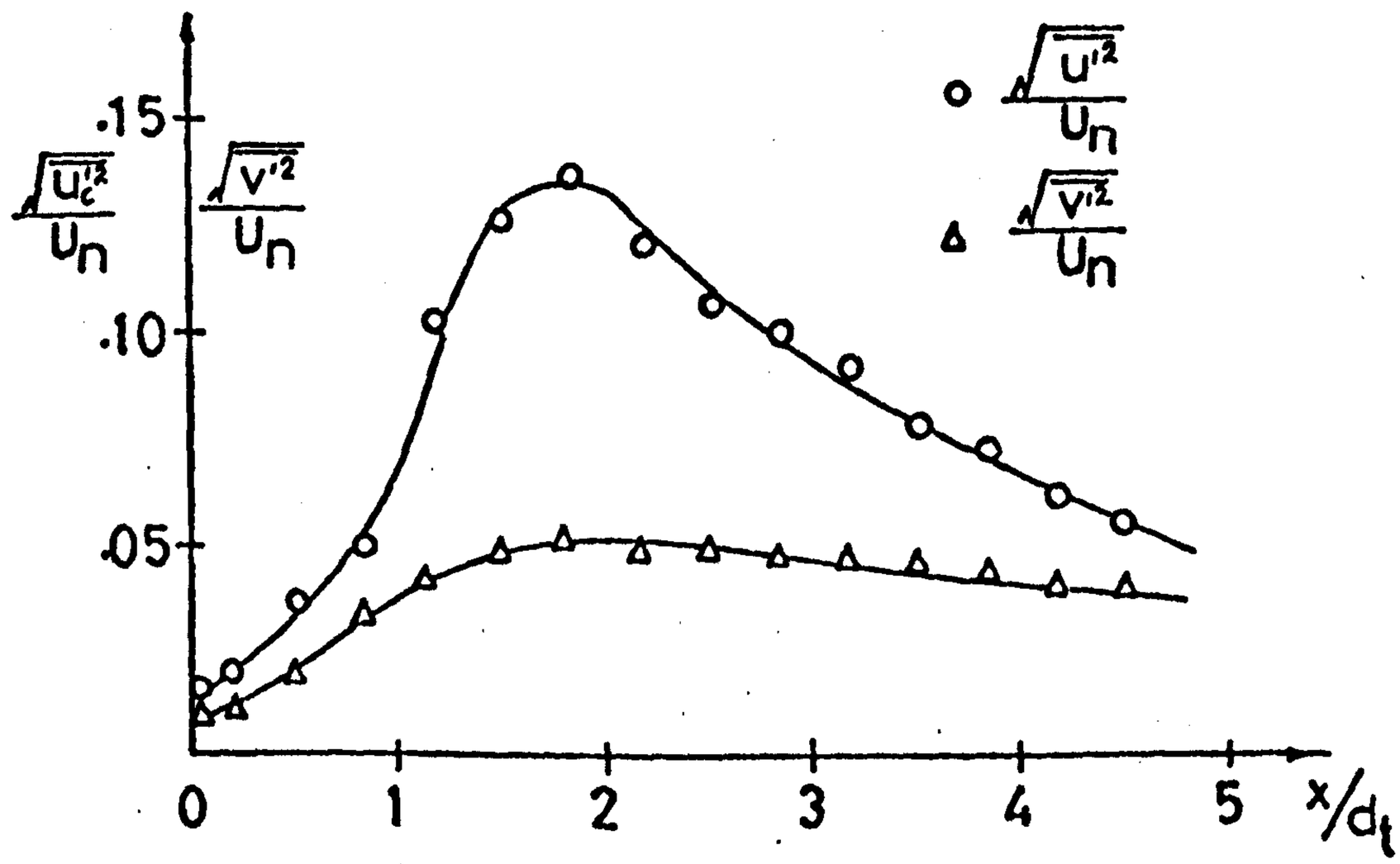

Fig. 6.5-4 Measured centre line r.m.s. velocity, r_n/r_t=0.171, U_n/U_e=4.67.

axial and radial r.m.s. velocities are close to each other at the nozzle exit, the axial value increases faster than the radial value and shows the greatest difference at their peak locations. The difference is more acute in the case of the mixing tube with a smaller radius ratio.

Fig. 6.5-5 and 6.5-6 show the measured mean velocity profiles at various sections downstream of the nozzle exit for the two cases investigated. The superimposed curves give an excellent qualitative description of the confined jet mixing.

Fig. 6.5-7 and 6.5-8 show the measured r.m.s. velocities profiles at the axial, tangential and radial directions. These curves reveal many important characteristics of confined jet mixing. In all cases, the peak values can be observed at a radial position corresponding to the nozzle wall position. The high peak at the beginning of of the mixing tube suggests that turbulent velocities are high at a thin zone separating the primary and secondary streams. As flow develops downstream, the high turbulent zone spreads and grows in width which reflects that the mixing between primary and secondary streams is spreading towards the wall and the axis. Further downstream, turbulent velocity profiles become flat and their levels reduce which suggest that the mixing process is diminishing.

Comparing the profiles of the three r.m.s. velocities, it can be observed that the absolute level of the three components are different especially in the strongly

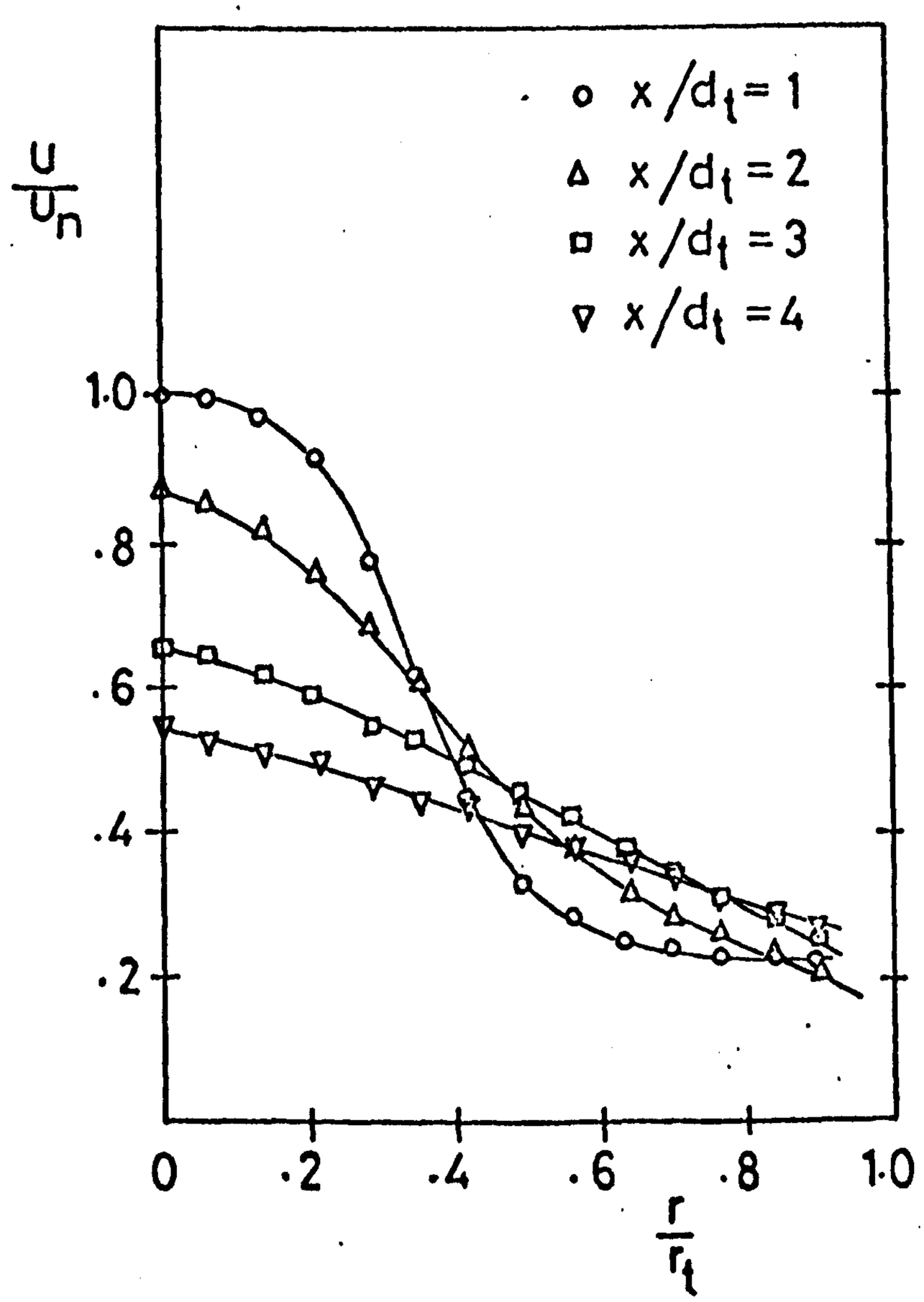

Fig.6.5-5 Measured mean velocity distribution across mixing tube, r_n/r_t=0.334, U_n/U_e=3.72.

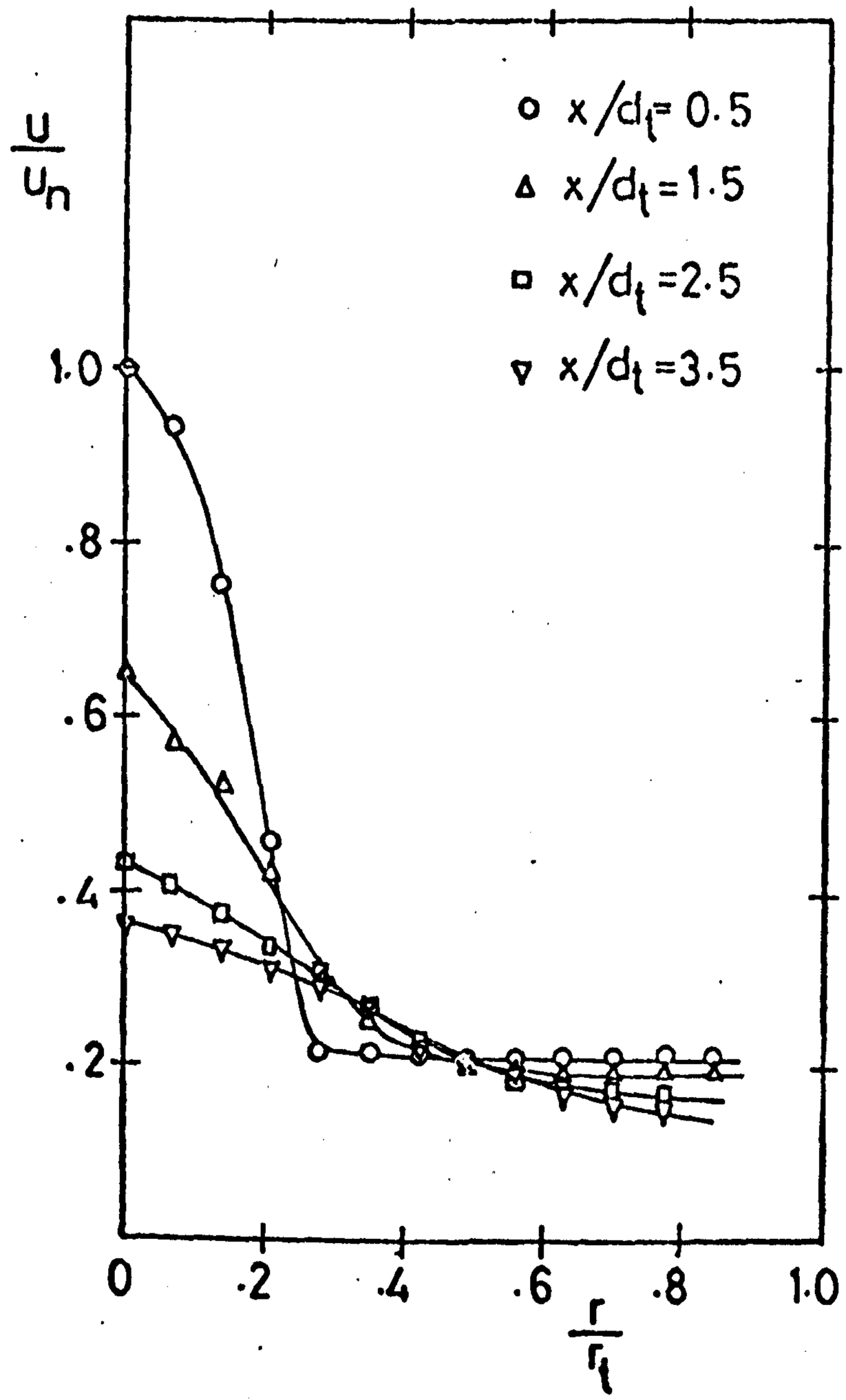

Fig.6.5-6. Measured mean velocity distribution across mixing tube, $r_n/r_t=0.171$, $U_n/U_e=4.67$.

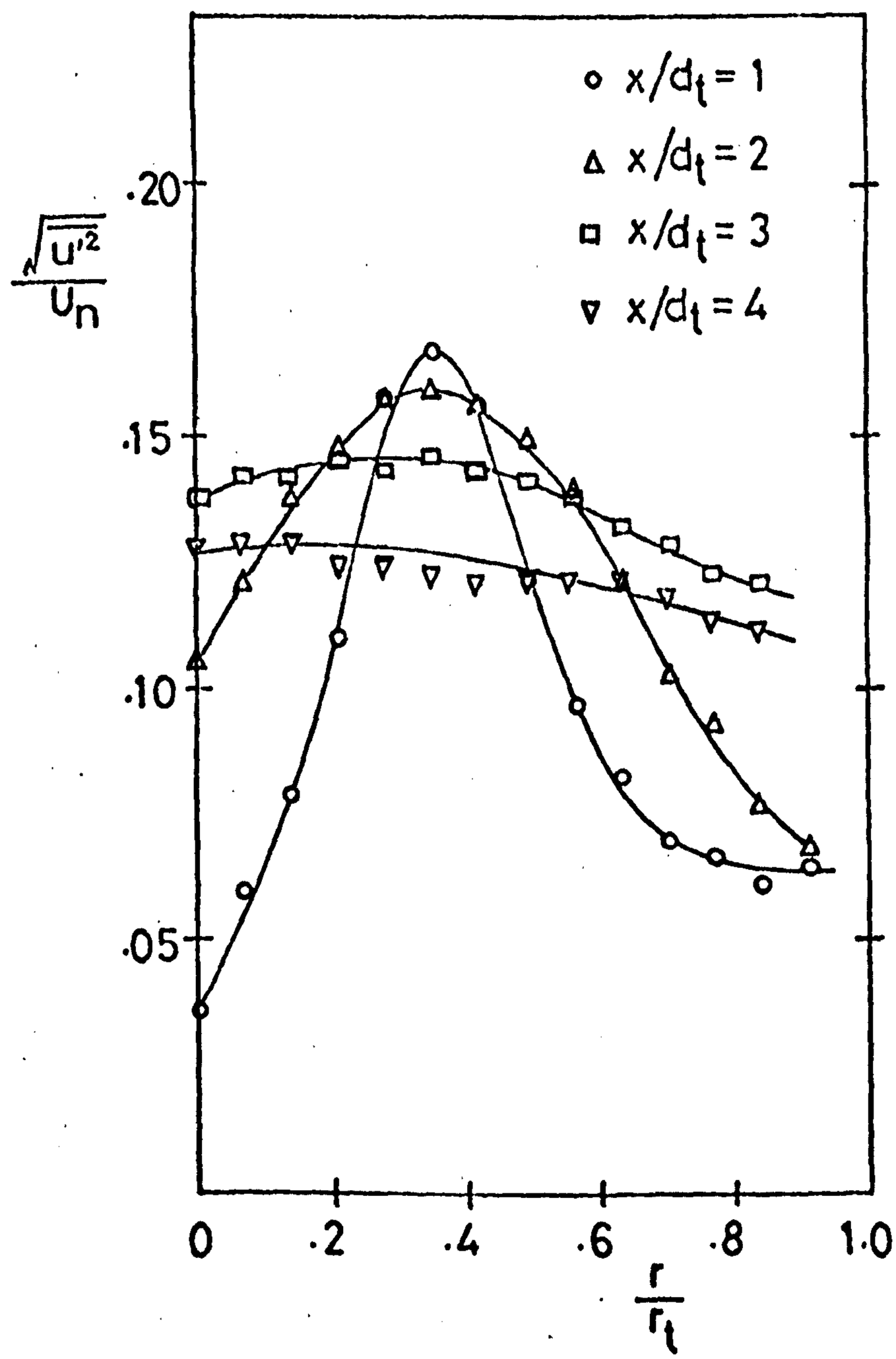

Fig.6.5-7(a) Measured axial r.m.s. velocity profiles, r_n/r_t=0.334, U_n/U_e=3.72.

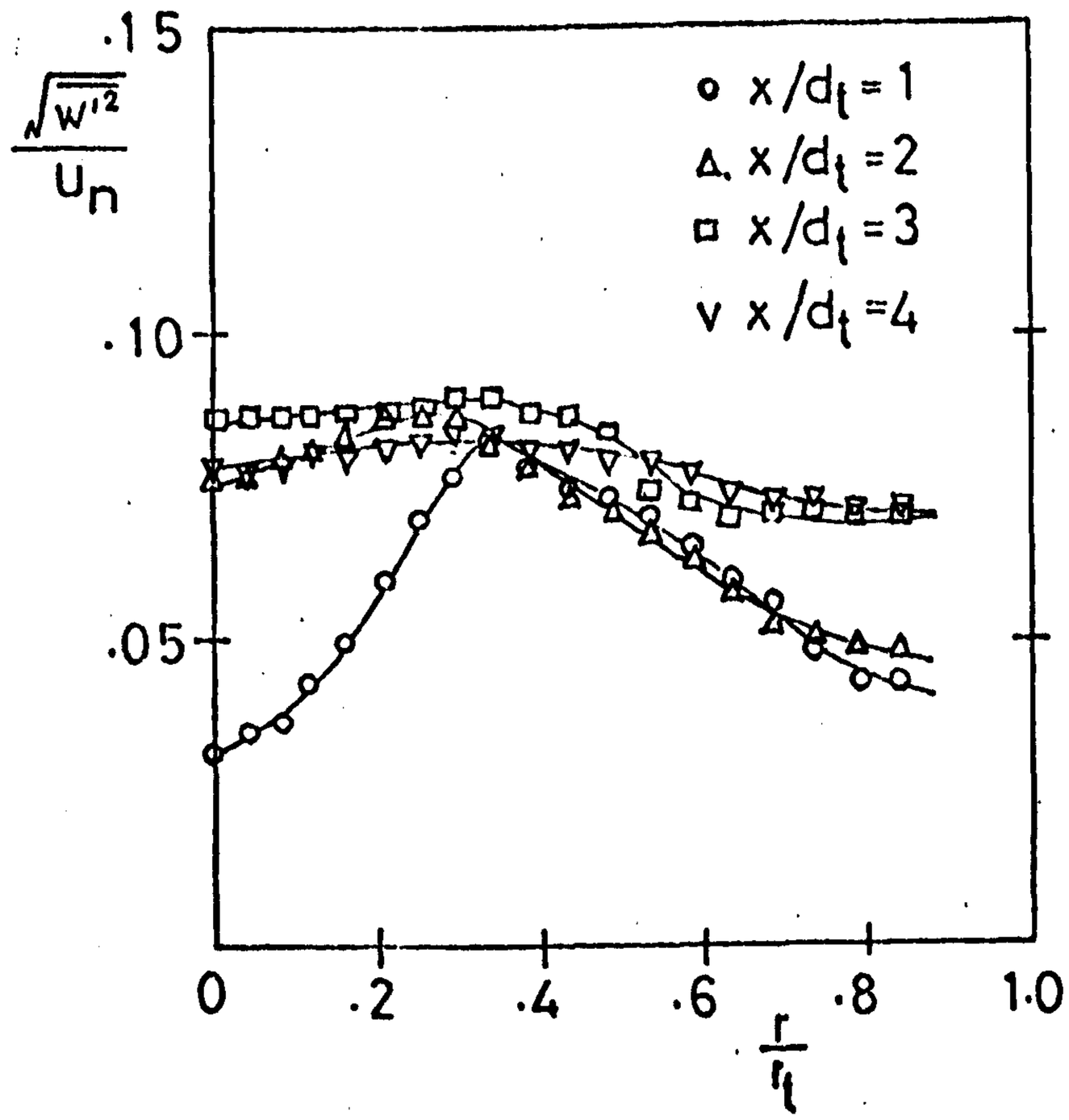

Fig.6.5-7(b) Measured tangential r.m.s. velocity profiles, r_n/r_t=0.334, U_n/U_e=3.72.

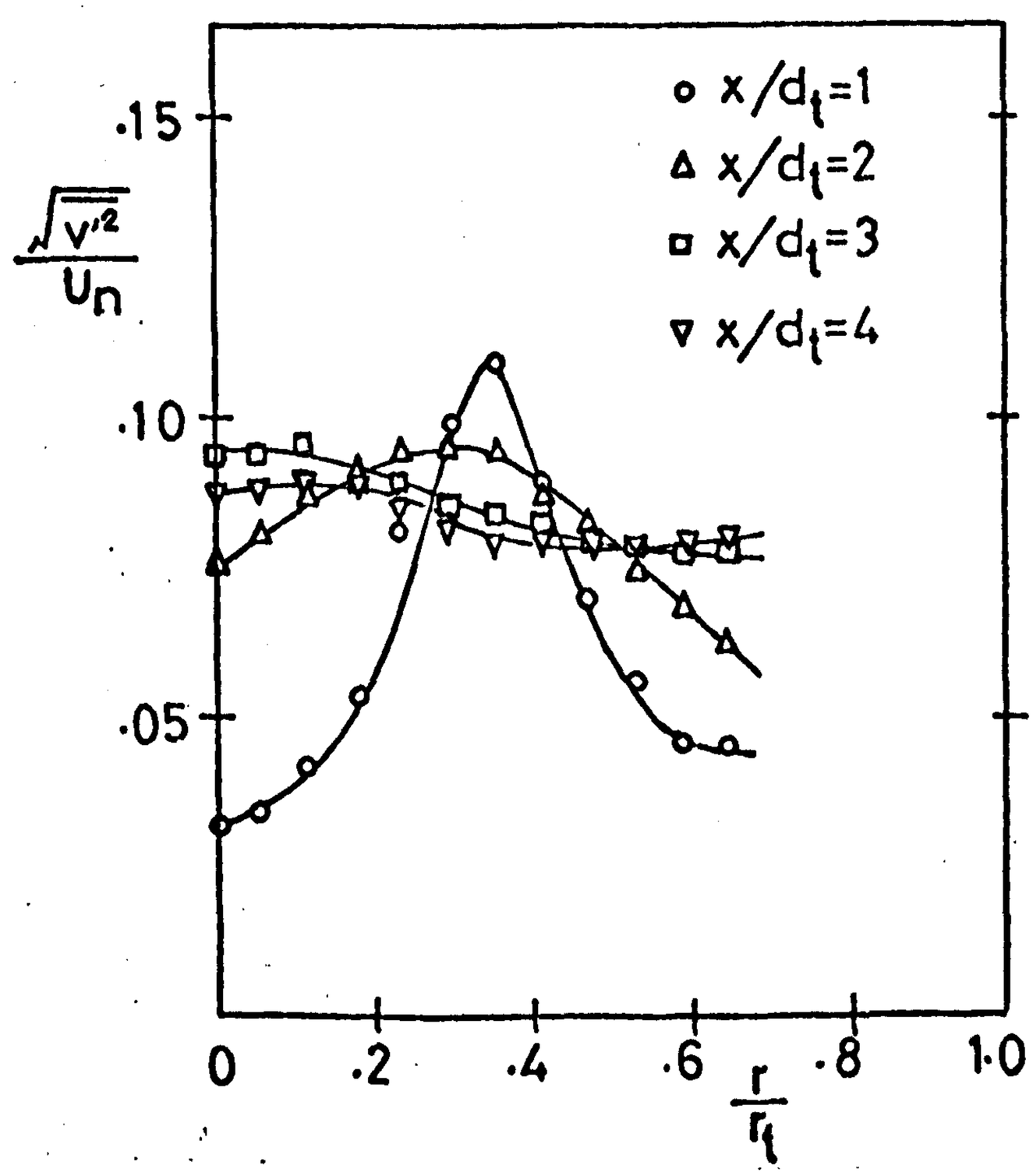

Fig.6.5-7(c) Measured radial r.m.s. velocity profiles, r_n/r_t=0.334, U_n/U_e=3.72.

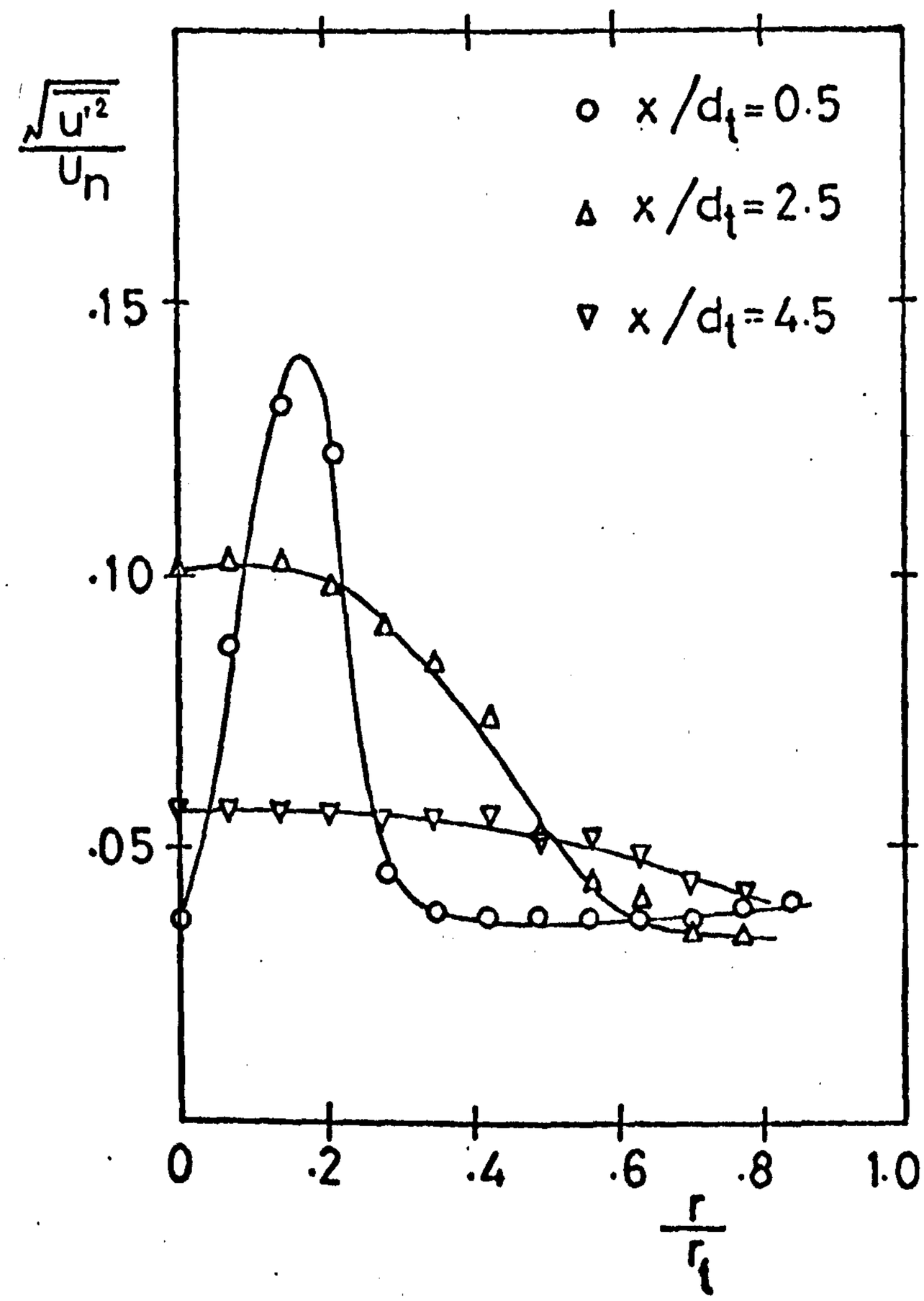

Fig.6.5-8(a) Measured axial r.m.s. velocity profiles, r_n/r_t=0.171, U_n/U_e=4.67.

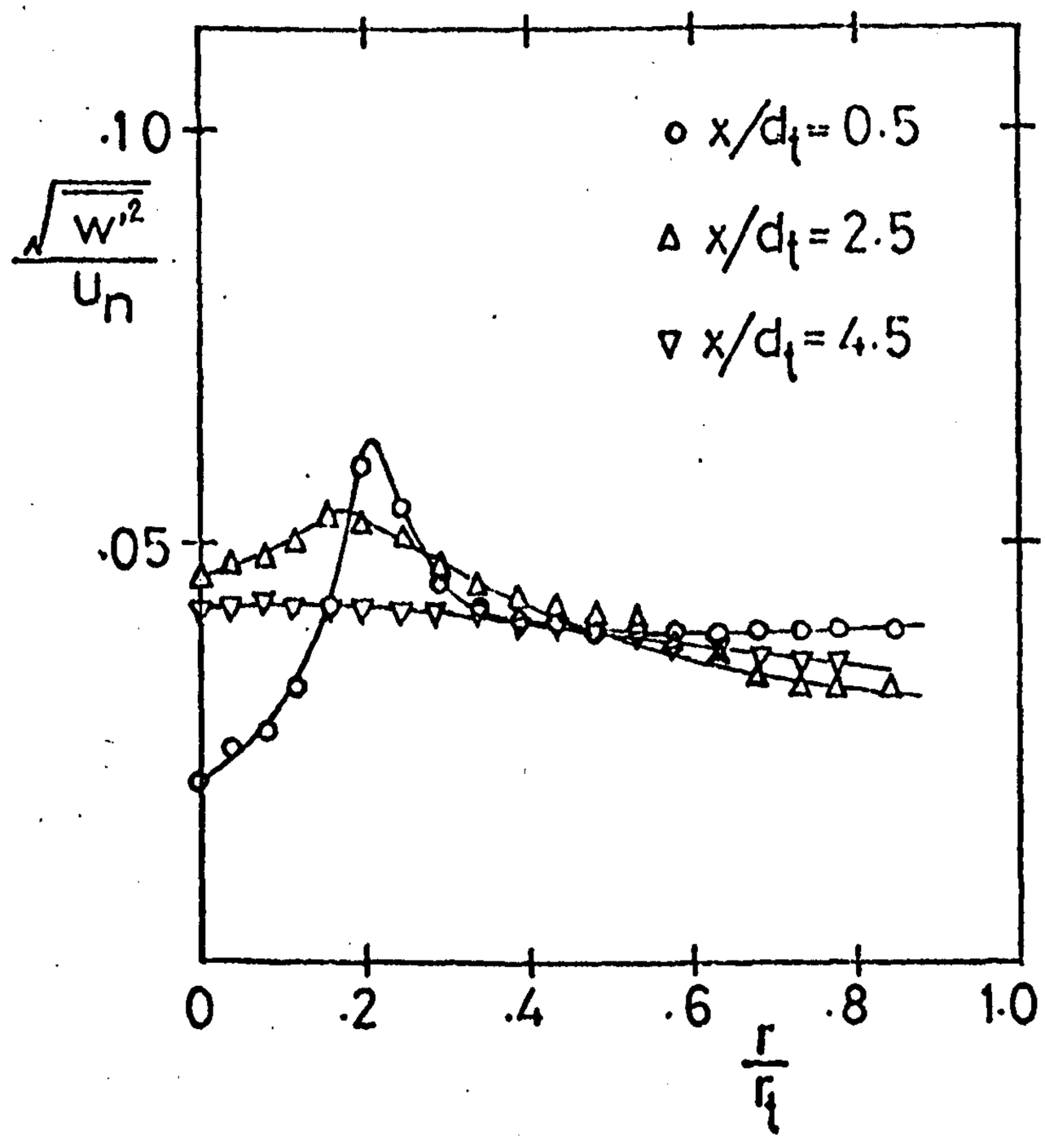

Fig.6.5-8(b) Measured tangential r.m.s. velocity profiles, r_n/r_t=0.171, U_n/U_e=4.67.

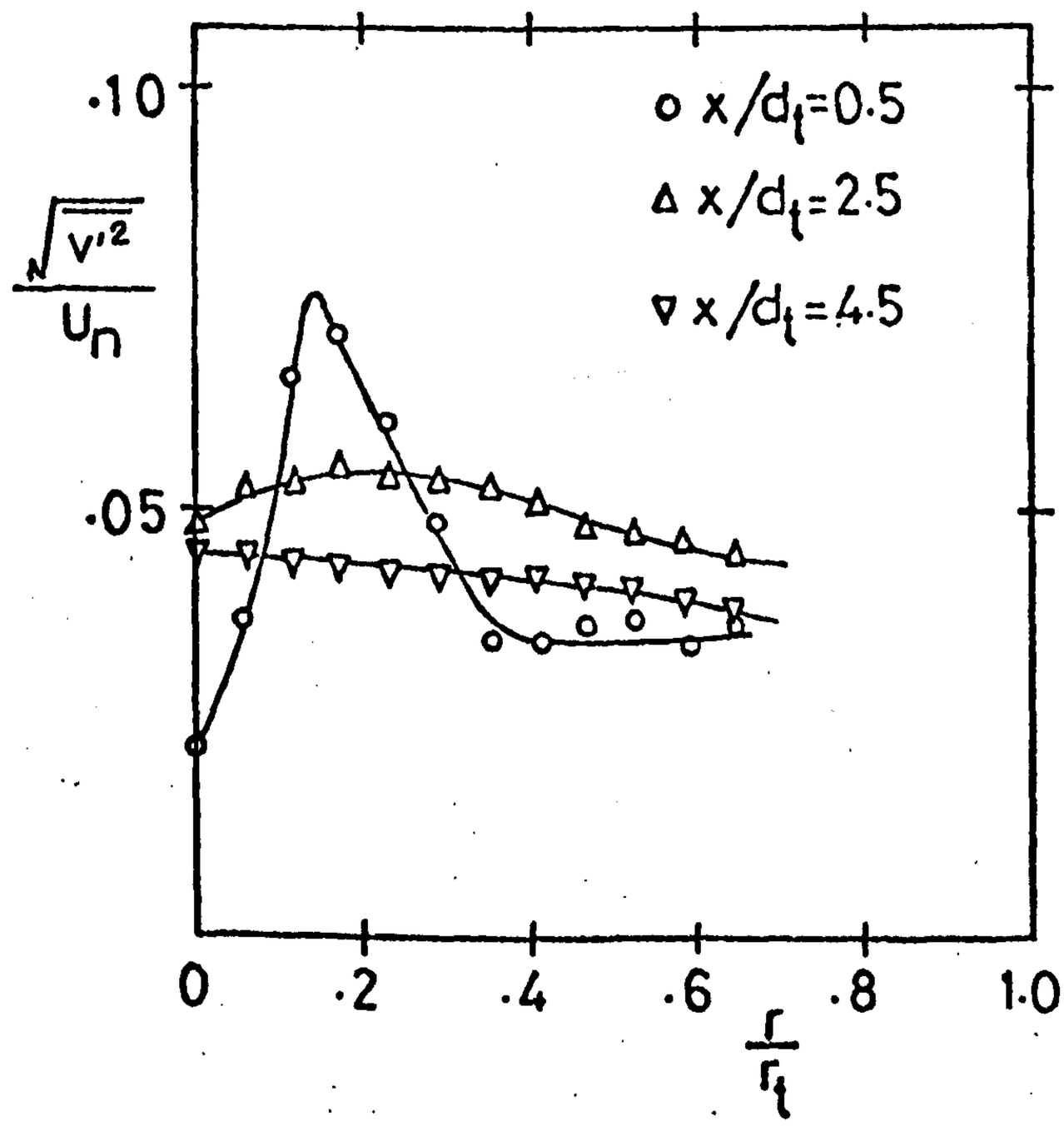

Fig.6.5-8(c) Measured radial r.m.s. velocity profiles, r_n/r_t=0.171, U_n/U_e=4.67.

mixing regions. The confined jet mixing is thus not an isotropic turbulent flow.

The mean and r.m.s. velocities at nozzle exit and secondary inlet were also measured. Their values were found to be closely uniform. The primary and secondary inlet k values were then calculated from the r.m.s. velocities. The results are tabulated in Table 6.5-2.

r_n/r_t	U_n	U_e	k_n	k_e
0.334	3.05	0.82	0.00486	0.0223
0.171	5.72	1.22	0.00697	0.0670

Table 6.5-2 Inlet conditions of mixing tube

6.5.2 Comparison of LDA Measurement with Prediction

The computer program for uniform diameter mixing tube was run for the geometrical and flow conditions used for the LDA measurement. The inlet values given in Table 6.5-2 were used as boundary conditions for the computer prediction. Inlet length scales were assumed to be 0.015* and 0.0085* of the mixing tube radius for the 12.7mm and 6.5mm nozzles respectively. The calculation was performed up to 8 diameters of the mixing tube with a 18 x 14 grid.

Fig. 6.5-9 and 6.5-10 show the comparison of the mean velocity and turbulent kinetic energy along the axis of the mixing tube. The agreement between the measurement

See Appendix A.9

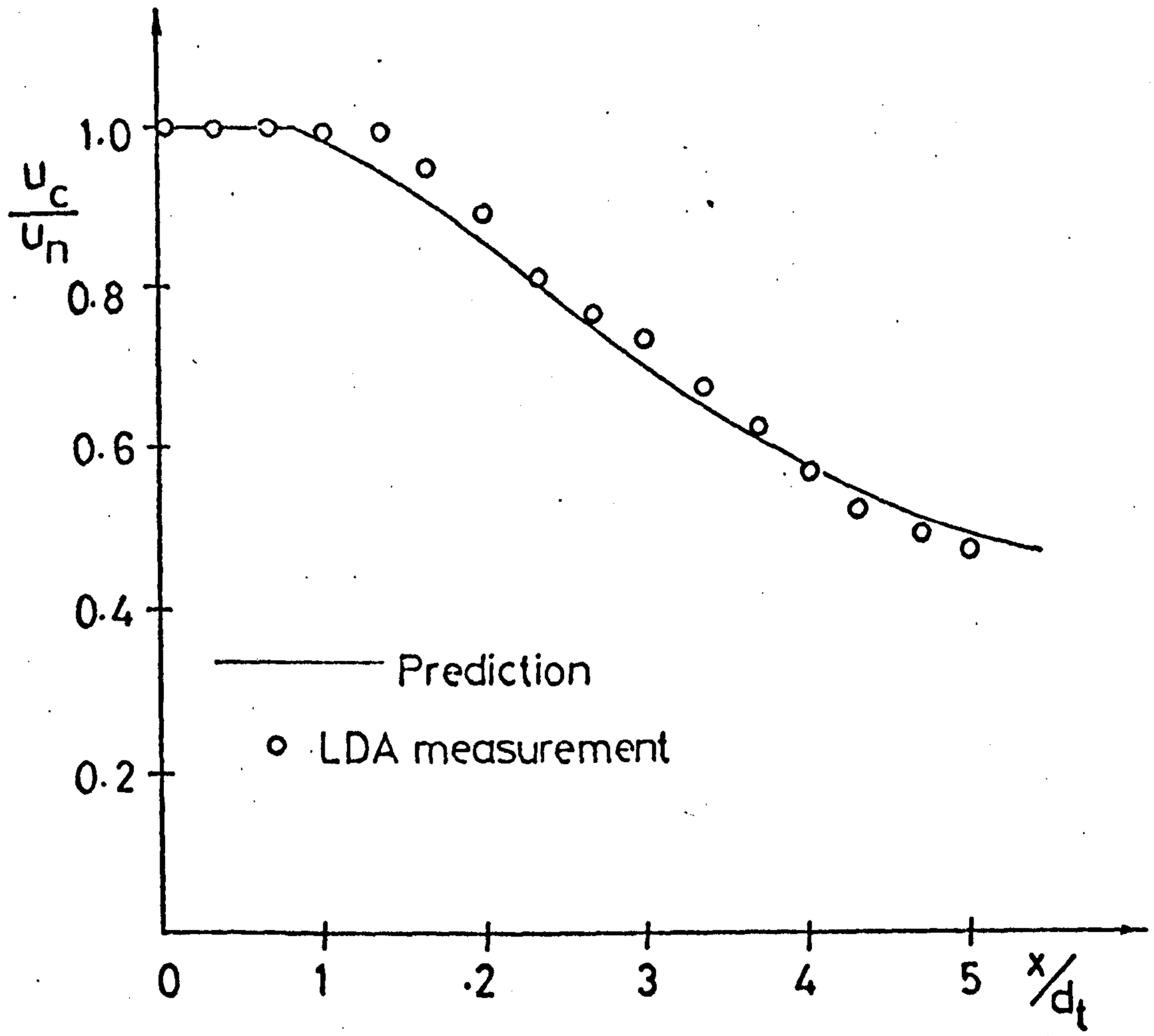

Fig.6.5-9(a) Comparison of predicted and measured centre line mean velocity, r_n/r_t=0.334, U_n/U_e=3.72.

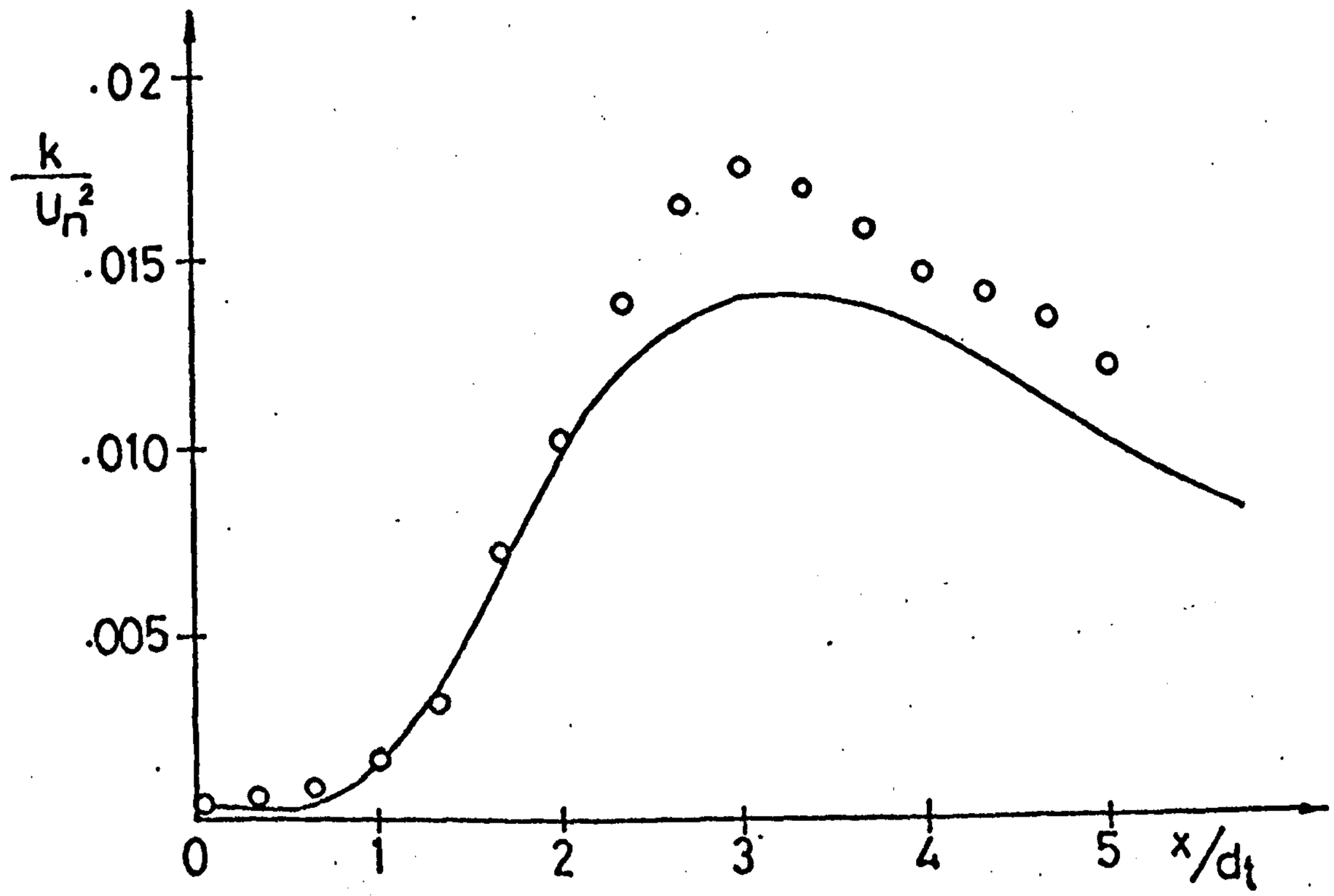

Fig.6.5-9(b) Comparison of predicted and measured centre line turbulent kinetic energy, r_n/r_t=0.334, U_n/U_e=3.72.

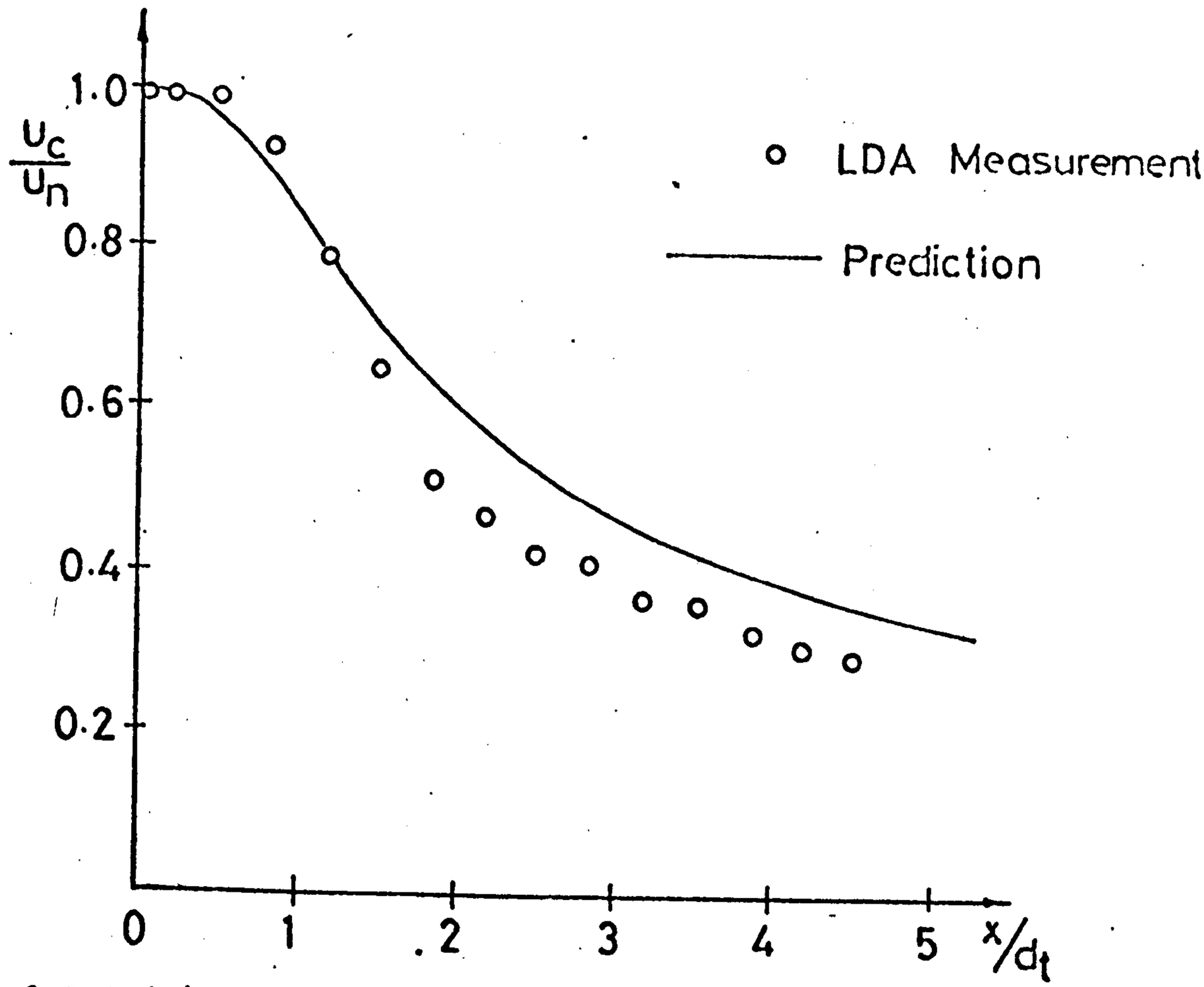

Fig.6.5-10(a) Comparison of predicted and measured centre line mean velocity, r_n/r_t=0.171, U_n/U_e=4.67.

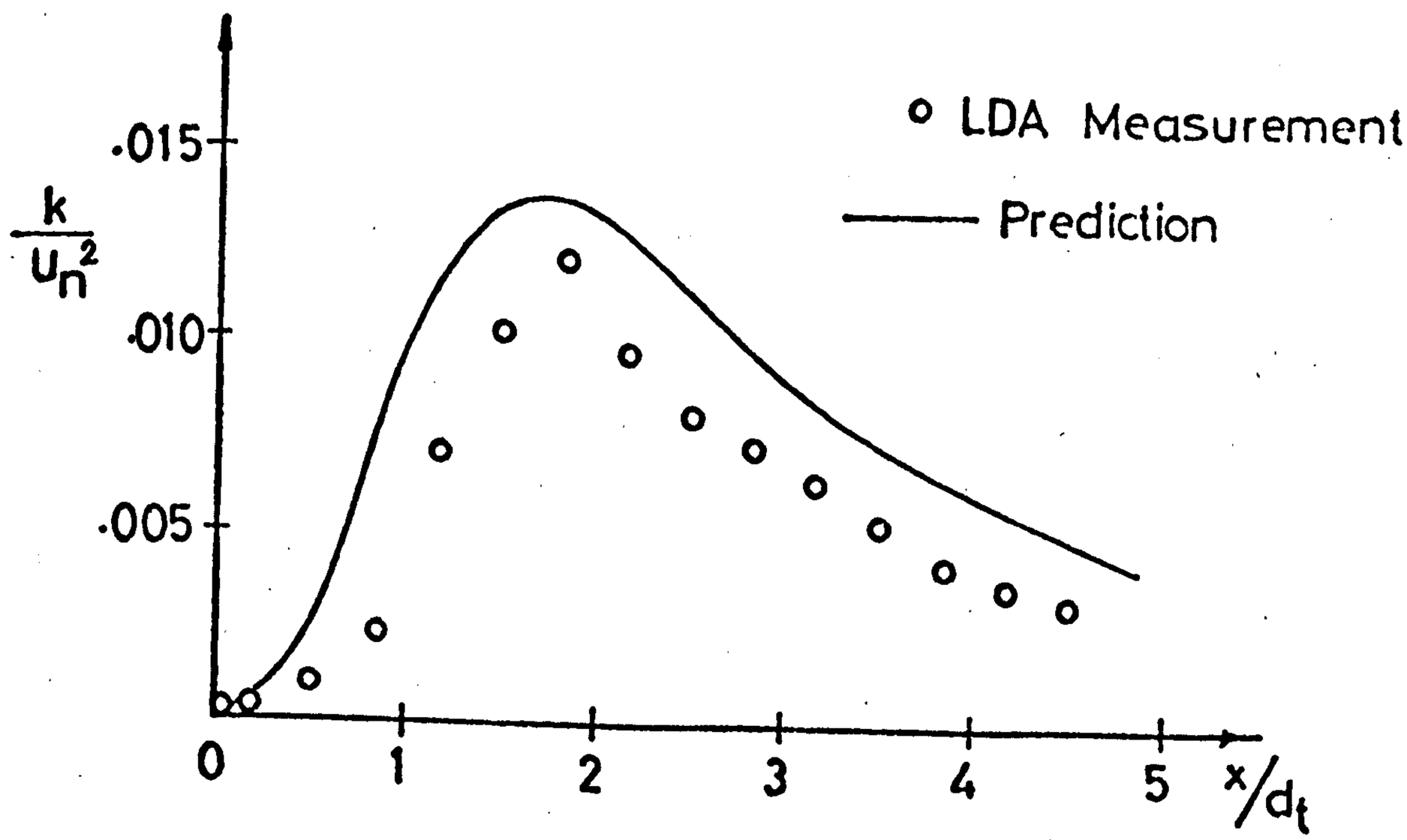

Fig.6.5-10(b) Comparison of predicted and measured centre line turbulent kinetic energy, r_n/r_t=0.171, U_n/U_e=4.67.

and prediction is excellent in the case of 0.334 radius ratio except for the k value at the region beyond 3 mixing tube diameters where a difference of 10 to 15% is observed. In the case of 0.171 radius ratio, the agreement can be considered as satisfactory where measurement and prediction confirm qualitatively with an average difference of 15%. In Fig. 6.5-11 and 6.5-12, comparisons of measured and predicted velocity profiles at various sections in the mixing tube are shown. Again, the agreement for the 0.334 radius ratio mixing tube is excellent, whereas for the case of 0.171 radius ratio, the predicted velocity profiles are somewhat 10% to 15% higher than the measured profiles. However, the shapes of the profiles agree closely with each other.

Fig. 6.5-13 and 6.5-14 show the comparisons of measured and predicted k profiles. The results have been non-dimensionalized by U_n^2. The agreement between the prediction and measurement is fairly good for 0.334 radius ratio. For the 0.171 radius ratio mixing tube, the predicted values are slightly higher than the measured values but it can still be considered as satisfactory especially when the shapes of the profiles are concerned.

6.5.3 Discussion

The measurements of mean and fluctuating velocities in confined jet mixing have been successfully carried out by a laser Doppler anemometer. The measurements of axial and tangential components were obtained down to 0.1 radius from the tube wall. However, measurement of the

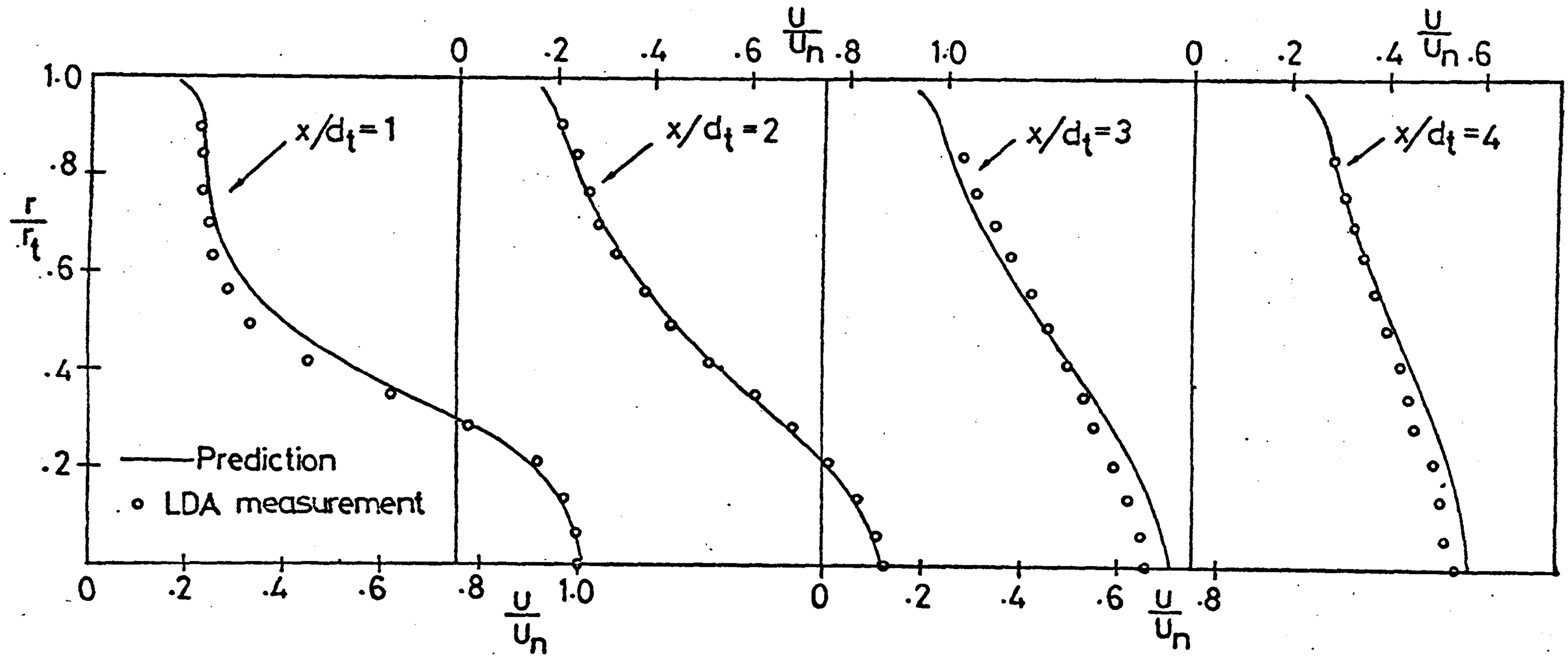

Fig.6.5-11 Comparison of predicted and measured mean velocity profiles, r_n/r_t=0.334, U_n/U_e=3.72.

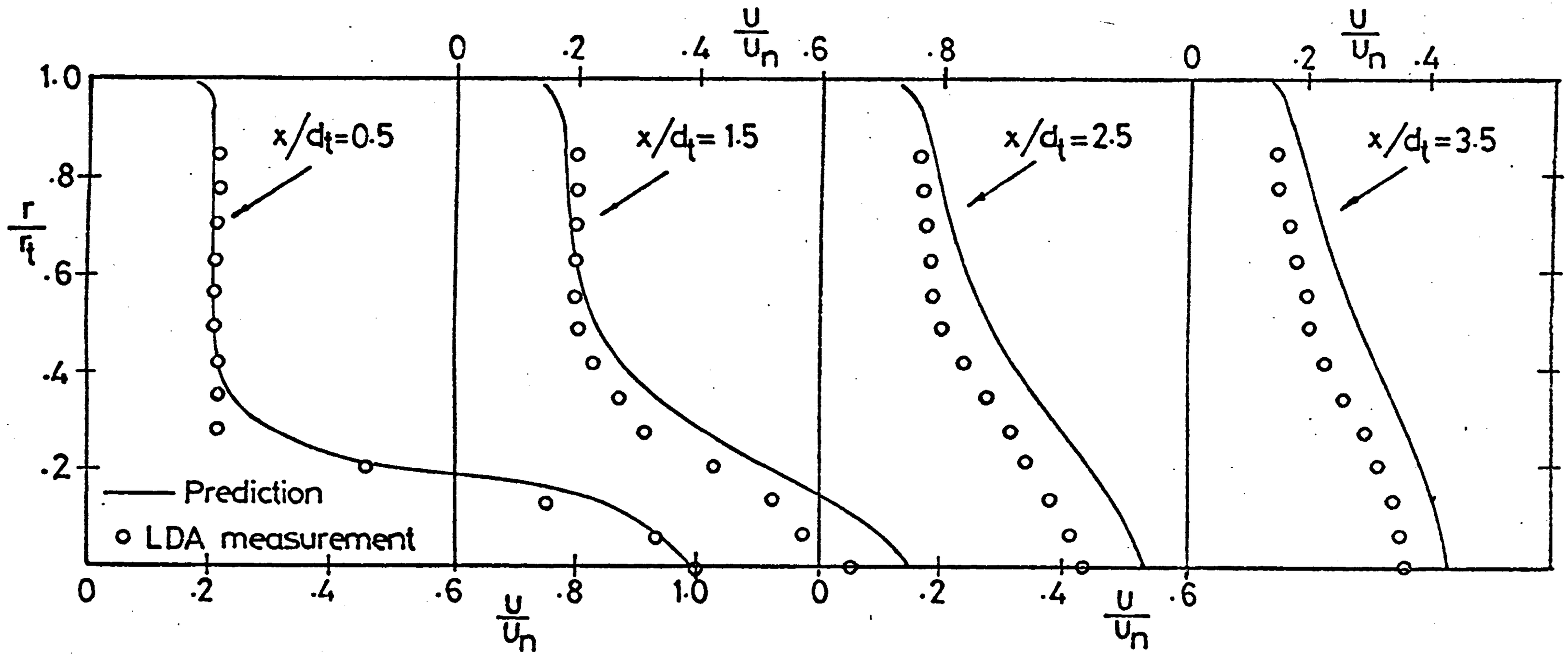

Fig.6.5-12 Comparison of predicted and measured mean velocity profiles, r_n/r_t=0.171, U_n/U_e=4.67.

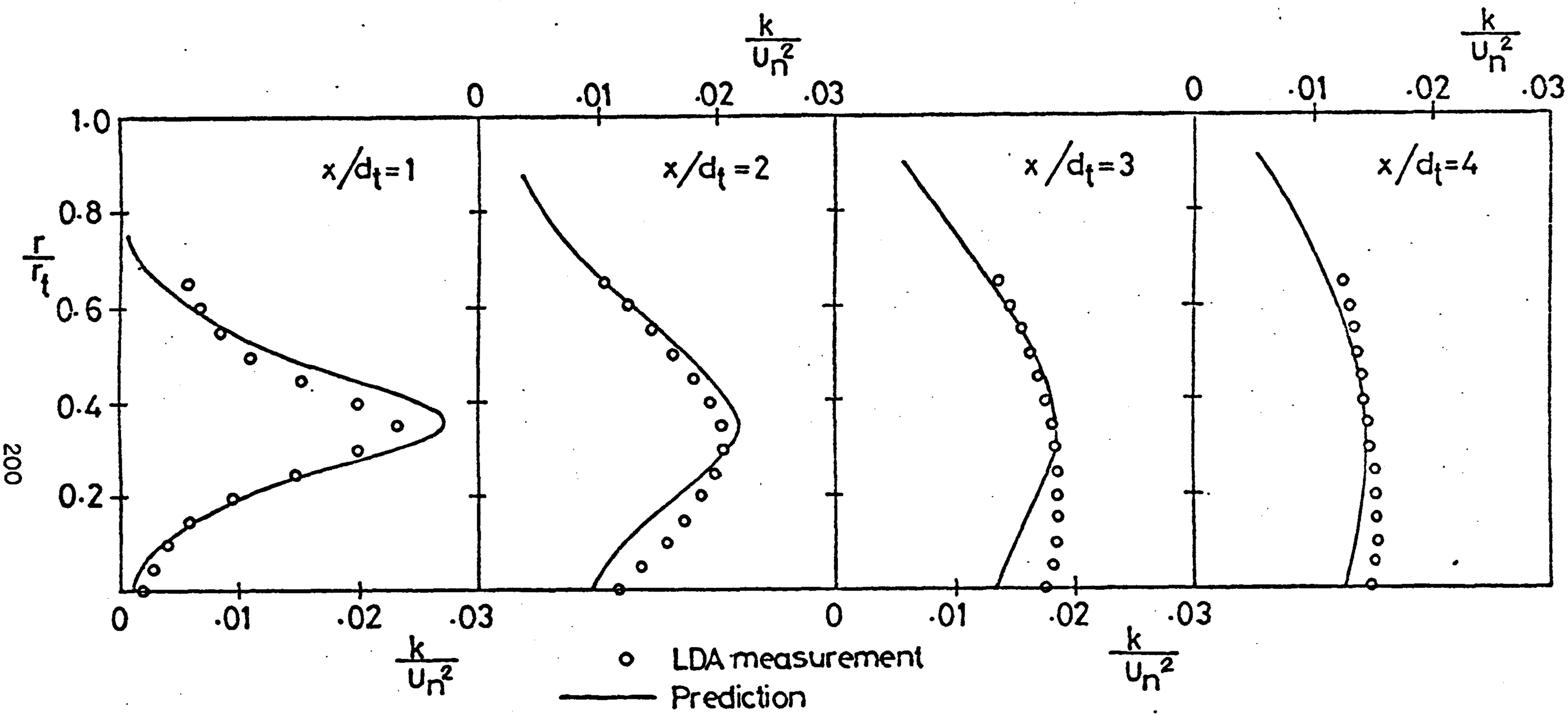

Fig.6.5-13 Comparison of predicted and measured turbulent kinetic energy, r_n/r_t=0.334, U_n/U_e=3.72.

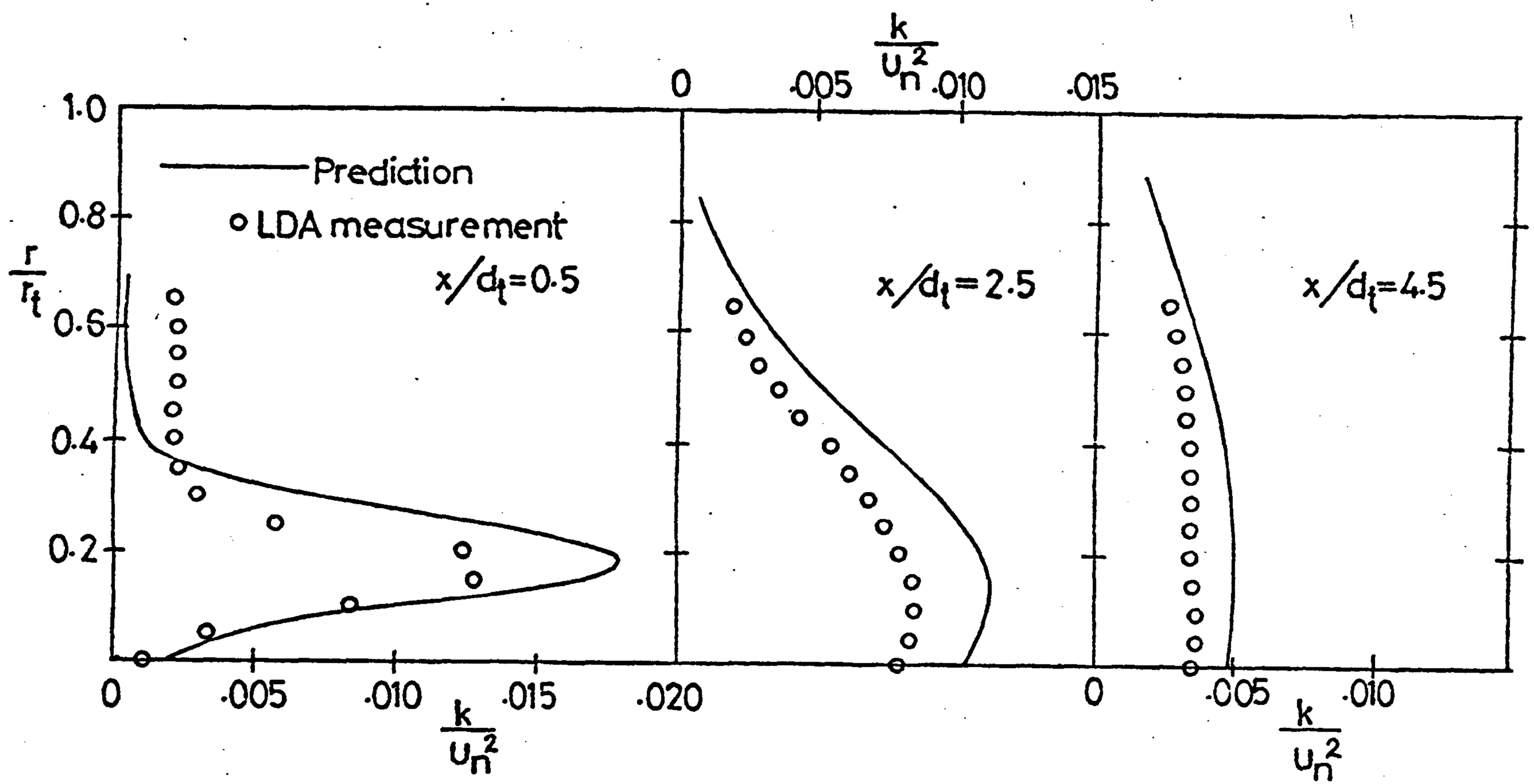

Fig.6.5-14 Comparison of predicted and measured turbulent kinetic energy, $r_n/r_t=0.171$, $U_n/U_e=4.67$.

radial component could only be obtained up to 0.65 radius from the axis of the tube under the present geometrical arrangement. Beyond that, it was extremely difficult to align the photomultiplier so that the measuring control volume could clearly be focused on the pinhole.

The possible error of measuring mean and fluctuating velocities using LDA may be attributed to any of the following sources: (1) poor beam intersection, (2) photomultiplier has not been correctly focused on the measuring volume, (3) scattering particle size has not been matched with the laser optics, (4) the density of scattering particles is too low or too high, (5) mean velocity gradient broadening, (6) transit-time broadening, and (7) electronic noise. The first three types of error can be eliminated by the proper set up of the optical system and careful design of the components. Item (4) is dependent on the water quality but for ordinary tap water, performance has been found satisfactory. Errors due to the gradient broadening and transit time broadening have been discussed in detail by Melling and Whitelaw (1973). According to the procedure outlined, these errors were estimated and found to be relatively small. Errors arising from electronic noise are dependent upon the design of the signal processing electronics. By using the upper portion of any frequency range of the tracker, such errors can be reduced to a minimum. For the DISA tracker, the electronic noise level was at most 0.2% of the mean output voltage.

The accuracy of the measurement also depends on the

elimination of noise and the dynamic response of the tracker. To remove as much noise as possible from the input signal, a narrow bandwidth setting of the I.F. filter in the tracker is necessary. However, such setting will inevitably restrict the rate at which the tracker can follow a changing input frequency. Thus, an optimum adjustment of the tracker is always a compromise between dynamic response and satisfactory rejection of noise. In a noisy turbulent signal, in order to eliminate noise satisfactorily, a lower r.m.s. velocity measurement can be expected due to the poor dynamic response of the tracker. This explains logically that the measured k-profiles are always lower than the predicted values at high turbulent regions.

The agreeement between the prediction and measurement is in general better in the case of 0.334 radius ratio than the case of 0.171. This is expected because for the smaller nozzle, it is necessary to have finer grids. However, our predictions for both cases use the same 18 x 14 grid owing to the computer time load. By increasing 50% of grid lines both radially and axially, the number of nodes will increase 125%. If the number of iteration remains unchanged, the computer time has to be increased by 125%. The present jet mixing computer program with 18 x 14 grid takes 15 minutes to run for 150 iterations on the IBM 370 computer. Any increase in the number of grids will be uneconomical. A compromise between accuracy and economy is always necessary. However, a study of the effect of

grid size are already given in section 5.1.2.

6.6 Measurement of Static Pressure in Mixing Tube and Diffuser

Measurements of static pressure were carried out in a test section consists of a mixing tube with internal diameter 25mm and a short diffuser with 7° included angles as described in section 6.2.2. The flow circuit was operated as an ordinary jet pump described in section 6.2.1. Two nozzles of geometrical details given in section 6.2.2 were used in the test. The nozzle exit was positioned to coincide with the mixing tube inlet. Geometrical and flow conditions for pressure measurement are tabulated in Table 6.6-1.

d_n/d_t	$M(Q_2/Q_1)$	d_t(mm)	d_n(mm)	Q_1(m^3/hr)
0.508	0.292	25	12.7	5.45
0.508	0.307	25	12.7	6.36
0.508	0.316	25	12.7	7.21
0.260	1.04	25	6.5	1.82
0.260	1.13	25	6.5	2.27
0.260	1.17	25	6.5	2.73

Table 6.6-1 Geometrical and flow conditions for static pressure testing

Static pressure tappings along the jet pump wall were connected into a manifold. Two gauge pressure meters, one for measuring positive gauge pressure of 0-1.6 bars and

the other for measuring negative gauge pressure of -1.0-0 bars were installed at the two ends of the manifold. Such arrangement provides facility for measuring static gauge pressure from -1.0 bar to 1.6 bars which is well beyond the pressure range of the testing jet pump.

The results of the measurements are presented in Fig. 6.6-1 and 6.6-2. The static pressure along the jet pump was plotted against the distance from the nozzle exit. Both figures demonstrate that a higher flow ratio, which was generated from a higher primary flow rate, gives a higher static pressure rise in the mixing tube. However, the static pressure rise in diffuser did not change much with different flow ratios.

The computer programs for mixing tube and diffuser were run to predict two measurements, one for each diameter ratio. The predicted result are compared with the measured values in Fig. 6.6-3 and 6.6-4. The static pressures were non-dimensionalized by the dynamic head of the nozzle exit velocity. The agreement between the measurement and prediction appears to be satisfactory.

By now, the computer model has been tested and compared with the experimental data from Razinsky and Brighton (1971), Sanger (1968a, 1968b) as well as the present measurements. All these comparisons suggest that the two equation k- ε model is capable of predicting pressure rise satisfactory in jet pump flows.

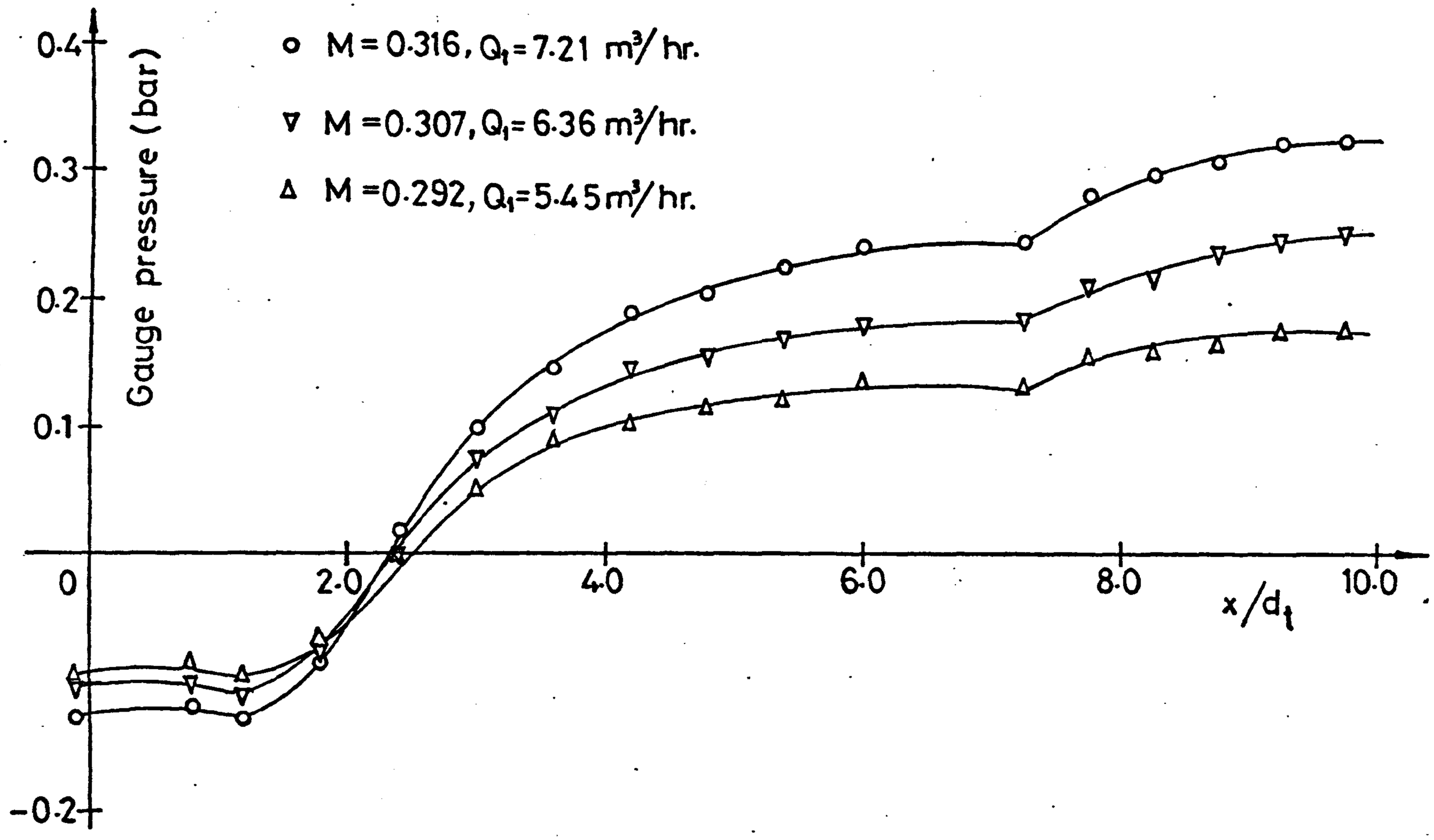

Fig. 6.6-1 Measured Static Pressure Variation Along Jet Pump, $d_n/d_t = 0.508$, $\theta = 7^o$.

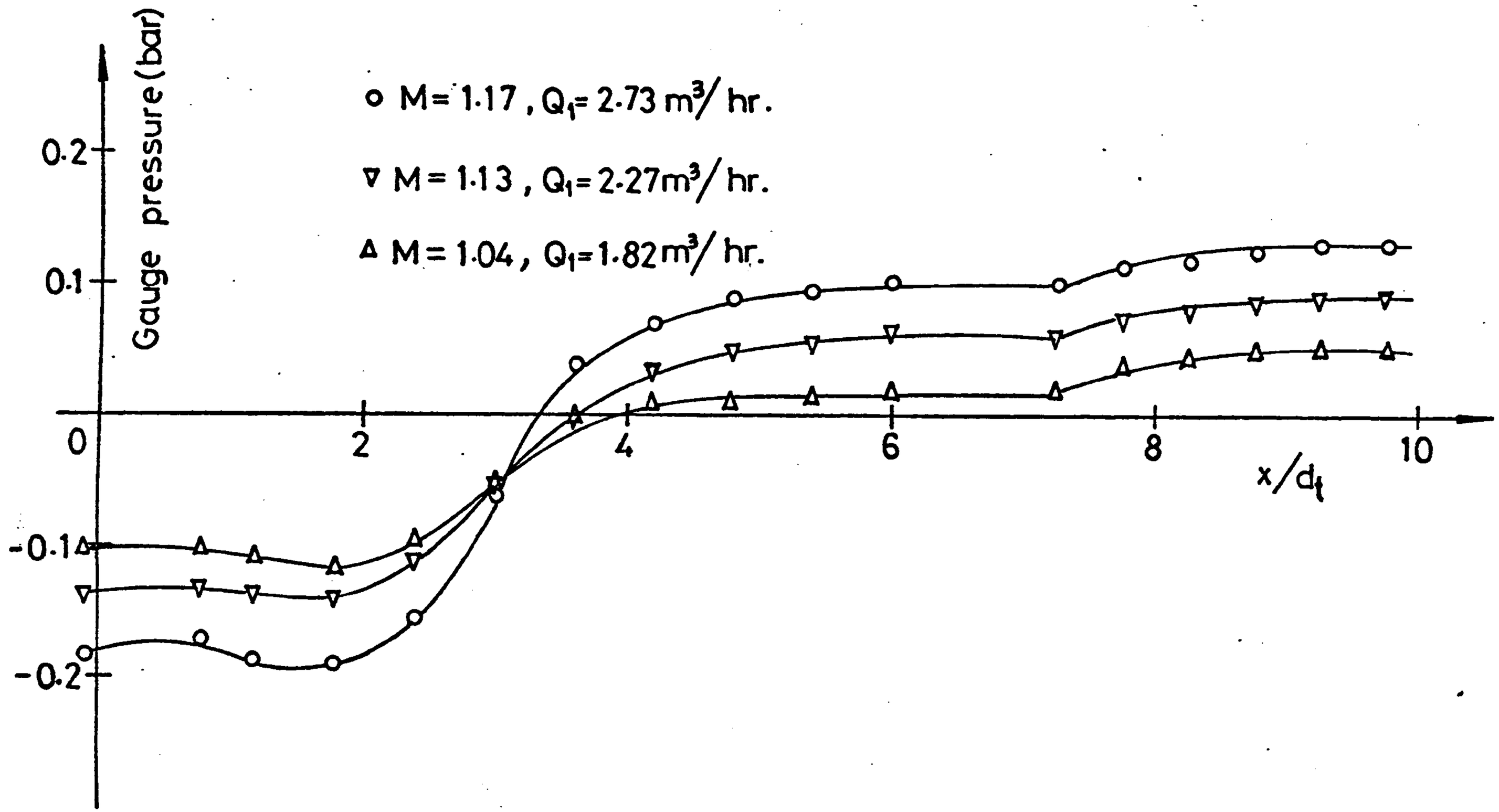

Fig. 6.6-2 Measured Static Pressure Variation Along Jet Pump, $d_n/d_t = 0.26$, $\theta = 7^{\circ}$.

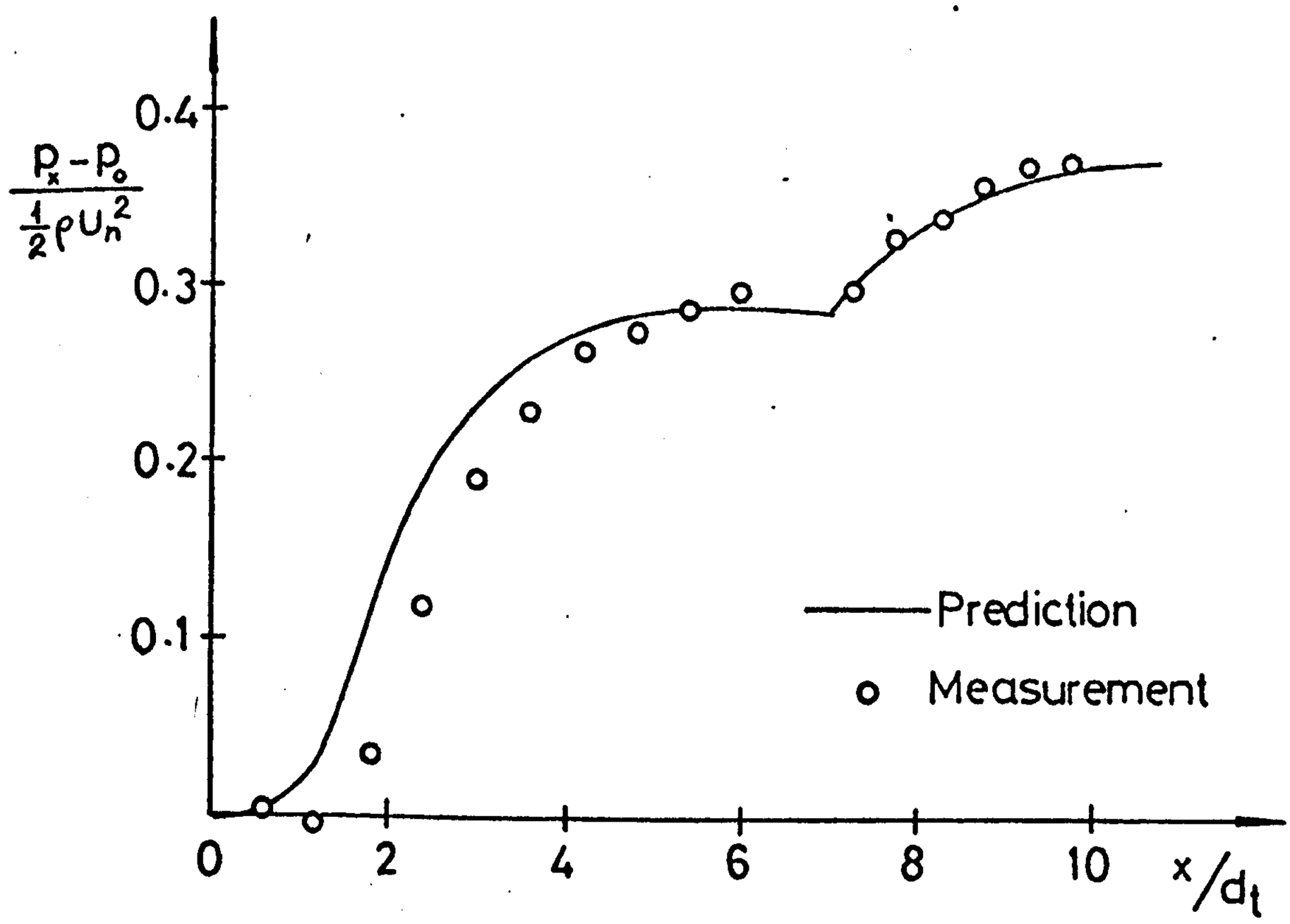

Fig. 6.6-3 Comparison of predicted and measured static pressure along jet pump, d_n/d_t=0.508, θ=7°.

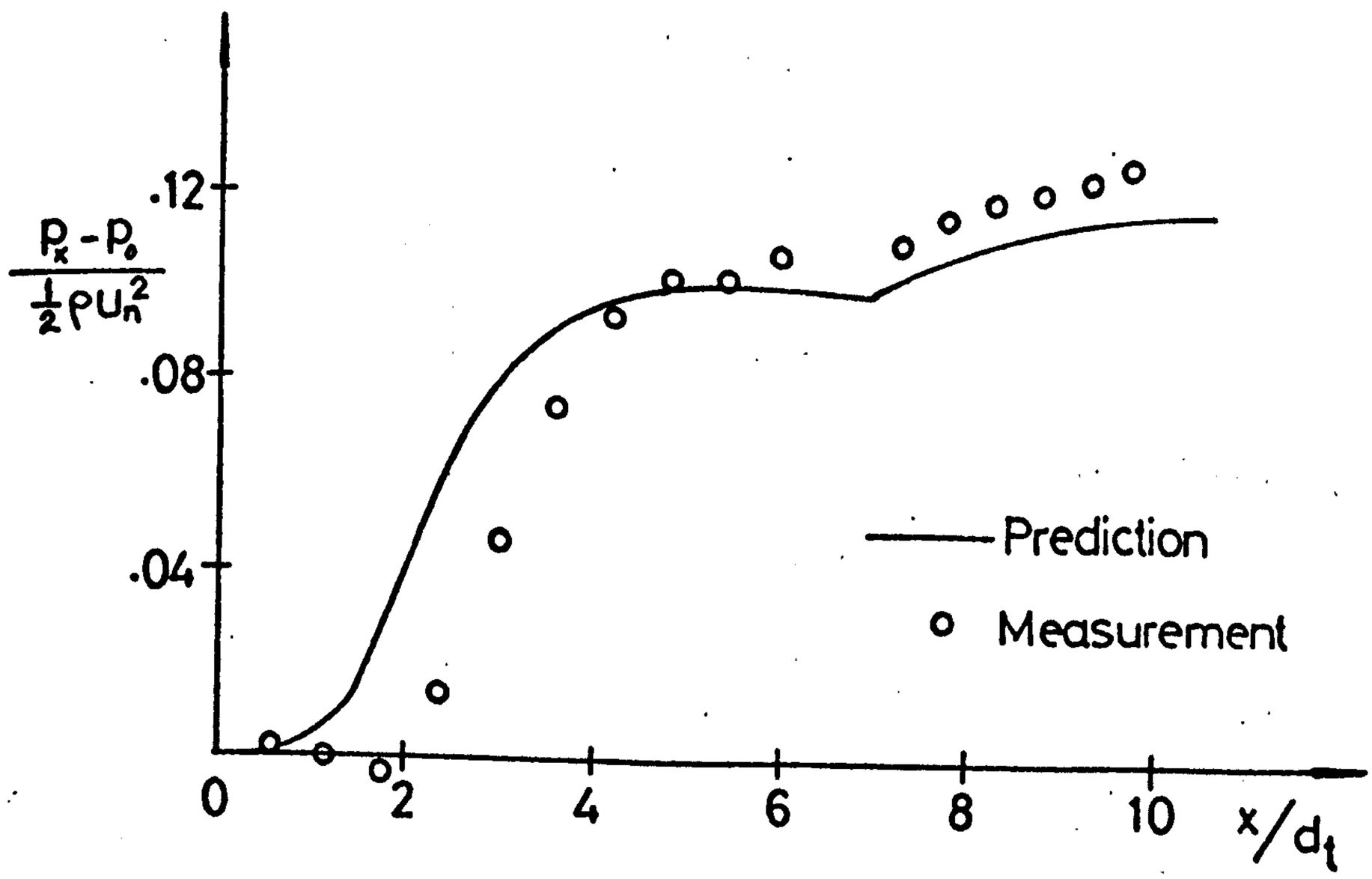

Fig. 6.6-4 Comparison of predicted and measured static pressure along jet pump, d_n/d_t=0.26, θ=7°.

CHAPTER 7

APPLICATION OF THE COMPUTER MODEL FOR JET PUMP DESIGN

The computer programs based on the two-equation k-ε turbulence model have successfully predicted the time-mean variables as well as the turbulent kinetic energy and turbulent shear stress throughout the flow field of the typical jet pumps. The predicted values have been compared with the available experimental data from various sources, both for air jet mixing and water jet mixing. The agreement in general is fairly good. The computer model will accurately predict the performance of any specified jet pump and may be used to optimise the geometry of a jet pump for a specific design requirement. The following sections illustrate the application of the mixing tube and diffuser computer programs for such design purposes.

7.1 Performance Prediction of Any Proposed Design

To predict the performance of any proposed jet pump with the geometry completely specified, the mixing tube program is run with a fixed primary flow rate and a variable secondary flow rate. The pressure and velocity fields of the mixing tube are then obtained. The mean velocity profile as well as the turbulent variables at the exit plane of the mixing tube are then used as the inlet boundary values for the diffuser program.

The variation of static pressure along the entire jet pump wall can thus be predicted for various flow ratios. Following the procedure outlined in section 5.4.2, the total head gained by the entrained fluid and the total head lost by the primary fluid can be evaluated. The head ratio and the efficiency can then be calculated and plotted against flow ratio for the proposed jet pump.

To illustrate such application of the computer model, a jet pump proposed by Sanger (1968a) was simulated by the computer programs to predict its performance. The predicted performance curves and the geometry of the pump are shown in Fig. 7.1-1. The result reveals that higher flow ratio will give lower head ratio and vice versa. This demonstrates that with a fixed primary flow rate, higher secondary flow rate can only be achieved at the expense of pressure head rise; on the other hand, it is only possible to pump less secondary fluid to a higher head. The optimum flow ratio corresponds to the maximum efficiency point where the flow rate and head rise compromise to give the best performance. Such performance predictions have two important applications in design,

(i) they permit a study of the performance of any new design;

(ii) they allow assessment of the performance of any existing pump when being used for off-design conditions.

Fig. 7.1-1 Predicted performance curves of Sanger's pump, $d_n/d_t=0.257$, $s/d_t=1.05$, $l_t/d_t=7.25$, $\theta=8.1^{\circ}$.

7.2 Effect of Geometry on Jet Pump Performance

The optimization of jet pump design in the past has largely depended on experimental testing and previous empirical data. As a result, the optimum geometrical configurations recommended by various workers differ from one another presumably due to the large number of geometrical variables involved and different flow conditions from which the results were derived. This can be attributed to the lack of basic detailed study of fluid flows in jet pumps. The present two equation k- ε model for calculating turbulent flows in the mixing tube and diffuser provides a powerful method for predicting the jet pump flows of various geometrical configurations. In this section, an attempt is made to demonstrate how the computer programs can be used to investigate the influence of various geometrical variables such as nozzle to mixing tube diameter ratio, mixing tube length, nozzle position and diffuser included angles. The primary flow rate is fixed at $1.77 \times 10^{-3} m^3/s$ and the flow ratio is assumed to be 3.5. In most cases, the primary flow rate is limited by the power source used to generate the flow and the flow ratio is usually a design requirement.

7.2.1 The Influence of Diameter Ratio

To study the effect of diameter ratio on jet pump performance, the diameter of the mixing tube was kept

constant at 34.2mm and the nozzle diameter was varied to give the diameter ratio changing from 0.2 to 0.4. With a fixed primary flow rate Q_1, a smaller diameter ratio produces a higher nozzle exit velocity. Other geometrical dimensions were kept at constant.

The predicted static pressure, expressed with reference to the secondary inlet value together with the geometry is shown in Fig. 7.2-1. The results reveal that for diameter ratio lower than 0.35, adverse pressure gradients are present in the mixing tube. The smaller the diameter ratio, the higher the pressure rise in the mixing tube. This may be seen as reflecting the degree of mixing between the primary and secondary flows since a smaller diameter ratio produces a higher velocity ratio at the inlet of the mixing tube for a fixed primary and secondary flow rates, and thus leads to more vigorous mixing between the two streams. For a diameter ratio of 0.4 which corresponds to a smaller velocity ratio at inlet, a favorable pressure gradient in the mixing tube is observed. This suggests that the influence of wall boundary layer due to friction outweighs the influence of mixing between the streams in determining the pressure variation. The influence of diameter ratio on pressure rise in the diffuser is insignificant compared with those in the mixing tube.

The results in Fig. 7.2-1 can be used to calculate the head ratio and thus efficiency of the jet pumps using the one-dimensional procedure outlined in section 5.4.2.

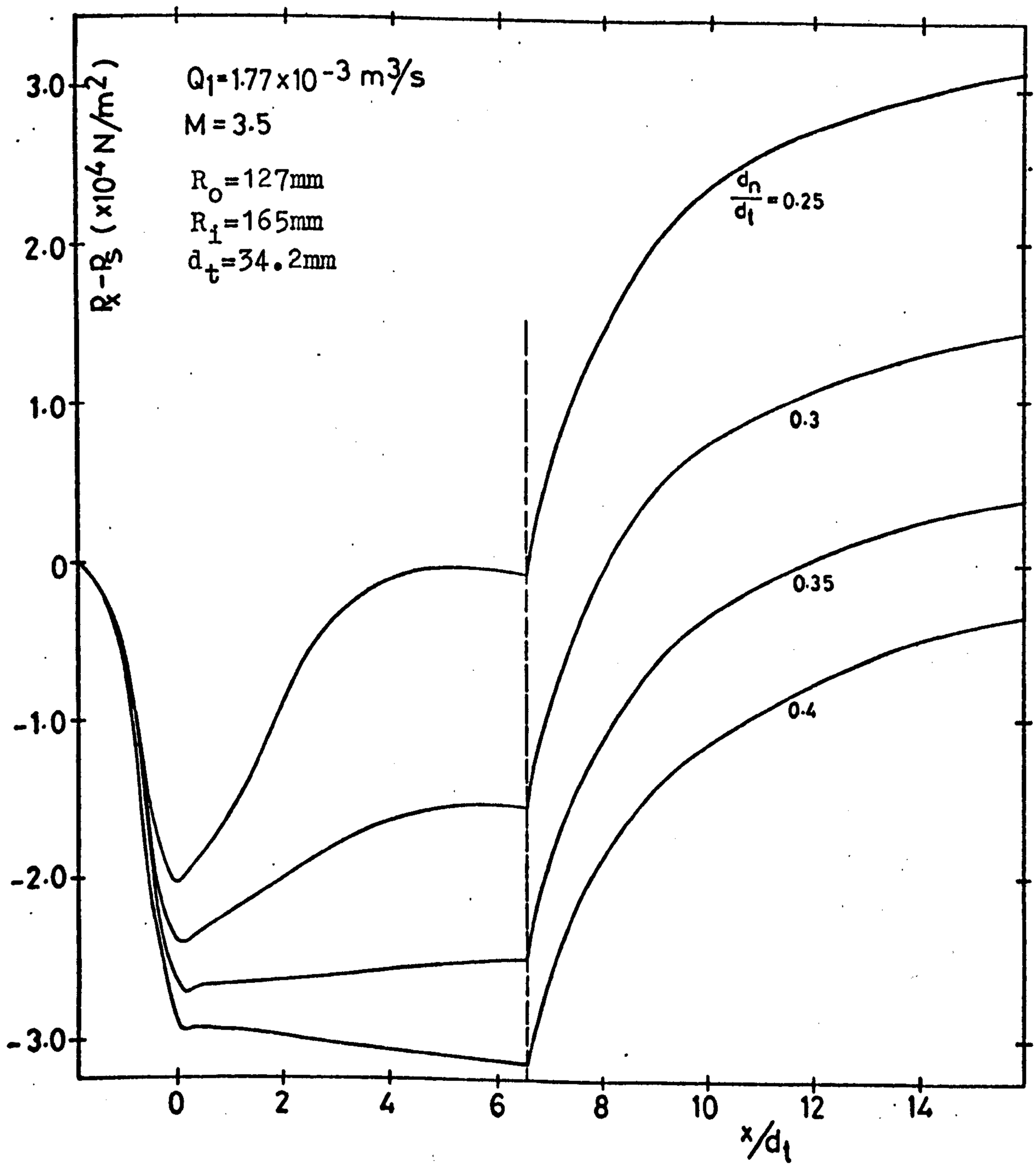

Fig. 7.2-1 Predicted static pressure variation of jet pumps with various diameter ratio, s/d_t=1.05, l_t/d_t=6.49, θ=7°.

The efficiency is plotted against the diameter ratio in Fig. 7.2-2. A maximum efficiency of 27% is observed at a diameter ratio of about 0.27. A small increase or decrease of diameter ratio will reduce the efficiency considerably. To maintain an efficiency of beyond 20% for this particular geometry and flow, the nozzle diameter should be selected so as to give a diameter ratio of 0.2 to 0.32. The diameter ratio is thus a very important and a sensitive geometrical parameter for optimizing jet pump performance.

7.2.2 The Influence of Mixing Tube Length

The study of the influence of mixing tube length on jet pump performance was carried out by running the mixing tube and diffuser programs with variable mixing tube length. A nozzle of fixed diameter was used to give a diameter ratio of 0.25 and a variable mixing tube length changing from 3.08 to 7.69 diameters. The predicted static pressure along the jet pump wall is plotted against the distance from the mixing tube inlet in Fig. 7.2-3. The results show that with a shorter mixing tube, the static pressure rise in the diffuser is smaller. This pressure rise increases with increase in mixing tube length. However, when the mixing tube length reaches around 6.5 diameters, any further increase in length only improves the pressure rise in diffuser slightly and such rise may easily be offset by the frictional loss in the mixing tube due to the extra length. This effect is due to the fact that with a shorter

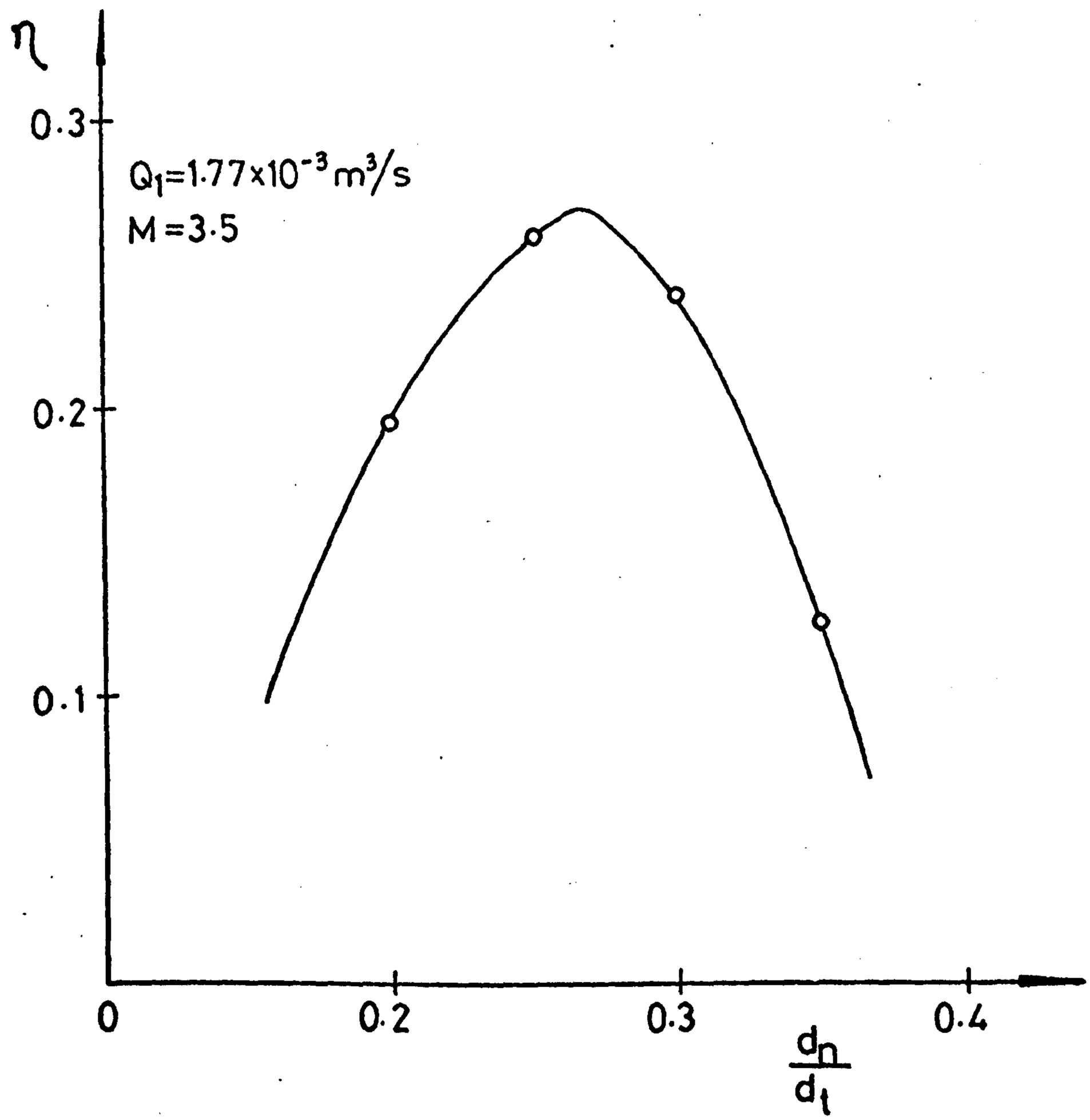

Fig. 7.2-2 The influence of diameter ratio on jet pump efficiency, $s/d_t=1.05$, $l_t/d_t=6.49$, $\theta=7^o$, $R_o=127mm$, $R_i=165mm$, $d_t=34.2mm$, $l_d=320mm$.

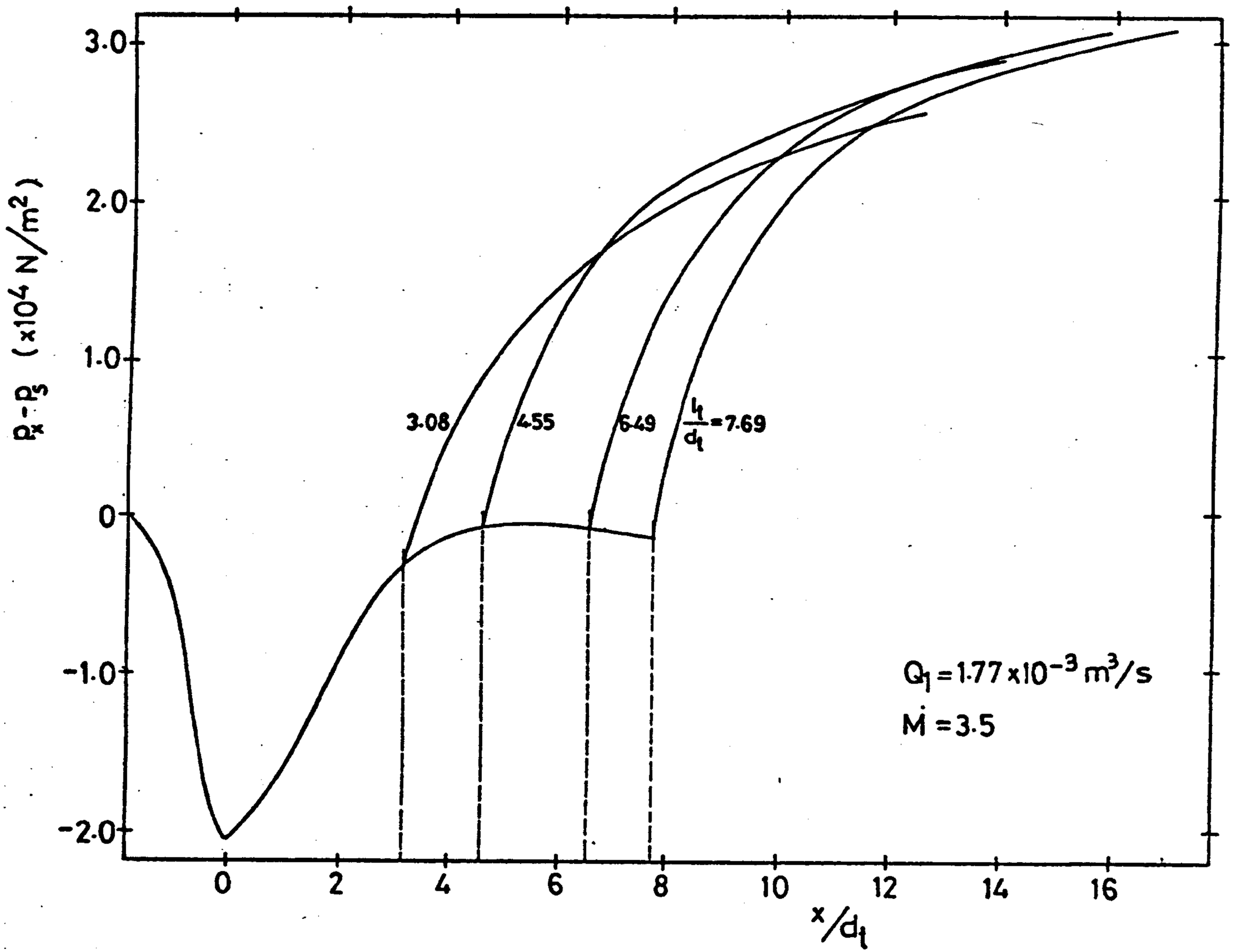

Fig.7.2-3 Predicted static pressure variation of jet pumps with various mixing tube length, d_n/d_t=0.25, s/d_t=1.05, θ=7°.

mixing tube, the mixing process is usually incomplete at the diffuser inlet. The relatively steep velocity profile at diffuser inlet gives less pressure rise due to more loss in the diffuser. With a longer mixing tube, mixing will almost be completed at the diffuser inlet and consequently the pressure rise in diffuser is expected to increase.

Fig. 7.2-4 shows the efficiency as a function of mixing tube length with flow conditions and other geometric variables kept constant. The curve reveals that a mixing tube length of about 5 to 7 diameters gives the best performance with efficiency up to around 26%. Any reduction of mixing length will reduce the efficiency considerably owing to the incomplete mixing. Mixing tube length beyond 6 diameters is unnecessary as the efficiency is diminishes with the increase in length due to the extra frictional loss of the additional length.

7.2.3 The Influence of Diffuser Included Angles

The influence of diffuser included angles was examined by varying the included angles from 3° to 9° while keeping the area ratio of the diffuser and other pump geometries and flow conditions unchanged. Fig. 7.2-5 shows the variation in static pressure along the jet pump wall for various diffuser included angles. The 7° diffuser seems to give a maximum pressure rise. A decrease in included angle to 5° causes the pressure at exit to drop considerably owing to the frictional loss in the extra length of the diffuser wall. On the other hand, an increase of included angle to 9° reduces the diffuser exit pressure

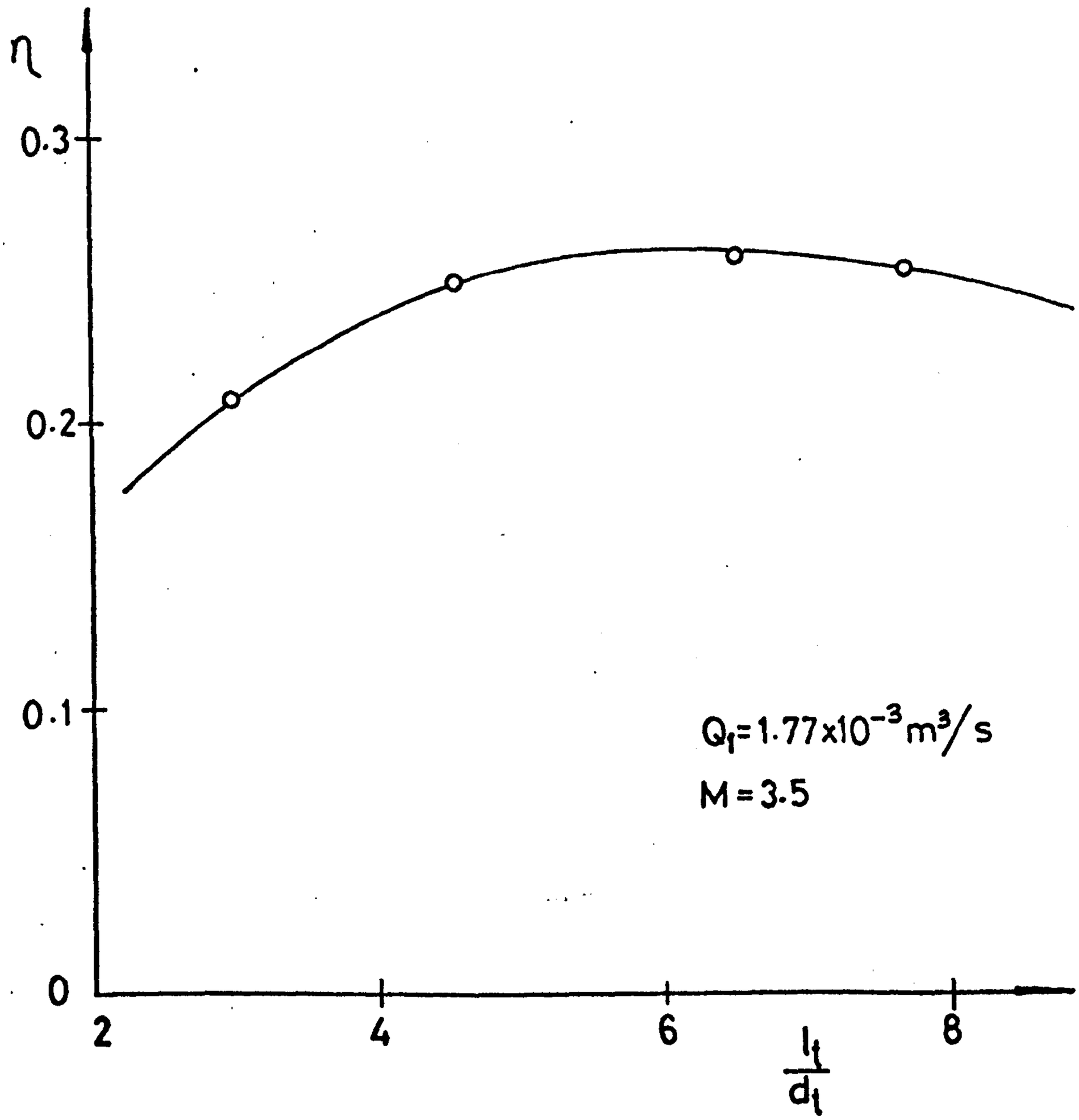

Fig.7.2-4 The influence of mixing tube length on jet pump efficiency, $d_n/d_t=0.25$, $s/d_t=1.05$, $\theta=7^o$.

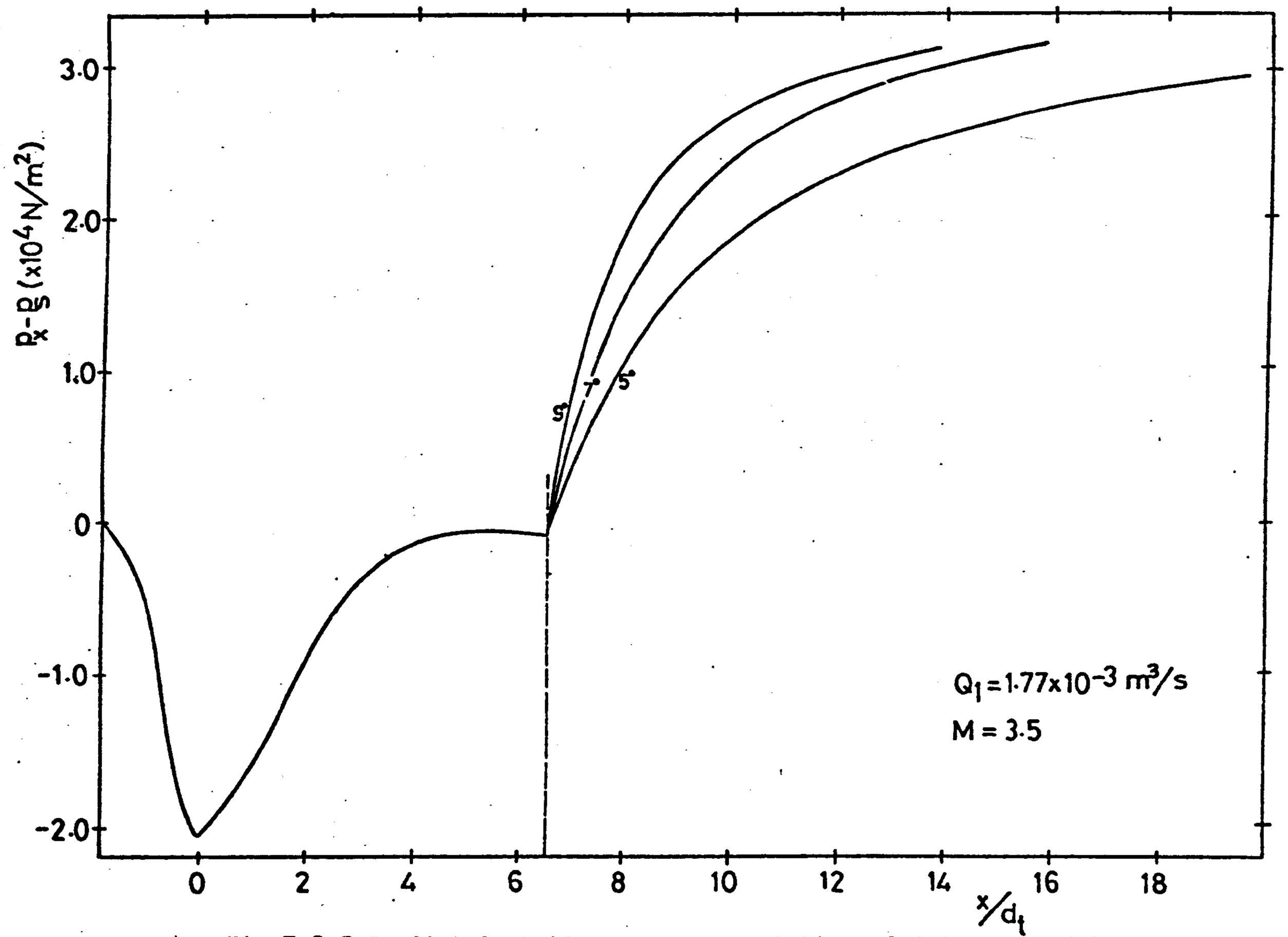

Fig.7.2-5 Predicted static pressure variation of jet pumps with various diffuser included angle, d_n/d_t=0.25, s/d_t=1.05, l_t/d_t=6.49.

slightly; the increased pressure loss caused by the more severe expansion outweighs the reduction in pressure loss due to the shorter length of diffuser.

The influence of diffuser included angles on the overall jet pump performance is shown in Fig. 7.2-6. For this particular geometry and flow condition, a 7° diffuser angle gives an optimum efficiency of 26%. It is also observed that the efficiency curve is rather flat which implies that the influence of diffuser included angle on performance is secondary. A shorter diffuser is always preferable as it saves both material and space. However, if the included angle is too large, there may be a danger of flow separation occurring in the diffuser region which will cause severe loss.

7.2.4 The Effect of Nozzle Exit to Mixing Throat Spacing

The effect of nozzle spacing on performance is related to other geometries such as mixing tube length, diameter ratio and secondary inlet contours of the jet pump. By keeping all other geometrical variables as constants, and varying the nozzle spacing over the range of 0.2 to 1.4 diameters of the mixing tube, the effect of nozzle position on performance can be investigated. Fig. 7.2-7 shows that the pressure in the mixing tube and diffuser is in general lower for smaller nozzle spacing. This phenomenon is expected because the decrease in annular area of the secondary inlet (due to shorter nozzle spacing) will certainly lower the static pressure in the region.

The overall performance of jet pump with varying nozzle

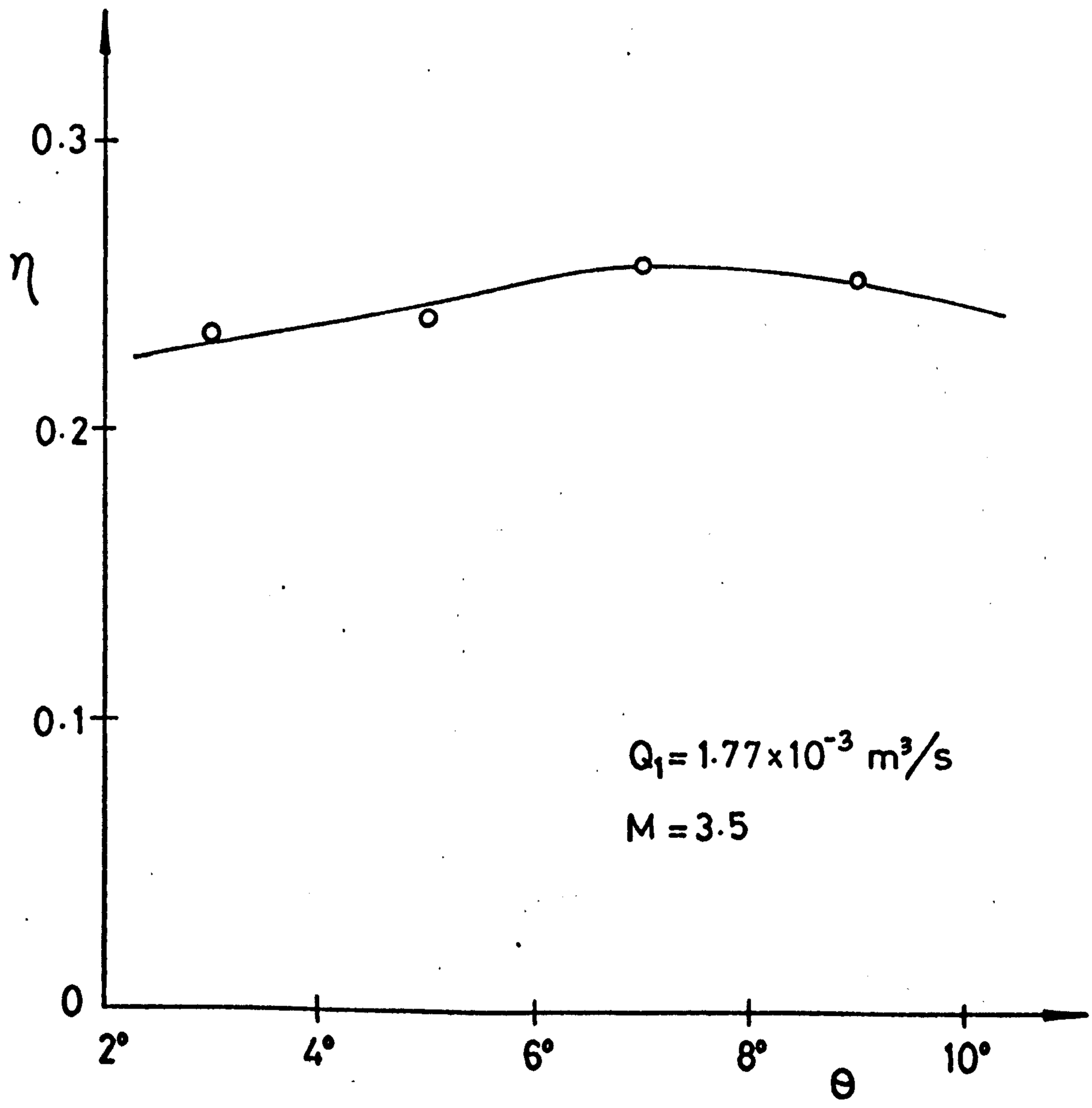

Fig. 7.2-6 The influence of diffuser included angle on jet pump efficiency, d_n/d_t=0.25, s/d_t=1.05, l_t/d_t=6.49.

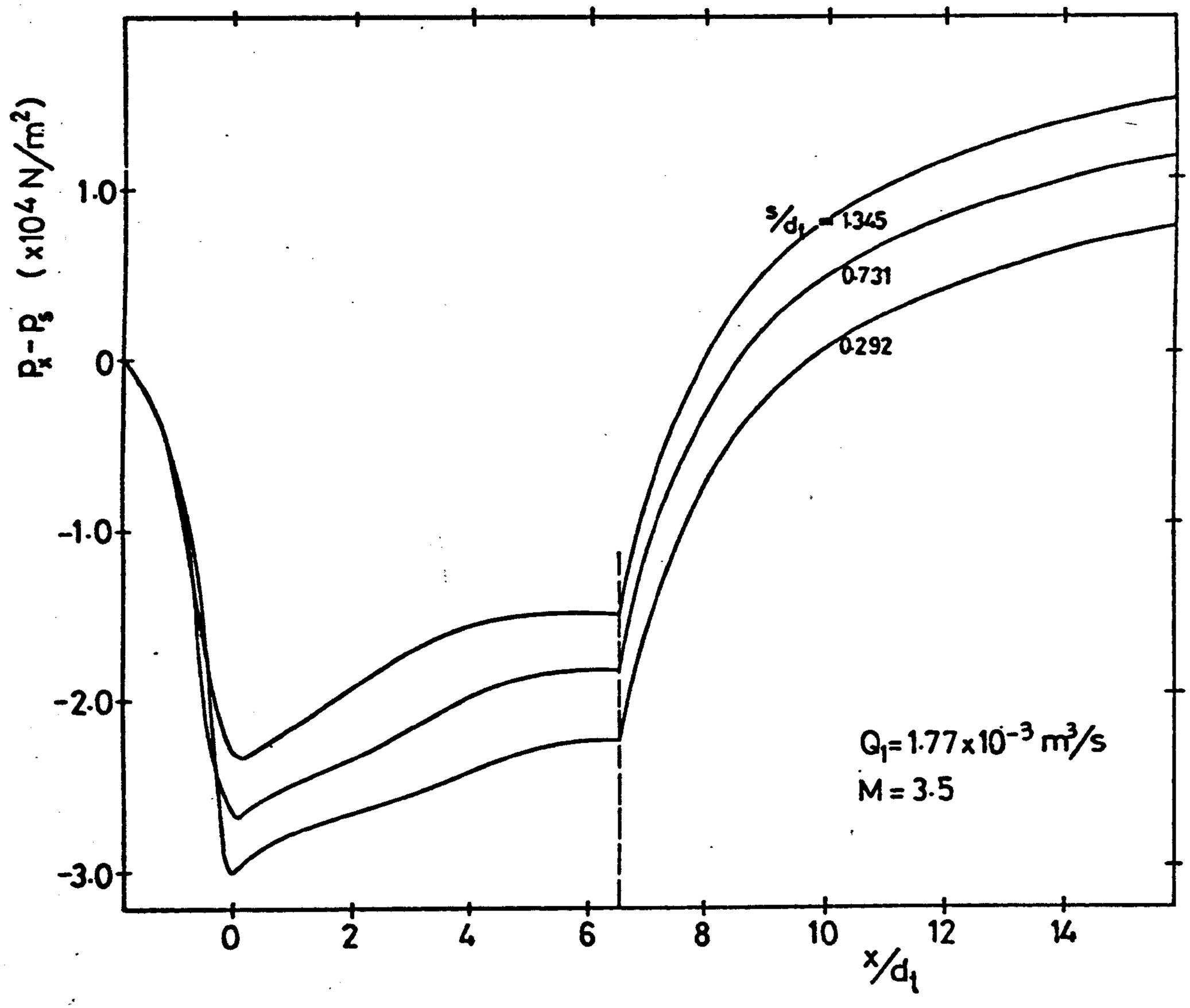

Fig. 7.2-7 Predicted static pressure variation of jet pumps with various nozzle spacing, d_n/d_t=0.3, l_t/d_t=6.49, θ=7°.

spacing is shown in Fig. 7.2-8. The efficiency of the jet pump increases from 13% at a position given by s/d_t=0.3 to a maximum of 26% at s/d_t = 1.2. The efficiency then decays gradually with further increase of nozzle spacing. The result suggests that for this particular configuration and flow condition, the mixing tube is not long enough to produce a maximum pressure rise in the mixing tube and therefore an increase in the spacing between nozzle outlet and mixing tube inlet would improve the performance. This optimum position change when the jet pump configuration and flow conditions vary.

7.3 An Optimizing Procedure for Jet Pump Design

In the previous section, the individual influence of various geometrical variables was studied and discussed. The present section attempts to outline a procedure for making use of the existing computer programs to generate an optimum geometry of a jet pump to fulfill a specified design requirement. In the usual design practice, the primary flow rate Q_1 is always limited by the independent power source which generates the primary flow. Another design parameter usually given is the flow ratio M which together with Q_1 determine the quantity of fluid can be pumped per unit time. The following procedure is recommended to obtain the optimum geometry:

(i) Fix the mixing tube diameter and specify initial values of mixing tube length, diffuser angle and nozzle spacing; run the mixing tube and diffuser

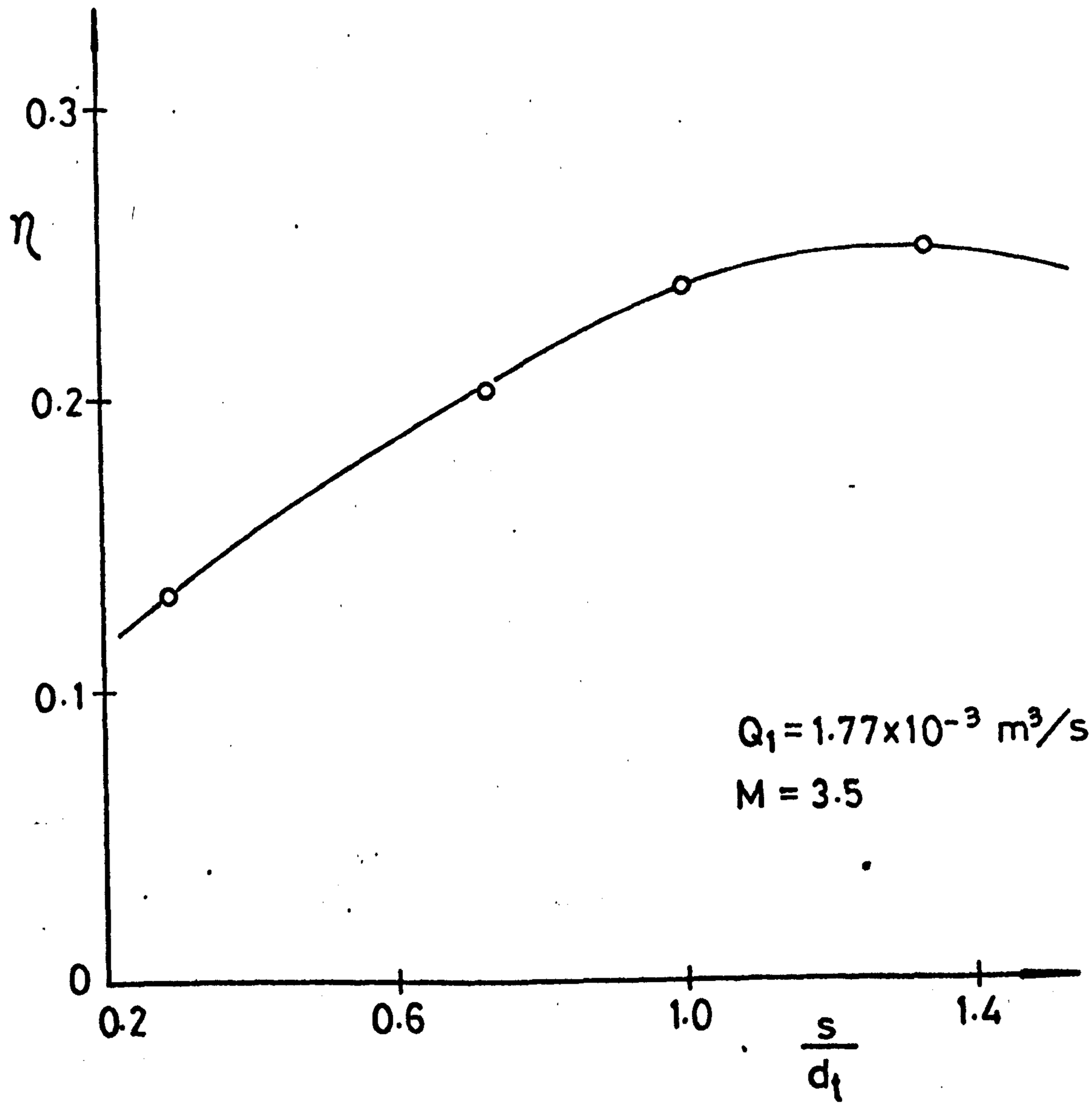

Fig. 7.2-8 The influence of nozzle spacing on jet pump efficiency, d_n/d_t=0.3, l_t/d_t=6.49, θ=7°.

programs with varying nozzles diameters while keeping other geometries constant to obtain the optimum diameter ratio corresponding to maximum head ratio.

(ii) Run the mixing tube and diffuser programs by using the newly obtained optimum nozzle diameter for various mixing tube lengths while keeping other geometries unchanged, to obtain the optimum mixing tube length.

(iii) Run the programs with optimum diameter ratio and mixing tube length obtained in (i) and (ii) to optimize the diffuser angle, keeping nozzle spacing unchanged.

(iv) Optimize the nozzle spacing with other geometries obtained in (i), (ii) and (ii).

(v) Using the optimum values of mixing tube length, diffuser angle and nozzle spacing obtained in (ii) (iii) and (iv), repeat step (i) to obtain a new optimum diameter ratio which together with other optimum geometrical variables suggest the best geometry for the particular design requirement.

An optimization example shows that for a primary flow rate of $1.77 \times 10^{-3} m^3/s$ and a flow ratio of 3.5, the following optimum geometrical variables were obtained: d_n/d_t = 0.27, l_t/d_t = 5.8, $\theta = 7^o$ and s/d_t = 1.25.

CHAPTER 8

CONCLUSIONS & SUGGESTIONS FOR FUTURE RESEARCH

8.1 Conclusions

The two-equation k- ε model of turbulence together with a finite difference procedure for solving pressure-velocity directly have been successfully applied to predict turbulent mixing in jet pumps. The predicted time-mean velocity, static pressure, turbulent kinetic energy and turbulent shear stresses in the mixing region have been compared with the existing data from various sources as well as the author's own measurements. The comparisons in general show good agreements which suggest that the two-equation k-ε model of turbulence is competent enough to predict turbulent flows in jet pumps.

The superiority of the present theoretical approach is its generality in calculating turbulent flows by solving the elliptic partial differential equations which describe the flow mathematically. This approach contrasts with the earlier ones which were based on empirical results and treated the various regions separately. The present method solves the same set of equations for various flow regions with different boundary conditions without using empirical coefficients derived from other jet pump testing or free jet data.

Measurements of time-mean velocity and r.m.s. fluctuating velocities in three orthogonal directions in a mixing tube with water as working fluid were carried out success-

fully using a laser Doppler anemometer. The data provides first hand information of r.m.s. velocities in confined jet mixing which is lacking in the existing literature. Difficulties in measuring radial and tangential fluctuating velocities are discussed. Methods of calculating measuring positions in pipe flow from laser beams configuration and pipe geometry have been devised. The measured values compare favourably with the computer predicted results.

The two computer programs, one for jet mixing in typical uniform bore mixing tube with bellmouth secondary inlet and the other for turbulent flow in conical diffuser, were used successively to predict the static pressure rise in typical jet pumps. The head ratio and efficiency were calculated from the predicted static pressure rise and flow ratio via a one-dimensional method normally employed in jet pump analysis. The predicted performance curves show an excellent agreement with test results although the predicted efficiency is slightly higher than measured.

The prediction also confirms the previous experimental studies that the efficiency of conventional jet pumps is relatively low and hardly ever exceeds 40%. This is due to the fact that the pumping effect is achieved wholly through turbulent mixing between the fluid streams. Unlike other mechanical pumping devices which suffer mainly from hydraulic loss due to friction, the flow in a jet pump encounters both frictional loss along the wall and a mixing loss between the primary and secondary streams. The mixing loss, which can be identified with

the turbulent shear stress at the mixing region, is proportional to the mean velocity gradient and the turbulent kinetic energy, according to the present turbulence model. To achieve the pumping effect, the turbulent mixing should be maintained at a certain level. This will result in the relatively high level of turbulent kinetic energy in the mixing region. The amount of loss due to turbulent mixing is always much more significant than the frictional loss in most jet pump flows. As a result of this high mixing loss, the efficiency of a jet pump is always relatively low. It is possible to reduce the mixing loss by reducing the mean velocity gradient or the turbulent kinetic energy in the mixing region. However, such a situation can only be created by increasing the flow ratio and this will lead to an increase in the frictional loss. An optimum design should achieve a minimum total energy loss, i.e., the best compromise between mixing loss and wall frictional loss.

It has been demonstrated that the programs can be used both to predict the performance of any proposed design of jet pump and to optimize any geometrical variable under specific flow conditions. Systematic repetition of the procedure will lead to an optimum overall geometry. Unlike the previous design procedures which rely largely on empirical test results and are always limited to a certain range of operation, the present computer programs provide a powerful tool for designer to obtain optimum geometry without going through actual

pump manufacture and testing.

8.2 Suggestions for Further Research

The present computer model, which successfully predicts all the possible flow regions in conventional jet pumps comprising a bellmouth secondary inlet, a uniform bore mixing tube and a conical diffuser, may also be used to study flow separation and recirculation in the mixing tube and diffuser so that an improved design can be proposed to avoid flow separation which normally causes large losses. Owing to their generality, there is a great potential to extend the present computer programs to predict and study many other flow problems associated with turbulent mixing.

The mixing tube program in its present structure can easily be modified to predict flow in a non-uniform bore, for example, the convergent-divergent mixing duct reported by Helmbold et al (1954) which is claimed to be more efficient than the conventional design. It is also possible to use the jet mixing program to study the pumping of one fluid by another of different density and viscosity. Since the density is treated as a variable rather than a constant, the program can be used to predict the compressible jet mixing in an ejector.

More systematic studies on the effects of varying the empirical constants used in the $k-\varepsilon$ turbulence model may be carried out such that better values can be employed to improve the flow prediction.

A more comprehensive three-equation model which uses the turbulent shear stress $\overline{u'v'}$ as another dependent variable, may also be used to predict the jet mixing and the diffuser flows so as to compare the accuracy and economy with the existing two-equation model.

On the experimental side, further research can be done to measure the radial r.m.s. velocity in the outer region of the mixing tube. A longer and adjustable photomultiplier holder is necessary so that the refracted laser beams from the measuring section can be detected at the most appropriate position.

Measurement of mean and r.m.s. fluctuating velocities by L.D.A. can also be extended to the diffuser region. A calculation procedure must be devised to locate the measuring point from the diffuser geometry and laser beams path. The success in measuring the mean and fluctuating velocities in a conical diffuser not only provides flow details for jet pump studies, but also widens the L.D.A. application and enriches the knowledge of turbulent flow in conical diffuser.

Fig. A.1-1

The One-Dimensional Theory assumes that

(i) the velocity at any cross-section is uniform,

(ii) the nozzle exit and the mixing tube inlet are in the same plane,

(ii) the thickness of the nozzle wall are negligible.

From Fig. A.1-1, the flow equations for the three connecting pipelines are:

Driving line: $$H_1 = \frac{P_a}{\gamma} + 0 + (1 + K_j)\frac{V_j^2}{2g} \qquad (A.1\text{-}1)$$

Suction line: $$H_2 = \frac{P_a}{\gamma} + 0 + (1 + K_s)\frac{V_s^2}{2g} \qquad (A.1\text{-}2)$$

Discharge Line: $$\frac{P_b}{\gamma} + \frac{V_t^2}{2g} + 0 = H_d + K_d\frac{V_t^2}{2g} \qquad (A.1\text{-}3)$$

where $\gamma = \rho g$ and K_j, K_s and K_d are frictional loss coefficients.

The continuity relations can be written as :

$$A_s + A_j = A_t$$

$$V_t = \frac{Q_1 + Q_2}{A_j + A_s} = \frac{Q_1 + Q_2}{A_t}$$

$$Q_1 = A_j V_j$$

$$Q_2 = A_s V_s$$

$$Q_1 + Q_2 = A_t V_t \qquad (A.1\text{-}4)$$

$$\frac{Q_2}{Q_1} = M$$

$$\frac{A_j}{A_t} = R$$

$$\frac{A_s}{A_j} = \frac{1 - R}{R}$$

The loss of energy due to friction at mixing tube wall is approximately given by

$$L_f = \gamma K_t (Q_1 + Q_2)\frac{V_t^2}{2g} \qquad (A.1\text{-}5)$$

where K_t is a resistance factor to be determined from experiment.

By applying the momentum equation and energy equation across the mixing tube and equating the two pressure rise terms the energy loss per unit time resulting from mixing can be written as:

$$L_m = Q_1 \gamma \frac{(V_j - V_t)^2}{2g} + Q_2 \gamma \frac{(V_s - V_t)^2}{2g} \qquad (A.1\text{-}6)$$

Equating the power supplied to the sum of the work done per second and the energy losses gives

$$Q_1\gamma(H_1 - H_d) = Q_2\gamma(H_d - H_2) + K_j Q_1 \gamma \frac{V_j^2}{2g} + K_s Q_2 \gamma \frac{V_s^2}{2g}$$
$$+ (K_d + K_t)(Q_1 + Q_2)\gamma \frac{V_t^2}{2g} + Q_1 \gamma \frac{(V_j - V_t)^2}{2g}$$
$$+ Q_2 \gamma \frac{(V_t - V_s)^2}{2g} \qquad (A.1\text{-}7)$$

By substituting equations (A.1-1) to (A.1-3) into equation (A.1-7) and simplifing the resulting expressions of $H_1 - H_d$ and $H_d - H_2$ using equations (A.1-4), the following head ratio can be obtained

$$N = \frac{H_d - H_2}{H_1 - H_d} = \frac{1 - L}{L + M}$$

where

$$L = \frac{1+K_s+(1+K_s)M^3\left(\frac{R}{1-R}\right)^2+(1+K_d+K_t)R^2(1+M)^3-2R(1+M)-2\frac{M^2R^2}{1-R}(1+M)}{1+K_j-(1+K_s)M^2\left(\frac{R}{1-R}\right)^2}$$

(A.1-8)

The efficiency can then be expressed as

$$\eta = \frac{Q_2(H_d - H_2)}{Q_1(H_1 - H_d)} = MN \qquad \text{(A.1-9)}$$

A.2 Momentum Integral Method of P.G. Hill (1965) for Axisymmetric Ducted Jets

The momentum equation for an axisymmetric free turbulent shear flow at high Reynolds number can be written as

$$U\frac{\partial U}{\partial x} + V\frac{\partial U}{\partial y} + \frac{1}{y}\frac{\partial(\overline{u'v'}y)}{\partial y} + \frac{1}{\rho}\frac{dP}{dx} = 0 \qquad \text{(A.2-1)}$$

The symbols are defined as follows:

x - direction: parallel to the jet axis

y - direction: normal to the jet axis

U,u' - time mean and fluctuating velocities in x-direction

V,v' - time mean and fluctuating velocities in y-direction

P - static pressure

ρ - density

The Reynolds shear stress is

$$\tau = -\rho\overline{u'v'}$$

When the stream outside the jet may be considered as a potential flow, the pressure gradient $\frac{dP}{dx}$ is given by

$$\frac{1}{\rho}\frac{dP}{dx} = -U_o\frac{dU_o}{dx} \qquad \text{(A.2-2)}$$

assuming $\overline{u'^2} - \overline{v'^2} \ll U_o$ and U_o is the free-stream velocity as illustrated in Fig. A.2-1.

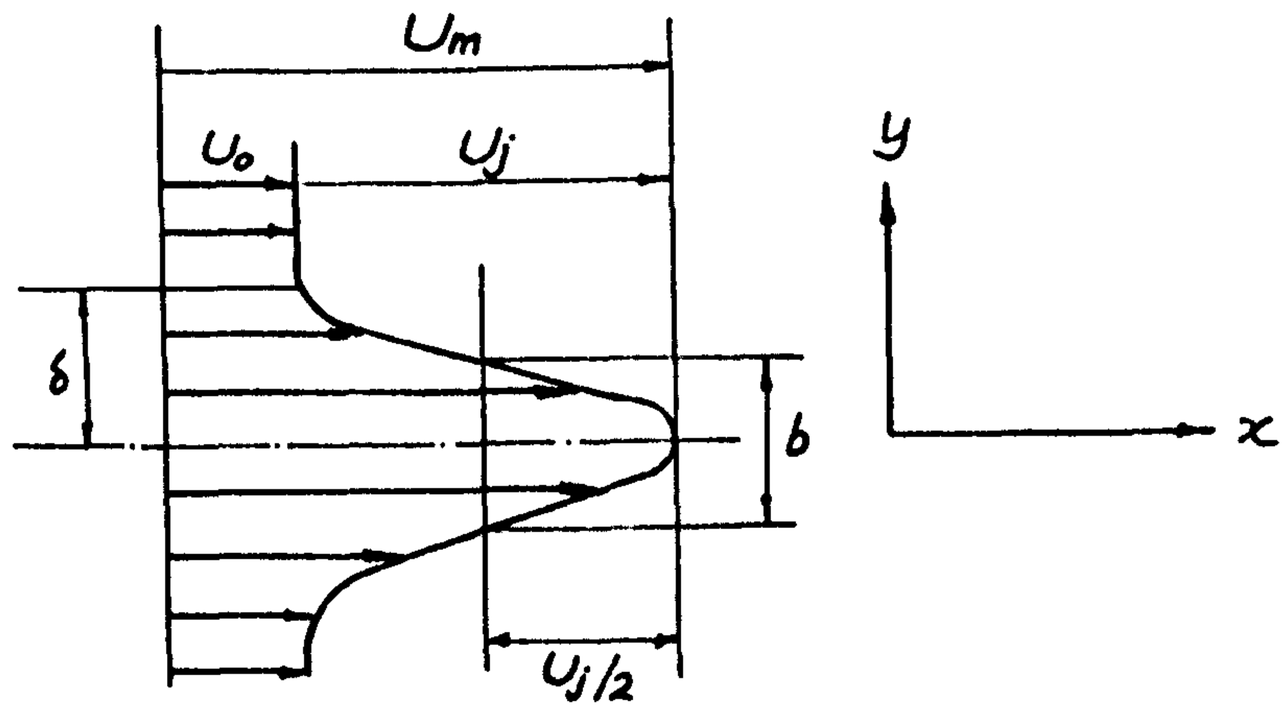

Fig. A.2-1 Nomenclature for velocity distribution.

If the jet flow is assumed to be self-preserving then the velocity and shear stress distribution may be expressed as

$$(U - U_o)/U_j = f(y/\delta) \qquad (A.2\text{-}3)$$

$$\tau/\rho U_j^{\,2} = g(y/\delta) \qquad (A.2\text{-}4)$$

where U_j is the difference between jet maximum velocity and free-stream velocity and δ is the distance from the centre-line of the jet to its edge.

The continuity equation is

$$\frac{\partial(Uy)}{\partial x} + \frac{\partial(Vy)}{\partial y} = 0 \qquad (A.2\text{-}5)$$

Defining $\lambda = U_o/U_j$ and $\eta = y/\delta$, and substituting these similarity expressions and the continuity relation in equation (A.2-1) the result may be expressed in a general integral form

$$\frac{1}{U_j}\frac{dU_j}{dx}\left[\lambda f + f^2 - \frac{f'}{\eta}\int_0^\eta f\eta_1 d\eta_1\right] + \frac{1}{U_o}\frac{dU_o}{dx}\left[\lambda f - \frac{\lambda f'\eta}{2}\right]$$

$$+ \frac{1}{\delta}\frac{d\delta}{dx}\left[-\lambda f'\eta - \frac{2f'}{\eta}\int_0^\eta f\eta_1 d\eta_1\right] = \frac{1}{\delta\eta}\frac{\partial}{\partial\eta}(g\eta) \qquad \text{(A.2-6)}$$

The general integral equation may be treated for three separate regions

(i) <u>Potential outer flow region</u>:

Multiplying equation (A.2-6) by η^2 to form a moment of momentum equation and integrating across the entire jet, it becomes

$$\frac{1}{U_j}\frac{dU_j}{dx}\left[\frac{7}{2}\lambda\phi_1 + \phi_2 + \phi_3\right] + \frac{1}{\delta}\frac{d\delta}{dx}\left[3\lambda\phi_1 + 2\phi_3\right] + \frac{1}{\lambda}\frac{d\lambda}{dx}\left[\frac{5}{2}\lambda\phi_1\right]$$

$$= \frac{\psi}{\delta} \qquad \text{(A.2-7)}$$

in which $\phi_1 = \int_0^1 f\eta^2 d\eta$

$$\phi_2 = \int_0^1 f^2\eta^2 d\eta$$

$$\phi_3 = -\int_0^1 \eta f' \int_0^\eta f\eta_1 d\eta_1 d\eta$$

and $\psi = \int_0^1 \eta\frac{\partial}{\partial\eta}\left(\frac{\tau\eta}{\rho U_j^2}\right)d\eta$

If the wall friction is negligible and the pressure P is approximately uniform across any transverse section then the momentum equation can be written as

$$0 = \pi R^2\frac{dP}{dx} + \frac{d}{dx}\int_0^R 2\pi\rho U^2 y dy \qquad \text{(A.2-8)}$$

where R is the radius of the duct.

The velocity within the jet U is given by

$$U = U_o + U_j f(\eta) \qquad (0<\eta<1) \qquad \text{(A.2-9)}$$

Substituting equation (A.2-2) and equation (A.2-9) into equation (A.2-8), it becomes

$$0=\pi R^2\rho\left[-d(\tfrac{1}{2}U_o^{\,2})/dx+R^{-2}d(U_o^{\,2}R^2)/dx+2R^{-2}\frac{d}{dx}\left\{\delta^2U_j^{\,2}(2\lambda\phi_4+\phi_5)\right\}\right] \qquad \text{(A.2-10)}$$

where $\phi_4 = \int_0^1 f\eta\, d\eta$ and $\phi_5 = \int_0^1 f^2\eta\, d\eta$

The integral form of the continuity equation may be expressed by

$$\frac{1}{U_j}\frac{dU_j}{dx} = \frac{\frac{d\lambda}{dx} + 4\phi_4\delta(\frac{d\delta}{dx})R^2}{\lambda + 2(\delta/R)^2\phi_4} \qquad \text{(A.2-11)}$$

In order to calculate the development of jet flow, equations (A.2-7), (A.2-10) and (A.2-11) are integrated using the Runge-Kutta-Merson procedure with values of ϕ_1 , ϕ_2 ....., ϕ_5, ψ directly evaluated from free-jet velocity measurements.

(ii) <u>Recirculation Region</u> :

In this region, the pressure gradient and free-stream velocity no longer obey equation(A.2-2). However, from experimental data, it is approximately true to assume constant static pressure in this region. Furthermore, the jet shape is approximately retained so that with appropriate modification, the foregoing equations may also be used

to predict the jet behaviour in the recirculation region.

(iii) Wall-jet Interaction Region:

When the jet has spread to the wall, it begins to undergo considerable changes in its velocity and shear distributions so that the preceeding self-preserving equations are not valid. As the free-stream velocity has disappeared the static pressure in the duct can no longer be given by equation (A.2-2). Instead it is assumed that the effective eddy viscosity distribution in this region of developing flow is given by

$$\nu_{eff} = \text{const.} U_j R g_1(\eta) \qquad \text{(A.2-12)}$$

in which the function of g_1 is given by

$$g_1 = 1 \qquad (0 < \eta < 0.28)$$

$$g_1 = 1.191 - 0.684\eta \qquad (0.28 < \eta < 1)$$

where $\eta = y/R$

The constant in equation (A.2-12) is evaluated from free-jet data. The velocity in this zone is set to

$$U = U_o + U_j\left[f(\eta) + \xi g(\eta)\right], \qquad \eta = y/R \qquad \text{(A.2-13)}$$

in which U_o is the velocity near the wall (the wall boundary layer is ignored), U_j is the difference between

U_o and the maximum velocity and ξ is a function of x only. If $f(\eta)$ is chosen as the one which was used for the preceding zones, then ξ equals zero when the jet 'touches' the wall and is a measure of the change in shape of velocity profile thereafter. If the function $g(\eta)$ is only required to satisfy the boundary conditions,

$$g(0) = g'(0) = 0$$
$$g(1) = g'(1) = 0$$

then a simple function may be used, e.g.

$$g(\eta) = \eta^2(1-\eta)^2$$

In the present case, four unknowns may be identified, i.e., U_j, λ, ξ and P. To form the necessary four equations, it is possible to take in addition to the continuity equation, three successive integrals of the momentum equation by multiplying equation (A.2-1) by y^j where j = 1,2,3 and integrating with respect to y. Using equations (A.2-12) and (A.2-13), the results may be expressed in the following form:

$$\begin{bmatrix} \beta_0 & \beta_1 & \beta_2 & \beta_3 \\ \beta_4 & \beta_5 & \beta_6 & \beta_7 \\ \beta_8 & \beta_9 & \beta_{10} & \beta_{11} \\ \beta_{12} & \beta_{13} & \beta_{14} & \beta_{15} \end{bmatrix} \begin{bmatrix} \overline{U}_j'/\overline{U}_j \\ \lambda' \\ \xi' \\ \overline{P}' \end{bmatrix} = \begin{bmatrix} \beta_{16} \\ \beta_{17} \\ \beta_{18} \\ \beta_{19} \end{bmatrix} \qquad \text{(A.2-14)}$$

in which the prime signifies differentiation with respect to x/D,

$$\overline{P} = \frac{2P_o}{M}$$

$$\overline{U_j} = \frac{U_j}{(M/\rho)^{\frac{1}{2}}}$$

where $M = 2\rho U_j^{\,2}\left[\frac{1}{3}\lambda^2 + 2\left(\frac{\delta}{R}\right)^2(2\lambda\phi_4 + \phi_5)\right]$

The matrix element β have the form

$$\beta_n = a_{1n}\lambda^{-2} + a_{2n}\lambda + a_{3n}\lambda^2 + a_{4n}\lambda\xi + a_{5n}\xi^2 + a_{6n}$$

in which the coefficients $a_{1n}, \ldots\ldots, a_{6n}$ depend only on various integrals across the shear layer of the velocity and shear distribution functions $f(\eta)$, $g(\eta)$ and $g_1(\eta)$. Equations(A.2-14) can then be integrated using the Runge-Kutta-Merson procedure.

A.3 Derivation of Momentum Equations for a Two-Dimensional Axisymmetric Flow

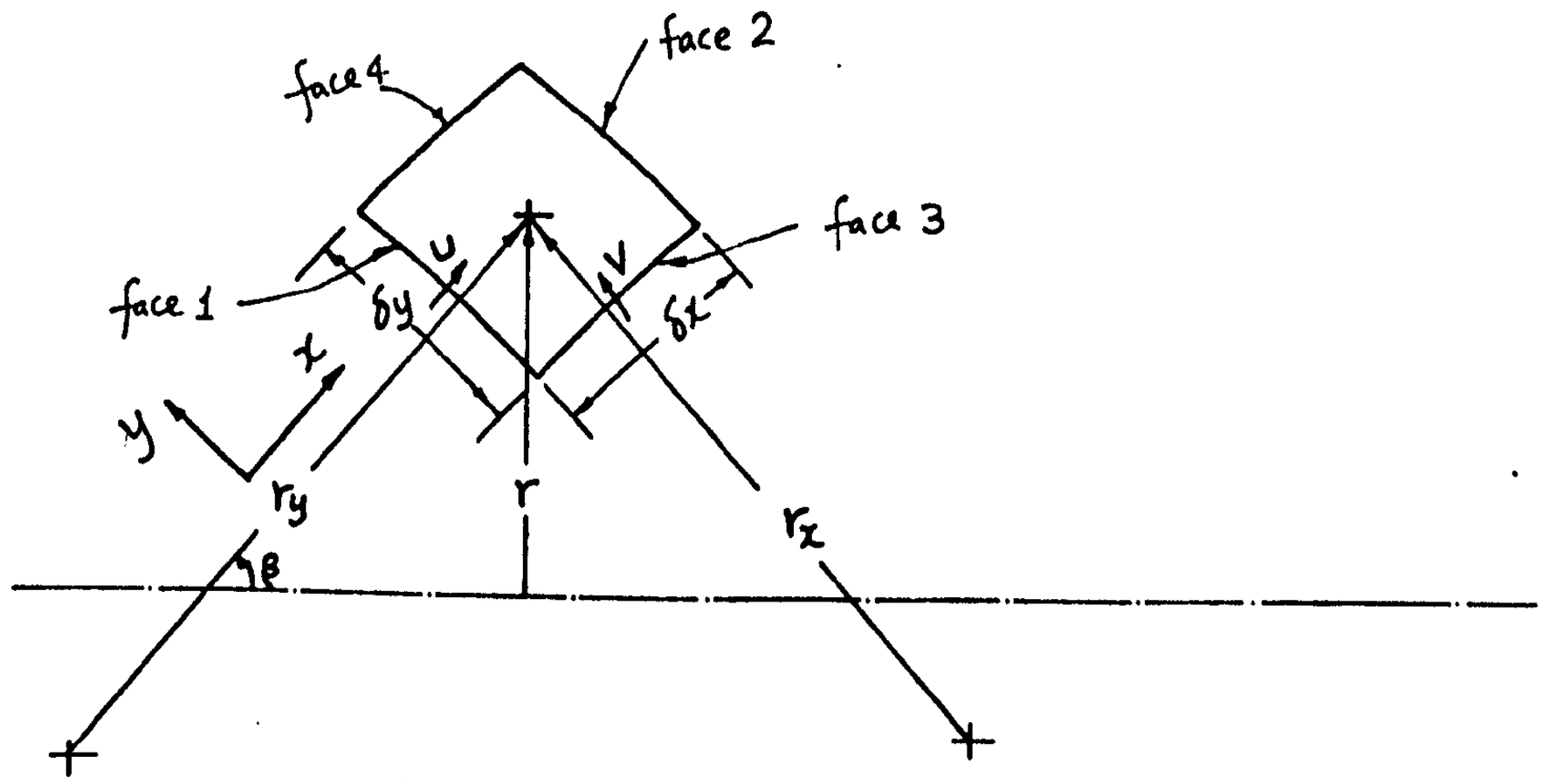

Fig. A.3-1

Consider the control volume shown in Fig. A.3-1 where x and y are the two orthogonal families of surfaces of revolution. r_x and r_y are the radii of curvature for x and y surfaces and r is the radius from the axis of symmetry. U and V are the velocities along x and y directions respectively. The U-momentum flux across surface 1 is

$$\rho U r \delta y \cdot U$$

U-momentum flux across surface 2 is

$$\rho U r \delta y \cdot U + \frac{\partial}{\partial x}(\rho U r \delta y \cdot U)\delta x$$

U-momentum flux across surface 3 is

$$\rho V r \delta x \cdot U$$

assuming that the control volume is small enough such that

the mean r's of surfaces 1 and 3 are approximately equal. U-momentum flux across surface 4 is

$$\rho V r \delta x \cdot U + \frac{\partial}{\partial y}(\rho V r \delta x \cdot U)\delta y$$

The net momentum flux flow out from the C.V. is then

$$(\dot{m}U)_x = \frac{\partial}{\partial x}(\rho U r \delta y \cdot U)\delta x + \frac{\partial}{\partial y}(\rho V r \delta x \cdot U)\,\delta y \quad (A.3\text{-}1)$$

There are several forces acting on the surfaces of the control volume due to pressure, centrifugal force and shear stresses.

The force acting on the C.V. due to pressure is

$$F_p = -\frac{\partial P}{\partial x}\,\delta x \cdot r \delta y \quad (A.3\text{-}2)$$

The centrifugal force acting on the C.V. due to V-velocity is

$$F_c = \rho r \delta x \delta y \,\frac{V^2}{r_y} \quad (A.3\text{-}3)$$

The shear stresses acting on the C.V. are shown in Fig. A.3-2

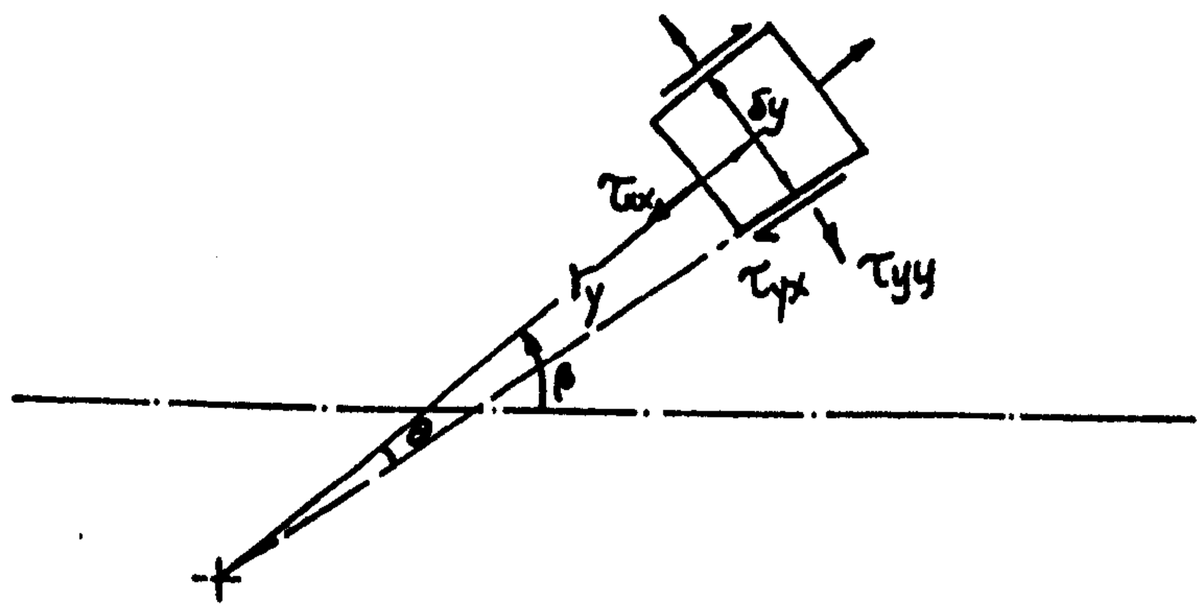

Fig. A.3-2

Shear force due to $\tau_{xx} = \frac{\partial}{\partial x}(\tau_{xx} \cdot r\,\delta y)\delta x$

Shear force due to $\tau_{yx} = \frac{\partial}{\partial y}(\tau_{yx} r\delta x)\delta y$

Force component acting in x-direction due to τ_{yy}

$$= -2r\delta x\,\tau_{yy}\sin\theta = -2r\delta x \cdot \tau_{yy} \cdot \frac{\frac{1}{2}\delta y}{r_y} = -\frac{\tau_{yy}}{r_y} \cdot r\delta x\delta y$$

since $\sin\theta \doteq \theta = \frac{\frac{1}{2}\delta y}{r_y}$.

Similarly, force acting in x-direction due to τ_{zz}

$$= -\frac{\tau_{zz}}{r} \cdot r\delta x\delta y \sin\beta$$

For a laminar flow, the components of shear stresses as derived by Goldstein (1957), are:

$$\tau_{xx} = \mu(2\frac{\partial U}{\partial x} + 2\frac{V}{r_x})$$

$$\tau_{yx} = \mu(\frac{\partial U}{\partial y} + \frac{\partial V}{\partial x})$$

$$\tau_{yy} = \mu(2\frac{\partial V}{\partial y} + 2\frac{U}{r_y})$$

$$\tau_{zz} = \mu\left[\frac{2(U\sin\beta + V\cos\beta)}{r}\right]$$

The overall shear forces acting on the C.V. in the x-direction can be written as

$$F_s = \Big[2\frac{\partial}{\partial x}(r\mu\frac{\partial U}{\partial x}) + \frac{\partial}{\partial y}(r\mu\frac{\partial U}{\partial y}) + \frac{\partial}{\partial y}(r\mu\frac{\partial V}{\partial x}) - 2\mu\frac{r}{r_y}(\frac{\partial V}{\partial y} + \frac{U}{r_y})$$

$$+ 2\mu\frac{\partial}{\partial x}(\frac{r}{r_x}V) - \mu\frac{2(U\sin\beta + V\cos\beta)}{r}\sin\beta\Big]\delta x\,\delta y \qquad \text{(A.3-4)}$$

It is possible to simplify the above expression for a flow with $r_x \gg r$ and $r_y \gg r$. In this case, those terms containing r/r_x or r/r_y will be small compared with other terms and can be neglected. Thus

$$F_s = \left[2\frac{\partial}{\partial x}(r\mu\frac{\partial U}{\partial x}) + \frac{\partial}{\partial y}(r\mu\frac{\partial U}{\partial y}) + \frac{\partial}{\partial y}(r\mu\frac{\partial V}{\partial x}) - \mu\frac{2(U\sin\beta + V\cos\beta)}{r}\sin\beta\right]\delta x\delta y \qquad (A.3\text{-}5)$$

Applying the Newton's 2nd Law, we have

$$(\dot{m}U)_x = F_p + F_c + F_s \qquad (A.3\text{-}6)$$

Substituting equations(A.3-1), (A.3-2), (A.3-3) and (A.3-5) into equation(A.3-6) and rearranging

$$\frac{1}{r}\left[\frac{\partial}{\partial x}(\rho UrU) + \frac{\partial}{\partial y}(\rho VrU) - \frac{\partial}{\partial x}(r\mu\frac{\partial U}{\partial x}) - \frac{\partial}{\partial y}(r\mu\frac{\partial U}{\partial y})\right] = -\frac{\partial P}{\partial x}$$

$$+\rho\frac{V^2}{r_y} + \frac{1}{r}\left[\frac{\partial}{\partial x}(r\mu\frac{\partial U}{\partial x}) + \frac{\partial}{\partial y}(r\mu\frac{\partial V}{\partial x}) - \mu\frac{2(U\sin\beta + V\cos\beta)}{r}\sin\beta\right]$$

(A.3-7)

Similar method can be applied to derive the V-momentum equation.

A.4 Derivation of k-Production Terms

The exact equation of k for a general 3-D orthogonal coordinates can be derived from the Navia-Stokes equations by multiplying the momentum equation for each coordinate direction by its corresponding fluctuating velocity; time averaging and summing the three equations (see for example, Williams (1972)) . The final form can be written

$$\rho\frac{Dk}{Dt} = -\frac{\partial}{\partial x_j}(\rho\overline{u'k'} + \overline{u_j'p'}) + \mu\frac{\partial^2 k}{\partial x_j^2} - \rho\overline{u_i'u_j'}\frac{\partial U_i}{\partial x_j} - \mu\overline{\left(\frac{\partial u_i'}{\partial x_j}\right)^2}$$

$$i,j = 1,2,3 \qquad (A.4\text{-}1)$$

Convection = Diffusion + Production - Dissipation

The various terms can be approximated to a simplified form according to Prandtl and Kolmogorov

$$-\frac{\partial}{\partial x_j}(\rho\overline{u_j'k'} + \overline{u_j'p'}) = \frac{\partial}{\partial x_j}(C_\mu \rho k^{\frac{1}{2}} l \frac{\partial k}{\partial x_j})$$

$$= \frac{\partial}{\partial x_j}(\frac{\mu_t}{\sigma_k}\frac{\partial k}{\partial x_j}) \qquad (A.4\text{-}2)$$

by using $\mu_t = C_\mu \rho k^{\frac{1}{2}} l$.

The dissipation term, following the local isotropy assumption, is given to as

$$\mu\overline{\left(\frac{\partial u_i'}{\partial x_j}\right)^2} = C_D \rho \frac{k^{3/2}}{l} \qquad (A.4\text{-}3)$$

For the production term G is given by

$$G = -\rho\overline{u_i'u_j'}\frac{\partial U_i}{\partial x_j} = \tau_{ij}\frac{\partial U_i}{\partial x_j} \qquad (A.4\text{-}4)$$

The turbulent shear stress components for a general 2-D orthogonal coordinates are obtained by substituting μ_t for μ in the stress components expressions by Goldstein (1957).

i.e.,

$$\tau_{xx} = \mu_t(2\frac{\partial U}{\partial x} + 2\frac{V}{r_x}) \qquad (A.4\text{-}5)$$

$$\tau_{yx} = \mu_t(\frac{\partial U}{\partial y} + \frac{\partial V}{\partial x}) \qquad (A.4\text{-}6)$$

$$\tau_{yy} = \mu_t(2\frac{\partial V}{\partial y} + 2\frac{U}{r_y}) \qquad (A.4\text{-}7)$$

Substituting (A.4-5), (A.4-6), (A.4-7) into equation (A.4-4) gives

$$G = 2\mu_t(\frac{\partial U}{\partial x} + \frac{V}{r_x})\frac{\partial U}{\partial x} + \mu_t(\frac{\partial U}{\partial y} + \frac{\partial V}{\partial x})^2$$

$$+ 2\mu_t(\frac{\partial V}{\partial y} + \frac{U}{r_y})\frac{\partial V}{\partial y}$$

$$= \mu_t\left\{2\left[(\frac{\partial U}{\partial x})^2 + (\frac{\partial V}{\partial y})^2 + \frac{V}{r_x}(\frac{\partial U}{\partial x}) + \frac{U}{r_y}(\frac{\partial V}{\partial y})\right]\right.$$

$$\left. + (\frac{\partial U}{\partial y} + \frac{\partial V}{\partial x})^2\right\} \qquad (A.4\text{-}8)$$

A.5 Derivation of the General Finite Difference Equation For ϕ

The general partial differential equation for ϕ is

$$\underbrace{\frac{\partial}{\partial x}(\rho U r\phi) + \frac{\partial}{\partial y}(\rho V r\phi)}_{\text{Convective terms}(I_{con})} - \underbrace{\frac{\partial}{\partial x}\left(\frac{r\mu_{eff}}{\sigma_\phi}\frac{\partial\phi}{\partial x}\right) - \frac{\partial}{\partial y}\left(\frac{r\mu_{eff}}{\sigma_\phi}\frac{\partial\phi}{\partial y}\right)}_{\text{Diffusive terms}(I_{dif})} = rS_\phi \tag{A.5-1}$$

Integrating the convective terms over the control volume (C.V.) around P with respect to x and y, we have

$$I_{con} = \int_y\int_x\left[\frac{\partial}{\partial x}(\rho U r\phi) + \frac{\partial}{\partial y}(\rho V r\phi)\right] dxdy$$

$$= \int_s^n \left[\rho U r\phi\right]_w^e dy + \int_w^e \left[\rho V r\phi\right]_s^n dx$$

$$= (\rho U r\delta y)_e\phi_e - (\rho U r\delta y)_w\phi_w$$

$$+(\rho V r\delta x)_n\phi_n - (\rho V r\delta x)_s\phi_s$$

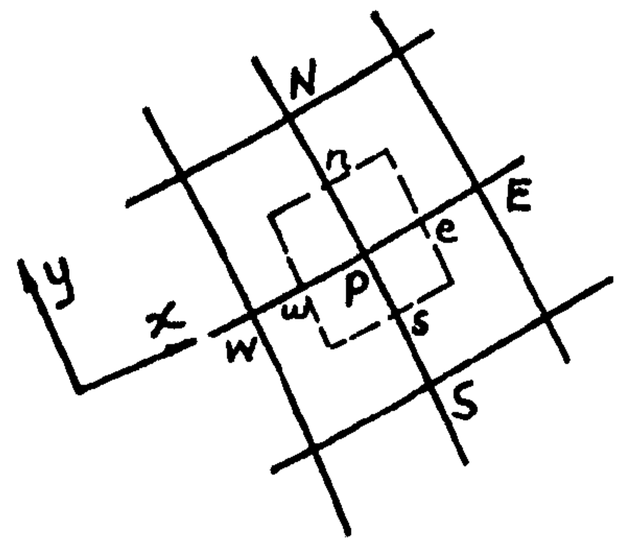

Similarly, integrating the diffusive terms over the C.V., one gets

$$I_{dif} = \int_y\int_x\left[\frac{\partial}{\partial x}\left(\frac{r\mu_{eff}}{\sigma_\phi}\frac{\partial\phi}{\partial x}\right) + \frac{\partial}{\partial y}\left(\frac{r\mu_{eff}}{\sigma_\phi}\frac{\partial\phi}{\partial y}\right)\right] dxdy$$

$$= \int_s^n \left[\frac{r\mu_{eff}}{\sigma_\phi}\frac{\partial\phi}{\partial x}\right]_w^e dy + \int_n^e \left[\frac{r\mu_{eff}}{\sigma_\phi}\frac{\partial\phi}{\partial y}\right]_s^n dx$$

$$= \left(\frac{r\mu_{eff}}{\sigma_\phi}\delta y\frac{\partial\phi}{\partial x}\right)_e - \left(\frac{r\mu_{eff}}{\sigma_\phi}\delta y\frac{\partial\phi}{\partial x}\right)_w + \left(\frac{r\mu_{eff}}{\sigma_\phi}\delta x\frac{\partial\phi}{\partial y}\right)_n$$

$$- \left(\frac{r\mu_{eff}}{\sigma_\phi}\delta x\frac{\partial\phi}{\partial y}\right)_s$$

Now,

$$\left(\frac{\partial\phi}{\partial x}\right)_e = \frac{\phi_E - \phi_P}{\delta x_e}$$

$$\left(\frac{\partial\phi}{\partial x}\right)_w = \frac{\phi_P - \phi_W}{\delta x_w}$$

$$\left(\frac{\partial\phi}{\partial y}\right)_n = \frac{\phi_N - \phi_P}{\delta y_n}$$

$$\left(\frac{\partial\phi}{\partial y}\right)_s = \frac{\phi_P - \phi_S}{\delta y_s}$$

Substituting into I_{dif} we have

$$I_{dif} = \left(\frac{\mu_{eff} r \delta y}{\sigma_\phi \delta x}\right)_e (\phi_E - \phi_P) + \left(\frac{\mu_{eff} r \delta y}{\sigma_\phi \delta x}\right)_w (\phi_W - \phi_P)$$

$$+\left(\frac{\mu_{eff} r \delta x}{\sigma_\phi \delta y}\right)_n (\phi_N - \phi_P) + \left(\frac{\mu_{eff} r \delta x}{\sigma_\phi \delta y}\right)_s (\phi_S - \phi_P)$$

Assuming $\left(\frac{\mu_{eff} r \delta y}{\sigma_\phi \delta x}\right)_e = D_e$,

$$\left(\frac{\mu_{eff} r \delta y}{\sigma_\phi \delta x}\right)_w = D_w \quad ,$$

$$\left(\frac{\mu_{eff} r \delta x}{\sigma_\phi \delta y}\right)_n = D_n \quad ,$$

and $\left(\frac{\mu_{eff} r \delta x}{\sigma_\phi \delta y}\right)_s = D_s$,

we have

$$I_{dif} = D_e(\phi_E - \phi_P) + D_w(\phi_W - \phi_P)$$

$$+ D_n(\phi_N - \phi_P) + D_s(\phi_s - \phi_P)$$

$$= D_e\phi_E + D_w\phi_W + D_n\phi_N + D_s\phi_S$$

$$-(D_e + D_w + D_n + D_s)\phi_P$$

If $(\rho U r \delta y)_e = C_e$

$(\rho U r \delta y)_w = C_w$

$(\rho V r \delta x)_n = C_n$

and $(\rho V r \delta x)_s = C_s$

we have

$$I_{con} = C_e\phi_e - C_w\phi_w + C_n\phi_n - C_s\phi_s$$

The values ϕ_e, ϕ_w, ϕ_n, ϕ_s must be calculated from the values of ϕ_E, ϕ_W, ϕ_N, ϕ_S. There are two schemes available for this calculation, i.e., (i) central difference scheme and (ii) upwind difference scheme.

(i) The central difference scheme suggests that the ϕ's at e, w, n, s can be calculated as the mean value of ϕ at the nodes P, E, W, N and S, i.e.,

$$\phi_e = 0.5(\phi_P + \phi_E)$$

$$\phi_n = 0.5(\phi_N + \phi_P)$$

$$\phi_w = 0.5(\phi_W + \phi_P)$$

$$\phi_s = 0.5(\phi_P + \phi_S)$$

Thus the convective term can be written as

$$I_{con} = 0.5C_e\phi_E - 0.5C_w\phi_W + 0.5C_n\phi_N - 0.5C_s\phi_S$$

$$+(0.5C_e - 0.5C_w + 0.5C_n - 0.5C_s)\phi_P$$

(ii) The upwind difference scheme suggests that since C's are directional, to accommodate the directional effect, the calculation of ϕ_e , ϕ_w , ϕ_n and ϕ_s depends on the sign of C. If C is positive, upstream value of ϕ is used, if C is negative then downstream value should be used. Thus

$$\phi_e = \phi_P \quad \text{if} \quad C_e \text{ is positive}$$

$$\phi_e = \phi_E \quad \text{if} \quad C_e \text{ is negative}$$

Thus $$C_e\phi_e = \left(\frac{|C_e| + C_e}{2}\right)\phi_P - \left(\frac{|C_e| - C_e}{2}\right)\phi_E$$

and likewise for others. By substituting $C_i\phi_i$ into I_{con} and rearranging, we have

$$I_{con} = 0.5(|C_e| - C_e)(\phi_P - \phi_E) + 0.5(|C_w| + C_w)(\phi_P - \phi_W)$$

$$+ 0.5(|C_n| - C_n)(\phi_P - \phi_N) + 0.5(|C_s| + C_s)(\phi_P - \phi_S)$$

$$+ (C_e + C_n - C_w - C_s)\phi_P$$

The total source in the control volume is linearized to the following expression

$$\int_y \int_x rS_\phi dxdy = S_P^\phi \phi_P + S_u^\phi$$

Assembling I_{con}, I_{dif} and the linearized source term into equation (A.5-1), we have

$$\left[(A_E + A_W + A_N + A_S) + (C_e - C_w + C_n - C_s) - S_P^\phi\right]\phi_P$$

$$= A_E\phi_E + A_W\phi_W + A_N\phi_N + A_S\phi_S + S_u^\phi$$

where

$$\left.\begin{aligned} A_E &= D_e - 0.5C_e \\ A_W &= D_w + 0.5C_w \\ A_N &= D_n - 0.5C_n \\ A_S &= D_s + 0.5C_s \end{aligned}\right\}$$

If central difference scheme is used for I_{con}.

or

$$\left.\begin{aligned} A_E &= D_e + 0.5(|C_e| - C_e) \\ A_W &= D_w + 0.5(|C_w| + C_w) \\ A_N &= D_n + 0.5(|C_n| - C_n) \\ A_S &= D_s + 0.5(|C_s| + C_s) \end{aligned}\right\} \text{If upwind difference scheme is used for } I_{con}$$

A.6 Linearization of Source Terms

U-momentum source terms

The source term is given by

$$S_u = -\frac{\partial P}{\partial x} + \frac{\rho V^2}{r_y} + \frac{1}{r}\left[\frac{\partial}{\partial x}(r\mu\frac{\partial U}{\partial x}) + \frac{\partial}{\partial y}(r\mu\frac{\partial V}{\partial x})\right]$$

$$- \frac{2\mu(U\sin\beta + V\cos\beta)}{r^2}\sin\beta$$

Integrating S_u over the control volume w. r. t. x and y,

$$\int_y\int_x rS_u dxdy = \int_y\int_x (-r\frac{\partial P}{\partial x} + \frac{r\rho V^2}{r_y})dxdy$$

$$+ \int_y\int_x \left[\frac{\partial}{\partial x}(r\mu\frac{\partial U}{\partial x}) + \frac{\partial}{\partial y}(r\mu\frac{\partial V}{\partial x})\right.$$

$$\left. - \frac{2\mu(U\sin\beta + V\cos\beta)}{r}\sin\beta\right] dxdy$$

The first integration represents the force acting on the control volume by pressure and centrifugal effects and the second integration represents the shear stress contribution. Thus

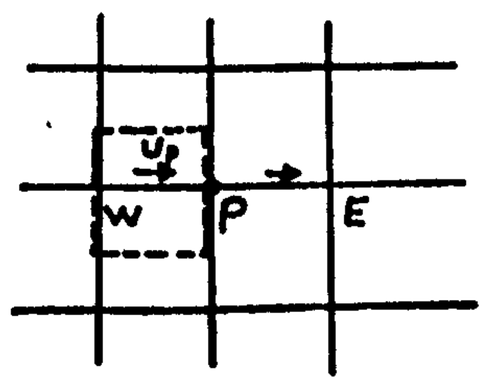

$$\int_y\int_x(-r\frac{\partial P}{\partial x} + r\frac{\rho V^2}{r_y})dxdy$$

$$= \frac{-(P_p - P_w)}{\delta x}\cdot\delta x r\delta y + (\frac{\rho V^2}{r_y})_P\cdot v_P$$

$$= \tfrac{1}{2}(a_e{}^u + a_w{}^u)(P_w - P_p) + (\frac{\rho V^2}{r_y})_P\cdot v_P$$

where v_P is the control volume

Here $\frac{\rho V^2}{r_y}$ is assumed to have its value at P prevail over the entire control volume.

As in the present study, the maximum possible value of angle β is relatively small, i.e., not more than 4° in diffuser region with a similar magnitude in the secondary flow region, the integration of the shear term can be approximated to a cylindrical polar coordinates case which is zero

Thus $$\int_y\int_x rS_u dxdy \simeq \tfrac{1}{2}(a_e^{\,u} + a_w^{\,u})(P_w - P_p) + \left(\frac{\rho V^2}{r_y}\right)_P \cdot v_P$$

<u>V-momentum source terms</u>

$$S_v = -\frac{\partial P}{\partial y} + \frac{\rho U^2}{r_x} + \frac{1}{r}\left[\frac{\partial}{\partial x}\left(r\mu\frac{\partial U}{\partial y}\right) + \frac{\partial}{\partial y}\left(r\mu\frac{\partial V}{\partial y}\right)\right]$$

$$- \frac{2\mu(U\sin\beta + V\cos\beta)}{r^2}\cos\beta$$

Using the similar integration procedure and approximation,

$$\int_y\int_x rS_v dxdy = \tfrac{1}{2}(a_n^{\,v} + a_s^{\,v})(P_S - P_P) + \left(\frac{\rho U^2}{r_x}\right)_P \cdot v_P$$

$$+ \int_y\int_x\left[\frac{\partial}{\partial x}\left(r\mu\frac{\partial U}{\partial y}\right) + \frac{\partial}{\partial y}\left(r\mu\frac{\partial V}{\partial y}\right) - \frac{2\mu(U\sin\beta + V\cos\beta)}{r}\cos\beta\right]dxdy$$

The shear terms when approximated to a cylindrical polar coordinates case is

$$\int_r\int_x \left[\frac{\partial}{\partial x}(r\mu\frac{\partial U}{\partial r}) + \frac{\partial}{\partial r}(r\mu\frac{\partial V}{\partial r}) - \frac{\mu V}{r}\right]dxdr - \int_r\int_x \frac{\mu V}{r}dxdr$$

$$= 0 - (\frac{\mu V}{r^2})_P \cdot v_P$$

since $\frac{\partial}{\partial x}(r\mu\frac{\partial U}{\partial r}) + \frac{\partial}{\partial r}(r\mu\frac{\partial V}{\partial r}) - \frac{\mu V}{r} = 0$ from the continuity equation.

Thus

$$\int_y\int_x rS_v dxdy = \tfrac{1}{2}(a_n{}^v + a_s{}^v)(P_S - P_P) + (\frac{\rho U^2}{r_x})_P \cdot v_P + (\frac{\mu}{r^2})_P v_P V$$

$$= S_p{}^v \cdot V + S_u{}^v$$

where $S_p{}^v = (\frac{\mu}{r^2})_P v_P$

$$S_u{}^v = \tfrac{1}{2}(a_n{}^v + a_s{}^v)(P_S - P_P) + (\frac{\rho U^2}{r_x})_P v_P$$

<u>k source terms</u>

$$\int_y\int_x rS_k dxdy = \int_y\int_x r(G - C_D\rho\varepsilon)dxdy$$

$$= \int_y\int_x r(G - \frac{C_D C_\mu \rho^2 k^2}{\mu_t})dxdy$$

$$= (G - \frac{C_D C_\mu \rho^2 k^2}{\mu_t})_P v_P$$

$$= S_p{}^k \cdot k + S_u{}^k$$

where $$S_P^k = -\left(\frac{C_D C_\mu \rho^2 k}{\mu_t}\right)_P v_P$$

$$S_u^k = G_P v_P$$

<u>ε source terms</u>

$$\int_y \int_x r S_\varepsilon \, dx dy = \int_y \int_x r(C_1 \varepsilon G/k - C_2 \rho \varepsilon^2/k) dx dy$$

$$= \int_y \int_x r\left(\frac{C_1 C_\mu \rho k G}{\mu_t} - C_2 \rho \varepsilon^2/k\right) dx dy$$

$$= \left(\frac{C_1 C_\mu \rho k G}{\mu_t}\right)_P v_P - (C_2 \rho \varepsilon/k)_P v_P \cdot \varepsilon$$

$$= S_p^\varepsilon \cdot \varepsilon + S_u^\varepsilon$$

where $$S_p^\varepsilon = -\left(\frac{C_2 \rho \varepsilon}{k}\right)_P v_P$$

$$S_u^\varepsilon = \left(\frac{C_1 C_\mu \rho k G}{\mu_t}\right)_P v_P$$

A.7 Derivation of the Finite Difference Equation for P'

The finite difference equation for U and U* can be written as

$$A_P^u U_P = \sum_{j=N,S,E,W} A_j^u U_j + 0.5(a_e^u + a_w^u)(P_W - P_P) + \left(\frac{\rho v^2}{r_y}\right)_P \cdot v_P \quad (A.7\text{-}1)$$

$$A_P^u U_P^* = \sum_{j=N,S,E,W} A_j^u U_j^* + 0.5(a_e^u + a_w^u)(P_W^* - P_P^*) + \left(\frac{\rho v^2}{r_y}\right) \cdot v_P \quad (A.7\text{-}2)$$

Substract (A.7-2) from (A.7-1) and use

$$P_j = P_j^* + P_j' \quad (A.7\text{-}3)$$

One gets

$$A_P^u(U_P - U_P^*) = \sum_{j=N,S,E,W} A_j^u(U_j - U_j^*) + 0.5(a_e^u + a_w^u)(P_W' - P_P') \quad (A.7\text{-}4)$$

By assuming $\sum_{j=N,S,E,W} A_j^u(U_j - U_j^*) = 0$, equation (A.7-4) becomes

$$U_P = U_P^* + D_w^u(P_W' - P_P') \quad (A.7\text{-}5)$$

where $$D_w^u = \frac{0.5(a_e^u + a_w^u)}{A_P^u}$$

Similarly for V,

$$V_P = V_P^* + D_s^v(P_S' - P_P') \quad (A.7\text{-}6)$$

where $$D_s^v = \frac{0.5(a_n^v + a_s^v)}{A_P^v}$$

The continuity equation is given by

$$\frac{\partial}{\partial x}(\rho r U) + \frac{\partial}{\partial y}(\rho r V) = 0$$

$$\int_{y_s}^{y_n}\int_{x_w}^{x_e}\left[\frac{\partial}{\partial x}(\rho r U) + \frac{\partial}{\partial y}(\rho r V)\right] dx dy$$

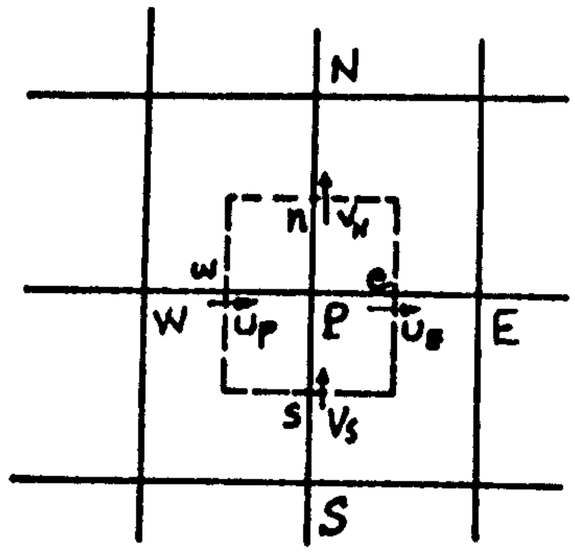

$$= (\rho U r \delta y)_e - (\rho U r \delta y)_w$$

$$+ (\rho V r \delta x)_n - (\rho V r \delta x)_s$$

$$= U_E(\rho r \delta y)_e - U_P(\rho r \delta y)_w$$

$$+ V_N(\rho r \delta x)_n - V_P(\rho r \delta x)_s = 0 \qquad \text{(A.7-7)}$$

Similarly to (A.7-5) and (A.7-6), one can obtian

$$U_E = U_E^* + D_e^u(P_P' - P_E') \qquad \text{(A.7-8)}$$

$$V_N = V_N^* + D_n^v(P_P' - P_N') \qquad \text{(A.7-9)}$$

Substituting U_P , U_E , V_P , V_N into equation (A.7-7), one gets

$$U_E^*(\rho r \delta y)_e - U_P^*(\rho r \delta y)_w + V_N^*(\rho r \delta x)_n - V_P^*(\rho r \delta x)_s$$

$$+ \left[D_e^u(\rho r \delta y)_e + D_w^u(\rho r \delta y)_w + D_n^v(\rho r \delta x)_n + D_s^v(\rho r \delta x)_s\right] P_p'$$

$$= D_e^u(\rho r \delta y)_e P_E' + D_w^u(\rho r \delta y)_w P_W' + D_n^v(\rho r \delta x)_n P_N'$$

$$+ D_s^v(\rho r \delta x)_s P_s' \qquad \text{(A.7-10)}$$

Since the net mass flow out of the control volume evaluated by U* and V* is $\dot{m}_P$, i.e.,

$$\dot{m}_P = U_E^*(\rho r\delta y)_e - U_P^*(\rho r\delta y)_w + V_N^*(\rho r\delta x)_n - V_P^*(\rho r\delta x)_s$$

and assuming $D_e^u(\rho r\delta y)_e = A_E$

$$D_w^u(\rho r\delta y)_w = A_W$$

$$D_n^v(\rho r\delta x)_n = A_N$$

$$D_s^v(\rho r\delta x)_s = A_S$$

Equation (A.7-10) can be rewritten as

$$(A_E + A_W + A_N + A_S)P_P' = A_E P_E' + A_W P_W' + A_N P_N' + A_S P_S' - \dot{m}_P \tag{A.7-11}$$

A.8 Calculation of Orthogonal Grid in the Secondary Inlet Region of Jet Pump

The secondary inlet region can be subdivided into two regions: (I) region between the duct wall and the nozzle wall, and (II) region between duct wall and the central jet. The two regions are considered separately below.

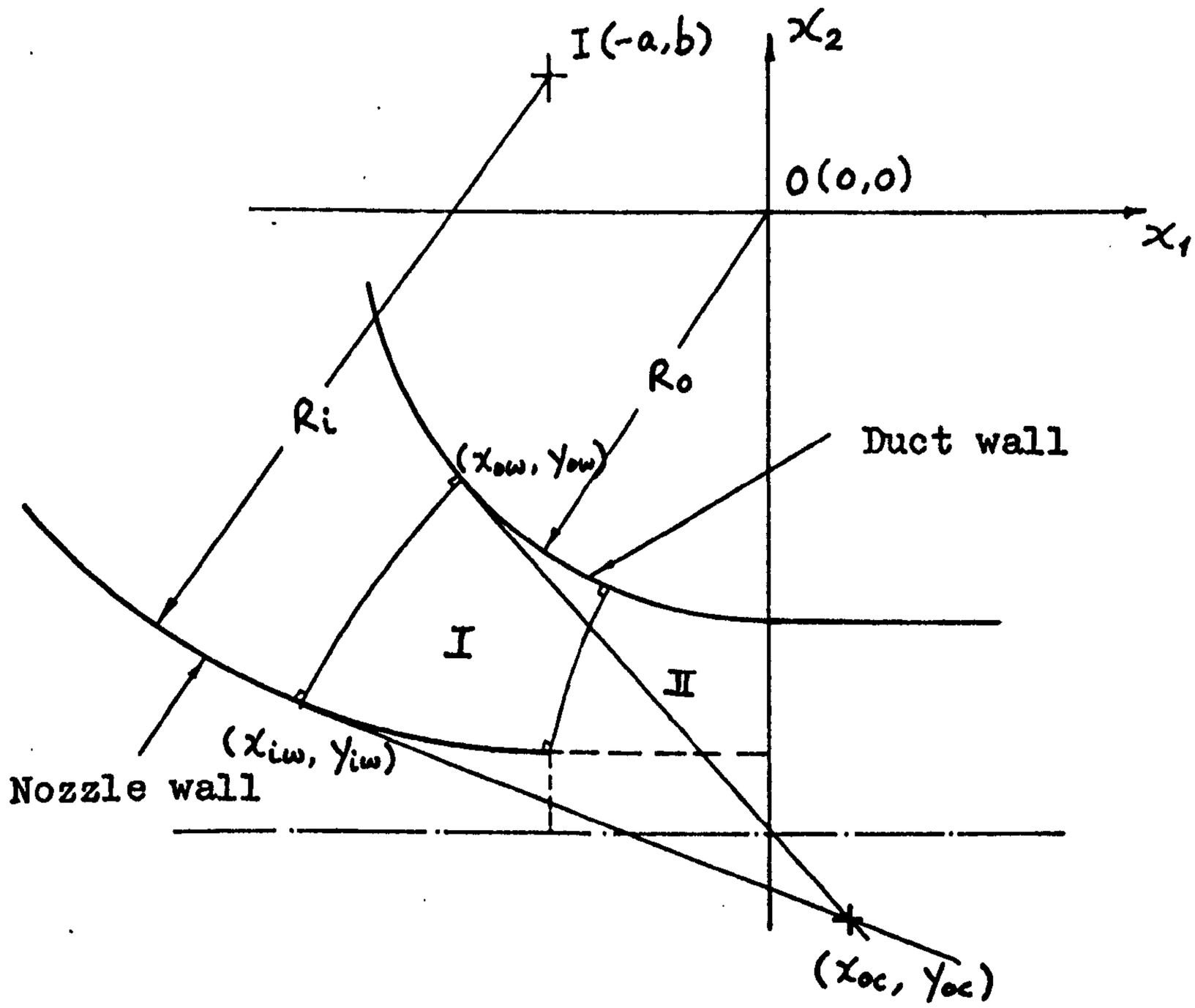

Fig. A.8-1 Geometry of secondary inlet

(I) The inner (nozzle) wall with centre at I(-a,b) can be described by

$$(x_1 + a)^2 + (x_2 - b)^2 = R_i^2 \qquad (A.8\text{-}1)$$

The outer (duct) wall with centre at O(0,0) can be

described by

$$x_1^2 + x_2^2 = R_o^2 \qquad (A.8\text{-}2)$$

From any point (x_{iw}, y_{iw}) on the inner wall, an orthogonal circle can be drawn to cut both inner and outer wall at right angles. Assuming that the centre of the orthogonal circle is at (x_{oc}, y_{oc}) and the intersection on the outer wall is (x_{ow}, y_{ow}), four equations can then be set up to solve for the four unknowns x_{oc}, y_{oc}, x_{ow} and y_{ow}.

For orthogonal condition,

$$\frac{y_{iw} - y_{oc}}{x_{iw} - x_{oc}} \times \frac{y_{iw} - b}{x_{iw} + a} = -1 \qquad (A.8\text{-}3)$$

$$\frac{y_{ow} - y_{oc}}{x_{ow} - x_{oc}} \times \frac{y_{ow}}{x_{ow}} = -1 \qquad (A.8\text{-}4)$$

Since (x_{ow}, y_{ow}) lies on the outer wall,

$$x_{ow}^2 + y_{ow}^2 = R_o^2 \qquad (A.8\text{-}5)$$

Equidistance from (x_{iw}, y_{iw}) and (x_{ow}, y_{ow}) to (x_{oc}, y_{oc}) gives

$$(x_{iw} - x_{oc})^2 + (y_{iw} - y_{oc})^2 = (x_{ow} - x_{oc})^2 + (y_{ow} - y_{oc})^2 \qquad (A.8\text{-}6)$$

Equations (A.8-3) to (A.8-6) are then solved for the four unknowns x_{ow}, y_{ow}, x_{oc} and y_{oc}. The solution procedure is as follows

(i) From equations (A.8-3) and (A.8-4), x_{oc} and y_{oc} can be expressed in terms of x_{ow} and y_{ow}.

(ii) Substituting x_{oc} and y_{oc} obtained in (i) into equation(A.8-6), the resulting equation now contains only x_{ow} and y_{ow}.

(iii) From equation(A.8-5) and the resulting equation obtained in (ii), solve for x_{ow} and y_{ow}, i.e.

$$x_{ow} = \frac{f^2 g - \sqrt{f^4 g^2 - (g^2+h^2)(f^4-h^2R_i^2)}}{g^2 + h^2} \qquad \text{(A.8-7)}$$

where $f^2 = x_{iw}(x_{iw} + a) + y_{iw}(y_{iw} - b) + R_i R_o$

$$g = (1 + \frac{R_i}{R_o})x_{iw} + a$$

$$h = (1+ \frac{R_i}{R_o})y_{iw} - b$$

and $$y_{ow} = -\sqrt{R_o^2 - x_{ow}^2} \qquad \text{(A.8-8)}$$

Now, since x_{ow} and y_{ow} are known, equations(A.8-3) and (A.8-4) can be used to solve for x_{oc} and y_{oc}. After appropriate algebraic simplification, one gets

$$x_{oc} = x_{ow} - F \cdot y_{ow} \qquad \text{(A.8-9)}$$

$$y_{oc} = y_{ow} + F \cdot x_{ow} \qquad \text{(A.8-10)}$$

where $$F = \frac{(x_{iw}+a)(x_{iw}-x_{ow}) + (y_{iw}-b)(y_{iw}-y_{ow})}{x_{ow}(y_{iw}-b) - y_{ow}(x_{iw}+a)}$$

and $$r_{oc} = \sqrt{(x_{iw} - x_{oc})^2 + (y_{iw} - y_{oc})^2} \qquad \text{(A.8-11)}$$

Thus, the grid line in the y-direction is defined by

$$(x_1 - x_{oc})^2 + (x_2 - y_{oc})^2 = r_{oc}^{\ 2} \qquad \text{(A.8-12)}$$

(II) This region is represented by ABCD in the diagram. The grid in this region is determined by the number of axial grid lines between C and D. The grid lines in ACD are the extensions of grid lines from the uniform mixing tube.

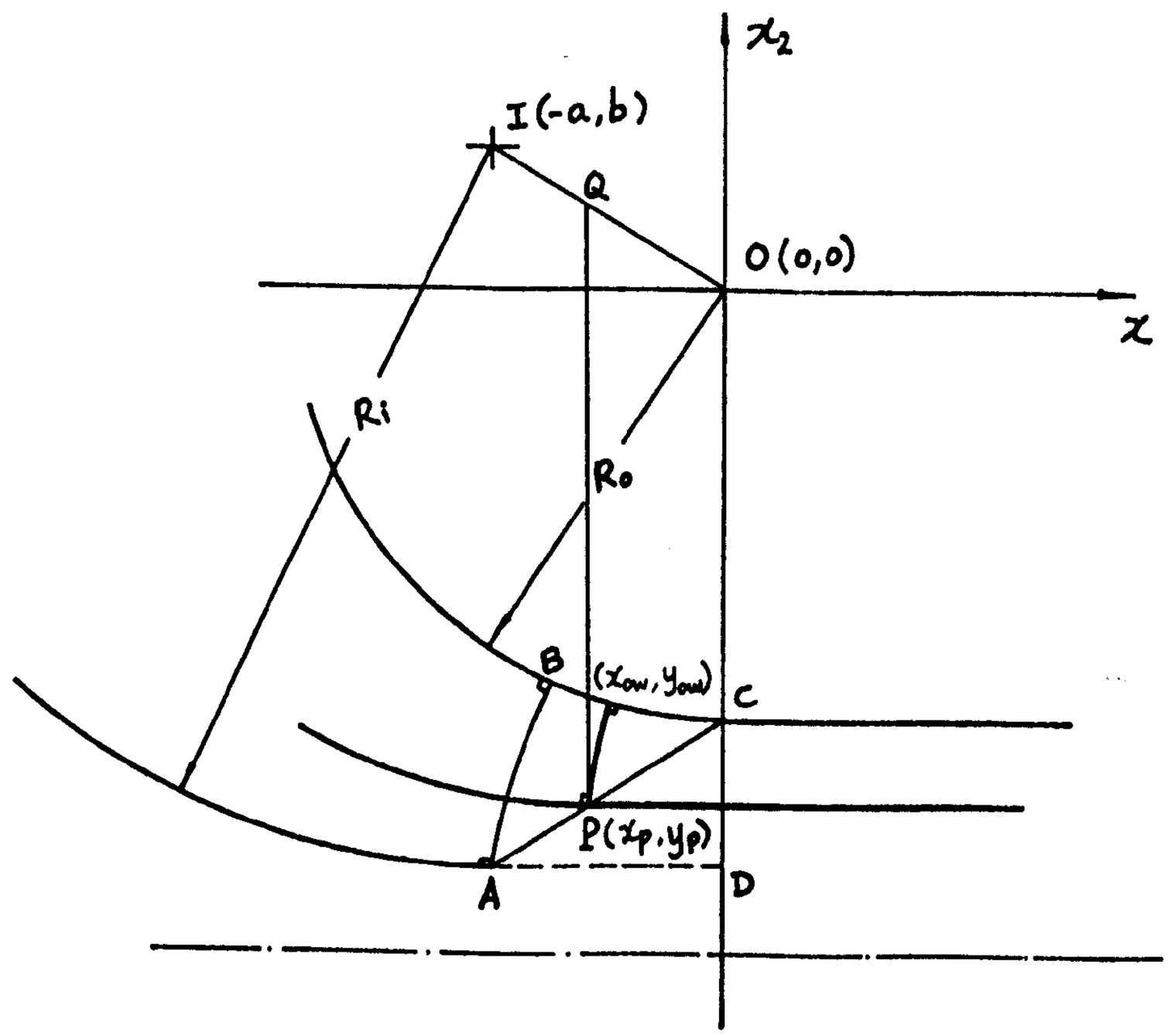

Fig. A.8-2

Any axial grid line will cut AC at a point P (x_P, y_P). From P, an orthogonal circle with centre (x_{oc}, y_{oc}) can be drawn to cut the duct wall BC at (x_{ow}, y_{ow}). Again, four equations can be set up to solve for the four unknowns x_{oc}, y_{oc}, x_{ow} and y_{ow}, i.e.,

$$y_{oc} = y_P \tag{A.8-13}$$

$$\frac{y_{ow} - y_{oc}}{x_{ow} - x_{oc}} \cdot \frac{y_{ow}}{x_{ow}} = -1 \tag{A.8-14}$$

$$x_{ow}^2 + y_{ow}^2 = R_o^2 \tag{A.8-15}$$

$$(x_{ow} - x_{oc})^2 + (y_{ow} - y_{oc})^2 = (x_{oc} - x_P)^2 \tag{A.8-16}$$

Equations(A.8-14) and (A.8-15) can be used to eliminate x_{ow} and y_{ow} in equation (A.8-16), thus giving

$$x_{oc} = \frac{R_o^2 + x_P^2 - y_P^2}{2x_P} \tag{A.8-17}$$

The grid line in y-direction drawn from $P(x_P, y_P)$ is defined by

$$(x_1 - x_{oc})^2 + (x_2 - y_{oc})^2 = (x_{oc} - x_P)^2 \tag{A.8-18}$$

The streamwise grid lines in the secondary inlet region are the extensions of axial grid lines in the mixing duct. From point P (Fig. A.8-2) a vertical line is drawn to cut

line OI at Q. The distance PQ and the coordinates of Q can be calculated. Using Q as the centre and PQ as the radius, a circle can be drawn which will join the axial grid line at P smoothly and cut all the orthogonal circles at right angles. A series of such circles can then be devised to form the streamwise grid lines in the secondary inlet region.

Appendix A.9

Inlet conditions for Turbulent Kinetic Energy 'k' and Length Scale 'l'

For the situations where measured and predicted flow parameters are being compared it is sometimes possible to use actual turbulence levels as inlet data for the computer model

When no empirical data is available, some estimation of 'k' and 'l' values at inlet must be made to initiate computation.

For the case of conical diffuser flows (McDonald et al (1966)), the value of 'k' at inlet (page 110) was specified by assuming the turbulence intensity to be 2.5%, based on the diffuser being fed from a large constant head chamber.

The value of inlet length scale chosen for the mixing tube is dependant upon the upstream boundary layer development and the thic kness of the nozzle wall. For a smooth and thin-walled nozzle, the length scale will always be small. Fig. 5.1-3 shows that even if the inlet length scale is altered by a factor of 1000 (i.e. from $0.0001r_o$ to $0.1r_o$), then the centre-line velocity in the strongly mixing region is only reduced by about 15%. The minimal effect of inlet length scale on static pressure distribution is shown in Fig. 5.1-6.

In this thesis, owing to the lack of published information on inlet lengths scales, the values for jet pump flows are taken in the region of $0.001\ r_o$ to $0.05\ r_o$. The exact choice is empirical. In the comparison with the experimental results of Razinsky and Brighton(1971) 'l' was taken as $0.005\ r_o$ since it gave good correlation for both time-mean variables and turbulent shear stress.

However, for the comparison of predicted values with the authors own LDA measurements, inlet length scales of $0.015\ r_t$ and $0.0085\ r_t$ for the 12.7 mm and 6.5 mm nozzles respectively were c hosen. The former value was determined from the comparison of measured and predicted centre-line K-distributions shown in Fig. A.9.-1. A correspondingly smaller value was chosen for the smaller (and thinner-sectioned) nozzle.

It is clear that no specific values for inlet length scale can be recommended at this time. The value will perhaps be a function of the nozzle dimensions and nozzle and duct wall surface conditions.

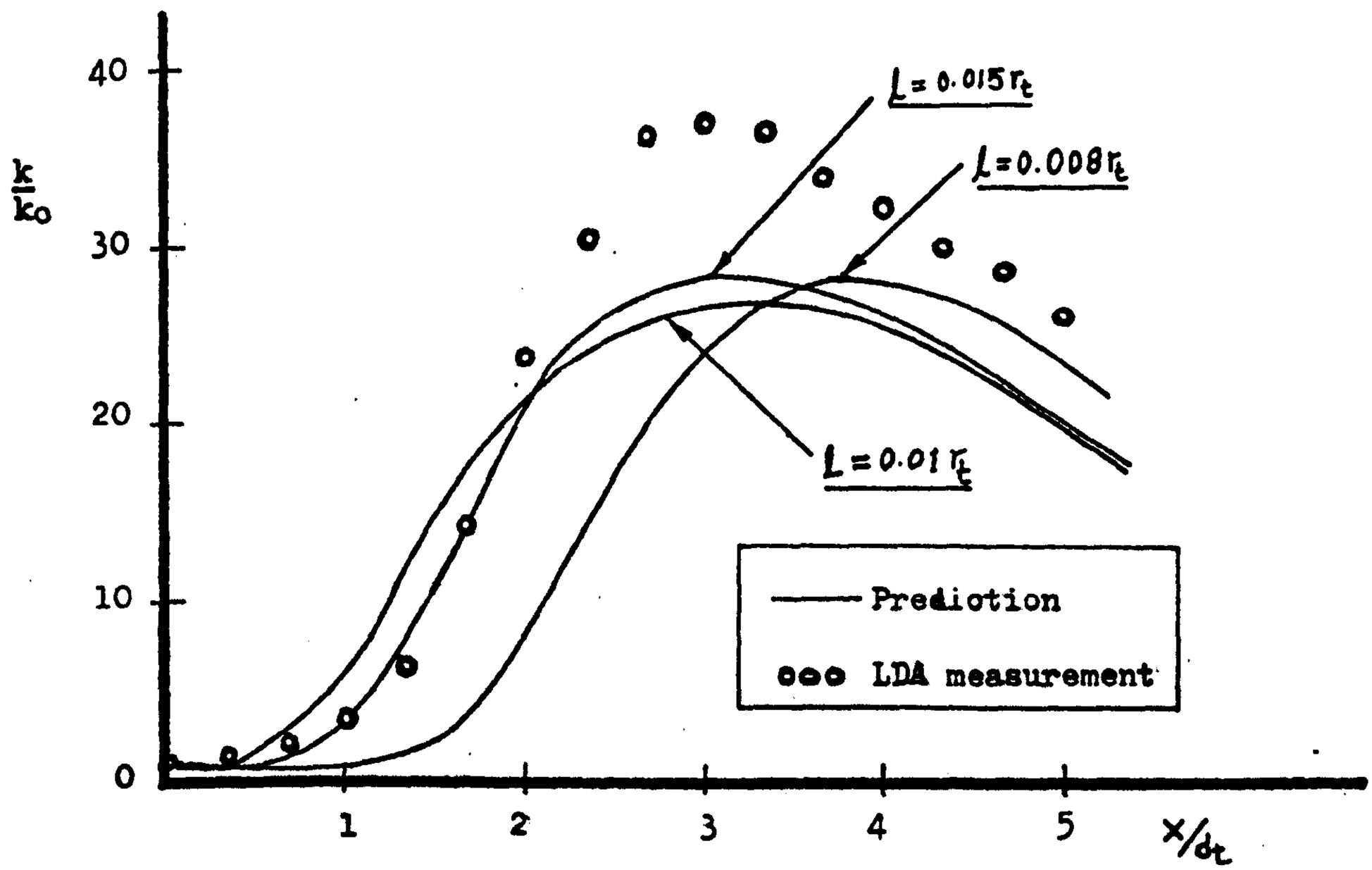

Fig.A.9 -1 Comparison of the predicted centre-line k-distributions using various inlet length scales with LDA measurement

By way of a concluding comment, it is relevant to say that the inlet length scale has only a marginal effect on the predicted mean flow behaviour. Thus for practical application where the emphasis is not on the turbulent structure of the flow but on the mean velocity and pressure distributions, values in the range of 0.001 r_o and 0.05 r_o for the mixing tube can be safely chosen. The computer model will itself predict values at the exit from the mixing tube and therefore at the entry to the diffuser. Only by future research, involving the measurement of average macroscopic length scale of eddies at the inlet, will the relationship between inlet length scales and upstream conditions be established

B.1 Listing of the Mixing Tube Program

```
      DIMENSION HEDU(6),HEDV(6),HEDP(6),HEDT(6),HEDK(6),HEDD(6),HEDM(6)
     1      ,HEDA(6),HEDB(6),HEDPP(6),HEDUN(6),HEDX(6),HEDY(6)
      COMMON/ALL/  IT,JT,NI,NJ,NIM1,NJM1,GREAT
     1/LVEL/RESCRU,NSWPU,URFU,DXEPU(26,12),DXPWU(26,12),SEWU(26,12),
     2       SNSU(26,12)
     1/VVEL/RESCRV,NSWPV,URFV,DYNPV(26,12),DYPSV(26,12),SNSV(26,12),
     2       SEWV(26,12),RCV(26,12)
     1/PCOR/RESCRM,NSWPP,URFP,DU(26,12),DV(26,12),IPREF,JPREF
     1/TEN/RESCRK,NSWPK,URFK
     1/TDIS/RESORE,NSWPD,URFE
     1/VAR/ U(26,12),V(26,12),P(26,12),PP(26,12),TE(26,12),ED(26,12)
     1/GEOM/INDCOS,XIW(18),YIW(18),XOW(18),YOW(26) ,XOC(18),YOC(18),
     2      RCC(18),XIC(18),YIC(18),RIC(18),X(26,12),Y(26,12),XU(26,12),
     3      YV(26,12),DXEP(26,12),DXPW(26,12),DYNP(26,12),DYPS(26,12),
     4      SNS(26,12),SEW(26,12),R(26,12),RV(26,12)
     1/FLUPR/URFVIS,VISCOS,DENSIT,PRANDT,DEN(26,12),VIS(26,12)
     1/KASE T5/UIN,TEIN,EDIN,FLOWIN,ALAMDA,UEN,FLOWEN, A,RSMALL,RMIX,
     2        INOZ,INP1,JNOZ,JNP1,IENT,IEP1
     1/TURB/GEN(26,12),CD,CMU,C1,C2,CAPPA,ELOG,PREC,PRTE
     1/WALLF/YPLUSN(28),TAUN(28),YPLUSS(18),TAUS(18)
     1/COEF/AP(26,12),AN(26,12),AS(26,12),AE(26,12),AW(26,12),SU(26,12),
     2       SP(26,12)
      LOGICAL INCALU,INCALV,INCALP,INPRC,INCALK,INCALD,INCALM,INCALA,
     1        INCALB
      GREAT=1.E30
      NITER=0
      IT=26
      JT=12
      NSWPU=1
      NSWPV=1
      NSWPP=5
      NSWPK=1
      NSWPD=1
      READ(9,010)HEDU,HEDV,HEDP,HEDT,HEDK,HEDD,HEDM,HEDA,HEDB,HEDPP,
     1HEDUN,HEDX,HEDY
  010 FORMAT(6A4)

C-----GRID
      NI=26
      NJ=12
      NIM1=NI-1
      NJM1=NJ-1
      NJM2=NJ-2
      INOZ=4
      JNOZ=4
      INP1=INOZ+1
      JNP1=JNOZ+1
      JNP2=JNOZ+2
      JMIX=NJM1-JNOZ
      IENT=INOZ+JMIX
      RNOZ=5.075E-3
      DY=RNOZ/FLOAT(JNOZ-1)
      A=3.59E-2
      RLARGE=16.5E-2
      RSMALL=12.7E-2
      RMIX=1.71E-2
      B=RLARGE+RNOZ-RSMALL-RMIX
      XENT=7.6E-2
      ALTCT=0.26
```

```
C DETERMINE THE INNER WALL GEOMETRY
      DXIW=(XENT-A)/FLOAT(INOZ-1)
      XIW(1)=-XENT-0.5*DXIW
      DO 100 I=2,INOZ
  100 XIW(I)=XIW(I-1)+DXIW
      DO 101 I=1,INOZ
  101 YIW(I)=B-SQRT(RLARGE*RLARGE-(XIW(I)+A)**2)
      YIW(INP1)=-(RSMALL+RMIX)+RNOZ
C DETERMINE THE OUTER WALL GEOMETRY
      RRAT=RLARGE/RSMALL
      DO 102 I=1,INOZ
      DSQ=XIW(I)*(XIW(I)+A)+YIW(I)*(YIW(I)-B)
      FSQ=DSQ+RRAT*RSMALL*RSMALL
      G=(1.0+RRAT)*XIW(I)+A
      H=(1.0+RRAT)*YIW(I)-B
      XOW(I)=(FSQ*G-SQRT(FSQ*FSQ*G*G-(G*G+H*H)*(FSQ*FSQ-H*H*RSMALL**2)))
     1/(G*G+H*H)
  102 YOW(I)=-SQRT(RSMALL*RSMALL-XOW(I)*XOW(I))
C DETERMINE THE CENTRE AND RADIUS OF O.C.
      DO 103 I=1,INOZ
      FUNCT=((XIW(I)+A)*(XIW(I)-XOW(I))+(YIW(I)-B)*(YIW(I)-YOW(I)))/(XOW
     1(I)*(YIW(I)-B)-YOW(I)*(XIW(I)+A))
      XOC(I)=XOW(I)-FUNCT*YOW(I)
      YOC(I)=YOW(I)+FUNCT*XOW(I)
  103 ROC(I)=SQRT((XIW(I)-XOC(I))**2+(YIW(I)-YOC(I))**2)
C DETERMINE THE CENTRE AND RADIUS OF INT. C.
      DXIC=A/FLOAT(JMIX)
      DYIC=B/FLOAT(JMIX)
      XIC(JNP1)=-A+0.5*DXIC
      YIC(JNP1)=B-0.5*DYIC
      DO 104 J=JNP2,NJM1
      XIC(J)=XIC(J-1)+DXIC
  104 YIC(J)=YIC(J-1)-DYIC
      DRIC=(RLARGE-RSMALL-B)/FLOAT(JMIX)
```



```
      DO 105 J=JNP1,NJM1
  105 RIC(J)=YIC(J)+RSMALL+(FLOAT(NJM1-J)+0.5)*DRIC
C DETERMINE THE GRIDS
      DO 106 I=1,INOZ
      DO 106 J=JNP1,NJM1
      Q=0.5*(RIC(J)**2-ROC(I)**2+XOC(I)**2+YOC(I)**2-(XIC(J)**2+YIC(J)**
     12))/(YOC(I)-YIC(J))
      S=(XIC(J)-XOC(I))/(YIC(J)-YOC(I))
      AI=S*S+1.0
      BI=XOC(I)+S*Q-S*YOC(I)
      CI=XOC(I)**2+(Q-YOC(I))**2-ROC(I)**2
      X(I,J)=(BI-SQRT(BI*BI-AI*CI))/AI
  106 Y(I,J)=Q-S*X(I,J)
      DO 107 I=1,JMIX
      X(INOZ+I,JNOZ+I)=XIC(JNOZ+I)
  107 Y(INOZ+I,JNOZ+I)=YIC(JNOZ+I)-RIC(JNOZ+I)
      DO 108 I=1,JMIX
      YOC(INOZ+I)=Y(INOZ+I,JNOZ+I)
      XOC(INOZ+I)=0.5*(RSMALL*RSMALL+X(INOZ+I,JNOZ+I)**2-Y(INOZ+I,JNOZ+I
     1)**2)/X(INOZ+I,JNOZ+I)
      ROC(INOZ+I)=XOC(INOZ+I)-X(INOZ+I,JNOZ+I)
      AC=XOC(INOZ+I)**2+YOC(INOZ+I)**2
      BO=-RSMALL*RSMALL*XOC(INOZ+I)
      CC=RSMALL**4-RSMALL*RSMALL*YOC(INOZ+I)**2
```

```
      XOW(INOZ+I)=-(BO+SQRT(BO*BO-AO*CO))/AO
  108 YOW(INOZ+I)=(RSMALL*RSMALL-XOC(INOZ+I)*XOW(INOZ+I))/YOC(INOZ+I)
      JMIXM1=JMIX-1
      DO 111 I=1,JMIXM1
      IP1=I+1
      DO 112 J=IP1,JMIX
      Q=0.5*(RIC(JNOZ+J)**2-ROC(INOZ+I)**2+XOC(INOZ+I)**2+YOC(INOZ+I)**2
     1-(XIC(JNOZ+J)**2+YIC(JNOZ+J)**2))/(YOC(INOZ+I)-YIC(JNOZ+J))
      S=(XIC(JNOZ+J)-XOC(INOZ+I))/(YIC(JNOZ+J)-YOC(INOZ+I))
      AI=S*S+1.0
      BI=XOC(INOZ+I)+S*Q-S*YOC(INOZ+I)
      CI=XOC(INOZ+I)**2+(Q-YOC(INOZ+I))**2-ROC(INOZ+I)**2
      X(INOZ+I,JNOZ+J)=(BI-SQRT(BI*BI-AI*CI))/AI
      Y(INOZ+I,JNOZ+J)=Q-S*X(INOZ+I,JNOZ+J)
  112 CONTINUE
  111 CONTINUE
      DO 113 J=2,JNOZ
      DO 113 I=INP1,NI
  113 Y(I,J)=-(RSMALL+RMIX)+(FLOAT(J)-1.5)*DY
      DO 114 J=1,JMIX
      IFIRST=INP1+J
      DO 115 I=IFIRST,NI
      Y(I,JNOZ+J)=Y(INOZ+J,JNOZ+J)
  115 CONTINUE
  114 CONTINUE
      DO 116 I=1,JMIX
      JLAST=JNOZ+I-1
      DO 117 J=2,JLAST
      X(INOZ+I,J)=X(INOZ+I,JNOZ+I)
  117 CONTINUE
```



```
  116 CONTINUE
      EPSX=1.15
      SUMX=0.5*EPSX**(NI-IENT-4)+(EPSX**(NI-IENT-3)-1.0)/(EPSX-1.0)+0.5
      DX=ALTOT/SUMX
      IEP1=IENT+1
      IEP2=IENT+2
      DO 109 I=IEP1,NI
  109 YOW(I)=-RSMALL
      DO 118 J=2,NJM1
  118 X(IEP1,J)=0.5*DX
      DO 121 I=IEP2,NIM1
      DO 122 J=2,NJM1
  122 X(I,J)=X(I-1,J)+DX
  121 DX=EPSX*DX
      DO 123 J=2,NJM1
  123 X(NI,J)=X(NIM1,J)-X(NI-2,J)+X(NIM1,J)
      DO 124 I=1,NI
      IF(I.LE.INOZ) JFIR=JNP1
      IF(I.GT.INOZ) JFIR=2
      DO 124 J=JFIR,NJM1
  124 R(I,J)=RSMALL+RMIX+Y(I,J)
      DO 125 J=2,JNOZ
  125 R(INOZ,J)=R(INP1,J)
C-----DEPENDENT VARIABLE SELECTION
      INCALU=.TRUE.
      INCALV=.TRUE.
      INCALP=.TRUE.
      INCALK=.TRUE.
```

```
      INCALC=.TRUE.
      INPRC=.TRUE.
C-----FLUID PROPERTIES
      DENSIT=1000.
C-----TURBULENCE CONSTANTS
      CMU=0.09
      CD=1.00
      C1=1.44
      C2=1.92
      CAPPA=.4187
      ELOG=9.793
      PRED=CAPPA*CAPPA/(C2-C1)/(CMU**.5)
      PRTE=1.0
C-----BOUNDARY VALUES
      UIN=22.0
      LEN=1.4435
      TURBIN=0.001
      TURBEN=0.003
      TEIN=TURBIN*UIN**2
      TEEN=TURBEN*UEN**2
      ALAMDA=0.005
      EDIN=TEIN**1.5/(ALAMDA*RMIX)
      EDEN=TEEN**1.5/(ALAMDA*RMIX)
      VISCOS=1.004E-3
C-----PRESSURE CALCULATION
      IPREF=2
```



```
      JPREF=JNP1
C-----PROGRAM CONTROL AND MONITOR
      MAXIT=133
      IMON=10
      JMON=10
      URFU=0.5
      URFV=0.5
      URFP=1.0
      URFE=0.7
      URFK=0.7
      URFVIS=0.7
      INCPRI=1
      SORMAX=1.0E-4
C
C-----CALCULATE GEOMETRICAL QUANTITIES AND SET VARIABLES TO ZERO
      CALL INIT
C-----INITIALISE VARIABLE FIELDS
      DO 202 J=2,JNOZ
      TE(INOZ,J)=TEIN
  202 ED(INOZ,J)=EDIN
      DO 211 J=JNP1,NJM1
      TE(1,J)=TEEN
  211 ED(1,J)=EDEN
      DO 200 I=INP1,NI
      DO 200 J=2,JNOZ
      U(I,J)=UIN
      TE(I,J)=TEIN
  200 ED(I,J)=EDIN
      FLOWIN=0.0
      AREEN=0.0
      DO 205 J=2,JNOZ
      AREEN=0.5*(DEN(INOZ,J)+DEN(INP1,J))*R(INP1,J)*SNS(INP1,J)
  205 FLOWIN=FLOWIN+AREEN*U(INP1,J)
```

```
      DO 201 I=2,NI
      DO 201 J=JNP1,NJM1
      TE(I,J)=TEEN
      ED(I,J)=EDEN
  201 L(I,J)=LEN
      FLOWEN=0.0
      ARDEN=0.0
      DO 206 J=JNP1,NJM1
      ARDEN=0.5*(DEN(1,J)+DEN(2,J))*0.25*(R(1,J)+R(2,J))*(SNS(1,J)+
     1SNS(2,J))
  206 FLOWEN=FLOWEN+ARDEN*U(2,J)
      DO 203 I=2,NIM1
  203 YPLUSN(I)=11.0
      DO 204 I=2,INOZ
  204 YPLUSS(I)=11.0
      SORMAX=SORMAX*(FLOWIN+FLOWEN)
      LM=(FLOWIN+FLOWEN)/(DENSIT*0.5*RMIX**2)
      FLORAT=FLOWEN/FLOWIN
      CALL PROPS
```

LEASE 2.0 MAIN DATE = MON DEC 11, 1978

```
C-----INITIAL OUTPUT
      WRITE(6,210)
      WRITE(6,220) UIN
      WRITE(6,221) UEN
      RE=UIN*RNOZ*2.0*DENSIT/VISCOS
      WRITE(6,230) RE
      RSDRL=RNOZ/RMIX
      WRITE(6,240) RSDRL
      WRITE(6,250) VISCOS
      WRITE(6,260) DENSIT
      WRITE(6,270) FLORAT
      WRITE(6,280) (XOW(I),I=1,NI)
      WRITE(6,280) (YOW(I),I=1,NI)
      WRITE(6,280) (XIW(I),I=1,INOZ)
      WRITE(6,280) (YIW(I),I=1,INOZ)
  280 FORMAT(1P10E11.3)
      CALL PRINT(2,2,NI,NJ,IT,JT,X,HEDX)
      CALL PRINT(2,2,NI,NJ,IT,JT,R,HEDY)
      CALL PRINT(2,2,NI,NJ,IT,JT,SEW ,HEDX)
      CALL PRINT(2,2,NI,NJ,IT,JT,SEWU,HEDX)
      CALL PRINT(2,2,NI,NJ,IT,JT,DYNP,HEDY)
      CALL PRINT(2,2,NI,NJ,IT,JT,DYPS,HEDY)
      IF(INCALU) CALL PRINT(2,2,NI,NJ,IT,JT,      U,HEDU)
      IF(INCALV) CALL PRINT(2,2,NI,NJ,IT,JT,      V,HEDV)
      IF(INCALP) CALL PRINT(2,2,NI,NJ,IT,JT,     P,HEDP)
      IF(INCALP) CALL PRINT(2,2,NI,NJ,IT,JT,     PP,HEDPP)
      IF(INCALK) CALL PRINT(2,2,NI,NJ,IT,JT,     TE,HEDK)
      IF(INCALD) CALL PRINT(2,2,NI,NJ,IT,JT,     ED,HEDD)
C
      WRITE(6,310) IMON,JMON
  300 NITER=NITER+1
C-----UPDATE MAIN DEPENDENT VARIABLES
      IF(INCALU) CALL CALCU
      IF(INCALV) CALL CALCV
      IF(INCALP) CALL CALCP
      IF(INCALK) CALL CALCTE
      IF(INCALD) CALL CALCED
```

```
C-----UPDATE FLUID PROPERITIES
      IF(INPRC) CALL PRCPS
C-----INTERMEDIATE OUTPUT
      DUMMY=0.0
      WRITE(6,311) NITER,RESORU,RESORV,RESORM,RESORT,RESORK,RESORE
     1             ,U(IMON,JMON),V(IMON,JMON),P(IMON,JMON),DUMMY,
     1                  TE(IMON,NJM1),ED(IMON,NJM1)
      IF(NITER.GT.2)INDPRI=40
      IF(ABS(FLOAT(NITER/INDPRI)-FLOAT(NITER)/INDPRI).GT.1.E-4)GO TO 301
      WRITE(6,312)
      IF(INCALU) CALL PRINT(2,2,NI,NJ,IT,JT,      U,HEDU)
      IF(INCALV) CALL PRINT(2,2,NI,NJ,IT,JT,      V,HEDV)
      IF(INCALP) CALL PRINT(2,2,NI,NJ,IT,JT,    P,HEDP)
```



```
      IF(INCALP) CALL PRINT(2,2,NI,NJ,IT,JT,    PP,HEDPP)
      IF(INCALK) CALL PRINT(2,2,NI,NJ,IT,JT,    TE,HEDK)
      IF(INCALD) CALL PRINT(2,2,NI,NJ,IT,JT,    ED,HEDD)
      WRITE(6,312)
      WRITE(6,310) IMON,JMON
  301 CONTINUE
C-----TERMINATION TESTS
      SORCE=RESORM
      IF(NITER.EQ.MAXIT) GO TO 302
      IF(SORCE.GT.SORMAX) GO TO 300
  302 CONTINUE
C
      IF(INCALU) CALL PRINT(2,2,NI,NJ,IT,JT,      U,HEDU)
      IF(INCALV) CALL PRINT(2,2,NI,NJ,IT,JT,      V,HEDV)
      IF(INCALP) CALL PRINT(2,2,NI,NJ,IT,JT,    P,HEDP)
      IF(INCALP) CALL PRINT(2,2,NI,NJ,IT,JT,    PP,HEDPP)
      IF(INCALK) CALL PRINT(2,2,NI,NJ,IT,JT,    TE,HEDK)
      IF(INCALD) CALL PRINT(2,2,NI,NJ,IT,JT,    ED,HEDD)
      IF(INPRO ) CALL PRINT(2,2,NI,NJ,IT,JT,    VIS,HEDM)
C-----CALCULATION OF NON DIMENSIONAL TURBULENCE ENERGY AND LENGTH SCALE
      DO 400 I=2,NIM1
      DO 400 J=2,NJM1
      U(I,J)=U(I,J)/UIN
      SU(I,J)=TE(I,J)*DEN(I,J)/ABS(TAUN(I))
  400 SP(I,J)=TE(I,J)**1.5/ED(I,J)/RMIX
      CALL PRINT(2,2,NI,NJ,IT,JT,      U,HEDUN)
      CALL PRINT(2,2,NI,NJ,IT,JT,    SU,HEDA)
      CALL PRINT(2,2,NI,NJ,IT,JT,    SP,HEDB)
  401 CONTINUE
      RINOZ=0.004405
      FLOWIN=0.5*RINOZ*RINOZ*DENSIT
      FLOWEN=0.0
      ARDEN=0.0
      DO 406 J=JNP1,NJM1
      ARDEN=0.5*(DEN(INOZ,J)+DEN(INP1,J))*R(INP1,J)*SNS(INP1,J)
  406 FLOWEN=FLOWEN+ARDEN*U(INP1,J)
      FLORAT=FLOWEN/FLOWIN
      WRITE(6,270)FLORAT
      STOP
C-----FORMAT STATEMENTS
  210 FORMAT(1H1,47X,33HKASE T5 - TURBULENT JETS MIXING  ////)
  220 FORMAT(////15X,33HINLET FLUID VELOCITY              ,1PE11.3)
  221 FORMAT(  //15X,33HENTRAINED VELOCITY                ,1PE11.3)
  230 FORMAT(  //15X,33HREYNOLDS NUMBER                   ,1PE11.3)
  240 FORMAT(  //15X,33HDIAMETER RATIO                    ,1PE11.3)
  250 FORMAT(  //15X,33HLAMINAR VISCOSITY                 ,1PE11.3)
```

```
  260 FORMAT(  //15X,33HFLUID DENSITY                                ,1PE11.3)
  270 FORMAT(  //15X,33HFLOW RATIO                                   ,1PE11.3)
  310 FORMAT(13HOITER     I---,  9X,29HABSOLUTE RESIDUAL SOURCE SUMS,9X,
     111H---I    I---,37H FIELD VALUES AT MONITORING LOCATION(,I2,1H,,I2,
     26H) ---I/14H  NO       UMOM,5X,4HVMOM,5X,4HMASS,5X,4HENER,5X,4HTKIN
     3,5X,4HDISP,9X,1HU,8X,1HV,8X,1HP,8X,1HT,8X,1HK,8X,1HD/)

LEASE 2.0                MAIN                    DATE = MON DEC 11, 1978

  311 FORMAT(1H ,I3,5X,1P6E9.2,3X,1P6E9.2)
  312 FORMAT(1H0,59(2H- ))
      END
LEASE 2.0                INIT                    DATE = MON DEC 11, 1978

      SUBROUTINE INIT
C
CHAPTER  C  C  C  C  0  0  0  0  PRELIMINARIES  0  0  0  0  0  0  0  0
C
      COMMON
     1/UVEL/RESORU,NSWPU,URFU,DXEPU(26,12),DXPWU(26,12),SEWU(26,12),
     2       SNSU(26,12)
     1/VVEL/RESORV,NSWPV,URFV,DYNPV(26,12),DYPSV(26,12),SNSV(26,12),
     2       SEWV(26,12),RCV(26,12)
     1/PCOR/RESORM,NSWPP,URFP,DU(26,12),DV(26,12),IPREF,JPREF
     1/VAR/ U(26,12),V(26,12),P(26,12),PP(26,12),TE(26,12),ED(26,12)
     1/ALL/IT,JT,NI,NJ,NIM1,NJM1,GREAT
     1/GEOM/INDCOS,XIW(18),YIW(18),XOW(18),YOW(26) ,XOC(18),YOC(18),
     2      ROC(18),XIC(18),YIC(18),RIC(18),X(26,12),Y(26,12),XU(26,12),
     3      YV(26,12),DXEP(26,12),DXPW(26,12),DYNP(26,12),DYPS(26,12),
     4      SNS(26,12),SEW(26,12),R(26,12),RV(26,12)
     1/FLUPR/URFVIS,VISCOS,DENSIT,PRANDT,DEN(26,12),VIS(26,12)
     1/KASE T5/UIN,TEIN,EDIN,FLOWIN,ALAMDA,UEN,FLOWEN, A,RSMALL,RMIX,
     2        INOZ,INP1,JNOZ,JNP1,IENT,IEP1
     1/TURB/GEN(26,12),CD,CMU,C1,C2,CAPPA,ELOG,PRED,PRTE
     1/COEF/AP(26,12),AN(26,12),AS(26,12),AE(26,12),AW(26,12),SU(26,12),
     2       SP(26,12)
C
CHAPTER  1  1  1  1  1  CALCULATE GEOMETRICAL QUANTITIES  1  1  1  1  1
C
      DO 101 J=JNP1,NJM1
      ILAST=INOZ+J-JNP1-1
      DO 101 I=1,ILAST
      GPX=(Y(I,J)-YIC(J))/(X(I,J)-XIC(J))
      GEX=(Y(I+1,J)-YIC(J))/(X(I+1,J)-XIC(J))
      ANGEP=ATAN((GEX-GPX)/(1.0+GEX*GPX))
      DXEP(I,J)=ANGEP*RIC(J)
  101 DXPW(I+1,J)=DXEP(I,J)
      DO 102 J=JNP1,NJM1
      I=INOZ+J-JNP1
      ANG=ATAN((X(I,J)-XIC(J))/(Y(I,J)-YIC(J)))
      DXEP(I,J)=ANG*RIC(J)
  102 DXPW(I+1,J)=DXEP(I,J)
      DO 103 J=2,JNOZ
      DXEP(INOZ,J)=2.0*(X(INP1,JNP1)+A)
  103 DXPW(INP1,J)=DXEP(INOZ,J)
      IEM1=IENT-1
      DO  104 I=INP1,NIM1
      IF(I.LT.IENT) JLAST=JNOZ+I-INOZ
      IF(I.GE.IENT) JLAST=NJM1
      DO 104 J=2,JLAST
      DXEP(I,J)=X(I+1,J)-X(I,J)
  104 DXPW(I+1,J)=DXEP(I,J)
```

```
      NJM2=NJ-2
      DO 106 J=JNP1,NJM2
      ILAST=J+INOZ-JNOZ
      DO 106 I=1,ILAST
      GPY=(Y(I,J)-YOC(I))/(X(I,J)-XOC(I))
      GNY=(Y(I,J+1)-YOC(I))/(X(I,J+1)-XOC(I))
      ANGNP=ATAN((GPY-GNY)/(1.0+GPY*GNY))
      DYNP(I,J)=ANGNP*ROC(I)
  106 DYPS(I,J+1)=DYNP(I,J)
      DO 109 I=1,IENT
      GNWY=(YOW(I)-YOC(I))/(XOW(I)-XOC(I))
      GPNWY=(Y(I,NJM1)-YOC(I))/(X(I,NJM1)-XOC(I))
      ANGNW=ATAN((GPNWY-GNWY)/(1.0+GPNWY*GNWY))
  109 DYNP(I,NJM1)=2.0*ANGNW*ROC(I)
      DO 110 I=1,INOZ
      GSWY=(YIW(I)-YOC(I))/(XIW(I)-XOC(I))
      GPSWY=(Y(I,JNP1)-YOC(I))/(X(I,JNP1)-XOC(I))
      ANGSW=ATAN((GSWY-GPSWY)/(1.0+GPSWY*GSWY))
  110 DYPS(I,JNP1)=2.0*ANGSW*ROC(I)
      DO 111 J=2,JNOZ
      DO 111 I=INP1,NI
      DYNP(I,J)=Y(I,J+1)-Y(I,J)
  111 DYPS(I,J+1)=DYNP(I,J)
      DO 112 J=JNP1,NJM2
      IFIR=J-JNOZ+INP1
      DO 112 I=IFIR,NI
      DYNP(I,J)=Y(I,J+1)-Y(I,J)
  112 DYPS(I,J+1)=DYNP(I,J)
      DO 114 I=IEP1,NI
  114 DYNP(I,NJM1)=DYNP(I,NJM2)
      DO 115 I=INP1,NI
  115 DYPS(I,2)=DYPS(I,3)
      DO 116 I=2,NIM1
      IF(I.LE.INOZ) JFIR=JNP1
      IF(I.GT.INOZ) JFIR=2
      DO 116 J=JFIR,NJM1
      SEW(I,J)=0.5*(DXEP(I,J)+DXPW(I,J))
      DXEPU(I,J)=SEW(I,J)
  116 DXPWU(I+1,J)=DXEPU(I,J)
      DO 117 I=1,NI
      IF(I.LE.INOZ) JFIR=JNP1
      IF(I.GT.INOZ) JFIR=2
      DO 117 J=JFIR,NJM1
      SNS(I,J)=0.5*(DYNP(I,J)+DYPS(I,J))
      DYNPV(I,J)=SNS(I,J)
  117 DYPSV(I,J+1)=DYNPV(I,J)
      DO 113 J=2,JNOZ
  113 SNS(INOZ,J)=SNS(INP1,J)
      DO 118 J=2,NJM1
  118 SEW(NI,J)=SEW(NIM1,J)
      DO 119 I=2,NI
      IF(I.LE.INOZ) JFIR=JNP1
      IF(I.GT.INOZ) JFIR=2
      DO 119 J=JFIR,NJM1
      SEWU(I,J)=0.5*(SEW(I,J)+SEW(I-1,J))
  119 SNSU(I,J)=0.5*(SNS(I,J)+SNS(I-1,J))
      DO 120 I=1,NI
      IF(I.LT.INOZ) JFIR=JNP1+1
      IF(I.GE.INOZ) JFIR=3
```

```
      DC 120 J=JFIR,NJM1
LEASE 2.C                    INIT                    DATE = MON DEC 11, 1978
      SEWV(I,J)=0.5*(SEW(I,J)+SEW(I,J-1))
  120 SNSV(I,J)=0.5*(SNS(I,J)+SNS(I,J-1))
      DC 121 I=1,NI
      IF(I.LT.INCZ) JFIR=JNP1
      IF(I.GE.INCZ) JFIR=2
      DC 121 J=JFIR,NJ
      RV(I,J)=C.5*(R(I,J)+R(I,J-1))
  121 RCV(I,J)=0.5*(RV(I,J)+RV(I,J-1))
C
CHAPTER  2  2  2  2  2  2  SET VARIABLES TO ZERC  2  2  2  2  2  2
C
      CO 200 I=1,NI
      IF(I.LE.INCZ) JFIR=JNOZ
      IF(I.GT.INCZ) JFIR=1
      DC 200 J=JFIR,NJ
      U(I,J)=0.0
      V(I,J)=0.0
      P(I,J)=0.0
      PP(I,J)=0.0
      TE(I,J)=0.0
      ED(I,J)=C.0
      DEN(I,J)=DENSIT
      VIS(I,J)=VISCCS
      DU(I,J)=0.0
      DV(I,J)=C.C
      SU(I,J)=0.0
      SP(I,J)=C.0
200   CCNTINUE
      RETURN
      END
LEASE 2.0                    PROPS                   DATE = MON DEC 11, 1978
      SUBRCUTINE PROPS
C
CHAPTER  0  0  0  0  0  0  0  0  PRELIMINARIES  0  0  C  C  0  0  0  0
C
      CCMMON
     1/FLUPR/URFVIS,VISCOS,DENSIT,PRANDT,DEN(26,12),VIS(26,12)
     1/VAR/ U(26,12),V(26,12),P(26,12),PP(26,12),TE(26,12),ED(26,12)
     1/ALL/IT,JT,NI,NJ,NIM1,NJM1,GREAT
     1/TURB/GEN(26,12),CC,CMU,C1,C2,CAPPA,ELOG,PRED,PRTE
C
CHAPTER   1   1   1   VISCOSITY   1   1   1
C
      CO 100 I=2,NIM1
      DC 100 J=2,NJM1
      VISOLD=VIS(I,J)
      IF(EC(I,J).EC.C.) GC TO 102
      VIS(I,J)=DEN(I,J)*TE(I,J)**2*CMU/ED(I,J)+VISCOS
      GC  TC  101
  102 VIS(I,J)=VISCCS
C-----UNDER-RELAX VISCOSITY
101   VIS(I,J)=URFVIS*VIS(I,J)+(1.-URFVIS)*VISCLD
  1CC CCNTINUE
C
CHAPTER  2  2  2  2  2  2  2  PROBLEM MODIFICATIONS  2  2  2  2  2  2
C
      CALL PROMOD(1)
```

```
C
      RETURN
      END
LEASE 2.0                CALCU                DATE = MON DEC 11, 1978

      SUBROUTINE CALCU
C
CHAPTER  0  0  0  0  0  0  0  0  PRELIMINARIES  0  0  0  0  0  0  0  0
C
      COMMON
     1/UVEL/RESORU,NSWPU,URFU,DXEPU(26,12),DXPWU(26,12),SEWU(26,12),
     2       SNSU(26,12)
     1/PCOR/RESORM,NSWPP,URFP,DU(26,12),DV(26,12),IPREF,JPREF
     1/VAR/ U(26,12),V(26,12),P(26,12),PP(26,12),TE(26,12),ED(26,12)
     1/ALL/IT,JT,NI,NJ,NIM1,NJM1,GREAT
     1/GEOM/INDCOS,XIW(18),YIW(18),XCW(18),YCW(26) ,XCC(18),YCC(18),
     2      ROC(18),XIC(18),YIC(18),RIC(18),X(26,12),Y(26,12),XU(26,12),
     3      YV(26,12),DXEP(26,12),DXPW(26,12),DYNP(26,12),DYPS(26,12),
     4      SNS(26,12),SEW(26,12),R(26,12),RV(26,12)
     1/FLUPR/URFVIS,VISCOS,DENSIT,PRANDT,DEN(26,12),VIS(26,12)
     1/COEF/AP(26,12),AN(26,12),AS(26,12),AE(26,12),AW(26,12),SU(26,12),
     2       SP(26,12)
     1/KASE T5/UIN,TEIN,EDIN,FLOWIN,ALAMDA,UEN,FLOWEN, A,RSMALL,RMIX,
     2        INOZ,INP1,JNOZ,JNP1,IENT,IEP1
C
CHAPTER  1  1  1  1  1  1  ASSEMBLY OF COEFFICIENTS  1  1  1  1  1  1  1
C
      DO 100 I=3,NIM1
      IF(I.LE.INP1) JFIR=JNP1
      IF(I.GT.INP1) JFIR=2
      DO 101 J=JFIR,NJM1
C-----COMPUTE AREAS AND VOLUME
      AREAN=0.5*(RV(I,J+1)+RV(I-1,J+1))*0.5*(SEWU(I,J)+SEWU(I,J+1))
      AREAS=0.5*(RV(I,J)+RV(I-1,J))*0.5*(SEWU(I,J)+SEWU(I,J-1))
      AREAE=0.125*(R(I-1,J)+2.0*R(I,J)+R(I+1,J))*(SNSU(I,J)+SNSU(I+1,J))
      AREAW=0.125*(R(I-2,J)+2.0*R(I-1,J)+R(I,J))*(SNSU(I,J)+SNSU(I-1,J))
      VOL=0.25*(R(I,J)+R(I-1,J))*SEWU(I,J)*(SNS(I-1,J)+SNS(I,J))
C-----CALCULATE CONVECTION COEFFICIENTS
      GN=0.5*(DEN(I,J+1)+DEN(I,J))*V(I,J+1)
      GNW=0.5*(DEN(I-1,J)+DEN(I-1,J+1))*V(I-1,J+1)
      GS=0.5*(DEN(I,J-1)+DEN(I,J))*V(I,J)
      GSW=0.5*(DEN(I-1,J)+DEN(I-1,J-1))*V(I-1,J)
      GE=0.5*(DEN(I+1,J)+DEN(I,J))*U(I+1,J)
      GP=0.5*(DEN(I,J)+DEN(I-1,J))*U(I,J)
      GW=0.5*(DEN(I-1,J)+DEN(I-2,J))*U(I-1,J)
      CN=0.5*(GN+GNW)*AREAN
      CS=0.5*(GS+GSW)*AREAS
      CE=0.5*(GE+GP)*AREAE
      CW=0.5*(GP+GW)*AREAW
C-----CALCULATE DIFFUSION COEFFICIENTS
      VISN=0.25*(VIS(I,J)+VIS(I,J+1)+VIS(I-1,J)+VIS(I-1,J+1))
      VISS=0.25*(VIS(I,J)+VIS(I,J-1)+VIS(I-1,J)+VIS(I-1,J-1))
      VISE=0.25*(VIS(I-1,J)+2.0*VIS(I,J)+VIS(I+1,J))
      VISW=0.25*(VIS(I-2,J)+2.0*VIS(I-1,J)+VIS(I,J))
      DN=VISN*AREAN/(0.5*(DYNP(I,J)+DYNP(I-1,J)))
      DS=VISS*AREAS/(0.5*(DYPS(I,J)+DYPS(I-1,J)))
      DE=VISE*AREAE/DXEPU(I,J)
      DW=VISW*AREAW/DXPWU(I,J)
C-----CALCULATE COEFFICIENTS OF SOURCE TERMS
```

```
      SMP=CN-CS+CE-CW
      CP=AMAX1(0.0,SMP)
      CFC=CP
C-----ASSEMBLE MAIN COEFFICIENTS
      AN(I,J)=DN-0.5*CN
      IF(ABS(0.5*CN).GT.DN) AN(I,J)=AN(I,J)+ABS(0.5*CN)
      AS(I,J)=DS+0.5*CS
      IF(ABS(0.5*CS).GT.DS) AS(I,J)=AS(I,J)+ABS(0.5*CS)
      AE(I,J)=DE-0.5*CE
      IF(ABS(0.5*CE).GT.DE) AE(I,J)=AE(I,J)+ABS(0.5*CE)
      AW(I,J)=DW+0.5*CW
      IF(ABS(0.5*CW).GT.DW) AW(I,J)=AW(I,J)+ABS(0.5*CW)
      DU(I,J)=0.5*(AREAE+AREAW)
      SU(I,J)=CPO*U(I,J)+DU(I,J)*(P(I-1,J)-P(I,J))
      SP(I,J)=-CP
  101 CONTINUE
  100 CONTINUE
C
CHAPTER  2  2  2  2  2  2  2  PROBLEM MODIFICATIONS  2  2  2  2  2  2  2
C
      CALL PROMOD(2)
C
CHAPTER  3  FINAL COEFF. ASSEMBLY AND RESIDUAL SOURCE CALCULATION  3  3
C
      RESORU=0.0
      DO 300 I=3,NIM1
      IF(I.LE.INP1) JFIR=JNP1
      IF(I.GT.INP1) JFIR=2
      DO 301 J=JFIR,NJM1
      AP(I,J)=AN(I,J)+AS(I,J)+AE(I,J)+AW(I,J)-SP(I,J)
      DU(I,J)=DU(I,J)/AP(I,J)
      RESOR=AN(I,J)*U(I,J+1)+AS(I,J)*U(I,J-1)+AE(I,J)*U(I+1,J)
     1      +AW(I,J)*U(I-1,J)-AP(I,J)*U(I,J)+SU(I,J)
      VOL=R(I,J)*SEW(I,J)*SNS(I,J)
      SORVOL=GREAT*VOL
      IF(-SP(I,J).GT.0.5*SORVOL)  RESOR=RESOR/SORVOL
      RESORU=RESORU+ABS(RESOR)
C-----UNDER-RELAXATION
      AP(I,J)=AP(I,J)/URFU
      SU(I,J)=SU(I,J)+(1.-URFU)*AP(I,J)*U(I,J)
      DU(I,J)=DU(I,J)*URFU
  301 CONTINUE
  300 CONTINUE
C
CHAPTER  4  4  4  SOLUTION OF DIFFERENCE EQUATION  4  4  4  4  4  4  4
C
      DO 400 N=1,NSWPU
  400 CALL LISOLV(3,2,NI,NJ,IT,JT,U)
      RETURN
      END
```

LEASE 2.0 CALCV DATE = MON DEC 11, 1978

```
      SUBROUTINE CALCV
C
CHAPTER  0  0  0  0  0  0  0  0  PRELIMINARIES  0  0  0  0  0  0  0  0
C
      COMMON
     1/VVEL/RESORV,NSWPV,URFV,DYNPV(26,12),DYPSV(26,12),SNSV(26,12),
     2       SEWV(26,12),RCV(26,12)
     1/PCOR/RESORM,NSWPP,URFP,DU(26,12),DV(26,12),IPREF,JPREF
```

```
      1/VAR/ U(26,12),V(26,12),P(26,12),PP(26,12),TE(26,12),ED(26,12)
      1/ALL/IT,JT,NI,NJ,NIM1,NJM1,GREAT
      1/GEOM/INDCCS,XIW(18),YIW(18),XOW(18),YOW(26) ,XOC(18),YOC(18),
      2      ROC(18),XIC(18),YIC(18),RIC(18),X(26,12),Y(26,12),XU(26,12),
      3      YV(26,12),DXEP(26,12),DXPW(26,12),DYNP(26,12),DYPS(26,12),
      4      SNS(26,12),SEW(26,12),R(26,12),RV(26,12)
      1/FLUPR/URFVIS,VISCOS,DENSIT,PRANDT,DEN(26,12),VIS(26,12)
      1/COEF/AP(26,12),AN(26,12),AS(26,12),AE(26,12),AW(26,12),SU(26,12),
      2       SP(26,12)
      1/KASE T5/UIN,TEIN,EDIN,FLOWIN,ALAMDA,UEN,FLOWEN, A,RSMALL,RMIX,
      2        INOZ,INP1,JNOZ,JNP1,IENT,IEP1
C
CHAPTER  1  1  1  1  1  1  ASSEMBLY OF COEFFICIENTS  1  1  1  1  1  1  1
CHAPTER  1  1  1  1  1  1  ASSEMBLY OF COEFFICIENTS  1  1  1  1  1  1  1
C
      DO 100 I=2,NIM1
      IF(I.LE.INOZ) JFIR=JNP1+1
      IF(I.GT.INOZ) JFIR=3
      DO 101 J=JFIR,NJM1
C-----COMPUTE AREAS AND VOLUME
      AREAN=RCV(I,J+1)*0.5*(SEWV(I,J)+SEWV(I,J+1))
      AREAS=RCV(I,J)*0.5*(SEWV(I,J)+SEWV(I,J-1))
      AREAE=0.25*(RV(I,J)+RV(I+1,J))*(SNSV(I,J)+SNSV(I+1,J))
      AREAW=0.25*(RV(I,J)+RV(I-1,J))*(SNSV(I,J)+SNSV(I-1,J))
      VOL=RV(I,J)*SEWV(I,J)*SNSV(I,J)
C-----CALCULATE CONVECTION COEFFICIENTS
      GN=0.5*(DEN(I,J+1)+DEN(I,J))*V(I,J+1)
      GP=0.5*(DEN(I,J)+DEN(I,J-1))*V(I,J)
      GS=0.5*(DEN(I,J-1)+DEN(I,J-2))*V(I,J-1)
      GE=0.5*(DEN(I+1,J)+DEN(I,J))*U(I+1,J)
      GSE=0.5*(DEN(I,J-1)+DEN(I+1,J-1))*U(I+1,J-1)
      GW=0.5*(DEN(I,J)+DEN(I-1,J))*U(I,J)
      GSW=0.5*(DEN(I,J-1)+DEN(I-1,J-1))*U(I,J-1)
      CN=0.5*(GN+GP)*AREAN
      CS=0.5*(GP+GS)*AREAS
      CE=0.5*(GE+GSE)*AREAE
      CW=0.5*(GW+GSW)*AREAW
C-----CALCULATE DIFFUSION COEFFICIENTS
      VISE=0.25*(VIS(I,J)+VIS(I+1,J)+VIS(I,J-1)+VIS(I+1,J-1))
      VISW=0.25*(VIS(I,J)+VIS(I-1,J)+VIS(I,J-1)+VIS(I-1,J-1))
      VISN=0.25*(VIS(I,J+1)+2.0*VIS(I,J)+VIS(I,J-1))
      VISS=0.25*(VIS(I,J)+2.0*VIS(I,J-1)+VIS(I,J-2))
      DN=VISN*AREAN/DYNPV(I,J)
      DS=VISS*AREAS/DYPSV(I,J)
      DE=VISE*AREAE/(0.5*(DXEP(I,J)+DXEP(I,J-1)))
      DW=VISW*AREAW/(0.5*(DXPW(I,J)+DXPW(I,J-1)))
```



```
C-----CALCULATE COEFFICIENTS OF SOURCE TERMS
      SMP=CN-CS+CE-CW
      CP=AMAX1(0.0,SMP)
      CPO=CP
C-----ASSEMBLE MAIN COEFFICIENTS
      AN(I,J)=DN-0.5*CN
      IF(ABS(0.5*CN).GT.DN) AN(I,J)=AN(I,J)+ABS(0.5*CN)
      AS(I,J)=DS+0.5*CS
      IF(ABS(0.5*CS).GT.DS) AS(I,J)=AS(I,J)+ABS(0.5*CS)
      AE(I,J)=DE-0.5*CE
      IF(ABS(0.5*CE).GT.DE) AE(I,J)=AE(I,J)+ABS(0.5*CE)
      AW(I,J)=DW+0.5*CW
      IF(ABS(0.5*CW).GT.DW) AW(I,J)=AW(I,J)+ABS(0.5*CW)
      DV(I,J)=0.5*(AREAN+AREAS)
```

```
      SU(I,J)=CPC*V(I,J)+CV(I,J)*(P(I,J-1)-P(I,J))
      IF(I.LE.INOZ) JED=JNP1+1
      IF(I.GT.INOZ) JED=JNP1+I-INOZ
      IF(I.LT.IENT.AND.J.GE.JED) SU(I,J)=SU(I,J)-(DEN(I,J)+DEN(I-1,J))
     1*(0.25*(U(I,J)+U(I+1,J)+U(I,J-1)+U(I+1,J-1)))**2*VOL/(RIC(J)
     1+RIC(J-1))
      SP(I,J)=-CP
      IF(INDCOS.EQ.2) SP(I,J)=SP(I,J)-VIS(I,J)*VOL/RV(I,J)**2
  101 CONTINUE
  100 CONTINUE
C
CHAPTER  2  2  2  2  2  2  2  PROBLEM MODIFICATIONS  2  2  2  2  2  2  2
C
      CALL PROMOD(3)
C
CHAPTER  3  FINAL COEFF. ASSEMBLY AND RESIDUAL SOURCE CALCULATION  3  3
C
      RESORV=0.0
      DO 300 I=2,NIM1
      IF(I.LE.INOZ) JFIR=JNP1+1
      IF(I.GT.INOZ) JFIR=3
      DO 301 J=JFIR,NJM1
      AP(I,J)=AN(I,J)+AS(I,J)+AE(I,J)+AW(I,J)-SP(I,J)
      DV(I,J)=DV(I,J)/AP(I,J)
      RESOR=AN(I,J)*V(I,J+1)+AS(I,J)*V(I,J-1)+AE(I,J)*V(I+1,J)
     1      +AW(I,J)*V(I-1,J)-AP(I,J)*V(I,J)+SU(I,J)
      VOL=R(I,J)*SEW(I,J)*SNS(I,J)
      SCRVOL=GREAT*VOL
      IF(-SP(I,J).GT.0.5*SCRVOL)  RESOR=RESCR/SCRVOL
      RESORV=RESORV+ABS(RESOR)
C-----UNDER-RELAXATION
      AP(I,J)=AP(I,J)/URFV
      SU(I,J)=SU(I,J)+(1.-URFV)*AP(I,J)*V(I,J)
      DV(I,J)=DV(I,J)*URFV
  301 CONTINUE
  300 CONTINUE
C
CHAPTER  4  4  4  SOLUTION OF DIFFERENCE EQUATION  4  4  4  4  4  4  4
C
      DO 400 N=1,NSWPV

LEASE 2.0                CALCV                DATE = MON DEC 11, 1978

  400 CALL LISOLV(2,3,NI,NJ,IT,JT,V)
      RETURN
      END
      SUBROUTINE CALCP
C
CHAPTER  0  0  0  0  0  0  0  0  PRELIMINARIES  0  0  0  0  0  0  0  0
C
      COMMON
     1/FCOR/RESCRM,NSWPP,URFP,DU(26,12),DV(26,12),IPREF,JPREF
     1/VAR/ U(26,12),V(26,12),P(26,12),PP(26,12),TE(26,12),ED(26,12)
     1/ALL/IT,JT,NI,NJ,NIM1,NJM1,GREAT
     1/GEOM/INDCOS,XIW(18),YIW(18),XOW(18),YOW(26) ,XOC(18),YOC(18),
     2      ROC(18),XIC(18),YIC(18),RIC(18),X(26,12),Y(26,12),XU(26,12),
     3      YV(26,12),DXEP(26,12),DXPW(26,12),DYNP(26,12),DYPS(26,12),
     4      SNS(26,12),SEW(26,12),R(26,12),RV(26,12)
     1/FLUPR/URFVIS,VISCOS,DENSIT,PRANDT,DEN(26,12),VIS(26,12)
     1/COEF/AP(26,12),AN(26,12),AS(26,12),AE(26,12),AW(26,12),SU(26,12),
     2       SP(26,12)
     1/KASE T5/UIN,TEIN,EDIN,FLOWIN,ALAMDA,UEN,FLOWEN, A,RSMALL,RMIX,
```

```
    2 ·       INCZ,INP1,JNOZ,JNP1,IENT,IEP1
      RESCRM=0.0
C
CHAPTER  1  1  1  1  1  1  ASSEMBLY OF COEFFICIENTS  1  1  1  1  1  1  1
C
      DO 100 I=2,NIM1
      IF(I.LE.INCZ) JFIR=JNP1
      IF(I.GT.INOZ) JFIR=2
      DO 101 J=JFIR,NJM1
      PP(I,J)=0.0
C-----COMPUTE AREAS AND VOLUME
      AREAN=RV(I,J+1)*0.5*(SEW(I,J)+SEW(I,J+1))
      AREAS=RV(I,J)*0.5*(SEW(I,J)+SEW(I,J-1))
      AREAE=0.25*(R(I,J)+R(I+1,J))*(SNS(I,J)+SNS(I+1,J))
      AREAW=0.25*(R(I,J)+R(I-1,J))*(SNS(I,J)+SNS(I-1,J))
      VOL=R(I,J)*SEW(I,J)*SNS(I,J)
C-----CALCULATE COEFFICIENTS
      DENN=0.5*(DEN(I,J)+DEN(I,J+1))
      DENS=0.5*(DEN(I,J)+DEN(I,J-1))
      DENE=0.5*(DEN(I,J)+DEN(I+1,J))
      DENW=0.5*(DEN(I,J)+DEN(I-1,J))
      AN(I,J)=DENN*AREAN*DV(I,J+1)
      AS(I,J)=DENS*AREAS*DV(I,J)
      AE(I,J)=DENE*AREAE*DU(I+1,J)
      AW(I,J)=DENW*AREAW*DU(I,J)
C-----CALCULATE SOURCE TERMS
      CN=DENN*V(I,J+1)*AREAN
      CS=DENS*V(I,J)*AREAS
      CE=DENE*U(I+1,J)*AREAE
      CW=DENW*U(I,J)*AREAW
      SMP=CN-CS+CE-CW
      SP(I,J)=0.0
      SU(I,J)=-SMP
C-----COMPUTE SUM OF ABSOLUTE MASS SOURCES
      RESCRM=RESCRM+ABS(SMP)
  101 CONTINUE
  100 CONTINUE
C
```

```
LEASE 2.C                    CALCP                    DATE = MON DEC 11, 1978

CHAPTER  2  2  2  2  2  2  2  PROBLEM MODIFICATIONS  2  2  2  2  2  2  2
C
      CALL PRCMOD(4)
C
CHAPTER  3  3  3  3  3  FINAL COEFFICIENT ASSEMBLY  3  3  3  3  3  3  3
C
      DO 300 I=2,NIM1
      IF(I.LE.INOZ) JFIR=JNP1
      IF(I.GT.INCZ) JFIR=2
      DO 301 J=JFIR,NJM1
  301 AP(I,J)=AN(I,J)+AS(I,J)+AE(I,J)+AW(I,J)-SP(I,J)
  300 CONTINUE
C
CHAPTER  4  4  4  4  4  SOLUTION OF DIFFERENCE EQUATIONS  4  4  4  4  4
C
      DO 400 N=1,NSWPP
  400 CALL LISOLV(2,2,NI,NJ,IT,JT,PP)
C
CHAPTER  5  5  5  5  CORRECT VELOCITIES AND PRESSURE  5  5  5  5  5  5
C
C-----VELOCITIES
```

```
      DC 500 I=2,NIM1
      CO 501 J=2,NJM1
      IF(I.NE.2) U(I,J)=U(I,J)+DU(I,J)*(PP(I-1,J)-PP(I,J))
      IF(J.NE.2) V(I,J)=V(I,J)+DV(I,J)*(PP(I,J-1)-PP(I,J))
  501 CCNTINUE
  5CC CCNTINUE
C-----PRESSURES (WITH PROVISICN FOR UNDER-RELAXATICN)
      PPREF=PP(IPREF,JPREF)
      CO 502 I=2,NIM1
      CC 503 J=2,NJM1
      P(I,J)=P(I,J)+URFP*(PP(I,J)-PPREF)
  503 CCNTINUE
  502 CCNTINUE
      DC 5C4 J=2,NJM1
  504 P(NI,J)=P(NIM1,J)
      RETURN
      END
```

LEASE 2.0 CALCTE DATE = MON DEC 11, 1978

```
      SUBRCUTINE CALCTE
C
CHAPTER  0  0  0  0  0  0  0  PRELIMINARIES  0  0  0  C  0  0  0
C
      CCMMON
     1/TEN/RESORK,NSWPK,URFK
     1/VAR/ U(26,12),V(26,12),P(26,12),PP(26,12),TE(26,12),ED(26,12)
     1/ALL/IT,JT,NI,NJ,NIM1,NJM1,GREAT
     1/GECM/INDCCS,XIW(18),YIW(18),XOW(18),YOW(26) ,XOC(18),YOC(18),
     2      ROC(18),XIC(18),YIC(18),RIC(18),X(26,12),Y(26,12),XU(26,12),
     3      YV(26,12),DXFP(26,12),DXPW(26,12),DYNP(26,12),DYPS(26,12),
     4      SNS(26,12),SEW(26,12),R(26,12),RV(26,12)
     1/FLUPR/URFVIS,VISCOS,DENSIT,PRANDT,DEN(26,12),VIS(26,12)
     1/CCEF/AP(26,12),AN(26,12),AS(26,12),AE(26,12),AW(26,12),SU(26,12),
     2       SP(26,12)
     1/TURB/GEN(26,12),CC,CMU,C1,C2,CAPPA,ELCG,PRED,PRTE
     1/WALLF/YPLLSN(28),TAUN(28),YPLUSS(18),TAUS(18)
     1/KASE T5/UIN,TEIN,EDIN,FLOWIN,ALAMDA,UEN,FLOWEN, A,RSMALL,RMIX,
     2        INCZ,INP1,JNCZ,JNP1,IENT,IEP1
     1/SUSP/SUKD(26,12),SPKD(26,12)
C
CHAPTER  1  1  1  1  1  1  ASSEMBLY CF COEFFICIENTS  1  1  1  1  1  1
C
      PRTE=1.0
      NJM2=NJ-2
      CC 100 I=2,NIM1
      IF(I.LE.INCZ) JFIR=JNP1
      IF(I.GT.INCZ) JFIR=2
      DC 101 J=JFIR,NJM1
C-----CCMPUTE AREAS AND VOLUME
      AREAN=RV(I,J+1)*0.5*(SEW(I,J)+SEW(I,J+1))
      AREAS=RV(I,J)*0.5*(SEW(I,J)+SEW(I,J-1))
      AREAE=0.25*(R(I,J)+R(I+1,J))*(SNS(I,J)+SNS(I+1,J))
      AREAW=0.25*(R(I,J)+R(I-1,J))*(SNS(I,J)+SNS(I-1,J))
      VCL=R(I,J)*SEW(I,J)*SNS(I,J)
C-----CALCLLATE CCNVECTICN CCEFFICIENTS
      GN=0.5*(DEN(I,J)+DEN(I,J+1))*V(I,J+1)
      GS=0.5*(DEN(I,J)+DEN(I,J-1))*V(I,J)
      GE=0.5*(DEN(I,J)+DEN(I+1,J))*U(I+1,J)
      GW=0.5*(DEN(I,J)+DEN(I-1,J))*U(I,J)
      CN=GN*AREAN
```

```
      CS=GS*AREAS
      CE=GE*AREAE
      CW=GW*AREAW
C-----CALCULATE DIFFUSION COEFFICIENTS
      GAMN=0.5*(VIS(I,J)+VIS(I,J+1))/PRTE
      GAMS=0.5*(VIS(I,J)+VIS(I,J-1))/PRTE
      GAME=0.5*(VIS(I,J)+VIS(I+1,J))/PRTE
      GAMW=0.5*(VIS(I,J)+VIS(I-1,J))/PRTE
      DN=GAMN*AREAN/DYNP(I,J)
      DS=GAMS*AREAS/DYPS(I,J)
      DE=GAME*AREAE/DXEP(I,J)
       DW=GAMW*AREAW/DXPW(I,J)
C-----SOURCE TERMS
```



```
      SMP=CN-CS+CE-CW
      CP=AMAX1(0.0,SMP)
      CPC=CP
      DUDX=(U(I+1,J)-U(I,J))/SEW(I,J)
      DVDY=(V(I,J+1)-V(I,J))/SNS(I,J)
      DUDY=((U(I,J)+U(I+1,J)+U(I,J+1)+U(I+1,J+1))/4.-(U(I,J)+U(I+1,J)+
     1U(I,J-1)+U(I+1,J-1))/4.)/SNS(I,J)
      DVDX=((V(I,J)+V(I,J+1)+V(I+1,J)+V(I+1,J+1))/4.-(V(I,J)+V(I,J+1)+V(
     1I-1,J)+V(I-1,J+1))/4.)/SEW(I,J)
      GEN(I,J)=(2.*(DUDX**2+DVDY**2)+(DUDY+DVDX)**2)*VIS(I,J)
C-----ASSEMBLE MAIN COEFFICIENTS
      AN(I,J)=DN-0.5*CN
      IF(ABS(0.5*CN).GT.DN) AN(I,J)=AN(I,J)+ABS(0.5*CN)
      AS(I,J)=DS+0.5*CS
      IF(ABS(0.5*CS).GT.DS) AS(I,J)=AS(I,J)+ABS(0.5*CS)
      AE(I,J)=DE-0.5*CE
      IF(ABS(0.5*CE).GT.DE) AE(I,J)=AE(I,J)+ABS(0.5*CE)
      AW(I,J)=DW+0.5*CW
      IF(ABS(0.5*CW).GT.DW) AW(I,J)=AW(I,J)+ABS(0.5*CW)
      SU(I,J)=CPC*TE(I,J)
      SUKD(I,J)=SU(I,J)
      SU(I,J)=SU(I,J)+GEN(I,J)*VCL
      SP(I,J)=-CP
      SPKD(I,J)=SP(I,J)
      SP(I,J)=SP(I,J)-CC*CMU*DEN(I,J)**2*TE(I,J)*VOL/VIS(I,J)
  101 CONTINUE
  100 CONTINUE
C
CHAPTER  2  2  2  2  2  2  PROBLEM MODIFICATIONS  2  2  2  2  2  2
C
      CALL PROMOD(6)
C
CHAPTER 3 FINAL COEFFICIENT ASSEMBLY AND RESIDUAL SOURCE CALCULATION 3
C
      RESORK=0.0
      DO 300 I=2,NIM1
      IF(I.LE.INCZ) JFIR=JNP1
      IF(I.GT.INCZ) JFIR=2
      DO 301 J=JFIR,NJM1
      AP(I,J)=AN(I,J)+AS(I,J)+AE(I,J)+AW(I,J)-SP(I,J)
      RESOR=AN(I,J)*TE(I,J+1)+AS(I,J)*TE(I,J-1)+AE(I,J)*TE(I+1,J)
     1       +AW(I,J)*TE(I-1,J)-AP(I,J)*TE(I,J)+SU(I,J)
```

```
      VOL=R(I,J)*SEW(I,J)*SNS(I,J)
      SCRVCL=GREAT*VCL
      IF(-SP(I,J).GT.0.5*SCRVCL)  RESCR=RESCR/SCRVCL
      RESCRK=RESCRK+ABS(RESCR)
C-----UNDER-RELAXATICN
      AP(I,J)=AP(I,J)/URFK
      SU(I,J)=SU(I,J)+(1.-URFK)*AP(I,J)*TE(I,J)
  301 CCNTINUE
```



```
  300 CCNTINUE
C
CHAPTER  4  4  4  4  4  SCLUTICN CF DIFFERENCE EQUATIONS  4  4  4  4  4
C
      DC 400 N=1,NSWPK
  400 CALL LISCLV(2,2,NI,NJ,IT,JT,TE)
      CO 401 J=2,NJM1
  401 TE(NI,J)=TE(NIM1,J)
      DC 402 J=JNP1,NJM1
  402 TE(1,J)=TE(2,J)
      RETURN
      END
```



```
      SUBROUTINE CALCED
C
CHAPTER  0  0  0  0  0  0  0  PRELIMINARIES  0  0  0  0  0  0  0
C
      CCMMCN
     1/TDIS/RESCRE,NSWPC,URFE
     1/ALL/IT,JT,NI,NJ,NIM1,NJM1,GREAT
     1/GEOM/INDCCS,XIW(18),YIW(18),XOW(18),YOW(26) ,XOC(18),YOC(18),
     2      ROC(18),XIC(18),YIC(18),RIC(18),X(26,12),Y(26,12),XU(26,12),
     3      YV(26,12),DXEP(26,12),DXPW(26,12),DYNP(26,12),DYPS(26,12),
     4      SNS(26,12),SEW(26,12),R(26,12),RV(26,12)
     1/FLUPR/URFVIS,VISCOS,DENSIT,PRANDT,DEN(26,12),VIS(26,12)
     1/CCEF/AP(26,12),AN(26,12),AS(26,12),AE(26,12),AW(26,12),SU(26,12),
     2       SP(26,12)
     1/TURB/GEN(26,12),CD,CMU,C1,C2,CAPPA,ELOG,PRED,PRTE
     1/WALLF/YPLUSN(28),TAUN(28),YPLUSS(18),TAUS(18)
     1/SUSP/SUKD(26,12),SPKD(26,12)
     1/VAR/ U(26,12),V(26,12),P(26,12),PP(26,12),TE(26,12),ED(26,12)
     1/KASE T5/UIN,TEIN,EDIN,FLCWIN,ALAMCA,UEN,FLOWEN, A,RSMALL,RMIX,
     2        INOZ,INP1,JNOZ,JNP1,IENT,IEP1
C
CHAPTER  1  1  1  1  1  1  ASSEMBLY CF CCEFFICIENTS  1  1  1  1  1  1
C
      DC 100 I=2,NIM1
      IF(I.LE.INOZ) JFIR=JNP1
      IF(I.GT.INCZ) JFIR=2
      CO 101 J=JFIR,NJM1
C-----CCMPUTE AREAS AND VCLUME
      AREAN=RV(I,J+1)*C.5*(SEW(I,J)+SEW(I,J+1))
      AREAS=RV(I,J)*0.5*(SEW(I,J)+SEW(I,J-1))
      AREAE=0.25*(R(I,J)+R(I+1,J))*(SNS(I,J)+SNS(I+1,J))
      AREAW=0.25*(R(I,J)+R(I-1,J))*(SNS(I,J)+SNS(I-1,J))
      VCL=R(I,J)*SEW(I,J)*SNS(I,J)
C-----CALCULATE CONVECTICN CCEFFICIENTS
      GN=0.5*(DEN(I,J)+DEN(I,J+1))*V(I,J+1)
```

```
      GS=0.5*(DEN(I,J)+DEN(I,J-1))*V(I,J)
      GE=0.5*(DEN(I,J)+DEN(I+1,J))*U(I+1,J)
      GW=0.5*(DEN(I,J)+DEN(I-1,J))*U(I,J)
      CN=GN*AREAN
      CS=GS*AREAS
      CE=GE*AREAE
      CW=GW*AREAW
C-----CALCULATE DIFFUSION COEFFICIENTS
      GAMN=0.5*(VIS(I,J)+VIS(I,J-1))/PRED
      GAMS=0.5*(VIS(I,J)+VIS(I,J-1))/PRED
      GAME=0.5*(VIS(I,J)+VIS(I+1,J))/PRED
      GAMW=0.5*(VIS(I,J)+VIS(I-1,J))/PRED
      DN=GAMN*AREAN/DYNP(I,J)
      DS=GAMS*AREAS/DYPS(I,J)
      DE=GAME*AREAE/DXEP(I,J)
       DW=GAMW*AREAW/DXPW(I,J)
C-----SOURCE TERMS
      SMP=CN-CS+CE-CW
      CP=AMAX1(0.0,SMP)
```



```
      CPC=CP
C-----ASSEMBLE MAIN COEFFICIENTS
      AN(I,J)=DN-0.5*CN
      IF(ABS(0.5*CN).GT.DN) AN(I,J)=AN(I,J)+ABS(0.5*CN)
      AS(I,J)=DS+0.5*CS
      IF(ABS(0.5*CS).GT.DS) AS(I,J)=AS(I,J)+ABS(0.5*CS)
      AE(I,J)=DE-0.5*CE
      IF(ABS(0.5*CE).GT.DE) AE(I,J)=AE(I,J)+ABS(0.5*CE)
      AW(I,J)=DW+0.5*CW
      IF(ABS(0.5*CW).GT.DW) AW(I,J)=AW(I,J)+ABS(0.5*CW)
      SU(I,J)=CPC*ED(I,J)
      SUKD(I,J)=SU(I,J)
      SU(I,J)=SU(I,J)+C1*CMU*GEN(I,J)*VOL*DEN(I,J)*TE(I,J)/VIS(I,J)
      SP(I,J)=-CP
      SPKD(I,J)=SP(I,J)
      SP(I,J)=SP(I,J)-C2*DEN(I,J)*ED(I,J)*VOL/TE(I,J)
  101 CONTINUE
  100 CONTINUE
C
CHAPTER  2  2  2  2  2  2  PROBLEM MODIFICATIONS  2  2  2  2  2  2
C
      CALL PROMOD(7)
C
CHAPTER 3 FINAL COEFFICIENT ASSEMBLY AND RESIDUAL SOURCE CALCULATION 3
C
      RESCRE=0.0
      DO 300 I=2,NIM1
      IF(I.LE.INOZ) JFIR=JNP1
      IF(I.GT.INOZ) JFIR=2
      DO 301 J=JFIR,NJM1
      AP(I,J)=AN(I,J)+AS(I,J)+AE(I,J)+AW(I,J)-SP(I,J)
      RESCR=AN(I,J)*ED(I,J+1)+AS(I,J)*ED(I,J-1)+AE(I,J)*ED(I+1,J)
     1       +AW(I,J)*ED(I-1,J)-AP(I,J)*ED(I,J)+SU(I,J)
      VOL=R(I,J)*SEW(I,J)*SNS(I,J)
      SORVOL=GREAT*VOL
      IF(-SP(I,J).GT.0.5*SCRVOL)  RESOR=RESOR/SORVOL
      RESCRE=RESCRE+ABS(RESCR)
C-----UNDER-RELAXATION
      AP(I,J)=AP(I,J)/URFE
      SU(I,J)=SU(I,J)+(1.-URFE)*AP(I,J)*ED(I,J)
```

```
  301 CONTINUE
  300 CONTINUE
C
CHAPTER  4  4  4  4  4  SOLUTION OF DIFFERENCE EQUATIONS  4  4  4  4  4
C
      DO 400 N=1,NSWPD
  400 CALL LISOLV(2,2,NI,NJ,IT,JT,ED)
      DO 401 J=2,NJM1
  401 ED(NI,J)=ED(NIM1,J)
      DO 402 J=JNP1,NJM1
  402 ED(1,J)=ED(2,J)
      RETURN
      END
```

LEASE 2.0 LISOLV DATE = MON DEC 11, 1978

```
      SUBROUTINE LISOLV(ISTART,JSTART,NI,NJ,IT,JT,PHI)
      DIMENSION PHI(IT,JT),E(32),B(32),C(32),D(32)
      COMMON
     1/COEF/AP(26,12),AN(26,12),AS(26,12),AE(26,12),AW(26,12),SU(26,12),
     2       SP(26,12)
     1/KASE T5/UIN,TEIN,EDIN,FLOWIN,ALAMDA,UEN,FLOWEN, A,RSMALL,RMIX,
     2        INOZ,INP1,JNOZ,JNP1,IENT,IEP1
      NIM1=NI-1
      NJM1=NJ-1
C-----COMMENCE W-E SWEEP
      DO 100 I=ISTART,NIM1
      IF(I.LE.(INOZ-2+ISTART)) JSTAR =JSTART+JNOZ-1
      IF(I.GT.(INOZ-2+ISTART)) JSTAR =JSTART
      JSTM1=JSTAR -1
      E(JSTM1)=0.0
      C(JSTM1)=PHI(I,JSTM1)
C-----COMMENCE S-N TRAVERSE
      DO 101 J=JSTAR ,NJM1
C-----ASSEMBLE TDMA COEFFICIENTS
      E(J)=AN(I,J)
      B(J)=AS(I,J)
      C(J)=AE(I,J)*PHI(I+1,J)+AW(I,J)*PHI(I-1,J)+SU(I,J)
      D(J)=AP(I,J)
C-----CALCULATE COEFFICIENTS OF RECURRENCE FORMULA
      TERM=1./(D(J)-B(J)*E(J-1))
      E(J)=E(J)*TERM
  101 C(J)=(C(J)+B(J)*C(J-1))*TERM
C-----OBTAIN NEW PHI+S
      DO 102 JJ=JSTAR ,NJM1
      J=NJ+JSTM1-JJ
  102 PHI(I,J)=E(J)*PHI(I,J+1)+C(J)
  100 CONTINUE
      RETURN
      END
```

LEASE 2.0 PRINT DATE = MON DEC 11, 1978

```
      SUBROUTINE PRINT(ISTART,JSTART,NI,NJ,IT,JT,  PHI,HEAD)
      DIMENSION PHI(IT,JT),HEAD(6),STORE(50)
      ISKIP=1
      JSKIP=1
      WRITE(6,110)HEAD
      ISTA=ISTART-13
  100 CONTINUE
      ISTA=ISTA+13
```

```
      IEND=ISTA+12
      IF(NI.LT.IEND)IEND=NI
      WRITE(6,111)(I,I=ISTA,IEND,ISKIP)
      WRITE(6,112)
      DO 101 JJ=JSTART,NJ,JSKIP
      J=JSTART+NJ-JJ
      DO 120 I=ISTA,IEND
      A=PHI(I,J)
      IF(ABS(A).LT.1.E-20) A=0.0
120   STORE(I)=A
  101 WRITE(6,113)J,(STORE(I),I=ISTA,IEND,ISKIP)
C-----------------------------------------------------
      IF(IEND.LT.NI)GO TO 100
      RETURN
  110 FORMAT(1H0,17(2H*-),7X,6A4,7X,17(2H-*))
  111 FORMAT(1H0,13H        I =      ,12,12I9)
  112 FORMAT(3H0 J)
  113 FORMAT(I3,8X,1P13E9.2)
      END
```

```
LEASE 2.0                PROMOD                DATE = MON DEC 11, 1978

      SUBROUTINE PROMOD (NCHAP)
C
CHAPTER  0  0  0  0  0  0  0  PRELIMINARIES  0  0  0  0  0  0  0  0  0
C
      COMMON
     1/UVEL/RESORU,NSWPU,URFU,DXEPU(26,12),DXPWU(26,12),SEWU(26,12),
     2       SNSU(26,12)
     1/VVEL/RESORV,NSWPV,URFV,DYNPV(26,12),DYPSV(26,12),SNSV(26,12),
     2       SEWV(26,12),RCV(26,12)
     1/PCOR/RESORM,NSWPP,URFP,DU(26,12),DV(26,12),IPREF,JPREF
     1/VAR/ U(26,12),V(26,12),P(26,12),PP(26,12),TE(26,12),ED(26,12)
     1/ALL/IT,JT,NI,NJ,NIM1,NJM1,GREAT
     1/GEOM/INDCOS,XIW(18),YIW(18),XCW(18),YCW(26) ,XOC(18),YOC(18),
     2      ROC(18),XIC(18),YIC(18),RIC(18),X(26,12),Y(26,12),XU(26,12),
     3      YV(26,12),DXEP(26,12),DXPW(26,12),DYNP(26,12),DYPS(26,12),
     4      SNS(26,12),SEW(26,12),R(26,12),RV(26,12)
     1/FLUPR/URFVIS,VISCOS,DENSIT,PRANDT,DEN(26,12),VIS(26,12)
     1/KASE T5/UIN,TEIN,EDIN,FLOWIN,ALAMDA,UEN,FLOWEN, A,RSMALL,RMIX,
     2        INDZ,INP1,JNDZ,JNP1,IENT,IEP1
     1/SLSP/SLKD(26,12),SPKD(26,12)
     1/COEF/AP(26,12),AN(26,12),AS(26,12),AE(26,12),AW(26,12),SU(26,12),
     2       SP(26,12)
     1/TURB/GEN(26,12),CD,CMU,C1,C2,CAPPA,ELOG,PREC,PRTE
     1/WALLF/YPLUSN(28),TAUN(28),YPLUSS(18),TAUS(18)
C
C
      GO TO (1,2,3,4,5,6,7),NCHAP
C
CHAPTER  1  1  1  1  1  1  1  1  PROPERTIES  1  1  1  1  1  1  1  1  1
C
    1 CONTINUE
C-----NO MODIFICATIONS FOR THIS PROBLEM
      RETURN
C
CHAPTER  2  2  2  2  2  2  2  2  U MOMENTUM  2  2  2  2  2  2  2  2  2
C
```

```
    2 CONTINUE
C-----TOP WALL
      CDTERM=CMU**0.25
      J=NJM1
      DO  210  I=3,NIM1
      YP=0.25*(DYNP(I,J)+DYNP(I-1,J))
      SQRTK=SQRT(0.5*(TE(I,J)+TE(I-1,J)))
      DENU=0.5*(DEN(I,J)+DEN(I-1,J))
      YPLUSA=0.5*(YPLUSN(I)+YPLUSN(I-1))
      IF(YPLUSA.LE.11.63)      GO  TO  211
      TMULT=DENU*CDTERM*SQRTK*CAPPA/ALOG(ELOG*YPLUSA)
      GO  TO  212
  211 TMULT=VISCOS/YP
  212 TAUN(I)=-TMULT*U(I,J)
      SP(I,J)=SP(I,J)-TMULT*SEWU(I,J)*0.5*(YOW(I)+YOW(I-1)+2.0*(RMIX+
     1RSMALL))
  210 AN(I,J)=0.0
      TAUN(2)=TAUN(3)
```



```
      TAUN(NI)=TAUN(NIM1)
C     INNER WALL
      J=JNP1
      DO 220 I=3,INP1
      YP=0.25*(DYPS(I,J)+DYPS(I-1,J))
      IF(I.EQ.INP1) YP=0.5*(DYPS(I-1,J))
      SQRTK=SQRT(0.5*(TE(I,J)+TE(I-1,J)))
      DENU=0.5*(DEN(I,J)+DEN(I-1,J))
      YPLUSA=0.5*(YPLUSS(I)+YPLUSS(I-1))
      IF(I.EQ.INP1) YPLUSA=YPLUSS(I-1)
      IF(YPLUSA.LE.11.63)      GO  TO  221
      TMULT=DENU*CDTERM*SQRTK*CAPPA/ALOG(ELOG*YPLUSA)
      GO TO 222
  221 TMULT=VISCOS/YP
  222 TAUS(I)=-TMULT*U(I,J)
      SP(I,J)=SP(I,J)-TMULT*SEWU(I,J)*0.5*(YIW(I)+YIW(I-1)+2.0*(RMIX+
     1RSMALL))
  220 AS(I,J)=0.0
      TAUS(2)=TAUS(3)
C-----SYMMETRY  AXIS
      DO 203 I=INP1,NI
  203 AS(I,2)=0.0
C-----OUTLET
      ARDENT=0.0
      FLOW=0.0
      DO  204  J=2,NJM1
      ARDEN=0.5*(DEN(NIM1,J)+DEN(NIM1-1,J))*0.25*(R(NIM1,J)+ R(NIM1-1,J)
     1)*(SNS(NIM1,J)+SNS(NIM1-1,J))
      ARDENT=ARDENT+ARDEN
  204 FLOW=FLOW+ARDEN*U(NIM1,J)
      UINC=(FLOWIN+FLOWEN-FLOW)/ARDENT
      DO  205  J=2,NJM1
  205 U(NI,J)=U(NIM1,J)+UINC
      RETURN
C
CHAPTER  3  3  3  3  3  3  3  3  V MOMENTUM  3  3  3  3  3  3  3  3  3
C
    3 CONTINUE
C-----TOP WALL
      DO 313 I=2,NIM1
  313 AN(I,NJM1)=0.0
```

```
C       INNER WALL
        DO 312 I=2,INCZ
  312   AS(I,JNCZ+2)=0.0
C-----SYMMETRY  AXIS
        DO 302 I=INP1,NIM1
  302   AS(I,3)=0.0
        RETURN
C
CHAPTER  4  4  4  4  4  4  PRESSURE CORRECTION  4  4  4  4  4  4  4  4
C
    4 CONTINUE
C
        RETURN
```

LEASE 2.0 PROMOD DATE = MON DEC 11, 1978

```
C
CHAPTER  5  5  5  5  5  5  5  THERMAL ENERGY  5  5  5  5  5  5  5  5  5
C
    5 CONTINUE
C-----NO MODIFICATIONS FOR THIS PROBLEM
        RETURN
C
CHAPTER  6  6  6  6  6  TURBULENT KINETIC ENERGY  6  6  6  6  6  6  6  6
C
    6 CONTINUE
C-----TOP WALL
        CDTERM=CMU**0.25
        J=NJM1
        DO  610  I=2,NIM1
        YP=0.5*DYNP(I,J)
        DENU=DEN(I,J)
        SQRTK=SQRT(TE(I,J))
        VOL=R(I,J)*SEW(I,J)*SNS(I,J)
        GENCDU=0.5*(ABS(TAUN(I+1)*U(I+1,J))+ABS(TAUN(I)*U(I,J)))/YP
        YPLUSN(I)=DENU*SQRTK*CDTERM*YP/VISCOS
        DUDY=((U(I,J)+U(I+1,J)+U(I,J+1)+U(I+1,J+1))/4.-(U(I,J)+U(I+1,J)+
       1U(I,J-1)+U(I+1,J-1))/4.)/SNS(I,J)
        GENRES=GEN(I,J)-VIS(I,J)*DUDY**2
        GEN(I,J)=GENRES+GENCDU
        IF(YPLUSN(I).LE.11.63)  GO  TO  611
        DITERM=DEN(I,J)*(CMU**.75)*SQRTK*ALOG(ELOG*YPLUSN(I))/(CAPPA*YP)
        GO  TO  612
  611   CONTINUE
        DITERM=DEN(I,J)*(CMU**.75)*SQRTK*YPLUSN(I)/YP
  612   CONTINUE
        SU(I,J)=GEN(I,J)*VOL+SUKD(I,J)
        SP(I,J)=-DITERM*VOL+SPKD(I,J)
  610   AN(I,J)=0.0
C       INNER WALL
        J=JNP1
        DO 620 I=2,INCZ
        YP=0.5*DYPS(I,J)
        DENU=DEN(I,J)
        SQRTK=SQRT(TE(I,J))
        VOL=R(I,J)*SEW(I,J)*SNS(I,J)
        GENCDU=0.5*(ABS(TAUS(I+1)*U(I+1,J))+ABS(TAUS(I)*U(I,J)))/YP
        YPLUSS(I)=DENU*SQRTK*CDTERM*YP/VISCOS
        DUDY=((U(I,J)+U(I+1,J)+U(I,J+1)+U(I+1,J+1))/4.-(U(I,J)+U(I+1,J)+
       1U(I,J-1)+U(I+1,J-1))/4.)/SNS(I,J)
        GENRES=GEN(I,J)-VIS(I,J)*DUDY**2
        GEN(I,J)=GENRES+GENCDU
```

```
      IF(YPLUSS(I).LE.11.63)  GO  TO  621
      DITERM=DEN(I,J)*(CMU**.75)*SQRTK*ALOG(ELOG*YPLUSS(I))/(CAPPA*YP)
      GO TO 622
  621 CONTINUE
      DITERM=DEN(I,J)*(CMU**.75)*SQRTK*YPLUSS(I)/YP
  622 CONTINUE
      SU(I,J)=GEN(I,J)*VOL+SUKD(I,J)
      SP(I,J)=-DITERM*VOL+SPKD(I,J)
```



```
  620 AS(I,J)=0.0
C-----SYMMETRY  AXIS
      J=2
      DO 630 I=INP1,NIM1
      DUDY=((U(I,J)+U(I+1,J)+U(I,J+1)+U(I+1,J+1))/4.-(U(I,J)+U(I+1,J)+
     1U(I,J-1)+U(I+1,J-1))/4.)/SNS(I,J)
      VOL=R(I,J)*SEW(I,J)*SNS(I,J)
      GEN(I,J)=GEN(I,J)-VIS(I,J)*DUDY**2
      SU(I,J)=SUKD(I,J)+GEN(I,J)*VOL
  630 AS(I,2)=0.0
      RETURN
C
CHAPTER  7  7  7  7  7  7  7  7  DISSIPATION  7  7  7  7  7  7  7  7  7
C
    7 CONTINUE
C-----TOP WALL
      J=NJM1
      DO  710  I=2,NIM1
      YP=0.5*DYNP(I,J)
      TERM=(CMU**.75)/(CAPPA*YP)
      SU(I,J)=GREAT*TERM*TE(I,J)**1.5
  710 SP(I,J)=-GREAT
C     INNER WALL
      J=JNP1
      DO 720 I=2,INCZ
      YP=0.5*DYPS(I,J)
      TERM=(CMU**.75)/(CAPPA*YP)
      SU(I,J)=GREAT*TERM*TE(I,J)**1.5
  720 SP(I,J)=-GREAT
C-----SYMMETRY  AXIS
      DO 730 I=INP1,NIM1
  730 AS(I,2)=0.0
      RETURN
      END
```

B.2 Listing of MAIN and Subroutine INIT for Uniform Mixing Tube

```
      DIMENSION HEDU(6),HEDV(6),HEDP(6),HEDT(6),HEDK(6),HEDD(6),HEDM(6)
     1          ,HEDA(6),HEDB(6),HEDPP(6),HEDUN(6)
      COMMON
     1/UVEL/RESORU,NSWPU,UREFU,DXFPU(32),DXPWU(32),SLKU(32)
     1/VVEL/RESORV,NSWPV,UREFV,DYNPV(32),DYPSV(32),SNSV(32),FCV(32)
     1/PCOR/RESORM,NSWPP,UREFP,DU(18,18),DV(18,18),IPREF,JPREF
     1/TEN/RESORK,NSWPK,UREFK
     1/TDIS/RESORE,NSWPD,UREFE
     1/VAR/ U(18,18),V(18,18),P(18,18),PP(18,18),TE(18 ,18),ED(18,18)
     1/ALL/IT,JT,NI,NJ,NIM1,NJM1,GREAT
     1/GEOM/INDCOS,X(32),Y(32),DXFP(32),DXPW(32),DYNP(32),DYPS(32),
     1        SNS(32),SEW(32),XU(32),YV(32),R(32),RV(32)
     1/FLUPR/UREFVIS,VISCOS,DENSIT,PRANDT,DEN(18,18),VIS(18,18)
     1/KASE T2/UIN,TEIN,EDIN,FLOWIN,ALAMDA, ULN,FLOWEN,
     2        RSMALL,RLARGE,AL1,AL2,JSTEP,ISTEP, ISTP1,JSTM1,ISTP1,ISTM1
     1/TURB/GEN(18,18),CC,CMU,C1,C2,CAPPA,ELCG,PRED,PRTE
     1/WALLF/YPLUSN(22),XPLUSW(22),TAUN(22),TAUW(22)
     1/COEF/AP(18,18),AN(18,18),AS(18,18),AE(18,18),AW(18,18),SU(18,18),
     1        SP(18,18)
      LOGICAL INCALU,INCALV,INCALP,INPRC,INCALK,INCALD,INCALM,INCALA,
     1        INCALB
      GREAT=1.E30
      NITER=0
      IT=18
      JT=18
      NSWPU=1
      NSWPV=1
      NSWPP=2
      NSWPK=1
      NSWPD=1
      READ(9,010)HEDU,HEDV,HEDP,HEDT,HEDK,HEDD,HEDM,HEDA,HEDB,HEDPP,
     1HEDUN
  010 FORMAT(6A4)
C
CHAPTER  1  1  1  1  1  PARAMETERS AND CONTROL INDICES  1  1  1  1  1  1
C
C-----GRID
      NI=14
      NJ=14
      NIM1=NI-1
      NJM1=NJ-1
      NJM2=NJ-2
      INDCOS=2
      JSTEP=5
      JSTP1=JSTEP+1
      JSTP2=JSTEP+2
      JSTM1=JSTEP-1
      RLARGE=0.15
      RSCRL=0.3333
      RSMALL=RLARGE*RSCRL
      ALTOT=3.0
      EPSX=1.05
      SUMX=0.5*EPSX**(NI-4)+(EPSX**(NI-3)-1.)/(EPSX-1.)+0.5
      DX=ALTOT/SUMX
      X(1)=-0.5*DX
      X(2)=-X(1)
      DO  100  I=3,NIM1
      X(I)=X(I-1)+DX
  100 DX=EPSX*DX
      X(NI)=X(NIM1)-X(NI-2)+X(NIM1)
      DY1=RSMALL/FLOAT(JSTM1)
      DY2=(RLARGE-RSMALL)/FLOAT(NJ-JSTEP-1)
      Y(1)=-0.5*DY1
```

```
      DO 101 J=2,JSTEP
  101 Y(J)=Y(J-1)+DY1
      Y(JSTP1)=Y(JSTEP)+0.5*(DY1+DY2)
      DO 102 J=JSTP2,NJ
  102 Y(J)=Y(J-1)+DY2
C-----DEPENDENT VARIABLE SELECTION
      INCALU=.TRUE.
      INCALV=.TRUE.
      INCALP=.TRUE.
      INCALK=.TRUE.
      INCALD=.TRUE.
      INPRO=.TRUE.
C-----FLUID PROPERTIES
      DENSIT=1.225
C-----TURBULENCE CONSTANTS
      CMU=0.09
      CD=1.00
      C1=1.44
      C2=1.92
      CAPPA=.4187
      ELOG=9.793
      PRED=CAPPA*CAPPA/(C2-C1)/(CMU**.5)
      PRTE=1.0
C-----BOUNDARY VALUES
      UIN=45.0
      UEN=4.5
      UM=(UIN*RSMALL**2+UEN*(RLARGE**2-RSMALL**2))/(RLARGE**2)
      ULARGE=UEN+(UIN-UEN)*(RSMALL/RLARGE)**2
      TURBIN=0.0003
      TEIN=TURBIN*UIN**2
      TURBEN=0.003
      TEEN=TURBEN*UEN**2
```



```
      ALAMDA=0.005
      EDIN=TEIN**1.5/(ALAMDA*RLARGE)
      EDEN=TEEN**1.5/(ALAMDA*RLARGE)
      VISCOS=1.8E-5
C-----PRESSURE CALCULATION
      IPREF=1
      JPREF=NJM1
C-----PROGRAM CONTROL AND MONITOR
      MAXIT=180
      IMON=6
      JMON=6
      URFU=0.5
      URFV=0.5
      URFP=1.0
      URFE=0.7
      URFK=0.7
      URFVIS=0.7
      INDPRI=1
      SORMAX=1.0E-4
C
CHAPTER 2 2 2 2 2 2 INITIAL OPERATIONS 2 2 2 2 2 2 2 2 2
C
C-----CALCULATE GEOMETRICAL QUANTITIES AND SET VARIABLES TO ZERO
      CALL INIT
C-----INITIALISE VARIABLE FIELDS
      DO 208 J=2,JSTEP
      TE(1,J)=TEIN
```

```
208 ED(1,J)=EDIN
    DO 209 J=JSTP1,NJM1
    TE(1,J)=TEEN
209 ED(1,J)=EDEN
    FLOWIN=0.0
    ARDEN=0.0
    DO 200 I=2,NI
    DO  200  J=2,JSTEP
    U(I,J)=UIN
    TE(I,J)=TEIN
200 ED(I,J)=EDIN
    DO 205 J=2,JSTEP
    ARDEN=0.5*(DEN(1,J)+DEN(2,J))*R(J)*SNS(J)
205 FLOWIN=FLOWIN+ARDEN*U(2,J)
    SORMAX=SORMAX*FLOWIN
    FLOWEN=0.0
    ARDEN=0.0
    DO 201 I=2,NI
    DO 201 J=JSTP1,NJM1
    TE(I,J)=TEEN
    ED(I,J)=EDEN
201 U(I,J)=UEN
    DO 206 J=JSTP1,NJM1
    ARDEN=0.5*(DEN(1,J)+DEN(2,J))*R(J)*SNS(J)
206 FLOWEN=FLOWEN+ARDEN*U(2,J)
    DO  203  I=2,NIM1
203 YPLUSN(I)=11.0
```

LEASE 2.0 MAIN DATE = SAT MAR 31, 1979

```
      CALL PROPS
C-----INITIAL OUTPUT
      WRITE(6,210)
      WRITE(6,220) UIN
      WRITE(6,221) UEN
      UK=UEN+(UIN-UEN)*(RSMALL/RLARGE)**2
      USTASQ=(UIN**2-UEN**2)*(RSMALL/RLARGE)**2+0.5*(UEN**2-UK**2)
      CT=UK/SQRT(USTASQ)
      WRITE(6,222) CT
      RE=UIN*RLARGE*2.0*DENSIT/VISCOS
      WRITE(6,230) RE
      WRITE(6,240) RSDRL
      WRITE(6,250) VISCOS
      WRITE(6,260) DENSIT
      IF(INCALU) CALL PRINT(2,2,NI,NJ,IT,JT,XU,Y,U,HEDU)
      IF(INCALV) CALL PRINT(2,2,NI,NJ,IT,JT,X,YV,V,HEDV)
      IF(INCALP) CALL PRINT(2,2,NI,NJ,IT,JT,X,Y,P,HEDP)
      IF(INCALK) CALL PRINT(2,2,NI,NJ,IT,JT,X,Y,TE,HEDK)
      IF(INCALD) CALL PRINT(2,2,NI,NJ,IT,JT,X,Y,ED,HEDD)
C
CHAPTER  3  3  3  3  3  3  3  ITERATION LOOP  3  3  3  3  3  3  3  3  3
C
      WRITE(6,310) IMON,JMON
  300 NITER=NITER+1
C-----UPDATE MAIN DEPENDENT VARIABLES
      IF(INCALU) CALL CALCU
      IF(INCALV) CALL CALCV
      IF(INCALP) CALL CALCP
      IF(INCALK) CALL CALCTE
      IF(INCALD) CALL CALCED
C-----UPDATE FLUID PROPERTIES
      IF(INPRO) CALL PROPS
C-----INTERMEDIATE OUTPUT
```

```
      DUMMY=0.0
      WRITE(6,311) NITER,RESORU,RESORV,RESORM,RESOPT,RESOEK,RESORD
     1             ,U(IMON,JMON),V(IMON,JMON),P(IMON,JMON),DUMMY,
     1                  TE(IMON,NJM1),ED(IMON,NJM1)
      IF(NITER.GT.2)INDPRI=40
      IF(ABS(FLOAT(NITER/INDPRI)-FLOAT(NITER)/INDPRI).GT.1.E-4)GO TO 301
      WRITE(6,312)
      IF(INCALU) CALL PRINT(2,2,NI,NJ,IT,JT,XU,Y,U,HEDU)
      IF(INCALV) CALL PRINT(2,2,NI,NJ,IT,JT,X,YV,V,HEDV)
      IF(INCALP) CALL PRINT(2,2,NI,NJ,IT,JT,X,Y,P,HEDP)
      IF(INCALK) CALL PRINT(2,2,NI,NJ,IT,JT,X,Y,TE,HEDK)
      IF(INCALD) CALL PRINT(2,2,NI,NJ,IT,JT,X,Y,ED,HEDD)
      WRITE(6,312)
      WRITE(6,310) IMON,JMON
  301 CONTINUE
C-----TERMINATION TESTS
      SORCE=RESORM
      IF(NITER.EQ.20.AND.SORCE.GT.1.0E4*SORMAX) GO TO  302
      IF(NITER.EQ.MAXIT) GO TO 302
      IF(SORCE.GT.SORMAX) GO TO 300
  302 CONTINUE

LEASE 2.0                MAIN                    DATE = SAT MAR 31, 1979

C
CHAPTER  4  4  4  4  4  4  FINAL OPERATIONS AND OUTPUT  4  4  4  4  4  4
C
      IF(INCALU) CALL PRINT(2,2,NI,NJ,IT,JT,XU,Y,U,HEDU)
      IF(INCALV) CALL PRINT(2,2,NI,NJ,IT,JT,X,YV,V,HEDV)
      IF(INCALP) CALL PRINT(2,2,NI,NJ,IT,JT,X,Y,P,HEDP)
      IF(INCALP) CALL PRINT(2,2,NI,NJ,IT,JT,X,Y,PP,HEDPP)
      IF(INCALK) CALL PRINT(2,2,NI,NJ,IT,JT,X,Y,TE,HEDK)
      IF(INCALD) CALL PRINT(2,2,NI,NJ,IT,JT,X,Y,ED,HEDD)
      IF(INPRO ) CALL PRINT(2,2,NI,NJ,IT,JT,X,Y,VIS,HEDM)
C-----CALCULATION OF NON DIMENSIONAL TURBULENCE ENERGY AND LENGTH SCALE
      DO 400 I=2,NIM1
      DO 400 J=2,NJM1
      U(I,J)=U(I,J)/UM
      SU(I,J)=TE(I,J)*DEN(I,J)/ABS(TAUN(I))
  400 SP(I,J)=TE(I,J)**1.5/ED(I,J)/RLARGE
      CALL PRINT(2,2,NI,NJ,IT,JT,XU,Y,U,HEDUN)
      CALL PRINT(2,2,NI,NJ,IT,JT,X,Y,SU,HEDA)
      CALL PRINT(2,2,NI,NJ,IT,JT,X,Y,SP,HEDB)
C-----CALCULATION OF SHEAR-STRESS COEFFICIENT ALONG LARGE DUCT WALL
      WRITE(6,402)
      DO  401  I=ISTEP,NIM1
      SSC=TAUN(I)/(1.0*DENSIT*ULARGE*ULARGE)
      XUD=XU(I)/RLARGE/2.
      WRITE(6,403) I,XUD,SSC
  401 CONTINUE
      STOP
C-----FORMAT STATEMENTS
  210 FORMAT(1H1,47X,47HKASE T2 - TURBULENT JETS MIXING IN UNIFORM DUCT/
     1////)
  220 FORMAT(  //15X,33HINLET JET VELOCITY                          ,1PE11.3)
  221 FORMAT(  //15X,33HANNULAR FLUID VELOCITY                      ,1PE11.3)
  222 FORMAT(  //15X,33HCRAYA-CURTET NUMBER                         ,1PE11.3)
  230 FORMAT(  //15X,33HREYNOLDS NUMBER                             ,1PE11.3)
  240 FORMAT(  //15X,33HDIAMETER RATIO                              ,1PE11.3)
  250 FORMAT(  //15X,33HLAMINAR VISCOSITY                           ,1PE11.3)
  260 FORMAT(  //15X,33HFLUID DENSITY                               ,1PE11.3)
```

```
  310 FORMAT(13HOITER     I---,  9X,29HABSOLUTE RESIDUAL SOURCE SUMS,9X,
     111H---I    I---,37H FIELD VALUES AT MONITORING LOCATION(,I2,1H,,I2,
     26H) ---I/14H  NO     UMOM,5X,4HVMOM,5X,4HMASS,5X,4HENER,5X,4HTKIN
     3,5X,4HDISP,9X,1HU,8X,1HV,8X,1HP,8X,1HT,8X,1HK,8X,1HD/)
  311 FORMAT(1H ,I3,5X,1P6E9.2,3X,1P6E9.2)
  312 FORMAT(1H0,59(2H- ))
  402 FORMAT(///5X,1HI,7X,5HXU(I),6X,10HS.S.COEFF.)
  403 FORMAT(/5X,I5,2(1PE11.3))
      END
LEASE 2.0                INIT                    DATE = SAT MAR 31, 1979

      SUBROUTINE INIT
C
CHAPTER  0  0  0  0  0  0  0  0  PRELIMINARIES  0  0  0  0  0  0  0  0
C
       COMMON
     1/UVEL/RESORU,NSWPU,URFU,DXEPU(32),DXPWU(32),SEWU(32)
     1/VVEL/RESORV,NSWPV,URFV,DYNPV(32),DYPSV(32),SNSV(32),RCV(32)
     1/PCOR/RESORM,NSWPP,URFP,DU(18,18),DV(18,18),IPREF,JPREF
     1/VAR/ U(18,18),V(18,18),P(18,18),PP(18,18),TE(18 ,18),ED(18,18)
     1/ALL/IT,JT,NI,NJ,NIM1,NJM1,GREAT
     1/GEOM/INDCOS,X(32),Y(32),DXEP(32),DXPW(32),DYNP(32),DYPS(32),
     1       SNS(32),SEW(32),XU(32),YV(32),R(32),RV(32)
     1/FLUPR/URFVIS,VISCOS,DENSIT,PRANDT,DEN(18,18),VIS(18,18)
     1/KASE T2/UIN,TEIN,EDIN,FLOWIN,ALAMDA, UEN,FLOWEN,
     2        RSMALL,PLARGE,AL1,AL2,JSTEP,ISTEP,JSTP1,JSTM1,ISTP1,ISTM1
     1/TURB/GEN(18,18),CD,CMU,C1,C2,CAPPA,ELOG,PRED,PRTE
     1/COEF/AP(18,18),AN(18,18),AS(18,18),AE(18,18),AW(18,18),SU(18,18),
     1       SP(18,18)
C
CHAPTER  1  1  1  1  1  CALCULATE GEOMETRICAL QUANTITIES  1  1  1  1  1
C
      DO 100 J=1,NJ
      R(J)=Y(J)
  100 IF(INDCOS.EQ.1)R(J)=1.0
      DXPW(1)=0.0
      DXEP(NI)=0.0
      DO 101 I=1,NIM1
      DXEP(I)=X(I+1)-X(I)
  101 DXPW(I+1)=DXEP(I)
      DYPS(1)=0.0
      DYNP(NJ)=0.0
      DO 102 J=1,NJM1
      DYNP(J)=Y(J+1)-Y(J)
  102 DYPS(J+1)=DYNP(J)
      SEW(1)=0.0
      SEW(NI)=0.0
      DO 103 I=2,NIM1
  103 SEW(I)=0.5*(DXEP(I)+DXPW(I))
      SNS(1)=0.0
      SNS(NJ)=0.0
      DO 104 J=2,NJM1
  104 SNS(J)=0.5*(DYNP(J)+DYPS(J))
      XU(1)=0.0
      DO 105 I=2,NI
  105 XU(I)=0.5*(X(I)+X(I-1))
      DXPWU(1)=0.0
      DXPWU(2)=0.0
      DXEPU(1)=0.0
      DXEPU(NI)=0.0
      DO 106 I=2,NIM1
      DXEPU(I)=XU(I+1)-XU(I)
```

```
  106 DXPWU(I+1)=DXEPU(I)
      SEWU(1)=0.0
      SEWU(2)=0.0
```



```
      DO 107 I=3,NIM1
  107 SEWU(I)=0.5*(DXEPU(I)+DXPWU(I))
      YV(1)=0.0
      RV(1)=0.0
      DO 108 J=2,NJ
      RV(J)=0.5*(R(J)+R(J-1))
      RCV(J)=0.5*(RV(J)+RV(J-1))
  108 YV(J)=0.5*(Y(J)+Y(J-1))
      DYPSV(1)=0.0
      DYPSV(2)=0.0
      DYNPV(NJ)=0.0
      DO 109 J=2,NJM1
      DYNPV(J)=YV(J+1)-YV(J)
  109 DYPSV(J+1)=DYNPV(J)
      SNSV(1)=0.0
      SNSV(2)=0.0
      SNSV(NJ)=0.0
      DO 110 J=3,NJM1
  110 SNSV(J)=0.5*(DYNPV(J)+DYPSV(J))
C
CHAPTER  2  2  2  2  2  2  SET VARIABLES TO ZERO  2  2  2  2  2  2
C
      DO 200 I=1,NI
      DO 200 J=1,NJ
      U(I,J)=0.0
      V(I,J)=0.0
      P(I,J)=0.0
      PP(I,J)=0.0
      TE(I,J)=0.0
      ED(I,J)=0.0
      DEN(I,J)=DENSIT
      VIS(I,J)=VISCOS
      DU(I,J)=0.0
      DV(I,J)=0.0
      SU(I,J)=0.0
      SP(I,J)=0.0
  200 CONTINUE
      RETURN
      END
```

B.3 Listing of MAIN and Subroutine INIT for Diffuser

```
 DIMENSION HEDU(6),HEDV(6),HEDP(6),HEDT(6),HEDK(6),HEDD(6),HEDM(6)
1       ,HEDA(6),HEDB(6),HEDPP(6),HEDUN(6)  ,HEDG(6)
 COMMON
1/UVEL/RESORU,NSWPU,URFU,DXEPU(32),DXPWU(32),SEWU(32)
1/VVEL/RESORV,NSWPV,URFV,DYNPV(28,14),DYPSV(28,14),SNSV(28,14),
2        RCV(28,14)
1/PCOR/RESORM,NSWPP,URFP,DU(28,14),DV(28,14),IPREF,JPREF
1/TEN/RESORK,NSWPK,URFK
1/TDIS/RESORE,NSWPD,URFE
1/VAR/ U(28,14),V(28,14),P(28,14),PP(28,14),TE(28,14),ED(28,14)
1/ALL/IT,JT,NI,NJ,NIM1,NJM1,GREAT
1/GEOM/INDCOS,X(32),DY(32),DXEP(32),DXPW(32),DYNP(28,14),
2        DYPS(28,14),SNS(28,14),SEW(32),XU(32),Y(28,14),YV(28,14),
3        R(28,14),RV(28,14)
1/FLUPR/URFVIS,VISCOS,DENSIT,PRANDT,DEN(28,14),VIS(28,14)
1/KASE T3/UIN,TEIN,EDIN,FLOWIN,ALAMDA,RIN,DAN
1/TURB/GEN(28,14),CD,CMU,C1,C2,CAPPA,ELOG,PRED,PRTE
1/WALLF/YPLUSN(32),XPLUSW(32),TAUN(32),TAUW(32)
1/COEF/AP(28,14),AN(28,14),AS(28,14),AE(28,14),AW(28,14),SU(28,14),
1        SP(28,14)
 LOGICAL INCALU,INCALV,INCALP,INPRO,INCALK,INCALD,INCALM,INCALA,
1        INCALB
 GREAT=1.E30
 NITER=0
 IT=28
 JT=14
 NSWPU=1
 NSWPV=1
 NSWPP=5
 NSWPK=1
      NSWPD=1
      READ(9,010)HEDU,HEDV,HEDP,HEDT,HEDK,HEDD,HEDM,HEDA,HEDB,HEDPP,
     1HEDUN,HEDG
  010 FORMAT(6A4)
C
CHAPTER  1  1  1  1  1  PARAMETERS AND CONTROL INDICES  1  1  1  1  1  1
C
C------GRID
      NI=14
      NJ=12
      NIM1=NI-1
```



```
      NJM1=NJ-1
      NJM2=NJ-2
      INDCOS=2
      ANGLE=4.05
      ANGLE=3.1416*ANGLE/180.0
      RIN=0.0171
      ALTOT=0.43
      EPSX=1.15
      SUMX=0.5*EPSX**(NI-4)+(EPSX**(NI-3)-1.)/(EPSX-1.)+0.5
      DX=ALTOT/SUMX
      XIN=RIN/SIN(ANGLE)
      X(1)=XIN-0.5*DX
      X(2)=XIN+0.5*DX
      DO  100  I=3,NIM1
      X(I)=X(I-1)+DX
  100 DX=EPSX*DX
      X(NI)=X(NIM1)-X(NI-2)+X(NIM1)
      DAN=ANGLE/FLOAT(NJ-2)
      DO 101 I=1,NI
```

```
      DY(I)=X(I)*DAN
  101 Y(I,1)=-0.5*DY(I)
      DO 102 I=1,NI
      DO 102 J=2, NJ
  102 Y(I,J)=Y(I,J-1)+DY(I)
C-----DEPENDENT VARIABLE SELECTION
      INCALU=.TRUE.
      INCALV=.TRUE.
      INCALP=.TRUE.
      INCALK=.TRUE.
      INCALD=.TRUE.
      INPRO=.TRUE.
C-----FLUID PROPERTIES
      DENSIT=1000.
C-----TURBULENCE CONSTANTS
      CMU=0.09
      CD=1.00
      C1=1.44
      C2=1.92
      CAPPA=.4187
      ELOG=9.793
      PRED=CAPPA*CAPPA/(C2-C1)/(CMU**.5)
      PRTE=1.0
C-----BOUNDARY VALUES
      UIN=2.47
      TURBIN=0.001
      TEIN=TURBIN*UIN**2
      ALAMDA=0.05
      EDIN=TEIN**1.5/(ALAMDA*RIN)
      VISCOS=1.004E-3
C-----PRESSURE CALCULATION
      IPREF=2
      JPREF=2
C-----PROGRAM CONTROL AND MONITOR
      MAXIT=190
```



```
      IMON=6
      JMON=6
      URFU=0.5
      URFV=0.5
      URFP=1.0
      URFE=0.7
      URFK=0.7
      URFVIS=0.7
      INDPRI=1
      SORMAX=1.0E-5
C
CHAPTER 2 2 2 2 2 2 INITIAL OPERATIONS 2 2 2 2 2 2 2 2 2
C
C-----CALCULATE GEOMETRICAL QUANTITIES AND SET VARIABLES TO ZERO
      CALL INIT
C-----INITIALISE VARIABLE FIELDS
      FLOWIN=0.0
      ARDEN=0.0
      READ(9,11) (U(2,J),J=2,NJM1)
   11 FORMAT(F10.3)
      DO 200  J=2,NJM1
      ARDEN=0.5*(DEN(I,J)+DEN(2,J))*0.25*(R(1,J)+R(2,J))*(SNS(1,J)+
     1SNS(2,J))
  200 FLOWIN=FLOWIN+ARDEN*U(2,J)
```

```
      DO 201 I=1,NI
      TE(I,NJ)=0.0
      ED(I,NJ)=0.0
  201 U(I,NJ)=0.0
      DO  203  I=2,NIM1
  203 YPLUSN(I)=11.0
      CALL PROPS
C-----INITIAL OUTPUT
      WRITE(6,210)
      WRITE(6,220) UIN
      RE=UIN*RIN*2.0*DENSIT/VISCOS
      WRITE(6,230) RE
      WRITE(6,250) VISCOS
      WRITE(6,260) DENSIT
      ANGLE=2.0*ANGLE*180./3.1416
      WRITE(6,270) ANGLE
      CALL PRINT(2,2,NI,NJ,IT,JT,X,Y,HEDG)
      IF(INCALU) CALL PRINT(2,2,NI,NJ,IT,JT,XU,  U,HEDU)
      IF(INCALV) CALL PRINT(2,2,NI,NJ,IT,JT,X,   V,HEDV)
      IF(INCALP) CALL PRINT(2,2,NI,NJ,IT,JT,X,  P,HEDP)
      IF(INCALP) CALL PRINT(2,2,NI,NJ,IT,JT,X,  PP,HEDPP)
      IF(INCALK) CALL PRINT(2,2,NI,NJ,IT,JT,X,  TE,HEDK)
      IF(INCALD) CALL PRINT(2,2,NI,NJ,IT,JT,X,  ED,HEDD)
C
CHAPTER  3  3  3  3  3  3  3  ITERATICN LOOP  3  3  3  3  3  3  3  3  3
C
      WRITE(6,310) IMON,JMCN
  300 NITER=NITER+1
C-----UPDATE MAIN DEPENDENT VARIABLES
      IF(INCALU) CALL CALCU
```



```
      IF(INCALV) CALL CALCV
      IF(INCALP) CALL CALCP
      IF(INCALK) CALL CALCTE
      IF(INCALD) CALL CALCED
C-----UPDATE FLUID PROPERITIES
      IF(INPRO) CALL PROPS
C-----INTERMEDIATE OUTPUT
      DUMMY=0.0
      WRITE(6,311) NITER,RESORU,RESORV,RESCRM,RESORT,RESCRK,RESORE
     1             ,U(IMON,JMON),V(IMON,JMON),P(IMON,JMON),DUMMY,
     1                  TE(IMON,NJM1),ED(IMON,NJM1)
      IF(NITER.GT.2)INDPRI=40
      IF(ABS(FLOAT(NITER/INDPRI)-FLOAT(NITER)/INDPRI).GT.1.E-4)GO TO 301
      WRITE(6,312)
      IF(INCALU) CALL PRINT(2,2,NI,NJ,IT,JT,XU,  U,HEDU)
      IF(INCALV) CALL PRINT(2,2,NI,NJ,IT,JT,X,   V,HEDV)
      IF(INCALP) CALL PRINT(2,2,NI,NJ,IT,JT,X,  P,HEDP)
      IF(INCALP) CALL PRINT(2,2,NI,NJ,IT,JT,X,  PP,HEDPP)
      IF(INCALK) CALL PRINT(2,2,NI,NJ,IT,JT,X,  TE,HEDK)
      IF(INCALD) CALL PRINT(2,2,NI,NJ,IT,JT,X,  ED,HEDD)
      WRITE(6,312)
      WRITE(6,310) IMON,JMCN
  301 CONTINUE
C-----TERMINATICN TESTS
      SORCE=RESORM
      IF(NITER.EQ.MAXIT) GO TO 302
      IF(SORCE.GT.SORMAX) GO TO 300
  302 CONTINUE
```

```
C
CHAPTER  4  4  4  4  4  4  FINAL OPERATIONS AND OUTPUT  4  4  4  4  4  4
C
      IF(INCALU) CALL PRINT(2,2,NI,NJ,IT,JT,XU,  U,HEDU)
      IF(INCALV) CALL PRINT(2,2,NI,NJ,IT,JT,X,   V,HEDV)
      IF(INCALP) CALL PRINT(2,2,NI,NJ,IT,JT,X,  P,HEDP)
      IF(INCALP) CALL PRINT(2,2,NI,NJ,IT,JT,X,  PP,HEDPP)
      IF(INCALK) CALL PRINT(2,2,NI,NJ,IT,JT,X,  TE,HEDK)
      IF(INCALD) CALL PRINT(2,2,NI,NJ,IT,JT,X,  ED,HEDD)
      IF(INPRO ) CALL PRINT(2,2,NI,NJ,IT,JT,X,  VIS,HEDM)
C-----CALCULATION OF NON DIMENSIONAL TURBULENCE ENERGY AND LENGTH SCALE
      DO 400 I=2,NIM1
      DO 400 J=2,NJM1
      U(I,J)=U(I,J)/UIN
      SU(I,J)=TE(I,J)*DEN(I,J)/ABS(TAUN(I))
  400 SP(I,J)=TE(I,J)**1.5/ED(I,J)/RIN
      CALL PRINT(2,2,NI,NJ,IT,JT,XU,  U,HEDUN)
      CALL PRINT(2,2,NI,NJ,IT,JT,X,  SU,HEDA)
      CALL PRINT(2,2,NI,NJ,IT,JT,X,  SP,HEDB)
C-----CALCULATION OF SHEAR-STRESS COEFFICIENT ALONG LARGE DUCT WALL
      WRITE(6,402)
      DO 401 I=2,NIM1
      SSC=TAUN(I)/(1.0*DENSIT*UIN*UIN)
      XUD=XU(I)/RIN/2.0
      WRITE(6,403) I,XUD,SSC
  401 CONTINUE
```



```
      STOP
C-----FORMAT STATEMENTS
  210 FORMAT(1H1,47X,36HKASE T3 - TURBULENT FLOW IN DIFFUSER////)
  220 FORMAT(  //15X,33HINLET VELOCITY                          ,1PE11.3)
  230 FORMAT(  //15X,33HREYNOLDS NUMBER                         ,1PE11.3)
  250 FORMAT(  //15X,33HLAMINAR VISCOSITY                       ,1PE11.3)
  260 FORMAT(  //15X,33HFLUID DENSITY                           ,1PE11.3)
  270 FORMAT(  //15X,33HINCLUDED ANGLE                          ,1PE11.3)
  310 FORMAT(13HOITER    I---,  9X,29HABSOLUTE RESIDUAL SOURCE SUMS,9X,
     111H---I    I---,37H FIELD VALUES AT MONITORING LOCATION(,I2,1H,,I2,
     26H) ---I/14H  NO       UMOM,5X,4HVMOM,5X,4HMASS,5X,4HENER,5X,4HTKIN
     3,5X,4HDISP,9X,1HU,8X,1HV,8X,1HP,8X,1HT,8X,1HK,8X,1HD/)
  311 FORMAT(1H ,I3,5X,1P6E9.2,3X,1P6E9.2)
  312 FORMAT(1H0,59(2H- ))
  402 FORMAT(///5X,1HI,7X,5HXU(I),6X,10HS.S.COEFF.)
  403 FORMAT(/5X,I5,2(1PE11.3))
      END
```

```
      SUBROUTINE INIT
C
CHAPTER  0  0  0  0  0  0  0  0  PRELIMINARIES  0  0  0  0  0  0  0  0
C
      COMMON
     1/UVEL/RESORU,NSWPU,URFU,DXEPU(32),DXPWU(32),SEWU(32)
     1/VVEL/RESORV,NSWPV,URFV,DYNPV(28,14),DYPSV(28,14),SNSV(28,14),
     2       RCV(28,14)
     1/PCOR/RESORM,NSWPP,URFP,DU(28,14),DV(28,14),IPREF,JPREF
     1/VAR/ U(28,14),V(28,14),P(28,14),PP(28,14),TE(28,14),ED(28,14)
     1/ALL/IT,JT,NI,NJ,NIM1,NJM1,GREAT
     1/GEOM/INDCOS,X(32),DY(32),DXEP(32),DXPW(32),DYNP(28,14),
     2       DYPS(28,14),SNS(28,14),SEW(32),XU(32),Y(28,14),YV(28,14),
     3       R(28,14),RV(28,14)
     1/FLUPR/URFVIS,VISCOS,DENSIT,PRANDT,DEN(28,14),VIS(28,14)
```

```
      1/KASE T3/UIN,TEIN,EDIN,FLOWIN,ALAMDA,RIN,DAN
      1/TURB/GEN(28,14),CD,CMU,C1,C2,CAPPA,ELCG,PRED,PRTE
      1/COEF/AP(28,14),AN(28,14),AS(28,14),AE(28,14),AW(28,14),SU(28,14),
      1       SP(28,14)
C
CHAPTER  1  1  1  1  1  CALCULATE GEOMETRICAL QUANTITIES  1  1  1  1  1
C
      DC 100 I=1,NI
      DO 100 J=1,NJ
      R(I,J)=X(I)*SIN((0.5+FLOAT(J-2))*DAN)
  100 IF(INDCCS.EC.1)R(I,J)=1.0
      DXPW(1)=0.0
      DXEP(NI)=0.0
      DO 101 I=1,NIM1
      DXEP(I)=X(I+1)-X(I)
  101 DXPW(I+1)=DXEP(I)
      DO 99 I=1,NIM1
      DYPS(I,1)=0.0
      DYNP(I,NJ)=0.0
      SNS(I,1)=0.0
   99 SNS(I,NJ)=0.0
      DO 102 I=1,NI
      DC 102 J=1,NJM1
      DYNP(I,J)=Y(I,J+1)-Y(I,J)
  102 DYPS(I,J+1)=DYNP(I,J)
      SEW(1)=0.0
      SEW(NI)=0.0
      DO 103 I=2,NIM1
  103 SEW(I)=0.5*(DXEP(I)+DXPW(I))
      DC 104 I=1,NI
      DO 104 J=2,NJM1
  104 SNS(I,J)=0.5*(DYNP(I,J)+DYPS(I,J))
      XU(1)=0.0
      DO 105 I=2,NI
  105 XU(I)=0.5*(X(I)+X(I-1))
      DXPWU(1)=0.0
      DXPWU(2)=0.0
      DXEPU(1)=0.0
      DXEPU(NI)=0.0
```



```
      DO 106 I=2,NIM1
      DXEPU(I)=XU(I+1)-XU(I)
  106 DXPWU(I+1)=DXEPU(I)
      SEWU(1)=0.0
      SEWU(2)=0.0
      DC 107 I=3,NIM1
  107 SEWU(I)=0.5*(DXEPU(I)+DXPWU(I))
      DO 98 I=1,NIM1
      YV(I,1)=0.0
      RV(I,1)=0.0
      DYPSV(I,1)=0.0
      DYPSV(I,2)=0.0
      DYNPV(I,NJ)=0.0
      SNSV(I,1)=0.0
      SNSV(I,2)=0.0
   98 SNSV(I,NJ)=0.0
      DO 108 I=1,NI
      DO 108 J=2,NJ
      RV(I,J)=0.5*(R(I,J)+R(I,J-1))
      RCV(I,J)=0.5*(RV(I,J)+RV(I,J-1))
  108 YV(I,J)=0.5*(Y(I,J)+Y(I,J-1))
```

```
      DC 109 I=1,NI
      DO 109 J=2,NJM1
      DYNPV(I,J)=YV(I,J+1)-YV(I,J)
  109 DYPSV(I,J+1)=DYNPV(I,J)
      CO 110 I=1,NI
      DO 110 J=3,NJM1
  110 SNSV(I,J)=0.5*(DYNPV(I,J)+DYPSV(I,J))
C
CHAPTER  2  2  2  2  2  2  SET VARIABLES TC ZERO  2  2  2  2  2  2
C
      DC 200 I=1,NI
      CC 200 J=1,NJ
      U(I,J)=UIN
      V(I,J)=0.0
      P(I,J)=0.0
      PP(I,J)=0.0
      TE(I,J)=TEIN
      ED(I,J)=EDIN
      DEN(I,J)=DENSIT
      VIS(I,J)=VISCOS
      DU(I,J)=0.0
      DV(I,J)=0.0
      SU(I,J)=0.0
      SP(I,J)=0.0
200   CONTINUE
      RETURN
      END
```

B.4 Listing of Program AREA for Calculating Secondary Inlet Flow Area

```
      RSMALL=0.127
      RLARGE=0.165
      RRAT=RLARGE/RSMALL
      A=3.59E-2
      RNOZ=5.075E-3
      RMIX=1.71E-2
      B=RLARGE+RNOZ-RSMALL-RMIX
      XIW=-0.076
      YIW=B-SQRT(RLARGE*RLARGE-(XIW+A)**2)
      DSQ=XIW*(XIW+A)+YIW*(YIW-B)
      FSQ=DSQ+RRAT*RSMALL*RSMALL
      G=(1.0+RRAT)*XIW+A
      H=(1.0+RRAT)*YIW-B
      XOW=(FSQ*G-SQRT(FSQ*FSQ*G*G-(G*G+H*H)*(FSQ*FSQ-H*H*RSMALL**2)))
     1/(G*G+H*H)
      YOW=-SQRT(RSMALL*RSMALL-XOW*XOW)
      FUNCT=((XIW+A)*(XIW-XOW)+(YIW-B)*(YIW-YOW))/(XOW*(YIW-B)-YOW*
     1(XIW+A))
      XOC=XOW-FUNCT*YOW
      YOC=YOW+FUNCT*XOW
      ROC=SQRT((XIW-XOC)**2+(YIW-YOC)**2)
      AREA=6.2832*ROC*(XOW-XIW)
      DELTA1=ATAN((YIW-YOC)/(XOC-XIW))
      DELTA2=ATAN((YOW-YOC)/(XOC-XOW))
      AREA=AREA+6.2832*(YOC+RMIX+RSMALL)*ROC*(DELTA2-DELTA1)
      WRITE(6,11) XIW,YIW,XOW,YOW,XOC,YOC,ROC,AREA
   11 FORMAT(//2F10.4,4X,2F10.4,5X,3F10.4,5X,F10.5)
      CALL EXIT
      END
```

B.5 Listing of Program for Calculating the Measuring Position and Geometry of Tangential Velocity Component

```
      FL=300.0
      ALFA=ATAN(25.0/FL)
      ROUT=25.4
      RIN=19.05
      RIP=1.49
      RIW=1.33
      WL=0.6328E-6
      A=1.0
      DA=1.0
    1 AIA=ATAN(A*SIN(ALFA)/SQRT(ROUT*ROUT-A*A*SIN(ALFA)*SIN(ALFA)))
      RP=ATAN(SIN(AIA)/SQRT(RIP*RIP-SIN(AIA)*SIN(AIA)))
      AIP=ATAN(ROUT*SIN(RP)/SQRT(RIN*RIN-(ROUT*SIN(RP))**2))
      RIPW=RIP/RIW
      RW=ATAN(RIPW*SIN(AIP)/SQRT(1.0-(RIPW*SIN(AIP))**2))
      ALFAP=ALFA+RW+RP-AIA-AIP
      AP=A*SIN(ALFA)/(RIW*SIN(ALFAP))
      SINAW=RIW*SIN(ALFAP)
      FS=0.5*WL/SINAW
      WRITE(6,10) A,AP,ALFAP,SINAW,FS
   10 FORMAT(4F10.3,E12.3)
      IF(A.GT.RIN) GO TO 2
      A=A+DA
      GO TO 1
    2 CALL EXIT
      END
```

B.6 Listing of Program for Calculating the Measuring Position and Geometry of Radial Velocity Component

```
      R=19.05
      A=31.75
      FL=300.0
      BS=25.0
      RIP=1.49
      RIW=1.33
      WL=0.6328E-6
      AIA=ATAN(BS/FL)
      SINRP=SIN(AIA)/RIP
      TANRP=SINRP/SQRT(1.0-SINRP*SINRP)
      RP=ATAN(TANRP)
      S=A*TANRP
      H=0.5
      DH=0.5
      A1=1.0+TANRP*TANRP
      A2=A1
    1 B1=-2.0*TANRP*(H+S-A*TANRP)
      C1=(H+S-A*TANRP)**2-R*R
      X1=-(B1+SQRT(B1*B1-4.0*A1*C1))/(2.0*A1)
      Y1=H+S-TANRP*(X1+A)
      B2=2.0*TANRP*(H-S+A*TANRP)
      C2=(H-S+A*TANRP)**2-R*R
      X2=-(B2+SQRT(B2*B2-4.0*A2*C2))/(2.0*A2)
      Y2=H-S+TANRP*(X2+A)
      ALFA1=ATAN(-Y1/X1)
      AIP1=ALFA1-RP
      SINRW1=RIP*SIN(AIP1)/RIW
      TANRW1=SINRW1/SQRT(1.0-SINRW1*SINRW1)
      RW1=ATAN(TANRW1)
      IF(ALFA1.GT.RW1) SLOP1=-TAN(ALFA1-RW1)
      IF(ALFA1.LE.RW1) SLOP1=TAN(RW1-ALFA1)
      ALFA2=ATAN(-Y2/X2)
      AIP2=ALFA2+RP
      SINRW2=RIP*SIN(AIP2)/RIW
      TANRW2=SINRW2/SQRT(1.0-SINRW2*SINRW2)
      RW2=ATAN(TANRW2)
      SLOP2=TAN(RW2-ALFA2)
      XP=(Y2-Y1+SLOP1*X1-SLOP2*X2)/(SLOP1-SLOP2)
      YP=Y1+SLOP1*(XP-X1)
      ANGLE=ATAN((SLOP2-SLOP1)/(1.0+SLOP2*SLOP1))
      RADIUS=SQRT(XP*XP+YP*YP)
      SINAN=RIW*SIN(0.5*ANGLE)
      FS=0.5*WL/SINAN
      T=(1.0-SLOP1*SLOP2)/(SLOP1+SLOP2)
      SLOP=(-2.0*T+SQRT(4.0*T*T+4.0))/2.0
      GRAD=YP/XP
      PROD=SLOP*GRAD
      WRITE(6,10) H,RADIUS,ANGLE,SINAN ,SLOP,GRAD,PROD,FS
   10 FORMAT(5F8.3,F10.3,F3.3,E12.3)
      IF(H.GE.(0.7*R)) GO TO 2
      H=H+DH
      GO TO 1
    2 CALL EXIT
      END
```

REFERENCES

1. Baker, H.A., Hottel, H.C. and Williams, G.C. (1962) 'Mixing and flow in ducted turbulent jets' Proc. Nine International Symposium on Combustion, Cornell.

2. Baker, R.J. (1974) 'The application of a filter bank to measurements of turbulence in fully developed jet flow.' Proc. of 2nd International Workshop on Laser Velocimetry, Purdue University, Vol. 1, 1974.

3. Bonnington, S.T. & King, A.L. (1972) 'Jet pumps and ejectors - A state of the Art Review and Bibliography'. BHRA Fluid Engineering, Nov. 1972.

4. Bourke, P.J., Brown, C.G. & Drain, L.E. (1971) 'Measurements of Reynolds shear stress in water by laser anemometry' DISA Information, No. 12.

5. Bradshaw, P., Ferriss, D.H. and Atwell, N.P. (1967) 'Calculation of boundary layer development using the turbulent energy equation' J. of Fluid Mechanics, 28.

6. Caretto, L.S., Gosman, A.D., Patankar, S.V. and Spalding, D.B. (1972) 'Two numerical procedures for three dimensional recirculating flows'. Proc. 2nd International Conference on Numerical Methods in Fluid Dynamics, Springer Verlag, New York.

7. Cunningham, R.G.(1954) 'The jet pump as a lubrication oil scavenge pump for aircraft engines.' WADC TR-55-143, Pennsylvania State University.

8. Cunningham, R.G.(1975) 'Liquid jet pump modelling: Effects of axial dimensions on theory-experiment agreement.' 2nd Symposium on Jet Pumps and Ejectors and Gas Lift Technique, Cambridge.

9. Curtet,R.(1958) 'Confined jets and recirculation phenomena with cold air.' Combustion and Flame, London, Vol.2,No.4.

10. Curtet, R. and Ricou, F.P. (1964) 'On the tendency of self-preservation in axisymmetric ducted jets'. J. of Basic Engineering, Trans. of ASME, Dec. 1964.

11. Daly, B.J. and Harlow, F.H. (1970) 'Transport equations in turbulence' Physics of Fluids Vol. 13 , 2634.

12. Dealy, J.M. (1964) 'The confined circular jet with turbulent source' A.S.M.E. Symposium on Fully Separated Flows at the Fluids Engineering Division Conference, May 1964.

13. Durao, D.F.G. and Whitelaw, J.H.(1974) 'Measurements in the region of recirculation behind a disc.' Imperial College, Mech. Eng. Dept. Report HTS/74/15.

14. Durst,F.(1972) 'Development and application of optical anemometers.' PhD Thesis, University of London.

15. Durst, F., Melling, A. and Whitelaw, J.H.(1976) 'Principles and Practice of Laser-Doppler Anemometry', Academic Press, London.

16. Durst, F. and Whitelaw, J.H.(1971) 'Measurements of mean velocity, fluctuating velocity and shear stress using a single channel anemometer.' DISA Information, No.12.

17. Durst, F., Wigley, G. and Zare, M.(1974) 'Laser-Doppler anemometry and its application to flow investigations in the environment of vegetation.' University of Karlsruhe, Report SFB 80/em/41.

18. Elghobashi, S.E. and Pun, W.M.(1974) 'A theoretical and experimental study of turbulent diffusion flames in cylindrical furnaces.' Proc. 15th Symposium on Combustion.

19. Escudier, M.P. and Nicoll, W.B.(1966) 'The shear-work-integral relation in calculations of turbulent boundary layers.' Imperial College, Mech. Eng. Dept. Report TWF/TN/18.

20. Escudier, M.P. and Spalding, D.B.(1965) 'A note on the turbulent uniform-property hydrodynamic boundary layer on a smooth impermeable wall; comparisons of theory with experiment.' A.R.C. C.P.875.

21. Exley, J.T. and Brighton, J.A.(1971) 'Flow separation and reattachment in confined jet mixing.' J. of Basic Engineering, Trans. ASME, June 1971.

22. Folsom, R.G.(1948) 'Predicting liquid jet pump performance.' Proc. of National Conference on Industrial Hydraulic, USA, Oct 1948.

23. Forstall, W. and Shapiro, A.H.(1950) 'Momentum and mass transfer in coaxial gas jets.' J. of Applied Mechanics, Vol.17.

24. Goldstein, S.(1957) 'Modern Developments in Fluid Dynamics' Oxford University Press, Oxford.

25. Goldstein, R.J. and Hagen, W.F.(1967) 'Turbulent flow measurements utilizing the Doppler shift of scattered laser radiation.' Physics of Fluids, Vol.10,1349.

26. Gosline, J.E. and O'Brien, M.P.(1934) 'The water jet pump.' University of California, Publication in Engineering, Vol.3, No.3

27. Gosman, A. D. and Pun, W.M.(1974) 'Calculation of recirculating flows.' HTS Course Notes, Imperial College, London, Report No. HTS/74/2.

28. Gosman, A.D., Pun, W.M., Runchal, A.K., Spalding, D.B. and Wolfshtein, M.(1969) 'Heat and mass transfer in recirculating flows.' Academic Press, London.

29. Ha Minh, H. and Chassaing, P.(1978) 'Some numerical predictions of incompressible turbulent flows.' Proc. 1st. Int. Conf. on Numerical Methods in Laminar and Turbulent Flow, Swansea, 1978.

30. Hansen, A.G. and Kinnavy, R.(1965) 'The design of water jet pumps. Part I-experimental determination of optimum design parameters.' ASME Paper 65-WA/FE-31, Nov.1965.

31. Hanjalic, K.(1970) 'Two-dimensional asymmetric turbulent flow in ducts.' PhD. Thesis, University of London.

32. Harlow, F.H. and Nakayama, P.I.(1968) 'Transport of turbulent energy decay rate.' Los Alamos Science Lab. University of California, Report LA-3854.

33. Head, M.R.(1960) 'Entrainment in the turbulent boundary layer.' A.R.C.R.and M. 3152.

34. Hedges, K.R. and Hill, P.G.(1972) 'A finite difference method for compressible jet mixing in converging-diverging ducts.' Queen's University Thermal Science Report No.3/72,1972.

35. Hedges, K.R. and Hill, P.G.(1974) 'Compressible flow ejectors -- Part I, Development of a finite difference flow model.' ASME Paper 74-FE-1.

36. Helmbold, H.B., Luessen, G. and Heinrich, A.M.(1954) 'An experimental comparison of constant pressure and constant diameter jet pumps.'University of Wichita, Engineering Report No.147, 1954.

37. Hill, B.J.(1973) 'Two-dimensional analysis of flow in jet pumps.' J. of Hydraulic Division, Proc. ASCE, Vol.99,No. HY7.

38. Hill, B.J.(1971) 'Analysis of confined jet flows with applications to the design of jet pumps.' PhD. Thesis, University of London, 1971.

39. Hill, P.G.(1965) 'Turbulent jets in ducted streams.'J.of Fluid Mechanics, Vol.22, Pt.1.

40. Hill, P.G.(1967) 'Incompressible jet mixing in converging-diverging axisymmetric ducts.' J. of Basic Engineering, Trans. ASME, Mar 1967.

41. Hinze, J.O.(1975) 'Turbulence', McGraw-Hill Inc., 2nd. Edition, New York.

42. Huffaker, R.M., Fuller, C.E.and Lawrence, T.R.(1969) 'Application of laser Doppler velocity instrumentation to the measurement of jet turbulence.' S.A.E. Conf., Detroit, 1969.

43. Jones, W.P. and Launder, B.E.(1973) 'Prediction of low Reynolds Number phenomena with a two-equation model of turbulence.'Int. J. of Heat and Mass Transfer, Vol.16,

44. Kastner, L.J. and Spooner, J.R.(1950) 'An investigation of the performance and design of the air ejector employing low-pressure air as driving fluid.' Proc.I.Mech.E. 162, Pt.2, 1950.

45. Keenan, J.H. and Neuman, E.P.(1942) 'A simple air ejector' J. of Applied Mechanics,Vol.9, No.2.

46. Kolmogorov, A.N.(1942) 'Equations of turbulent motion of an incompressible turbulent fluid.' Izv. Akad. Nauk SSSR Ser Phys. VI, No.1-2,56.

47. Launder, B.E., Morse, A., Rodi, W. and Spalding, D.B. (1972) 'The prediction of free shear flows-A comparison of the performance of six turbulence models.' Proc. of NASA Conf. on Free Shear Flows, Langley, 1972.

48. Launder, B.E. and Spalding, D.B.(1972) 'Mathematical Models of Turbulence', Academic Press, London, 1972.

49. Launder, B.E. and Spalding, D.B.(1974) 'The numerical computation of turbulent flows.' Computer Methods in Applied Mechanics and Engineering, Vol.3.

50. Lewis, R.D.,Foreman, J.W., Watson, H.J. and Thornton, J. R.(1968) 'Laser-Doppler velocimeter for measuring flow-velocity fluctuations.' Physics of Fluids, Vol.11, 433.

51. Matthews, L. and Whitelaw, J.H.(1971) 'The prediction of film cooling in the presence of recirculating flows with a two-equation model of turbulence.' Imperial College, Mech. Eng. Dept. Report HTS/71/31.

52. McDonald, A.T. and Fox, R.w.(1966) 'An experimental investigation of incompressible flow in conical diffusers' Int. J. of Mechanical Science, Vol.8,1966.

53. Melling, A. and Whitelaw, J.H.(1973) 'Measurements in turbulent water flows by laser anemometer.' Proc. of 3rd Biennial Symposium on Turbulence in Liquids, Roller, 115. Also, Imperial College, Mech.Eng.Dept.Report HTS/73/44.

54. Mikhail, S.(1960) 'Mixing of coaxial streams inside a closed conduit.' J. of Mechanical Engineering Science, Vol.2, No.1.

55. Morton, J.B. and Clark, W.H.(1971) 'Measurement of two point velocity correlations in pipe flow using laser anemometer.' J. of Physics E: Sci. Instrum., No.4.

56. Mueller, N.H.G.(1964) 'Water jet Pump.' Proc. ASCE, Vol. 90, No.HY3.

57. Nee, V.W. and Kovasznay, L.S.G.(1968) 'The calculation of the incompressible turbulent boundary layer by a simple theory.' Proc. of AFOSR/IFP Conf. on Computation of Turbulent Boundary Layers, Vol.I, Stanford University.

58. Neilson, P.V.(1973) 'Prediction of air distribution in a forced ventilation room.' Ingenioreus Ugeblad, Nr.5.

59. Ng, K.H. and Spalding, D.B.(1972) 'Some applications of a model of turbulence to boundary layer near walls.' Physics of Fluids, 15.

60. Patankar, S.V, and Spalding, D.B.(1967) 'Heat and Mass Transfer in Boundary Layers.' Morgan-Grampian, London.

61. Patankar, S.V. and Spalding, D.B.(1972) 'A calculation procedure for heat, mass and momentum transfer in three dimensional parabolic flows.' Int. J. of Heat and Mass Transfer, Vol.15.

62. Pope, S.B.(1972) 'Injector pump performance -- The influence of duct and nozzle geometry.' MSc.Dissertation Imperial College, London.

63. Prandtl, L.(1925) 'Bericht uber Untersuchungen zur Ausgebildeten Turbulenz.' ZAMM 5, 136.

64. Prandtl, L.(1945) 'Uber ein neues Formelsystem fur die ausgebildete Turbulenz.' Nachrichten von der Akad. der Wissenschaft in Gottingen.

65. Pun, W.M. and Spalding, D.B.(1967) 'A procedure for predicting the velocity and temperature distributions in a confined, steady, turbulent, gaseous, diffusion flame.' Imperial College, Mech.Eng.Dept. Report SF/TN/1/.

66. Rankine, J.M.(1870) 'On the mathematical theory of combined streams.' Proc. Royal Society, London, Vol.19.

67. Razinsky, E. and Brighton, J.A.(1971) 'Confined jet mixing for nonseparating conditions.' J. of Basic Engineering, Trans. ASME, Sept.1971.

68. Reddy, Y.R. and Kar, S.(1968) 'Theory and performance of water jet pumps.' J. of Hydraulic Div., ASCE, Vol.94, No.HY5.

69. Rodi, W.(1972) 'The prediction of free turbulent boundary layers by use of two-equation model of turbulence' PhD. Thesis, University of London, 1972.

70. Rotta, J.(1951) 'Statistische Theorie nichthomogener Turbulenz.' Zeitch fur Physik, 129,547, and 131,51.

71. Rotta, J.(1971) 'Recent attempt to develop a generally applicable calculation method for turbulent shear flow layers.' Proc. of AGARD Conf. on Turbulent Shear Flows, London.

72. Rudd, M.J.(1969) 'A new theoretical model for the laser Dopplermeter.' J. of Physics E., Sci.Instrum. Vol.2,55.

73. Runchal, A.K.(1969) 'Transfer processes in steady two-dimensional separated flows.' PhD. Thesis, Imperial College, London.

74. Sanger, N.L.(1968a) 'Noncavitating performance of two low-area-ratio water jet pumps having throat length of 7.25 diameters.' NASA TN D-4445, 1968.

75. Sanger, N.L.(1968b) 'Noncavitating and cavitating performance of two low-area-ratio water jet pumps with throat length of 5.66 diameters.' NASA TN D-4759, 1968.

76. Sanger, N.L.(1971) 'Fortran programs for the design of liquid-to-liquid jet pumps.' NASA TN D-6453,1971.

77. Sanger, N.L.(1970) 'An experimental investigation of several low-area-ratio water jet pumps.' J. of Basic Engineering, Trans.ASME, Series D, 92, 1970.

78. Schlichting, H.(1960) 'Boundary Layer Theory' McGraw-Hill Book Co., 4th.Ed., New York.

79. Schulz, F.(1952) 'Model tests for water jet pumps.' Abhandlungen des Dokumentations zentrums fur Technik und Wirtschaft, No.3, 2nd Ed. Vienna.

80. Schulz, F. and Fasol, K.H.(1958) 'Wasserstrahlpumpen zur Forderung von Flussigkeiten.' Springer Verlag, Vienna.

81. Sharma, R.N.(1972) 'Momentum and mass transfer in turbulent conical wall jets.' PhD.Thesis, Indian Institute of Technology, Kanpur.

82. Spalding, D.B.(1967) 'The calculation of length scale of turbulence in some turbulent boundary layers remote from walls.' Imperial College, Mech.Eng.Dept.Report TWF/TN/31.

83. Spalding, D.B.(1969) 'The prediction of two-dimensional, steady turbulent flows.' Imperial College, Mech.Eng.Dept. report EF/TN/A/16.

84. Truckenbrodt, E.(1952) 'Ein Quadraturverfahren zur Berechnung der laminaren und turbulenten Reibungsschicht ber ebener und rotationssysnmetrischer Stromung.' Ing. Arch.20.

85. Vogel, R.(1956) 'Theoretical and exeprimental investigation of air ejectors.' Maschinenbautechnik, Vol. 5.

86. Wang, C.P. and Snyder, D.(1974) 'Laser Doppler velocimetry experimental study.' Applied Optics, Vol.13.

87. Welch, N.E. and Tomme, W.J.(1967) 'Analysis of turbulence from data obtained with a laser velocimeter.' AIAA Paper No. 67-179.

88. Williams, P.D.(1972) 'Numerical and Experimental studies of turbulent flow in diffusers at low Reynolds Numbers.' PhD Thesis, University of Exeter.

89. Wolfshtein, M.(1968) 'Convection processes in turbulent impinging jets.' PhD. Thesis, Imperial College, London.

90. Yeh, Y and Cummins, H. Z.(1964) 'Localized flow measurements with an He-Ne laser spectrometer.' Applied Physics Letters, Vol.4., 176.

The computer modelling and experimental study of confined jet mixing with application to jet pump design
(S.N. TAY)

SUMMARY

As an aid to jet pump design and performance analysis, a theoretical investigation on turbulent confined jet mixing in a non-uniform axisymmetric duct typically used in jet pumps and ejectors has been undertaken. A so-called Prandtl-Kolmogorov two-equation turbulence model, with turbulent kinetic energy k and turbulent energy dissipation rate ε as the two parameters, is incorporated into the time-mean Navier-Stokes equations to form a complete set of partial differential equations which describes the turbulent flow mathematically. The equations are solved numerically via a primitive pressure-velocity finite-difference procedure using a digital computer. The time-mean static pressure, velocities, turbulent kinetic energy and dissipation rate are predicted directly throughout the whole flow field.

To validate the computer model, predicted time-mean static pressure and velocity as well as turbulent shear stress for flow in a uniform bore mixing tube are compared with the published results. The method is then extended to predict flows in conical diffusers and typical jet pumps. The predictions are also compared with the available experimental data.

A laser Doppler anemometer is used to measure the mean and fluctuating velocities of water jet mixing in a uniform perspex mixing tube with a centrally located

nozzle. The measured data which enable turbulent kinetic energy to be evaluated, are compared with the computer predictions to further consolidate the theoretical model.

Finally, the computer model is used to predict the performance of a proposed jet pump and to investigate the influence of various geometrical parameters on jet pump performance. The capability of the computer model as a useful design tool is also demonstrated via an optimization procedure to give the optimum geometry for a given design specification.